

VOLUME 79

APRIL 10, 1975

NUMBER 8

JPCHAX

---

THE JOURNAL OF

PHYSICAL

CHEMISTRY

---

PUBLISHED BIWEEKLY BY THE AMERICAN CHEMICAL SOCIETY

# THE JOURNAL OF PHYSICAL CHEMISTRY

---

**BRYCE CRAWFORD, Jr.**, *Editor*  
**STEPHEN PRAGER**, *Associate Editor*  
**ROBERT W. CARR, Jr.**, **FREDERIC A. VAN-CATLEDGE**, *Assistant Editors*

**EDITORIAL BOARD:** C. A. ANGELL (1973-1977), F. C. ANSON (1974-1978), V. A. BLOOMFIELD (1974-1978), J. R. BOLTON (1971-1975), L. M. DORFMAN (1974-1978), H. L. FRIEDMAN (1975-1979), E. J. HART (1975-1979), W. J. KAUZMANN (1974-1978), R. L. KAY (1972-1976), D. W. McCLURE (1974-1978), R. M. NOYES (1973-1977), J. A. POPLE (1971-1975), B. S. RABINOVITCH (1971-1975), S. A. RICE (1969-1975), F. S. ROWLAND (1973-1977), R. L. SCOTT (1973-1977), A. SILBERBERG (1971-1975), J. B. STOTHERS (1974-1978), W. A. ZISMAN (1972-1976)

AMERICAN CHEMICAL SOCIETY, 1155 Sixteenth St., N.W., Washington, D.C. 20036

## Books and Journals Division

**JOHN K CRUM** *Director*  
**VIRGINIA E. STEWART** *Assistant to the Director*

---

**CHARLES R. BERTSCH** *Head, Editorial Processing Department*  
**D. H. MICHAEL BOWEN** *Head, Journals Department*  
**BACIL GUILLEY** *Head, Graphics and Production Department*  
**SELDON W. TERRANT** *Head, Research and Development Department*

©Copyright, 1975, by the American Chemical Society. Published biweekly by the American Chemical Society at 20th and Northampton Sts., Easton, Pa. 18042. Second-class postage paid at Washington, D.C., and at additional mailing offices.

All manuscripts should be sent to *The Journal of Physical Chemistry*, Department of Chemistry, University of Minnesota, Minneapolis, Minn. 55455.

*Additions and Corrections* are published once yearly in the final issue. See Volume 78, Number 26 for the proper form.

*Extensive or unusual alterations in an article after it has been set in type are made at the author's expense*, and it is understood that by requesting such alterations the author agrees to defray the cost thereof.

The American Chemical Society and the Editor of *The Journal of Physical Chemistry* assume no responsibility for the statements and opinions advanced by contributors.

Correspondence regarding accepted copy, proofs, and reprints should be directed to Editorial Processing Department, American Chemical Society, 20th and Northampton Sts., Easton, Pa. 18042. Department Head: CHARLES R. BERTSCH. Associate Department Head: MARIANNE C. BROGAN. Assistant Editor: CELIA B. MCFARLAND. Editorial Assistant: JOSEPH E. YURVATI.

Advertising Office: Centcom, Ltd., 50 W. State St., Westport, Conn. 06880.

## Business and Subscription Information

Send all new and renewal subscriptions *with payment* to: Office of the Controller, 1155 16th Street, N.W., Washington, D.C. 20036. Subscriptions should be renewed promptly to avoid a break in your series. All correspondence and telephone calls regarding

changes of address, claims for missing issues, subscription service, the status of records, and accounts should be directed to Manager, Membership and Subscription Services, American Chemical Society, P.O. Box 3337, Columbus, Ohio 43210. Telephone (614) 421-7230. For microfiche service, contact ACS Journals Department, 1155 16th St. N.W., Washington, D.C. 20036. Telephone (202) 872-4444.

On changes of address, include both old and new addresses with ZIP code numbers, accompanied by mailing label from a recent issue. Allow four weeks for change to become effective.

Claims for missing numbers will not be allowed (1) if loss was due to failure of notice of change in address to be received before the date specified, (2) if received more than sixty days from date of issue plus time normally required for postal delivery of journal and claim, or (3) if the reason for the claim is "issue missing from files."

Subscription rates (hard copy or microfiche) in 1975: \$20.00 for 1 year to ACS members; \$80.00 to nonmembers. Extra postage \$4.50 in Canada and PUAS, \$5.00 other foreign. Supplementary material (on microfiche only) available on subscription basis, 1975 rates: \$15.00 in U.S., \$19.00 in Canada and PUAS, \$20.00 elsewhere. All microfiche airmailed to non-U.S. addresses; air freight rates for hard-copy subscriptions available on request.

Single copies for current year: \$4.00. Rates for back issues from Volume 56 to date are available from the Special Issues Sales Department, 1155 Sixteenth St., N.W., Washington, D.C. 20036.

Subscriptions to this and the other ACS periodical publications are available on microfilm. For information on microfilm write Special Issues Sales Department at the address above.

THE JOURNAL OF  
PHYSICAL CHEMISTRY

Volume 79, Number 8 April 10, 1975

JPCA 79(8) 765-858 (1975)

ISSN 0022-3654

Kinetics of the Reaction of Hydroxyl Radicals with Ethylene, Propylene, 1-Butene, and <i>trans</i> -2-Butene	Andres V. Pastrana and Robert W. Carr, Jr.*	765
Photolysis of Hydrogen Selenide	D. C. Dobson, F. C. James, I. Safarik, H. E. Gunning, and O. P. Strausz*	771
Abstraction of Sulfur Atoms from Carbonyl Sulfide by Atomic Hydrogen	S. Tsunashima, T. Yokota, I. Safarik, H. E. Gunning, and O. P. Strausz*	775
Reaction between Ozone and Hydrogen Sulfide	Sotirios Glavas and Sidney Toby*	779
Effects of Solutes, Deuteration, and Annealing on the Production and Decay of Radicals in $\gamma$ Irradiated 3-Methylpentane Glasses	M. A. Neiss and J. E. Willard*	783
Temperature Dependence of the Heat Capacities of Activation for the Aquations of Bromo- and Sulfatopentaamminecobalt(III) Ions in Acidic Aqueous Solution	Anthony M. Newton and Thomas W. Swaddle*	795
The Use of the Enthalpy of Transfer of Slightly Soluble Salts in the Study of Water-Nonelectrolyte Structural Interactions. The <i>tert</i> -Butyl Alcohol-, Dioxane-, and Urea-Water Systems	Linford L. Bright and John R. Jezorek*	800
Electrochemistry of Chemisorbed Molecules. III. Determination of the Oxidation State of Halides Chemisorbed on Platinum. Reactivity and Catalytic Properties of Adsorbed Species	Ross F. Lane and Arthur T. Hubbard*	808
Dissolution Rates of Aqueous Silver Halide Dispersions	D. D. F. Shiao,* L. J. Fortmiller, and A. H. Herz	816
Vibrational Spectra of Liquid Crystals. IX. Calculation of Infrared and Raman Active Lattice Vibration Frequencies of 4,4'-Azoxydianisole	Dolores Grunbaum and Bernard J. Bulkin*	821
Spectrophotometric Study of the Vapors of Iron(III) Chloride and of Mixtures of Iron(III) Chloride and Aluminum(III) Chloride. Evidence for Formation of Mixed Metal Dimer Molecules	Chyi-Feng Shieh and N. W. Gregory*	828
Electron Spin Resonance Study of the Sulfide Radical Adducts to Unsaturated Compounds	Yutaka Kirino and Richard W. Fessenden*	834
Protonation Reactions at Carbon Sites in the Anion Radicals of Certain Unsaturated Compounds and Aromatic Amino Acids	C. Van Paemel, H. Frumin, V. L. Brooks, R. Failor, and M. D. Sevilla*	839
Complexes of Aromatic Electron Donors with <i>N</i> -Methylsuccinimide and <i>N</i> -Methylmaleimide	Norman Kulevsky* and Roy Foster	846
Magnetic Criteria for Aromaticity	Rois Benassi, Paolo Lazzarotti,* and Ferdinando Taddei	848
Search for Isotope Effects in the Self-Diffusion of Benzene and Cyclohexane at 25°	R. Mills	852
Kinetics of the Conversion of Monetite to Calcium Pyrophosphate	Nancy Wolejko Wikholm, Ralph A. Beebe,* and J. S. Kittelberger	853

## COMMUNICATIONS TO THE EDITOR

Rotational Freedom of Adsorbed Molecules . . . . .	D. M. Ruthven 856
A Correction and Improvement of "On the Kinetics of Step-Wise Micelle Association" by E. A. G. Aniansson and S. N. Wall . . . . .	E. A. G. Aniansson* and S. N. Wall 857
Rate of Phase Separation in Liquid Mixtures Studied by T-Jump Experiments under Pressure A. Jost and G. M. Schneider* . . . . .	858

■ Supplementary material for this paper is available separately, in photocopy or microfiche form. Ordering information is given in the paper.

\* In papers with more than one author, the asterisk indicates the name of the author to whom inquiries about the paper should be addressed.

## AUTHOR INDEX

Aniansson, E. A. G., 857	Glavas, S., 779	Lane, R. F., 808	Shiao, D. D. F., 816
Beebe, R. A., 853	Gregory, N. W., 828	Lazzeretti, P., 848	Shieh, C.-F., 828
Benassi, R., 848	Grunbaum, D., 821	Mills, R., 852	Strausz, O. P., 771, 775
Bright, L. L., 800	Gunning, H. E., 771, 775	Neiss, M. A., 783	Swaddle, T. W., 795
Brooks, V. L., 839	Herz, A. H., 816	Newton, A. M., 795	Taddei, F., 848
Bulkin, B. J., 821	Hubbard, A. T., 808	Pastrana, A. V., 765	Toby, S., 779
Carr, R. W., Jr., 765	James, F. C., 771	Ruthven, D. M., 856	Tsunashima, S., 775
Dobson, D. C., 771	Jezorek, J. R., 800	Safarik, I., 771, 775	Van Paemel, C., 839
Failor, R., 839	Jost, A., 858	Schneider, G. M., 858	Wall, S. N., 857
Fessenden, R. W., 834	Kirino, Y., 834	Sevilla, M. D., 839	Wikholm, N. W., 853
Fortmiller, L. J., 816	Kittelberger, J. S., 853		Willard, J. E., 783
Foster, R., 846	Kulevsky, N., 846		Yokota, T., 775
Frumin, H., 839			

# THE JOURNAL OF PHYSICAL CHEMISTRY

Registered in U. S. Patent Office © Copyright, 1975, by the American Chemical Society

VOLUME 79, NUMBER 8 APRIL 10, 1975

## Kinetics of the Reaction of Hydroxyl Radicals with Ethylene, Propylene, 1-Butene, and *trans*-2-Butene<sup>1</sup>

Andres V. Pastrana and Robert W. Carr, Jr.\*

Department of Chemical Engineering and Materials Science, University of Minnesota, Minneapolis Minnesota 55455  
(Received March 20, 1974; Revised Manuscript Received December 30, 1974)

Publication costs assisted by the U.S. Atomic Energy Commission

The kinetics of the decay of hydroxyl radicals in the presence of ethylene, propylene, 1-butene, and *trans*-2-butene were studied at approximately 1 Torr and 300°K in a tubular discharge-flow reactor. Hydroxyl radicals were produced by the reaction of atomic hydrogen with nitrogen dioxide,  $\text{H} + \text{NO}_2 = \text{OH} + \text{NO}$  (1), and their decay was followed by line absorption photometry at 308.328 nm in an excess of olefin. The decays were pseudo-first order, and the kinetics were first order with respect to both hydroxyl and olefin for each of the olefins studied. The second-order rate constants are  $nk_{\text{OH}+\text{C}_2\text{H}_4} = (2.13 \pm 0.13) \times 10^{-12} \text{ cm}^3 \text{ molecule}^{-1} \text{ sec}^{-1}$ ,  $nk_{\text{OH}+\text{C}_3\text{H}_6} = (5 \pm 1) \times 10^{-12} \text{ cm}^3 \text{ molecule}^{-1} \text{ sec}^{-1}$ ,  $nk_{\text{OH}+1\text{-C}_4\text{H}_8} = (1.5 \pm 0.1) \times 10^{-11} \text{ cm}^3 \text{ molecule}^{-1} \text{ sec}^{-1}$ , and  $nk_{\text{OH}+\textit{trans}\text{-2-butene}} \cong (1.2 \pm 1) \times 10^{-11} \text{ cm}^3 \text{ molecule}^{-1} \text{ sec}^{-1}$ . The reaction with propylene is susceptible to secondary reactions since  $n$ , the stoichiometric coefficient, decreased by a factor of 3.5 as  $[\text{C}_3\text{H}_6]_0/[\text{OH}]_0$  increased from 1.5 to 30. The stoichiometric coefficients for the  $\text{C}_2\text{H}_4$  reaction and the  $\text{C}_3\text{H}_6$  reaction at the higher (olefin)/(OH) ratios are nearly unity. The reaction with butenes is accompanied by the formation of a white solid. With propylene and the butenes H abstraction from the allyl position is predicted to be competitive with addition to the double bond.

### Introduction

Hydroxyl radicals may play an extremely important role in the chemistry of urban atmospheres. The production of hydroxyl and some of its possible reactions in photochemical smog were discussed by Leighton in 1961,<sup>2</sup> while later suggestions linked hydroxyl with NO to NO<sub>2</sub> conversion<sup>3,5</sup> and postulated that reaction of hydroxyl radicals with olefins was a significant chain-propagating step for olefin consumption.<sup>3,4</sup> Support for this postulate was obtained from computer simulation of smog chamber experiments on the propylene-NO<sub>x</sub> system.<sup>6</sup> Niki, Daby, and Weinstock<sup>6</sup> showed that although the rates of attack of atomic oxygen and ozone on propylene were too slow to account for observed propylene consumption rates, inclusion of a chain reaction involving hydroxyl radicals as a chain carrier, with reaction of hydroxyl with olefin initiating the chain, could account for the "excess" rate of propylene consumption. Furthermore, the computed rates of propylene consumption were sensitive to the bimolecular rate coefficient used for the hydroxyl radical-propylene reaction.

In view of the above considerations, accurate values of

hydroxyl radical plus olefin reaction rate coefficients will be necessary for the description of atmospheric reactions to be used in modelling photochemical smog. Although the reaction of hydroxyl with ethylene has been studied by discharge-flow,<sup>7-9</sup> flash photolysis,<sup>10,11</sup> and resonance fluorescence<sup>12</sup> methods, the reported rate coefficients at 298 K differ by a factor of 3. The 298 K rate coefficient for hydroxyl plus propylene is also not accurately known. In this case two measurements in discharge-flow apparatus differ by a factor of 3,<sup>8,9</sup> while a resonance fluorescence determination<sup>12</sup> and a steady-illumination photolysis method<sup>13</sup> yielded rate coefficients bracketed by the former pair. Thus we considered further investigation of these important reactions to be necessary.

In this work we have studied the hydroxyl-ethylene and hydroxyl-propylene reactions, and have made the first direct measurements of the kinetics of hydroxyl with 1-butene and with *trans*-2-butene in a tubular discharge-flow apparatus by an improved hydroxyl line absorption photometry method. The production of hydroxyl via the reaction of atomic hydrogen with nitrogen dioxide was done in excess nitrogen dioxide.

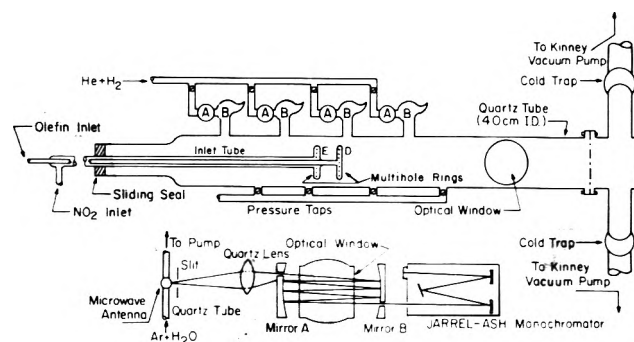


**Figure 1.** Flow reactor and optical arrangement: A, microwave discharge cavities; B, Wood's horns; D and E, reactant inlets.

## Experimental Section

**Apparatus.** The reactor shown schematically in Figure 1 was used for these experiments. The 4-cm i.d. flow tube was 150 cm long, with a pair of planar quartz windows serving as observation ports for [OH] measurement by line absorption photometry at 308.939 nm. Linear flow velocities of approximately  $3 \times 10^3$  cm sec<sup>-1</sup> at 1–5 Torr of dilute reactants in He ( $N_{Re} < 10$ ) were obtained with a Kinney KDH 130 pump. Four side arms, 20 cm apart, were provided for introduction of atomic hydrogen following 2450-MHz dissociation of ~10% H<sub>2</sub> in 1 Torr He in a tuned cavity.<sup>14</sup> In practice the upstream side arm nearest the NO<sub>2</sub> inlet was used to minimize H decay prior to reaction with NO<sub>2</sub>. The reactor wall was lined with a thin Teflon sheet, which was found to be effective for retarding heterogeneous removal of H and OH. Olefins and NO<sub>2</sub> were admitted through a coaxial sliding-seal inlet tube having two ring-shaped flow dispersers which allowed their injection in the radial direction. The entire injection assembly was able to translate in the axial direction, providing a variable reaction distance from the observation ports. Nitrogen dioxide entered from the upstream disperser, and olefins from the other. Mixing effectiveness was verified by visual observations of the airglow,  $O + NO \rightarrow NO_2 + h\nu$ ,<sup>15</sup> and by measuring [OH] vs. distance with NO<sub>2</sub> only entering from the downstream disperser. Second-order kinetic plots of OH decay,  $(OH)_0/(OH)$  vs. distance, increased monotonically from 1.0 at  $z = 0$  cm, the disperser position, and the airglow was of uniform intensity. Pressure measurements at the four pressure taps with either a Pirani gauge or a tilting McLeod gauge revealed negligible pressure drop during experiments.

Flow rates of He, H<sub>2</sub>, NO<sub>2</sub>, and C<sub>2</sub>H<sub>4</sub> were controlled by needle valves and measured with calibrated rotameters. The flow rates of propylene and butene were measured by the rate of pressure loss in a bulb of known volume.<sup>16</sup>

**Hydroxyl Radical Generation.** Hydroxyl radicals were generated by the reaction of atomic hydrogen with NO<sub>2</sub>.<sup>17</sup> The mechanism of the production and decay of OH in the absence of olefins consists of the following steps:

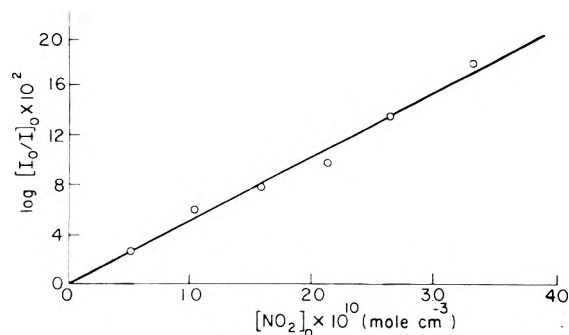
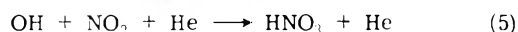
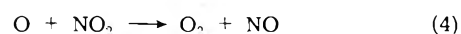
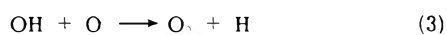
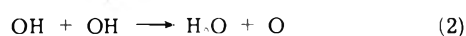
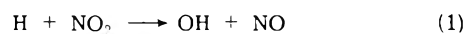


**Figure 2.** Logarithm of maximum absorption at 308.328 nm vs. initial NO<sub>2</sub> concentrations.

To avoid reactions of H with olefins, NO<sub>2</sub> was in excess in reaction 1,  $[NO_2]_0/[H]_0$  being in the range 3–10, and H decay was pseudo-first order to an approximation,  $-d[H]/dt = k_1'[H]$ , where  $k_1' = k_1[NO_2]$ . Using  $k_1 = 4.8 \times 10^{-11}$  cm<sup>3</sup> molecule<sup>-1</sup> sec<sup>-1</sup>,<sup>18</sup> and  $[NO_2]_0 = 4 \times 10^{14}$  molecules cm<sup>-3</sup>, the half-life of OH is  $\sim 3 \times 10^{-5}$  sec. Thus in the 1 cm between mixing ring inlets, with  $\bar{v} = 3 \times 10^3$  cm/sec, [H] will decay by more than 10 half-lives or >99.9% before the olefin is added. Also, in the absence of olefin, OH decay after the first centimeter is given by the following equation:

$$-d[OH]/dt = 2k_2[OH]^2 + k_3[O][OH] + k_5[OH][NO_2][He] + k_w[OH] \quad (7)$$

In excess [NO<sub>2</sub>], (3) is immediately followed by (1), the net being reaction 4. Thus, the kinetics of OH decay are predicted to follow a concurrent first- and second-order rate law. (Reaction 5 is pseudo-first order in OH.) Second-order plots,  $[OH]^{-1}$  vs.  $t$ , showed upward curvature, corroborating this analysis, but with increasing  $[OH]_0$  the amount of curvature decreased, showing the increased contribution of the first term on the right-hand side of the above rate equation.

**Hydroxyl Concentration Measurement.** A light source emitting the OH A<sup>2</sup>Σ<sup>+</sup> → OH X<sup>2</sup>Π spectrum, a set of spherical concave mirrors forming a folded light path as described by Herriott et al.,<sup>19</sup> a Suprasil lens, and a 0.5-m monochromator with a 1 P28 photomultiplier comprised the equipment for OH detection by line photometry. The OH light source consisted of a mixture of 0.6% by volume of H<sub>2</sub>O in 18 Torr of Ar, flowing through a tuned 2450-MHz microwave cavity.<sup>14</sup> With the mirrors set at a nonconfocal distance, emission from the discharge was focussed to pass through a 3-mm hole drilled in the first mirror, and traversed the reactor nine times or more in an elliptical pattern before exiting to the monochromator through a similar 3-mm hole in the second mirror. The ellipse was limited to a 3 mm width along the reactor axis, and the [OH] detectability (1% absorption) was  $\sim 10^{12}$  cm<sup>-3</sup>.

Transmitted intensity of the Q<sub>1</sub> – 5 line at 308.328 nm was isolated by the monochromator. Provided  $I_0/I \leq 1.5$ , where  $I_0$  is incident intensity, and  $I$  is transmitted intensity, Beer's law,  $[OH] = (t)^{-1} \log(I_0/I)$ , can be used for the "line absorption" measurement.<sup>20</sup> For production of OH by the reaction of H with NO<sub>2</sub> in a large excess of H, and provided mixing is efficient,  $[OH]_0 = [NO_2]_0$ .<sup>21</sup> Excess H was only used in these experiments designed to test Beer's law, where olefins were absent. The linearity of Figure 2 demonstrates the validity of Beer's law up to  $I_0/I = 1.5$ . In this work the optical transmission was always greater than 0.75.

**Flow Considerations.** Laminar flow was always obtained. Viscous pressure drop was negligible ( $\Delta p/p \sim 10^{-3}$ ), as demonstrated by direct measurement, and corroborated by applying Poiseuille's equation for the pressure drop to typical experimental conditions. Reaction times were calculated by  $t = zA/Q$ , where  $z$  is axial distance,  $A$  is the flow cross-sectional area, and  $Q$  is volumetric flow rate. This will be accurate provided  $D/kC_0R^2 \geq 1.0$ ,<sup>22</sup> where, applied to the present case,  $D$  = binary diffusion coefficient of OH,  $R$  = reactor radius,  $k$  = second-order rate constant, and  $C_0$  = initial concentration of olefin. In these experiments  $D/kC_0R^2 > 12$  was always attained. This condition describes the situation where radial diffusion is fast enough to make the concentration profile uniform. The contribution of axial dispersion was estimated by examining the mass balance on OH for first-order kinetics, which were always observed. In the approximation that radial concentration gradients are negligible, and using the boundary conditions  $[OH] = [OH]_0$  at  $z = 0$  and  $[OH] = C$  at  $z = \infty$

$$D \frac{\partial^2 [OH]}{\partial z^2} - \bar{v} \frac{\partial [OH]}{\partial z} - k_1 [OH] = 0 \quad (8)$$

yields  $k_0 = k_{\text{obsd}}[1 + k_{\text{obsd}}D/\bar{v}^2]$  where  $k_{\text{obsd}}$  is the experimentally determined first-order rate coefficient. For a typical  $k_{\text{obsd}}$  of  $600 \text{ sec}^{-1}$  at  $\bar{v} = 3 \times 10^3 \text{ cm sec}^{-1}$ ,  $p = 1 \text{ Torr}$ , and  $D = (690/p) \text{ cm}^2 \text{ sec}^{-1}$ , the last estimated from data in ref 23,  $k_{\text{obsd}}D/\bar{v}^2 = 5 \times 10^{-2}$ . If  $k_{\text{obsd}}D/\bar{v}^2$  is regarded as a correction, the magnitude of the correction to  $k_{\text{obsd}}$  is probably less than the accumulated errors from other sources.

We have tested this apparatus by measuring OH decay in the absence of added olefin. With either H in excess of  $\text{NO}_2$ , or vice versa, the kinetics are predominantly second order in OH, with some concurrent first-order decay. A kinetic analysis yielded values of  $k_2$  for either of the above conditions,<sup>24</sup> in good agreement with recent reports.<sup>25,26</sup>

### Experimental Results

When measuring the rate of decay of hydroxyl radicals, an excess of olefin over  $[OH]_0$  was used. With this condition OH decay always obeyed a first-order rate law. The first-order rate coefficients, however, depended upon the olefin concentration. In Figure 3 are typical first-order plots of OH decay in the presence of propylene for various initial concentrations of propylene. In these experiments, as in all of the work presented here,  $[\text{NO}_2]_0$  was in excess of  $[\text{H}]_0$  to prevent the reaction of H atoms with the olefins. Typically  $[\text{NO}_2]_0$  was  $4 \times 10^{14}$  molecules  $\text{cm}^{-3}$ , and  $[\text{H}_2]$  was in the range  $3-7 \times 10^{13}$  molecules  $\text{cm}^{-3}$ . In propylene experiments  $[OH]_0$  was varied from  $1.0 \times 10^{13}$  to  $1.75 \times 10^{13}$  molecules  $\text{cm}^{-3}$ ,  $[\text{C}_3\text{H}_6]_0$  was from  $3.3 \times 10^{13}$  to  $7.1 \times 10^{14}$  molecules  $\text{cm}^{-3}$ , and  $[\text{C}_3\text{H}_6]_0/[OH]_0$  varied from about 2 to 34. The results were invariant to a threefold variation in  $[\text{NO}_2]_0$ .

With ethylene, 1-butene, or *trans*-2-butene present as the excess reactant the OH decay kinetics were also first order in OH, and the pseudo-first-order rate constant increased with increasing olefin concentration in each case. Initial OH concentration ranged from  $3 \times 10^{13}$  to  $8 \times 10^{13}$  molecules  $\text{cm}^{-3}$  while the ethylene concentration was varied from  $8 \times 10^{13}$  to  $3.9 \times 10^{14}$  molecules  $\text{cm}^{-3}$ . The ratio of  $[\text{C}_2\text{H}_4]_0/[OH]_0$  was kept as high as was possible, consistent with reliable measurement of the OH decay. In the experiments with 1-butene a tenfold excess of nitrogen dioxide over atomic hydrogen was used. Initial OH concentration was maintained at values ranging from  $1.0 \times 10^{13}$  to  $4.7 \times$

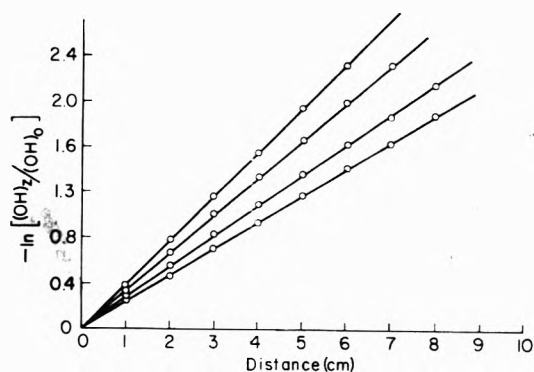


Figure 3. Typical experimental first-order OH decay plots for various initial concentrations of  $\text{C}_3\text{H}_6$ ,  $[\text{C}_3\text{H}_6]_0$ . The slope increases with increasing  $[\text{C}_3\text{H}_6]_0$ .

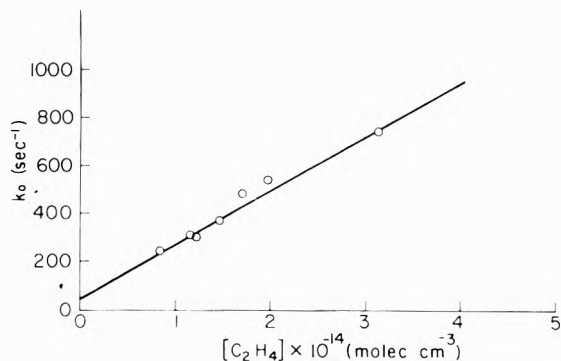


Figure 4. Pseudo first-order rate constants vs.  $[\text{C}_2\text{H}_4]$ .

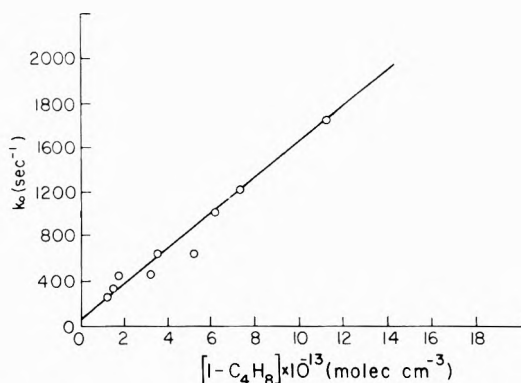


Figure 5. Pseudo first-order rate constants vs.  $[1-\text{C}_4\text{H}_8]$ .

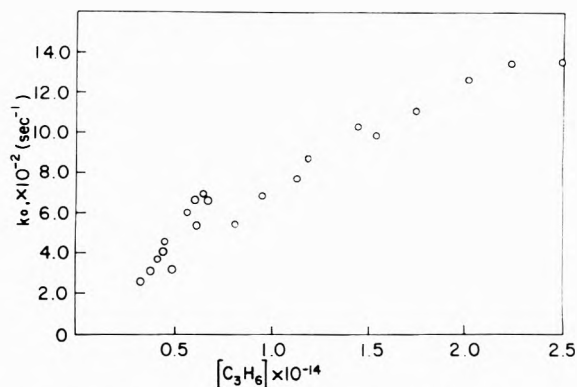


Figure 6. Pseudo first-order rate constants vs.  $[\text{C}_3\text{H}_6]$ .

$10^{13}$  molecules  $\text{cm}^{-3}$  and the 1-butene concentration was changed from  $1.2 \times 10^{13}$  to  $1.1 \times 10^{14}$  molecules  $\text{cm}^{-3}$ . In this case, due to the high rate,  $[\text{1-C}_4\text{H}_8]_0/[\text{OH}]_0 = 10$ , was the largest attainable ratio. The same conditions were used in the reaction with 2-butene. Also, the butene reactions were accompanied by a white solid which coated the reactor walls, and made light intensity measurements extremely difficult. With 2-butene this effect was so severe that reliable measurements were virtually impossible, and only an estimate of the rate constant was attempted. The dependence of the pseudo-first-order rate constants on olefin concentration was determined by plotting  $k_0$  vs. [olefin]. A linear dependence was found for ethylene and 1-butene as illustrated by Figures 4 and 5. Thus the kinetics in these two systems were second order, first order in OH and first order in olefin. The kinetic behavior with propylene was more complex, as illustrated by Figure 6.

### Kinetic Analysis

Figures 4–6 show that the first-order OH decay consists of two components, one proportional to olefin concentration and the other independent of olefin concentration. The differential rate expression required by the data is given by eq 9, where  $n$  is the stoichiometric coefficient of

$$-d[\text{OH}]/dt = 2k_2[\text{OH}]^2 + nk[\text{olefin}][\text{OH}] + k''[\text{OH}] \quad (9)$$

OH. The term which is second order in [OH] is included (see eq 7) since close examination of the ethylene data indicated the need to take reaction 2 into account. Inclusion of the second two terms on the right-hand side is consistent with the data as plotted in Figures 4 and 5. Equation 9 is also consistent with Figure 6, although only if  $n$  is variable. The intercept of each of these plots,  $k''$ , refers to first-order decay of OH which is independent of olefin concentration, and is due to reactions 5 and 6. In the cases of propylene and the two butenes the second-order term was negligible since  $2k_2[\text{OH}]_0/nk[\text{C}_3\text{H}_6] \leq 0.001$ . For 1-butene  $nk$  and  $k''$  were obtained from linear least-squares fit (eq 10) to the

$$\begin{aligned} -d[\text{OH}]/dt &= nk[\text{olefin}][\text{OH}] + k''[\text{OH}] \\ &= k_3[\text{OH}] \end{aligned} \quad (10)$$

data in Figure 5, while for propylene a linear least-squares fit was made to two regions of Figure 6. The data for lower  $[\text{C}_3\text{H}_6]$  and the data for higher  $[\text{C}_3\text{H}_6]$  were fit separately. The results are given in Table I.

For the case of ethylene, the bimolecular contribution was more significant and therefore eq 9 was used to obtain the rate constants. By using a known value of the bimolecular rate constant  $k_2$ , and assuming two unknown parameters,  $[\text{OH}]_0$  and  $k_0$ , the experimental data,  $[\text{OH}]_t$  against reaction time, was fitted by a non-linear least-squares computer program. In this situation the integrated concurrent first- and second-order rate expression may be written as

$$[\text{OH}]_t^{-1} = \{[\text{OH}]_0^{-1} + 2k_2/k_0\} \exp[k_0 t] - 2k_2/k_0$$

Three different values of  $k_2$  were tested in obtaining  $k_0$  and  $[\text{OH}]_0$  from this equation. These corresponded to three different values reported in the literature for the measured rate constant of the disproportionation reaction 2. They were  $2.57 \times 10^{-12}$  cc/molecule sec, recommended by Wilson,<sup>27</sup>  $1.40 \times 10^{-12}$  cc/molecule sec, presented by Kaufman and Del Greco,<sup>17</sup> and the value reported by Breen and Glass,<sup>28</sup>  $0.84 \times 10^{-12}$  cc/molecule sec. Although no very large differences were found, the value recommended by

TABLE I

Reaction	$nk$ , $\text{cm}^3 \text{ molecule}^{-1} \text{ sec}^{-1}$	$k''$ , $\text{sec}^{-1}$
$\text{OH} + \text{C}_2\text{H}_4$	$(2.31 \pm 0.13) \times 10^{-12}$	$45 \pm 26$
$\text{OH} + \text{C}_3\text{H}_6^a$	$(1.70 \pm 0.06) \times 10^{-11}$	
$\text{OH} + \text{C}_3\text{H}_6^b$	$(0.49 \pm 0.03) \times 10^{-11}$	$60 \pm 30^c$
$\text{OH} + \text{1-C}_4\text{H}_8$	$(1.53 \pm 0.05) \times 10^{-11}$	$109 \pm 30$
$\text{OH} + \text{trans-2-C}_4\text{H}_8$	$(1.2 \pm 1) \times 10^{-11}$	

<sup>a</sup> From linear least-squares fit to data with  $[\text{C}_3\text{H}_6]_0/[\text{OH}]_0$  between 1.5 and 2.1. <sup>b</sup> From linear least-squares fit to data with  $[\text{C}_3\text{H}_6]_0/[\text{OH}]_0$  between 5 and 30. <sup>c</sup> From Figure 6.

Wilson gave the smallest standard error of the measured experimental data, and therefore the results of  $k_0$  presented in this work for these particular reactions were computed using that value.

The difficulties inherent in having a two-parameter fit can be avoided by using  $[\text{OH}]_0$  as a constant parameter and then calculating the value of  $k_0$  using the same nonlinear computer technique for a given value of  $[\text{OH}]_0$ . Since  $[\text{OH}]_0$  could be calculated from the slope of Figure 2, we tested the effect of  $[\text{OH}]_0$  on the fitted value of  $k_0$ . Negligible change could be observed for a variation of 4 or more in the assumed value of  $[\text{OH}]_0$ .

The second-order rate coefficients obtained for each of the four olefins investigated are given in Table I, as are the value of  $k''$ . For propylene, the value of  $k''$  in Table I is only approximate, since it was obtained by extrapolating Figure 6 to the intercept. The contribution of reaction 5 to  $k''$  for each reaction was calculated from  $k'' = k_6 + k_5[\text{NO}_2][\text{He}]$ . The pseudo-first-order decay constant,  $k_5[\text{NO}_2][\text{H}] = 15 \text{ sec}^{-1}$  was obtained by using  $k_5 = 1 \times 10^{-30} \text{ cm}^6 \text{ molecule}^{-2} \text{ sec}^{-1}$ ,<sup>29</sup> and  $[\text{NO}_2] = 4 \times 10^{14} \text{ molecules cm}^{-3}$ .

**Surface Reactions.** Assuming that  $k_6 = k'' - 15 \text{ sec}^{-1}$ , the following values of  $k_6$  are computed:  $30 \text{ sec}^{-1}$  ( $\text{C}_2\text{H}_4$ );  $45 \text{ sec}^{-1}$  ( $\text{C}_3\text{H}_6$ );  $95 \text{ sec}^{-1}$  ( $\text{1-C}_4\text{H}_8$ ). In experiments without olefins, values of  $k_6$  were obtained by computer simulation of OH decay using reactions 1–6. With  $\text{NO}_2$  in excess of H,  $k_6 = 15 \text{ sec}^{-1}$  was obtained, while for H in excess of  $\text{NO}_2$ ,  $k_6 = 10 \pm 5 \text{ sec}^{-1}$  was obtained. The least-squares error limits of the intercepts of Figures 4–6 are sufficiently large that the determinations of  $k_6$  for  $\text{C}_2\text{H}_4$ ,  $\text{C}_3\text{H}_6$ , and the two cases without any olefin reactant cannot be considered to be significantly different from one another. Thus there is no evidence that  $\text{C}_2\text{H}_4$  and  $\text{C}_3\text{H}_6$  play any role in surface removal of OH, and there is no evidence that OH consumption via steps other than the overall olefin reaction plus (5) and (6) occur to a significant extent in the  $\text{C}_2\text{H}_4$  and  $\text{C}_3\text{H}_6$  systems. For 1-butene, the higher value of  $k_6$  may indicate that solids formation catalyzed surface removal of OH, or that other unknown OH reactions are occurring, but the former appears more likely. We wish to emphasize that the only reactions of OH contributing to  $nk$  are those that are proportional to [olefin], and since coverage of a Teflon surface by adsorbed olefins must be low, surface removal of OH by a reaction proportional to [olefin] is almost certainly negligible. Thus  $nk$  can be attributed to homogeneous reactions.

### Discussion

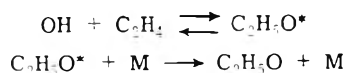
**Ethylene.** The rate constant reported here for  $\text{OH} + \text{C}_2\text{H}_4$ ,  $nk = (2.31 \pm 0.13) \times 10^{-12} \text{ cm}^3 \text{ molecule}^{-1} \text{ sec}^{-1}$ , is in good agreement with two other determinations, also by



discharge-flow methods. Morris, Stedman, and Niki<sup>8</sup> used mass spectrometric detection of OH to obtain  $nk = 2.5 \times 10^{-12} \text{ cm}^3 \text{ molecule}^{-1} \text{ sec}^{-1}$  in excess  $\text{C}_2\text{H}_4$ , while Bradley et al.<sup>9</sup> used electron spin resonance measurement of OH decay in excess (5.5- to 13.1-fold)  $\text{C}_2\text{H}_4$ . The latter authors measured stoichiometric coefficients,  $n$ , by mass spectrometry, and reported  $k = (1.7 \pm 0.5) \times 10^{-12} \text{ cm}^3 \text{ molecule}^{-1} \text{ sec}^{-1}$ . This is in excellent agreement with  $nk = 1.8 \times 10^{-12} \text{ cm}^3 \text{ molecule}^{-1} \text{ sec}^{-1}$  reported by Morris et al.<sup>8</sup> in OH-rich experiments, where they argued that  $n$  should be unity. The linearity of Figure 4 shows that  $n$  did not change detectably over about a tenfold variation of  $[\text{C}_2\text{H}_4]_0/[\text{OH}]_0$  in our experiments. This, together with the agreement of our rate constants with those from ref 8 and 9 suggests that the stoichiometric coefficient in our ethylene experiments is probably not much greater than unity, and that the results of discharge-flow experiments are independent of whether OH is produced by titrating H nearly to completion (ref 9), or to completion (ref 8) with  $\text{NO}_2$ , or whether excess  $\text{NO}_2$  is used.

Four other investigations have yielded somewhat higher rate constants. Wilson and Westenberg's<sup>7</sup> determination of  $nk = 5 \times 10^{-12} \text{ cm}^3 \text{ molecule}^{-1} \text{ sec}^{-1}$  by discharge-flow ESR is not necessarily in disagreement because  $n$  was not measured. Stuhl<sup>12</sup> reported  $k = (3 \pm 1) \times 10^{-12} \text{ cm}^3 \text{ molecule}^{-1} \text{ sec}^{-1}$  by resonance fluorescence of OH following flash photolysis of  $\text{H}_2\text{O}-\text{C}_2\text{H}_4$  mixtures. While the value is larger than reported here, the error limits overlap those from the other investigations discussed. Two other investigations, both by flash photolysis, report significantly larger values:  $k = 5 \times 10^{-12} \text{ cm}^3 \text{ molecule}^{-1} \text{ sec}^{-1}$ <sup>10</sup> and  $5.2 \times 10^{-12} \text{ cm}^3 \text{ molecule}^{-1} \text{ sec}^{-1}$ .<sup>11</sup> Photolysis of  $\text{H}_2\text{O}$ , used by Greiner<sup>10</sup> to generate OH, has been criticized because of likely complications resulting from the presence of  $\text{HO}_2$ .<sup>27</sup> Furthermore, Morris et al.<sup>8</sup> pointed out the possibility that OH reactions with the products of  $\text{C}_2\text{H}_4$  photolysis, which occurred at the short wavelengths used, could have influenced OH decay rates. Smith and Zellner<sup>11</sup> generated OH by both  $\text{H}_2\text{O}$  photolysis, and photolysis of  $\text{N}_2\text{O}-\text{H}_2$  mixtures, and obtained results in excellent agreement via the two techniques. Photolysis of  $\text{C}_2\text{H}_4$  could not have occurred since  $\text{C}_2\text{H}_4$  was used as a light filter, and the authors found no evidence for secondary reactions of OH. However, H atoms were produced in the OH generation reactions. While not suggesting that H atoms were a complicating factor in the flash work, we have noticed that H atoms accelerate OH decay in the presence of olefins in discharge-flow experiments.

A more likely reason for the observed differences lies in the effect of pressure. Although the total pressures at which the flash photolysis work was done is not given in ref 10 or 11, they are almost certainly larger than the 1 Torr prevalent in discharge-flow experiments. Thus if the reverse of the association reaction



could compete with collisional deactivation at 1 Torr the lower rate constants from discharge-flow work would be explained. In fact, Morris et al.<sup>8</sup> observed (mass spectrometrically) enhancement of the peak at  $m/e$  corresponding to  $\text{C}_2\text{H}_5\text{O}^*$  when the pressure was increased from 1 to 4 Torr.

*Propylene.* Assuming eq 11, where  $p$  is the order of the

$$k_0 = nk[\text{C}_3\text{H}_6]^p + k'' \quad (11)$$

reaction with respect to propylene, the curvature of Figure 6 can be attributed either to  $p$  or to changing values of  $n$ . Taking the logarithm of eq 11 yields

$$\log k_0 = \log k'' + \log nk + p \log [\text{C}_3\text{H}_6] \quad (12)$$

A plot of  $\log k_0$  vs.  $\log [\text{C}_3\text{H}_6]$  was linear with a slope of 1 plus or minus about 10%. Thus the curvature of Figure 5 could be ascribed to variation of  $n$ . A surface reaction which is dependent upon  $[\text{C}_3\text{H}_6]$  cannot explain the curvature of Figure 6, because then the rate of first-order decay, i.e.,  $k_0$  would exhibit a curve of monotonically increasing slope, rather than the observed decreasing slope. A tangent to the curve of Figure 6 at larger  $[\text{C}_3\text{H}_6]$  has a lower slope than at a lesser  $[\text{C}_3\text{H}_6]$ , showing that  $n$  decreases with increasing  $[\text{C}_3\text{H}_6]$  as expected. Data taken at lower values of  $[\text{C}_3\text{H}_6]$ , where  $[\text{C}_3\text{H}_6]_0/[\text{OH}]_0$  is in the range 2-4, could be approximated by a straight line yielding  $nk = 1.7 \times 10^{-11} \text{ cm}^3 \text{ molecule}^{-1} \text{ sec}^{-1}$ . These conditions of  $[\text{C}_3\text{H}_6]_0/[\text{OH}]_0$  are similar to those reported by Morris, Stedman, and Niki,<sup>8</sup> who obtained  $nk = 5 \times 10^{-11} \text{ cm}^3 \text{ molecule}^{-1} \text{ sec}^{-1}$ . The difference in rate constants may be related to the effect of  $n$  of the different initial concentrations used in the two investigations. The slope of the best straight line through the data shown in Figure 6 at larger  $[\text{C}_3\text{H}_6]_0$ , where  $[\text{C}_3\text{H}_6]_0/[\text{OH}]_0$  was as large as 34, yielded  $nk = 5.0 \times 10^{-12} \text{ cm}^3 \text{ molecule}^{-1} \text{ sec}^{-1}$ . This is a factor of 3 smaller than the rate constant recently reported by Stuhl,<sup>12</sup>  $k = (1.45 \pm 0.22) \times 10^{-11} \text{ cm}^3 \text{ molecule}^{-1} \text{ sec}^{-1}$ , but in excellent agreement with  $k = (5 \pm 2) \times 10^{-12} \text{ cm}^3 \text{ molecule}^{-1} \text{ sec}^{-1}$  reported by Bradley et al.<sup>9</sup> Some of the discrepancy between ref 12 and this work and ref 9 may lie in the formation of a chemically activated adduct, as suggested above for ethylene, although it would have to be a smaller effect for the larger propylene molecule.

The propensity of the OH plus  $\text{C}_3\text{H}_6$  system toward secondary reactions is clearly illustrated by Figure 6. Thus work done at low  $[\text{C}_3\text{H}_6]/[\text{OH}]$  ratios must be regarded with caution, and the occurrence of secondary reactions may account for some of the discrepancies in reported rate coefficients. Our data at higher  $[\text{C}_3\text{H}_6]/[\text{OH}]$ , while probably not entirely free of secondary reactions, must be less so than at lower  $[\text{C}_3\text{H}_6]/[\text{OH}]$ . The value  $5 \times 10^{-12} \text{ cm}^3 \text{ molecule}^{-1} \text{ sec}^{-1}$ , which is smaller than all but one of those previously reported, is consistent with the idea that secondary reactions are relatively unimportant at the highest  $[\text{C}_3\text{H}_6]/[\text{OH}]_0$  attained in this work, and that the present value of  $nk$  may be reasonably close to  $k$  for  $\text{C}_3\text{H}_6$ .

*Effect of  $\text{NO}_2$ .* One aspect of this work which sets it apart from earlier discharge-flow investigations of OH-olefin reactions is the excess of  $\text{NO}_2$  over H. The rate of (1) is therefore accelerated sufficiently that H is reduced to a negligible amount within 1 cm of the  $\text{NO}_2$  inlet, and olefin can be introduced before significant OH decay occurs, thus suppressing O production via (2). In this way possible complications due to O and H reactions are minimized. These species, and particularly O, would introduce radicals and other reactive intermediates following facile addition to the olefin. Furthermore, there is evidence that excess  $\text{NO}_2$  has negligible effect on the reactions being studied. First, a threefold variation of  $[\text{NO}_2]_0$  did not cause any change of  $nk$  for  $\text{C}_2\text{H}_4$ . Second, a recent determination of the rate coefficient for reaction of OH with  $\text{C}_2\text{H}_2$ ,<sup>30</sup> using this technique, yielded a value in good agreement with a discharge-flow determination<sup>31</sup> where  $\text{NO}_2$  was not in excess. Third, the rate coefficients for OH with  $\text{C}_2\text{H}_4$  are in good agree-

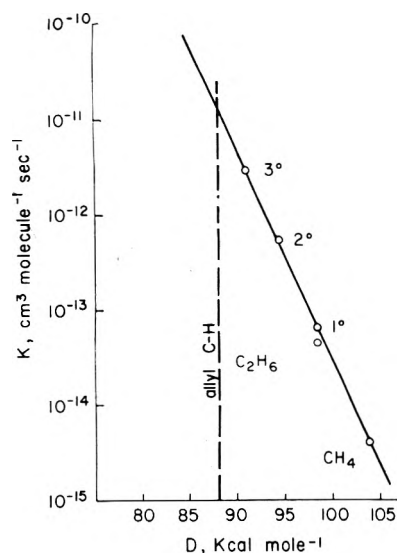


**Figure 7.** Per bond rate constants for H-atom transfer to OH, vs. bond dissociation energy,  $D$ , in alkanes: 1°, 2°, and 3° refer to primary, secondary, and tertiary C-H, respectively.

ment with the two other discharge flow determinations where  $\text{NO}_2$  was not in excess.<sup>8,9</sup>

**Mechanism.** Greiner first suggested that the reaction between hydroxyl and ethylene was an addition to the double bond.<sup>32</sup> Morris, Stedman, and Niki,<sup>8</sup> by mass spectrometry, later detected signals at  $m/e$  values corresponding to adduct species in both the ethylene and propylene reactions with hydroxyl. In the ethylene case a comparison of the observed rate constant with the rate constant for H abstraction by OH from methane, which is more than 100 times smaller<sup>27</sup> and has a bond dissociation energy of 104 kcal/mol, compared with 103 kcal/mol for vinyl C-H in ethylene, makes it almost certain that addition occurs to the virtual exclusion of abstraction. Propylene and the butenes contain relatively weak (88 kcal/mol) allyl C-H bonds, which might allow abstraction to compete with addition.

Hydroxyl radicals abstract H atoms from alkanes with increasing facility with decreasing dissociation energy of the attacked bond. Reliable data are available for  $\text{H}_2$ ,  $\text{CH}_4$ , and  $\text{C}_2\text{H}_6$ .<sup>27</sup> In addition, Greiner<sup>33</sup> has studied a number of alkanes, and has suggested an additivity principle, summarized by the expression

$$k = 6.5 \times 10^{11} N_p \exp(-820/T) + 14.1 \times 10^{11} N_s \exp(-425/T) + 12.6 \times 10^{11} N_t \exp(+85/T) \text{ cm}^3 \text{ mol}^{-1} \text{ sec}^{-1} \quad (13)$$

where  $N_p$ ,  $N_s$ , and  $N_t$  are the number of primary, secondary, and tertiary C-H bonds in a given alkane, respectively. We plotted  $\log k$ , per C-H bond, obtained from the available data on  $\text{CH}_4$  and  $\text{C}_2\text{H}_6$ , and from eq 13, vs. bond

dissociation energy, Figure 7. The plot is remarkably linear, extrapolating to about  $5 \times 10^{-11} \text{ cm}^3 \text{ molecule}^{-1} \text{ sec}^{-1}$  at a bond dissociation energy of 88 kcal/mol. We do not claim this as an accurate value for abstraction of H from the allyl position of an olefin by hydroxyl, since the preexponential factor for H abstraction from an olefin should differ from that for H abstraction from an alkane, but only wish to illustrate that such an abstraction may occur with appreciable rate. The bond dissociation energy correlation predicts a rate constant which is larger than the observed values for either propylene or 1-butene. This may be a reflection of the activation energies used in eq 13, which were suggested to be slightly low in a recent review.<sup>27</sup> Nevertheless, the possibility that abstraction may occur competitively with addition in propylene and higher alkanes should be considered.

**Acknowledgment.** The authors thank Professor Robert Collins for assistance with the optical arrangement.

## References and Notes

- (1) Supported by the U.S. Atomic Energy Commission. This is AEC Document No. C00-2026-15.
- (2) P. A. Leighton, "The Photochemistry of Air Pollution", Academic Press, New York, N.Y., 1961.
- (3) D. H. Stedman, E. D. Morris, Jr., E. E. Daby, H. Niki, and B. Weinstock, presented at the 160th National Meeting of the American Chemical Society, Chicago, Ill., Sept 1970, Abstract WATR No. 26.
- (4) B. Weinstock, E. E. Daby, and H. Niki, "Chemical Reactions in Urban Atmospheres", C. S. Tuesday, Ed., American Elsevier, New York, N.Y., 1971, p. 54.
- (5) J. Heicklen, K. Westberg, and N. Cohen in ref 4, p. 55.
- (6) H. Niki, E. E. Daby, and B. Weinstock, *Adv. Chem. Ser.*, **No. 113**, 16 (1972).
- (7) W. E. Wilson, Jr., and A. Westenberg, *Symp. (Int.) Combust.*, [Proc.], **11th**, 1967, 1143 (1968).
- (8) E. D. Morris, Jr., D. H. Stedman, and H. Niki, *J. Am. Chem. Soc.*, **93**, 3570 (1971).
- (9) J. N. Bradley, W. Hack, K. Hogermann, and H. G. G. Wagner, *J. Chem. Soc., Faraday Trans. 1*, **69**, 1889 (1973).
- (10) N. R. Greiner, *J. Chem. Phys.*, **53**, 1284 (1970).
- (11) I. W. M. Smith and R. Zellner, *J. Chem. Soc., Faraday Trans. 2*, **69**, 1617 (1973).
- (12) F. Stuhl, XI. International Symposium on Free Radicals, Berchtesgaden-Kongress, 1973, Preprint No. 34.
- (13) R. Simonaitis and J. Heicklen, *Int. J. Chem. Kinet.*, **5**, 231 (1973).
- (14) F. C. Fehsenfeld, K. M. Evenson, and H. P. Broida, *Natl. Bur. Stand. Rep.*, **No. 8701** (1964).
- (15) P. Harteck, R. R. Reeves, and G. Manella, *J. Chem. Phys.*, **29**, 133 (1958).
- (16) W. Brennen and R. L. Brown, *Rev. Sci. Instrum.*, **39**, 608 (1968).
- (17) K. Kaufman and F. P. Del Greco, *Symp. (Int.) Combust.*, [Proc.], **9th**, 1963, 659 (1964).
- (18) L. F. Phillips and H. I. Schiff, *J. Chem. Phys.*, **37**, 1233 (1962).
- (19) D. Herriott, H. Kogelnik, and R. Kompfner, *Appl. Opt.*, **3**, 523 (1963).
- (20) I. G. Mitchell and M. W. Zemansky, "Resonance Radiation and Excited Atoms", Cambridge University Press, New York, N.Y., 1961.
- (21) R. V. Poirier, Ph.D. Thesis, University of Minnesota, 1970.
- (22) R. V. Poirier and R. W. Carr, Jr., *J. Phys. Chem.*, **75**, 1593 (1971).
- (23) Marrero and E. A. Mason, *J. Phys. Chem. Ref. Data*, **1**, 3 (1972).
- (24) A. V. Pastrana, Ph.D. Thesis, University of Minnesota, 1973.
- (25) A. A. Westenberg and N. de Haas, *J. Chem. Phys.*, **58**, 4066 (1973).
- (26) A. McKenzie, M. F. R. Mulcahy, and J. R. Steven, *J. Chem. Phys.*, **59**, 3244 (1973).
- (27) W. E. Wilson, Jr., *J. Phys. Chem. Ref. Data*, **1**, 535 (1972).
- (28) J. E. Breen and G. P. Glass, *J. Chem. Phys.*, **52**, 1082 (1970).
- (29) J. G. Anderson and F. Kaufman, *Chem. Phys. Lett.*, **16**, 375 (1972).
- (30) A. V. Pastrana and R. W. Carr, Jr., *Int. J. Chem. Kinet.*, in press.
- (31) J. E. Breen and G. P. Glass, *Int. J. Chem. Kinet.*, **3**, 145 (1970).
- (32) N. R. Greiner, *J. Chem. Phys.*, **53**, 1284 (1970).
- (33) N. R. Greiner, *J. Chem. Phys.*, **53**, 1070 (1970).

## Photolysis of Hydrogen Selenide

D. C. Dobson, F. C. James, I. Safarik, H. E. Gunning, and O. P. Strausz\*

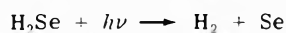
Department of Chemistry, University of Alberta, Edmonton, Alberta, Canada

(Received May 20, 1974; Revised Manuscript Received December 2, 1974)

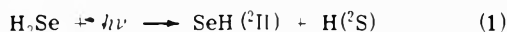
Publication costs assisted by the National Research Council of Canada

The photochemical decomposition of hydrogen selenide has been studied by flash photolysis-kinetic spectroscopy, ESR spectroscopy, and continuous photolysis techniques. From the combined results including those obtained in scavenging experiments with added ethylene, it was concluded that the only primary step operative in the  $\lambda > 200.0$  nm photolysis is the free-radical mode of decomposition,  $\text{H}_2\text{Se} + h\nu \rightarrow \text{H} + \text{SeH}$ , with a quantum efficiency of unity. The intermediacy of H and SeH in the reaction, and the presence of Se and  $\text{Se}_2$  originating from the secondary reactions of the SeH radical under flash conditions, has been demonstrated by spectroscopic means. The SeH radicals decay largely by the cisproportionation reaction  $2\text{SeH} \rightarrow \text{H}_2\text{Se} + \text{Se}({}^3\text{P})$ . The rate constant for the abstraction reaction,  $\text{H} + \text{H}_2\text{Se} \rightarrow \text{H}_2 + \text{SeH}$  has been determined in competition with the  $\text{H} + \text{C}_2\text{H}_4 \rightarrow \text{C}_2\text{H}_5$  reaction to have the value of  $(7.1 \pm 2.0) \times 10^{12} \text{ cm}^3 \text{ mol}^{-1} \text{ sec}^{-1}$ .

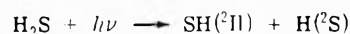
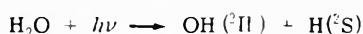
The photolysis of hydrogen selenide has received little attention compared with studies on the photolysis of water and hydrogen sulfide. An early study<sup>1</sup> using a mercury arc lamp, and tungsten-steel and aluminum spark lamps identified the primary photolytic step as decomposition into molecular hydrogen and selenium atoms



This contrasts with the anticipated primary decomposition



which is analogous to the well-established free-radical mode of decomposition of both water<sup>2,3</sup> and hydrogen sulfide:<sup>4,5</sup>



The presence of  $\text{OH}^6$  and  $\text{SH}^{4,7}$  radicals in the  $\text{H}_2\text{O}$  and  $\text{H}_2\text{S}$  systems has been detected by flash spectroscopy. Porter<sup>4</sup> looked for the SeH radical in flash photolyzed hydrogen selenide and attributed the failure to detect this species to either the predissociative nature of the  $0,0$  transition of the  $\text{A}^3\Sigma - \text{X}^2\Pi$  system, or to the chemical reactivity of the radical. Later Radford,<sup>8</sup> and more recently Carrington,<sup>9</sup> succeeded in obtaining the ESR spectrum of SeH. As the experimental part of this work was near completion,<sup>10</sup> Lindgren<sup>11</sup> reported the observation of the SeH radical as a weak diffuse spectrum in the region 300.0–325.0 nm following the flash photolysis of  $\text{H}_2\text{Se}$ . More recently Donovan et al.<sup>12</sup> have reported the observation of strong Rydberg bands of SeH in the vacuum uv.

The present study was undertaken to elucidate the nature of the primary step in the photodecomposition of the hydrogen selenide molecule, to obtain spectral information on the SeH radical, and to gain an insight into the chemistry of SeH radicals. The present article describes the primary processes while the rates of recombination of the transient SeH, Se, and  $\text{Se}_2$  species and the spectrum of the SeH radical will be reported in forthcoming communications.

### Experimental Section

**Flash Photolysis.** The uv flash photolysis apparatus used was similar in design to that described in earlier articles from this laboratory.<sup>13</sup>

Continuous time-absorption records for specific wavelengths were obtained by replacing the spectroscopic lamp with a 450-W xenon arc lamp and the photographic plate with a photomultiplier (EMI-6265B) slit combination. The 18,0 band of the  $\text{B}^3\Sigma_u^- - \text{X}^3\Sigma_g^-$  system of  $\text{Se}_2$  at 334.0 nm<sup>14</sup> was monitored in these experiments.

The far-uv spectra were obtained in a flash apparatus incorporating a 0.5-m Jarell Ash (Type 78-650) Seya Namioka vacuum monochromator in which spectra were recorded photographically.

The pressures of  $\text{H}_2\text{Se}$  and inert gases used in the flash experiments were in the ranges 0.05–1 and 50–350 Torr, respectively.

**Electron Spin Resonance Experiments.** ESR spectra were obtained in a Varian V4502 spectrometer. Photolyses were conducted in situ at 77 K in the cavity using an Osram high-pressure mercury arc and Vycor 7910 and Pyrex filters.

**Continuous Photolysis Experiments.** A medium-pressure mercury lamp (Hanovia) and a cadmium resonance lamp (Osram) were used to irradiate a quartz cell 10 cm long and 5 cm in diameter. Pyrex and Vycor 7910 filters could be interposed between the lamp and the air-cooled face of the cell. An interference filter was used to isolate the 228.8-nm resonance line of cadmium used for quantum yield measurements. Carbonyl sulfide was used as an actinometric gas ( $\phi_{\text{CO}}$  from  $\text{COS} = 1.8$  at  $\lambda$  228.8 nm and  $\lambda$  253.7 nm),<sup>15</sup> and the pressures of hydrogen selenide used were such that total absorption occurred within the cell (above ca. 100 Torr). Yields of noncondensable products of photolysis were measured with a gas burette and analyzed by gas chromatography using a 10-ft. molecular sieve 13X column.

**Materials.**  $\text{H}_2\text{Se}$  and  $\text{D}_2\text{Se}$  (Matheson 98.0 and 99.8%, respectively),  $\text{SF}_6$  (Matheson 98%), and  $\text{CO}_2$  (Matheson 99.8% "bone dry") were purified by distillation in vacuo and degassed before use.  $\text{C}_2\text{H}_4$  (Phillips 99.99%) was passed through traps at 77 K.  $\text{COS}$  (Matheson 97.5%) was purified by a method previously described.<sup>15</sup> Tank  $\text{N}_2$  (Union Car-

**TABLE I: Hydrogen Yield in the Flash Photolysis of Hydrogen Selenide**

Pressure, Torr		Diluent	Yield of H <sub>2</sub> , μmol/flash
H <sub>2</sub> Se	Total		
0.53	53	SF <sub>6</sub>	3.01
0.54	162	SF <sub>6</sub>	3.70
0.55	176	SF <sub>6</sub>	3.54
0.46	276	SF <sub>6</sub>	3.34
0.98	98	CO <sub>2</sub>	5.91
0.81	244	CO <sub>2</sub>	6.00
1.29	129	C <sub>2</sub> H <sub>4</sub>	0.28
0.98	98	CO <sub>2</sub>	5.91
0.94	94	SF <sub>6</sub>	6.90

bide Canada Ltd. 99.993%) and He (Canadian Liquid Air Co. 99.999%) were used without further purification.

## Results

The absorption spectroscopic experiments showed the presence of the following intermediates in flash photolyzed mixtures: Se<sub>2</sub>, Se, and SeH. The most prominent feature of the uv spectrum was the Se<sub>2</sub>(B<sup>3</sup>Σ<sub>u</sub><sup>-</sup>) - (X<sup>3</sup>Σ<sub>g</sub><sup>-</sup>) band system.<sup>14</sup> Bands at λ 300.0, 310.0, and 322.0 nm, attributed to the A<sup>2</sup>Σ<sup>+</sup> - X<sup>2</sup>Π system of SeH,<sup>11</sup> were seen only at short delay times. Absorption by H<sub>2</sub>Se, and after photolysis, reduction of the overall transmission by solid deposits, prevented studies at wavelengths below 250 nm in the uv experiments. The resonance lines of Se(<sup>3</sup>P<sub>J</sub>) were observed in the vacuum uv at 206.3, 204.0, and 196.1 nm, corresponding to J = 0, 1, and 2, respectively.<sup>16</sup> A careful search for <sup>1</sup>D<sub>2</sub> and <sup>1</sup>S<sub>0</sub> state selenium atoms which absorb at 188.5 nm and at 199.5 nm, respectively,<sup>16</sup> with transition probabilities comparable to that of Se(5<sup>3</sup>S<sub>1</sub>) ← (4<sup>3</sup>P<sub>2</sub>),<sup>17</sup> indicated the absence of these species. SeH and Se<sub>2</sub> were also observed in the vacuum uv region, the SeH at 179.0 nm<sup>12</sup> corresponding to the C<sub>1</sub> ← X<sup>3</sup>Π<sub>3/2</sub> transition and Se<sub>2</sub>(<sup>3</sup>Σ<sub>g</sub><sup>-</sup>) as the C ← X and D ← X band systems.<sup>18</sup>

The concentration of Se<sub>2</sub> rapidly rose to a maximum and subsequently decayed by second-order kinetics in the presence of He, N<sub>2</sub>, or CO<sub>2</sub> as inert diluents. With SF<sub>6</sub> as diluent the decay was complex; nevertheless the amounts of H<sub>2</sub> per flash formed were independent of the nature of diluent gas used, Table I. Ethylene when used as diluent exhibited a strong suppressing effect on both Se<sub>2</sub>(X<sup>3</sup>Σ<sub>g</sub><sup>-</sup>) and the hydrogen product.

The most important feature of the Se(<sup>3</sup>P<sub>J</sub>) spectrum was that it appeared weakly at zero delay time and its rate of growth was intermediate between that of SeH and Se<sub>2</sub>. In the presence of added ethylene the spectrum of ethylene episelenide could be seen.<sup>19</sup> This molecule is known to form from the addition of selenium atoms to ethylene.<sup>20</sup>

When H<sub>2</sub>Se was photolyzed in an ice matrix at 77 K the two-line proton spectrum with a splitting of 505 G appeared.<sup>21</sup> In similar experiments with D<sub>2</sub>Se the three-line deuterium spectrum with a splitting of 77 G was observed. The ESR spectrum with a g value of 0.808 attributed by Radford<sup>8</sup> to the gaseous SeH radical could not, of course, be detected under these conditions.

The kinetics of H<sub>2</sub> formation was studied quantitatively in continuous photolysis experiments. A plot of the quantum yield of hydrogen formation as a function of hydrogen selenide pressure is shown in Figure 1. The value of Φ(H<sub>2</sub>) is 1.0 ± 0.05 in the pressure range, 200–800 Torr, studied.

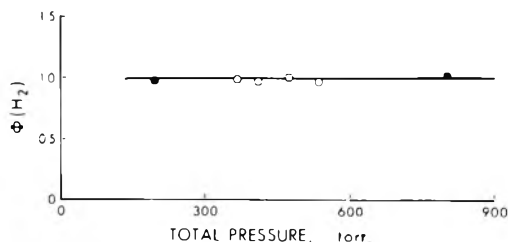


**Figure 1.** Plot of the quantum yield of hydrogen production as a function of H<sub>2</sub>Se pressure in the photolysis of pure H<sub>2</sub>Se (open circles) and with added SF<sub>6</sub> (filled circles).

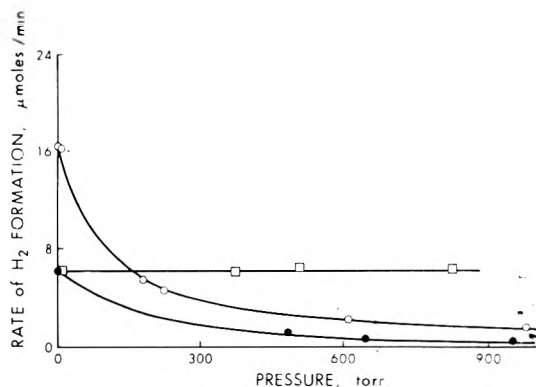


**Figure 2.** Variation of the rate of hydrogen production in the photolysis of H<sub>2</sub>Se with the pressure of added ethylene and sulfur hexafluoride: 10 Torr of H<sub>2</sub>Se + C<sub>2</sub>H<sub>4</sub> no filter (open circles); as above but with a Vycor 7910 filter (filled circles); 10 Torr of H<sub>2</sub>Se + SF<sub>6</sub> with a Vycor 7910 filter (squares). Photolysis by medium-pressure mercury lamp (Hanovia).

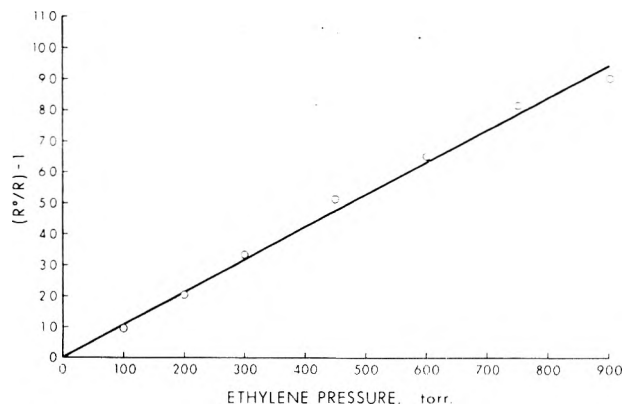
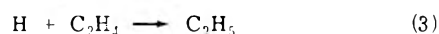
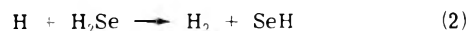


**Figure 3.** Plot of  $[R^0(\text{H}_2)/R(\text{H}_2)] - 1$  vs. ethylene pressure (eq 1).

Ethylene was used to scavenge atomic hydrogen and any radical species present. The suppressing effect of ethylene on the yield of hydrogen is shown in Figure 2. This suppression is evidently due to the competing reaction of ethylene with hydrogen selenide for H atoms:



Steady-state treatment of the two reactions leads to the rate expression

$$[R^0(\text{H}_2)/R(\text{H}_2)] - 1 = (k_3/k_2)([\text{C}_2\text{H}_4]/[\text{H}_2\text{Se}]) \quad (1)$$

where  $R^0(\text{H}_2)$  and  $R(\text{H}_2)$  are the rates of hydrogen production in the absence and presence of ethylene, respectively.

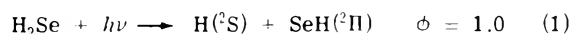
Plotting the left-hand side of (I) against ethylene pressure (at a fixed pressure of 10 Torr of H<sub>2</sub>Se) a straight line relation is obtained, Figure 3, as predicted.

From the slope,  $k_3/k_2$  equals  $0.105 \pm 0.01$ . The value of  $k_3$  is uncertain although a recent review article<sup>22</sup> includes most high-pressure values in the range  $(7.5 \pm 1.0) \times 10^{11} \text{ cm}^3 \text{ mol}^{-1} \text{ sec}^{-1}$ . Using this average value of  $k_3$  we obtain  $k_2 = (7.1 \pm 2.0) \times 10^{12} \text{ cm}^3 \text{ mol}^{-1} \text{ sec}^{-1}$ . Thus, it appears that all the hydrogen produced in the reaction is scavengable with ethylene, but because of the high value of  $k_2$  a more substantial excess of ethylene than was used here would be required for the complete suppression of hydrogen. The  $k_3/k_2$  ratio does not seem to be affected by the wavelength of the photolysis. Figure 2 also illustrates that the diluent gas SF<sub>6</sub> has no effect on the quantum yield of hydrogen, indicating that the hydrogen producing sequence does not involve an intermediate species that can be collisionally deactivated.

### Discussion

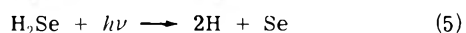
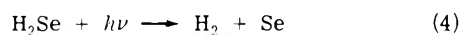
The electronic absorption spectrum of H<sub>2</sub>Se consists of a continuum from 340.0 nm to below 190.0 nm ( $\epsilon_{\text{max}} 1.5 \times 10^3 \text{ M}^{-1} \text{ cm}^{-1}$  at 215.0 nm),<sup>1</sup> with strong discrete bands starting in the vacuum uv at 169.0 nm.<sup>23</sup> Weak vibrational structure in the 250.0-nm absorption region of H<sub>2</sub>S indicates that the lowest excited state of H<sub>2</sub>S is nominally a Rydberg state. Although no fine structure has been detected in the 340–190-nm region of H<sub>2</sub>Se, it has been suggested that this absorption also corresponds to excitation to a Rydberg state.<sup>23</sup>

The only primary step which is consistent with the pressure independent unit efficiency of hydrogen production, the suppressing effect of added ethylene, the appearance of the intense spectrum of SeH, even at short delay times, and the ESR spectrum of H, is the free radical mode of decomposition



Using a value of 76 kcal mol<sup>-1</sup> for the HSe–H bond dissociation energy,<sup>25</sup> the threshold for reaction 1 is at ~380.0 nm.

Of the two alternative primary steps



neither can be important; the former on account of the suppressing effect of added ethylene on the yield of hydrogen, and the latter on energetic grounds. Step 5 is endothermic by 146 kcal mol<sup>-1</sup> and would become feasible only at wavelengths below 197.0 nm.

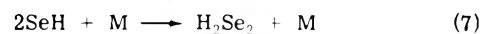
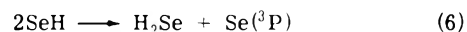
This photobehavior of H<sub>2</sub>Se may be compared to that of H<sub>2</sub>O and H<sub>2</sub>S both of which undergo primary decompositions analogous to step 1 in their first absorption region,<sup>28,29</sup> although molecular hydrogen production has been observed on photolysis of hydrogen sulfide at  $\lambda < 200.0 \text{ nm}$ .<sup>30</sup>

In continuous photolysis where the H<sub>2</sub>Se concentration is sufficiently high, step 1 is followed by the hydrogen abstraction reaction

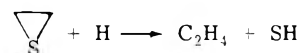


From the measured high value of the rate constant of this reaction it may be estimated that the H<sub>2</sub>Se pressure required for complete scavenging of H atoms would only be a few Torr. Thus, in the continuous photolysis experiments,

Figure 1, the quantum yield of SeH formation should be two and subsequent decay should take place without the release of additional hydrogen. The choice for the decay mode is then entirely analogous to that of SH decay

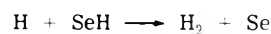


Hydrogen diselenide has been described as a comparatively stable molecule, volatile at room temperature.<sup>31</sup> Since no reaction product that could be ascribed to hydrogen diselenide was found, and as elemental selenium formation was observed, one must conclude that the principal mode of decay is via (6). This conclusion then makes the analogy between the H<sub>2</sub>S and H<sub>2</sub>Se photochemical systems complete in that the dominant mode of disproportionation of the SH radical has been shown to be  $2\text{SH} \rightarrow \text{H}_2\text{S} + \text{S}(\text{}^3\text{P})$ <sup>29,30</sup> resulting in a quantum yield of unity for hydrogen formation in conventional photolysis systems. The hydrogen sulfide yield from the disproportionation of SH has been shown to be less than unity; in the

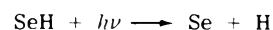


system, for example, a value of 0.41 has been obtained.<sup>32</sup> The loss has been ascribed<sup>33</sup> to the cross combination and disproportionation reactions of SH with the S<sub>2-7</sub> and HS<sub>2-8</sub> radicals present in the system. It is plausible and quite likely that similar reactions occur in the SeH systems.

The likely occurrence of reaction 6 is also in line with the observation of Se(<sup>3</sup>P<sub>*J*</sub>) and Se<sub>2</sub>(X<sup>3</sup>Σ<sub>*g*</sub><sup>-</sup>) spectra in the flash photolysis experiments, although under flash conditions the conversions were usually high ([H<sub>2</sub>Se] ~ [SeH]<sub>max</sub>), and consequently a contribution to Se(<sup>3</sup>P<sub>*J*</sub>) formation from other reactions such as

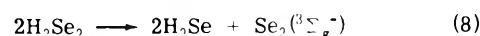


and



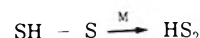
cannot be excluded.

It should also be noted that H<sub>2</sub>Se<sub>2</sub>, though not found as a stable product, could be detected in small quantities in flashed H<sub>2</sub>Se by kinetic mass spectrometry.<sup>27</sup> The H<sub>2</sub>Se<sub>2</sub>, if formed, would probably follow a route similar to the decomposition of the sulfur analog H<sub>2</sub>S<sub>2</sub> where sulfur and H<sub>2</sub>S are produced in the reaction but not hydrogen. A possible reaction might be



Experiments with a Pyrex filter limited the photolysis of H<sub>2</sub>Se to the tail end of the absorption region, 280–340 nm, and resulted in a small percentage decomposition (<1%).

In the flash photolysis of hydrogen sulfide the spectrum of the HS<sub>2</sub> radical has been detected.<sup>4,7</sup> The radical arises via the combination reaction



and/or the disproportionation  $\text{SH} + \text{S}_{3-7} \rightarrow \text{HS}_2 + \text{S}_{2-6}$ .<sup>34</sup> In the flash photolysis of hydrogen selenide no spectrum that could be assigned to the HSe<sub>2</sub> radical was discernible, although this may be due to unfavourable spectral characteristics or too short a lifetime.

Thus, the reaction sequence in high-pressure (200–800 Torr) conventional photolysis can be adequately described by the following elementary steps:

**TABLE II: Input Parameters Used in the Bond-Energy-Bond-Order Calculations**

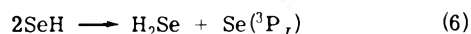
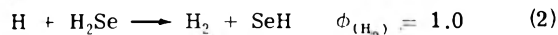
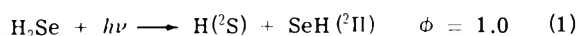
	Bond			Morse parameter, A
	Energy, kcal <sup>a</sup>	Distance, Å	Energy index	
H-H	109.4	0.74	1.041	
HO-H	124.3	0.96	1.036	2.19
HS-H	92.8	1.35	0.936	1.83
HSe-H	76.2-79.2 <sup>b</sup>	1.46	0.887	1.79

<sup>a</sup> Zero point energy included. <sup>b</sup> Preferred value, calculated from a spectroscopic value of  $D(\text{Se-H}) = 70 \text{ kcal mol}^{-1}$  and  $D(\text{HSe-H}) = 76 \text{ kcal mol}^{-1}$ .<sup>26,27</sup>

**TABLE III: Activation Energies for Hydrogen Abstraction by Hydrogen Atoms from the Group VI Hydrides**

	$E_a, \text{ kcal mol}^{-1}$		Ref
	Calcd	Exptl	
H + H <sub>2</sub> O	18.6	21.0	36
H + D <sub>2</sub> O	18.6	20.9	37
H + H <sub>2</sub> S	2.6	1.7	29
H + D <sub>2</sub> S	2.6	5.0	37, 38
H + H <sub>2</sub> Se	1.1-1.4 <sup>a</sup>	~1.5	This work

<sup>a</sup> Based on the preferred value of  $D(\text{HSe-H}) = 79.2 \text{ kcal mol}^{-1}$  which includes the zero point energy.



followed by the self- and cross-combination and disproportionation reactions of the SeH, Se, and Se<sub>2</sub> radicals. These latter processes, however, do not yield hydrogen. The selenium atoms from (6) can only be formed in their ground state for energetic reasons.

Abstraction reaction 2 is very rapid, its rate constant is 9.5 times larger than that for addition to ethylene. The H atoms probably carry a substantial excess of translational energy, since primary step 1 is exothermic in the entire absorption region, 190-340 nm. In the photolysis of H<sub>2</sub>O<sup>6</sup> and H<sub>2</sub>S<sup>29,35</sup> it has been shown that nearly all the initial excess electronic energy of the system is converted into kinetic energy. If this is the case for H<sub>2</sub>Se, as is likely, essentially all the estimated excess energy, about 40 kcal mol<sup>-1</sup> at 253.7 nm, would appear as the excess translational energy of the hydrogen atoms. This excess translational energy would preferentially increase the reactivity of the hydrogen atoms for the reaction having the higher activation energy, and would cause the yield of H<sub>2</sub> to deviate from the values predicted by eq 1. The fact that eq 1 is obeyed (Figure 3) suggests that the activation energy of abstraction reaction 2 is approximately equal to the activation energy of the addition reaction 3, that is ~1.5 kcal mol<sup>-1</sup>.<sup>22</sup> This value for  $E_a$  is consistent with the value of 1.7 kcal mol<sup>-1</sup> reported for abstraction from H<sub>2</sub>S,<sup>30</sup> since  $D(\text{HS-H})$  is about 13-14 kcal mol<sup>-1</sup> higher than  $D(\text{HSe-H})$ .

In order to compare this value of the activation energy with that predicted by the bond-energy-bond-order

(BEBO) method<sup>36</sup> a calculation was carried out for the H + H<sub>2</sub>Se as well as the H + H<sub>2</sub>O and H + H<sub>2</sub>S systems. The input parameters used in the calculations are compiled in Table II. Bond energy indices and the Morse parameters were obtained by utilizing the formulae  $p = [0.26 \ln (E/E_x)]/(R_x - R)$ , and  $\beta = 1.2177 \times 10^7 \omega_e (\mu/E)^{1/2}$ , respectively. The values obtained for the potential energies of activation are tabulated in Table III, along with the experimental activation energies. The agreement between the computational and the experimental results for H<sub>2</sub>O and H<sub>2</sub>S are satisfactory and the computed value of 1.4 kcal for H<sub>2</sub>Se is consistent with that estimated from experiment. Taking this value for the activation energy, the A factor of the reaction becomes equal to  $8.8 \times 10^{13} \text{ cm}^3 \text{ mol}^{-1} \text{ sec}^{-1}$ , which is about one-third of the gas kinetic collision frequency and corresponds to an entropy of activation of  $\Delta S^\ddagger = -10.5 \text{ gibbs mol}^{-1}$ . The value of  $\Delta S^\ddagger$  can be compared with an estimate based on a simple procedure adapted by Benson,<sup>40</sup> where the entropy of the activated complex is calculated by comparison with analogous molecules. The standard entropy of the H-H-SeH activated complex ( $S^\ddagger$ ) can be approximated from  $S^\circ(\text{H}_2\text{Se})$  considering that spin and loss of symmetry will each contribute an  $R \ln 2$  term. Thus  $S^\ddagger = S^\circ(\text{H}_2\text{Se}) + 2.8 \text{ gibbs mol}^{-1}$  and the entropy of activation is  $\Delta S_p^\ddagger = S^\circ(\text{H}_2\text{Se}) + 2.8 - S^\circ(\text{H}_2\text{Se}) - S^\circ(\text{H}) = -24.6 \text{ gibbs mol}^{-1}$  or transformed to the standard state of 1 M  $\Delta S_e^\ddagger = \Delta S_p^\ddagger - R \Delta n - (\Delta n) R \ln (RT) = -16.2 \text{ gibbs mol}^{-1}$ . The 5.7 gibbs mol<sup>-1</sup> difference from the experimental value can then be attributed to the vibrational contribution from the degenerate bending modes of the new H-H-SeH bond. This contribution is equivalent to a vibrational frequency of 150 cm<sup>-1</sup> for the degenerate mode and indicates a rather loose structure for the activated complex.

*Acknowledgment.* The authors thank the National Research Council of Canada for financial support and Dr. P.S.H. Bolman for experimental assistance.

## References and Notes

- C. F. Goodeve and N. O. Stein, *Trans. Faraday Soc.*, **27**, 393 (1931).
- G. Black and G. Porter, *Proc. Roy. Soc., Ser. A*, **266**, 185 (1962); A. Y. M. Ung and R. A. Back, *Can. J. Chem.*, **42**, 753 (1964).
- J. R. McNesby and H. Okabe, *Adv. Photochem.*, **3**, 157 (1964). For review see D. G. Volman, *ibid.*, **1**, 43 (1963).
- G. Porter, *Discuss. Faraday Soc.*, **9**, 60 (1950).
- B. de B. Darwent and R. Roberts, *Proc. Roy. Soc., Ser. A*, **216**, 344 (1953).
- K. H. Welge and F. Stuhl, *J. Chem. Phys.*, **46**, 2440 (1967).
- P. Fowles, M. de Sorigo, A. J. Yarwood, O. P. Strausz, and H. E. Gunning, *J. Am. Chem. Soc.*, **89**, 1352 (1967).
- H. E. Radford, *J. Chem. Phys.*, **40**, 2732 (1964).
- A. Carrington, G. N. Currie, and N. J. D. Lucas, *Proc. Roy. Soc., Ser. A*, **315**, 355 (1970).
- O. P. Strausz, R. J. Donovan, and M. de Sorigo, *Ber. Bunsenges. Phys. Chem.*, **72**, 253 (1968).
- B. Lindgren, *J. Mol. Spectrosc.*, **28**, 536 (1968).
- R. J. Donovan, D. J. Little, and J. Konstantatos, *J. Chem. Soc., Faraday Trans. 2*, **68**, 1812 (1972).
- P. Fowles, M. de Sorigo, A. J. Yarwood, O. P. Strausz, and H. E. Gunning, *J. Am. Chem. Soc.*, **89**, 1352 (1967); J. Connor, G. Greig, and O. P. Strausz, *ibid.*, **91**, 1622 (1969); P. J. Young, G. Greig, and O. P. Strausz, *ibid.*, **92**, 413 (1970); J. Connor, R. W. Fair, A. von Roodseelaar, and O. P. Strausz, *ibid.*, **93**, 563 (1971); J. Connor, P. J. Young, and O. P. Strausz, *ibid.*, **93**, 822 (1971); P. J. Young, E. Hardwidge, S. Tsunashima, G. Greig, and O. P. Strausz, *ibid.*, **96**, 5723 (1974).
- R. F. Barrow, G. C. Chandler, and C. B. Meyer, *Phil. Trans. Roy. Soc., Ser. A*, **260**, 395 (1966).
- K. S. Sidhu, I. G. Csizmadia, O. P. Strausz, and H. E. Gunning, *J. Am. Chem. Soc.*, **88**, 2412 (1966).
- C. E. Moore, Ed., *Natl. Bur. Stand. Circ.*, **No. 467** (1958).
- G. M. Lawrence, *Astrophys. J.*, **148**, 261 (1967).
- C. Shin-Piaw, *Ann. Phys.*, **10**, 173 (1938).

- (19) A. B. Callear and W. J. R. Tyerman, *Trans. Faraday Soc.*, **62**, 371 (1966).
- (20) W. J. R. Tyerman, P. Kerbarle, W. B. O'Callaghan, O. P. Strausz, and H. E. Gunning, *J. Am. Chem. Soc.*, **88**, 4277 (1966).
- (21) D. H. Volman, J. Wolstenholme, and S. C. Hadley, *J. Phys. Chem.*, **71**, 1798 (1967).
- (22) W. E. Jones, S. D. MacKnight, and L. Teng, *Chem. Rev.*, **73**, 407 (1973).
- (23) W. C. Price, J. P. Teegan, and A. D. Walsh, *Proc. Roy. Soc., Ser. A*, **201**, 600 (1950).
- (24) (a) S. D. Thompson, D. G. Carroll, F. Watson, M. O'Donnell, and S. P. McGlynn, *J. Chem. Phys.*, **45**, 1367 (1966); (b) D. G. Carroll, A. T. Armstrong, and S. P. McGlynn, *ibid.*, **44**, 1865 (1966).
- (25) Since the average  $D(\text{Se-H})$  in  $\text{H}_2\text{Se}$  is  $73 \text{ kcal mol}^{-1}$ <sup>26</sup> and, from the absorption spectrum,  $D(\text{Se-H}) = 70 \text{ kcal mol}^{-1}$ ,<sup>11,27</sup> it follows that  $D(\text{HSe-H}) = 76 \text{ kcal mol}^{-1}$ .
- (26) S. R. Gunn, *J. Phys. Chem.*, **68**, 949 (1964).
- (27) D. C. Dobson, F. C. James, S. C. Barton, and O. P. Strausz, to be submitted for publication.
- (28) J. R. McNesby, I. Tanaka, and H. Okabe, *J. Chem. Phys.*, **36**, 605 (1962).
- (29) B. de B. Darwent, R. L. Wadlinger, and M. J. Allard, *J. Phys. Chem.*, **71**, 2346 (1967).
- (30) M. J. Kurylo, N. C. Peterson, and W. Braun, *J. Chem. Phys.*, **54**, 943 (1971).
- (31) J. P. Nielson, S. Maeser, and D. S. Jennings, *J. Am. Chem. Soc.*, **61**, 440 (1939).
- (32) T. Yokota, M. Ahmed, O. P. Strausz, and H. E. Gunning, to be submitted for publication.
- (33) S. Tsunashima, T. Yokota, I. Safarik, H. E. Gunning, and O. P. Strausz, *J. Phys. Chem.*, submitted for publication.
- (34) M. de Sorigo, Ph.D. Thesis, University of Alberta.
- (35) R. G. Gann and J. Dubrin, *J. Chem. Phys.*, **47**, 1867 (1967).
- (36) H. S. Johnston, "Gas Phase Reaction Rate Theory", Ronald Press, New York, N.Y., 1966, pp 179 and 339.
- (37) F. Kaufman and F. P. Del Greco, *Symp. (Int.) Combust., [Proc.], 9th, 1962*, 659 (1963).
- (38) G. Dixon-Lewis, M. M. Sutton, and A. Williams, *Symp. (Int.) Combust., [Proc.], 10th, 1964*, 495 (1965).
- (39) B. de B. Darwent and R. Roberts, *Discuss. Faraday Soc.*, **14**, 55 (1953).
- (40) S. W. Benson, "Thermochemical Kinetics", Wiley, New York, N.Y., 1968.

## Abstraction of Sulfur Atoms from Carbonyl Sulfide by Atomic Hydrogen

S. Tsunashima, T. Yokota, I. Safarik, H. E. Gunning, and O. P. Strausz\*

Department of Chemistry, University of Alberta, Edmonton, Alberta, Canada (Received July 9, 1974)

Publication costs assisted by the National Research Council of Canada

The reaction of H atoms, produced by the mercury photosensitized decomposition of  $\text{H}_2$ , with COS was investigated in the temperature range 27–252°. The only primary reaction of importance is  $\text{H} + \text{COS} \rightarrow \text{CO} + \text{SH}$  (1). The rate coefficient of reaction 1 was determined in competition with the reaction  $\text{H} + \text{H}_2\text{S} \rightarrow \text{H}_2 + \text{SH}$  to have the value  $k_1 = (9.1 \pm 1.2) \times 10^{12} \exp(-3900 \pm 370)/RT$  cc mol<sup>-1</sup> sec<sup>-1</sup>.

### Introduction

Relatively few studies have been reported on the reaction of hydrogen atoms with sulfur compounds.<sup>1</sup>

In a concurrent study at this laboratory<sup>2</sup> the only detectable reaction of hydrogen atoms with ethylene episulfide was found to be sulfur atom abstraction with a rate coefficient of  $5.6 \times 10^{13} \exp(-1940/RT)$  cc mol<sup>-1</sup> sec<sup>-1</sup>. The analogous sulfur atom abstraction from carbonyl sulfide



was demonstrated by Oldershaw and Forter<sup>3</sup> and by Rommel and Schiff.<sup>4</sup> The latter authors reported a value for  $k_1$  of  $1.3 \times 10^{10}$  cc mol<sup>-1</sup> sec<sup>-1</sup> at 298°K.

The main purpose of the present study was to determine the Arrhenius parameters of reaction 1 and to examine its kinetic, mechanistic features.

### Experimental Section

The apparatus consisted of a  $5 \times 10$  cm quartz cell fitted to a circulatory system with total volume of 510 ml. The fan type circulator was constructed of glass and Teflon and was driven by an induction motor. A small side arm containing liquid mercury at room temperature was connected close to the cell. The cell itself was surrounded by an aluminum block furnace which was fitted with pencil heaters;

the temperature was measured by standardized iron-constantan thermocouples.

The light source was a Hanovia low-pressure mercury arc equipped with a 2537-Å interference filter and a collimating quartz lens.

Hydrogen atoms were produced by the mercury photosensitized decomposition of hydrogen. In most experiments the pressure of hydrogen was kept at  $500 \pm 20$  Torr and the pressure of COS and/or  $\text{H}_2\text{S}$  at less than 10 Torr. At these concentrations the direct photolysis or mercury sensitized decomposition of COS or  $\text{H}_2\text{S}$  was negligible. Thermolysis of COS could also be discounted since the onset of decomposition lies higher than the highest temperature, 252°, employed.<sup>5</sup>

Carbonyl sulfide (Matheson) was purified as described previously.<sup>6</sup>  $\text{H}_2$  (Matheson, stated purity 99.9%) was used as received.  $\text{H}_2\text{S}$  (Matheson) was purified by bulb-to-bulb distillation at -130°.

After irradiation, the reaction mixture was slowly pumped through two 5-ft long spiral traps at -196°, the second one being packed with molecular sieve. Carbon monoxide and traces of hydrogen were then removed from the second trap at 100°, measured in a gas buret, and transferred to a copper oxide furnace at 380°. The resulting carbon dioxide was then analyzed by gas chromatography on a 5-ft long Poropak Q column at 50°.

TABLE I: Effect of Temperature and H<sub>2</sub>S-COS Concentration on the Quantum Yield of CO Formation<sup>a</sup>

Pressure, Torr				
H <sub>2</sub> S	COS	H <sub>2</sub> S/COS	$\phi(\text{CO})$	$1/\phi(\text{CO})$
27°				
1.01	15.8	0.064	0.581	1.72
1.01	10.4	0.097	0.450	2.22
1.02	10.0	0.102	0.395	2.53
1.02	10.0	0.102	0.391	2.56
1.03	10.0	0.103	0.441	2.27
1.04	10.0	0.104	0.420	2.38
1.05	10.0	0.105	0.422	2.37
1.01	5.21	0.194	0.251	3.98
1.02	5.18	0.197	0.269	3.72
2.08	10.34	0.201	0.273	3.66
1.04	4.13	0.252	0.214	4.67
0.998	3.38	0.295	0.187	5.36
1.02	3.37	0.303	0.181	5.54
1.02	3.37	0.303	0.160	6.25
1.03	3.40	0.303	0.169	5.91
1.02	3.36	0.304	0.168	5.96
1.03	3.31	0.311	0.183	5.45
2.06	6.00	0.343	0.156	6.41
1.02	2.60	0.392	0.140	7.14
81°				
1.03	9.75	0.103	0.592	1.69
1.01	10.0	0.101	0.606	1.65
1.01	5.26	0.192	0.386	2.59
1.01	3.34	0.302	0.281	3.56
1.05	3.37	0.312	0.259	3.86
121°				
1.04	9.96	0.104	0.754	1.33
1.05	10.0	0.105	0.679	1.47
1.01	9.37	0.108	0.734	1.36
1.00	5.23	0.191	0.512	1.96
1.01	5.23	0.193	0.529	1.89
1.01	3.32	0.304	0.370	2.70
252°				
1.01	10.6	0.095	1.12	0.893
1.02	10.0	0.102	1.04	0.961
1.03	10.0	0.103	0.935	1.07
1.05	10.0	0.105	0.992	1.01
1.01	5.23	0.193	0.810	1.23
1.01	3.32	0.304	0.592	1.69

<sup>a</sup>  $P_{\text{H}_2} = 500 \pm 10$  Torr.

Light intensities were determined by propane actinometry<sup>7</sup> using  $\phi(\text{H}_2) = 0.58$  at 27°. The approximate value of the maximal absorbed intensity was  $3 \times 10^{-8}$  einstein  $\text{min}^{-1}$ .

## Results

The Hg(<sup>3</sup>P<sub>1</sub>) (Hg\*) photosensitization of hydrogen and carbonyl sulfide mixtures at room temperature leads to the formation of CO, H<sub>2</sub>S, sulfur, and HgS. The latter product is deposited on the cell face in the form of a thin black film, decreasing the window transparency, and attenuating the absorbed light intensity. The attenuation, which rendered quantitative product yield measurements difficult, was more serious at room temperature than at elevated temperatures. In order to correct for the gradual changes in trans-

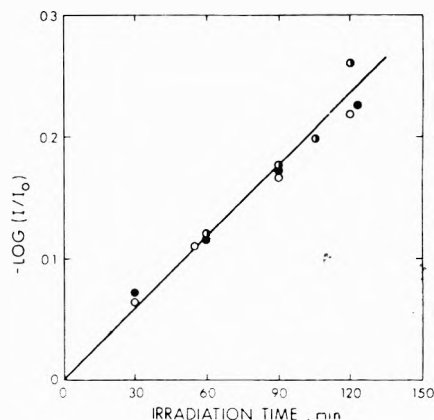


Figure 1.  $-\log I/I_0$  as a function of irradiation time for  $P_{\text{COS}} = 10.0$  Torr,  $P_{\text{H}_2\text{S}} = 0$  (O);  $P_{\text{H}_2\text{S}} = 1.0$  Torr,  $P_{\text{COS}} = 10.0$  Torr (●);  $P_{\text{H}_2\text{S}} = 1.0$  Torr,  $P_{\text{COS}} = 3.36$  Torr (◐),  $P_{\text{H}_2} = 500 \pm 20$  Torr in every case.

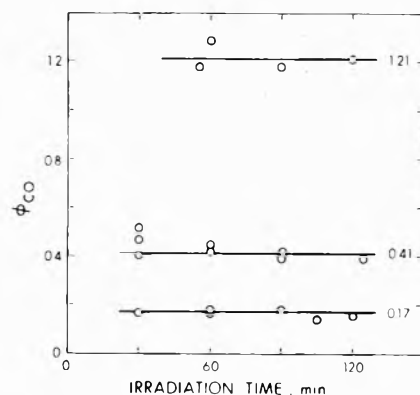


Figure 2. Corrected  $\phi_{\text{CO}}$  as a function of radiation time. From top to bottom,  $P_{\text{H}_2\text{S}} = 0$ ,  $P_{\text{COS}} = 10$  torr ( $\phi_{\text{CO}} = 1.21$ );  $P_{\text{H}_2\text{S}} = 1.0$  Torr,  $P_{\text{COS}} = 10.0$  torr ( $\phi_{\text{CO}} = 0.41$ );  $P_{\text{H}_2\text{S}} = 1.0$  Torr,  $P_{\text{COS}} = 3.36$  Torr ( $\phi_{\text{CO}} = 0.17$ );  $P_{\text{H}_2} = 500 \pm 20$  Torr in every case.

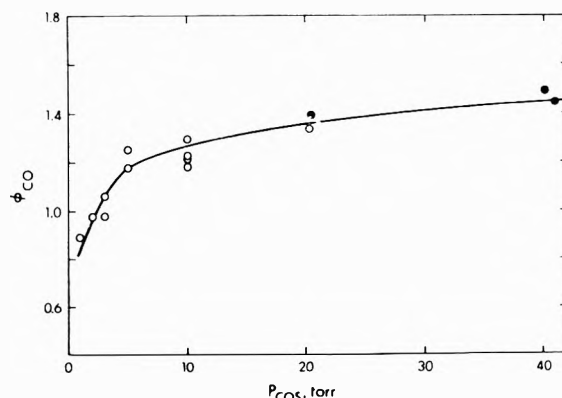


Figure 3.  $\phi_{\text{CO}}$  as a function of  $P_{\text{COS}}$  for  $P_{\text{H}_2} = 480$  Torr (O) and 1005 Torr (●).

parency, actinometric determinations of light intensities were done before and after photolyses.

The results of a series of experiments in which the photolysis time was varied using COS-H<sub>2</sub> and COS-H<sub>2</sub>S-H<sub>2</sub> mixtures are shown in Figure 1. The plot of  $\log(I/I_0)$  vs. irradiation time, where  $I_0$  and  $I$  are the initial and final intensities, is linear, satisfying the relationship  $-\log(I/I_0) = (\beta/2.303)t$ . Absorbed light intensities in the quantum yield



determinations were then calculated using the integrated form of the above equation

$$I(t) = I_0(1 - e^{-\beta t})/\beta \quad (I)$$

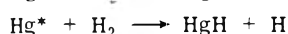
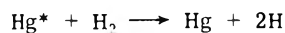
where  $\beta/2.303$  is the slope of the plot in Figure 1. The corrections at a fixed pressure of hydrogen, 500 Torr, were independent of the COS concentrations used or of the presence of added hydrogen sulfide.

The quantum yields of CO formation were determined as a function of COS concentration at a fixed pressure of hydrogen. The measured yields became independent of the exposure time only when they were corrected for light intensity attenuation by eq I, Figure 2. From the plot in Figure 3, it is seen that the limiting value of  $\phi(\text{CO})$  is about 1.45 at COS pressures above 30 Torr in 500–1000 Torr of hydrogen.

In order to determine the value of the absolute rate coefficient for reaction 1, competitive experiments were carried out with added hydrogen sulfide. The quantum yields of CO formation were monitored as a function of the  $[\text{H}_2\text{S}]/[\text{COS}]$  ratios at four different temperatures. The results are compiled in Table I.

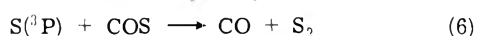
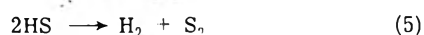
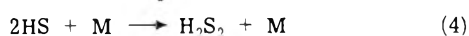
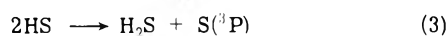
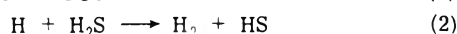
## Discussion

Under the prevailing experimental conditions of this study excited mercury atoms are totally quenched by hydrogen

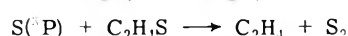
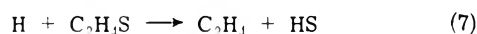


Although the quantum yield of HgH formation is high, 0.67,<sup>8</sup> the lifetime of HgH with respect to dissociation is short and the overall kinetics would be indistinguishable from that of H atoms. Thus, the system can be treated as a source of H atoms with  $\Phi(\text{H}) = 2.0$ .<sup>9</sup>

The principal elementary reactions occurring in the  $\text{H}_2\text{S}$ –COS– $\text{H}_2$  mixtures are



If scavenging of the H and S atoms by COS were complete at the concentrations involved, this mechanism would predict a quantum yield of CO formation of between two and three. As the experimental value of  $\phi(\text{CO})$  is only 1.45, it is evident that the scavenging of neither atoms is complete. Complete scavenging of both atoms was achieved in the analogous system  $\text{H}_2$ – $\text{Hg}^*$ –ethylene episulfide: there, the quantum yield of ethylene formation via the abstraction reactions

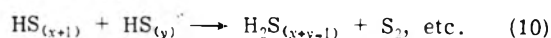
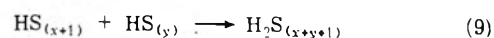
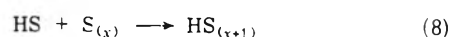


had a value of 2.4, and it was also shown that at room temperature 41% of the HS radicals disappeared via the disproportionation step 3<sup>2</sup> and the remainder via steps 4 and 5 and by combination reactions with the  $\text{S}_2$ – $\text{S}_7$  sulfur radicals and  $\text{S}_3\text{H}$ – $\text{S}_7\text{H}$  sulphydryl radicals present as transient intermediates in the system

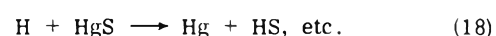
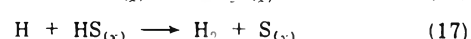
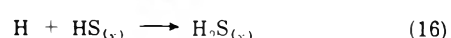
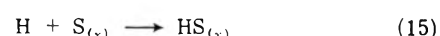
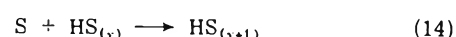
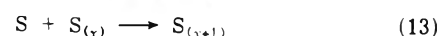
TABLE II: Arrhenius Parameters for Sulfur Atom Abstraction by Hydrogen Atoms and Methyl Radicals

Reaction	$\text{Log } A, \text{ cc mol}^{-1} \text{ sec}^{-1}$	$E_a, \text{ kcal mol}^{-1}$	$k(300^\circ\text{K}), \text{ cc mol}^{-1} \text{ sec}^{-1}$	Ref
H + COS	12.96	3.9	$1.3 \times 10^{10}$	This work
H + H <sub>2</sub> S	12.89	1.7	$4.5 \times 10^{11}$	4
H + S	13.75	1.9	$2.3 \times 10^{12}$	4
CD + COS	11.58	11.35	$2.0 \times 10^3$	11
CH + S	11.35	7.4 <sup>a</sup>	$8.9 \times 10^5$	11
CH + S	11.33	7.5 <sup>a</sup>	$7.3 \times 10^5$	b
CH + S	12.31	6.8 <sup>a</sup>	$2.2 \times 10^7$	b
S( <sup>3</sup> P) + COS	13.7 (assumed)	~5	$\sim 1.1 \times 10^{10}$	11
S( <sup>3</sup> P) + S			$1.7 \times 10^{13}$	c

<sup>a</sup> Uncorrected for secondary  $\text{C}_2\text{H}_4$  producing reactions. <sup>b</sup> M. G. Ahmed, M.Sc. Thesis, University of Alberta, Edmonton, Alberta, 1974. <sup>c</sup> A. van Roodselaar and O. P. Strausz, to be submitted for publication.



The difference between the CO and  $\text{C}_2\text{H}_4$  yields from the respective systems is attributable to the difference in the rates of the reactions involved. From the rate constant values compiled in Table II it can be predicted that abstraction of sulfur by H and S atoms will go to completion with  $\text{C}_2\text{H}_4\text{S}$ ; however with COS both reactions will be slow and loss of H atoms, S atoms, and HS radicals may occur via the reactions



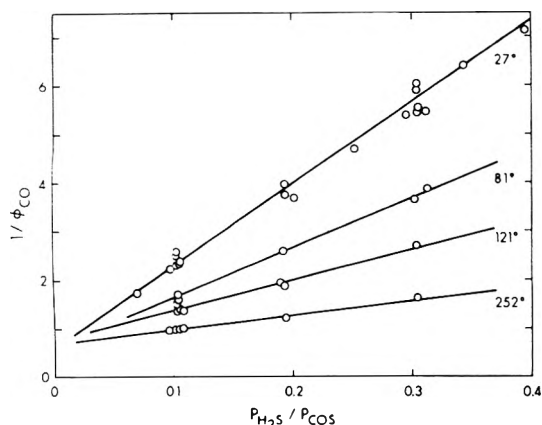
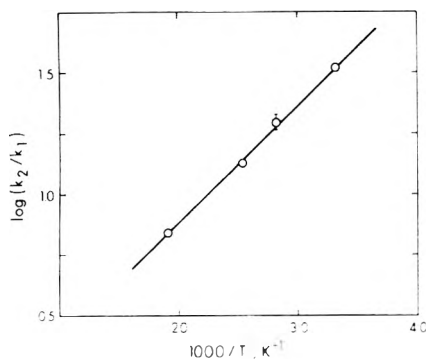
Since the amount of HS produced is independent of the ratio  $[\text{H}_2\text{S}]/[\text{COS}]$ , it may be assumed that the rates of steps 15–18 relative to step 1 are constant, and that step 6 is negligibly slow as compared to other reactions consuming S atoms. On this basis one can derive the following expression for the quantum yield of CO formation:

$$1/\phi(\text{CO}) = \frac{1}{2} \left( 1 + \alpha + \frac{k_7[\text{H}_2\text{S}]}{k_1[\text{COS}]} \right) \quad (II)$$

where  $\alpha$  is the sum of the rates of steps 15–18 relative to that of step 1. Equation II is plotted at four different temperatures, 27, 81, 121, and 252° within the  $[\text{H}_2\text{S}/\text{COS}]$  range 0.06–0.4, Figure 4. From the values given in Table III it is seen that the intercept is independent of temperature

**TABLE III: Slope and Intercept Values of the Plots in Figure 5**

$T, ^\circ\text{C}$	Slope	Intercept	$k_2/k_1$
27	$16.6 \pm 0.4$	$0.656 \pm 0.081$	$33.2 \pm 0.8$
81	$9.86 \pm 0.41$	$0.688 \pm 0.054$	$19.7 \pm 0.8$
181	$6.80 \pm 0.15$	$0.624 \pm 0.029$	$13.6 \pm 0.3$
252	$3.50 \pm 0.02$	$0.677 \pm 0.041$	$7.0 \pm 0.04$

**Figure 4.**  $\phi_{\text{CO}}$  as a function of  $\text{H}_2\text{S}/\text{COS}$  at 27, 81, 121, and 252°.**Figure 5.**  $\log(k_2/k_1)$  as a function of  $T^{-1}$ .

but the slope gradually decreases with increasing temperature. The Arrhenius plot for  $k_2/k_1$  is shown in Figure 5 from which the value of the rate coefficient ratio is  $\log k_2/k_1 = -(0.068 \pm 0.015) + (2190 \pm 190)/2.3RT$ . Accepting Braun and coworkers<sup>10</sup> value for the Arrhenius parameters of reaction 2 of  $A_2 = (7.77 \pm 0.90) \times 10^{12} \text{ cc mol}^{-1} \text{ sec}^{-1}$  and  $E_a = 1709 \pm 60 \text{ cal mol}^{-1}$ , the Arrhenius parameters of reaction 1 are computed to be  $A = (9.1 \pm 1.2) \times 10^{12} \text{ cc mol}^{-1} \text{ sec}^{-1}$  and  $E_a = 3.9 \pm 0.4 \text{ kcal mol}^{-1}$ . These lead to a rate constant value of  $1.3 \times 10^{10} \text{ cc mol}^{-1} \text{ sec}^{-1}$  at room temperature,<sup>12</sup> in excellent agreement with that measured by Rommel and Schiff<sup>4</sup> in a discharge flow system at room temperature using mass spectrometric detection.

The  $A$  factor of the reaction is  $9.1 \times 10^{12} \text{ cc mol}^{-1} \text{ sec}^{-1}$  which corresponds to an entropy of activation of  $-15.0 \text{ gibbs mol}^{-1}$ . It is interesting to compare this value with an estimate based on a simple procedure adopted by Benson,<sup>13</sup> where the entropy of the activated complex is calculated by comparison with analogous molecules.

For the estimate of the standard entropy of the  $\text{H} \cdots \text{S} \cdots \text{CO}$  activated complex,  $S^{0\dagger}$ , we start with the stan-

dard entropy of the  $\text{SCO}$  molecule. There is a rotational contribution of  $0.6 \text{ gibbs mol}^{-1}$  from the increased principal moments of inertia in the activated complex and a spin contribution of  $R \ln 2$ . Thus

$$S^{0\dagger} = S^0(\text{COS}) + 0.6 + 1.4$$

and the entropy of activation at 300°K is  $\Delta S_p^\ddagger = S^0(\text{COS}) + 2.0 - S^0(\text{COS}) - S^0(\text{H}) = -25.4 \text{ gibbs mol}^{-1}$  or, converted to the standard state of 1  $M$ ,  $\Delta S_c^\ddagger = \Delta S_p^\ddagger - R \Delta n - (\Delta n)R \ln(RT) = -25.4 + 8.4 = -17.0 \text{ gibbs mol}^{-1}$ . Agreement with the experimental value can be achieved by assuming a vibrational contribution of  $2.0 \text{ gibbs mol}^{-1}$  from the  $\text{H} \cdots \text{S} \cdots \text{C}$  degenerate bending modes. This is equivalent to a vibrational frequency of  $400 \text{ cm}^{-1}$  and indicates a rather tight structure for the activated complex.

For the reaction  $\text{H} + \text{H}_2\text{S} = \text{HS} + \text{H}_2$  the experimental  $A$  factor is  $7.77 \times 10^{12} \text{ cc mol}^{-1} \text{ sec}^{-1}$ <sup>10</sup> and the corresponding entropy of activation is  $-15.3 \text{ gibbs mol}^{-1}$ . The standard entropy of the  $\text{H} \cdots \text{H} \cdots \text{SH}$  activated complex can be estimated in a similar manner from the standard entropy of the  $\text{H}_2\text{S}$  molecule. There will be a rotational contribution of  $1.0 \text{ gibbs mol}^{-1}$  and spin and loss of symmetry will contribute each an  $R \ln 2$  term. Thus

$$S^{0\dagger} = S^0(\text{H}_2\text{S}) + 1.0 + 2.8$$

and the entropy of activation at 300°K is  $\Delta S_p^\ddagger = S^0(\text{H}_2\text{S}) + 3.8 - S^0(\text{H}_2\text{S}) - S^0(\text{H}) = -23.6 \text{ gibbs mol}^{-1}$  or, converted to the standard state of 1  $M$ ,  $\Delta S_c^\ddagger = \Delta S_p^\ddagger + 8.4 = -15.2 \text{ gibbs mol}^{-1}$  in agreement with the experimental value.

In this estimate any vibrational contribution from the degenerate bending modes of the  $\text{H} \cdots \text{H} \cdots \text{S}$  bonds is neglected. However, a negligibly small vibrational contribution to the entropy requires a vibrational frequency of at least  $800 \text{ cm}^{-1}$  at 300°K and this again indicates a tight structure for the activated complex.

*Acknowledgment.* We thank the National Research Council of Canada for financial support.

## References and Notes

- (1) For example, W. E. Jones, S. D. MacKnight, and L. Teng, *Chem. Rev.*, **73**, 407 (1973).
- (2) T. Yokota, M. G. Ahmed, O. P. Strausz, and H. E. Gunning, submitted for publication to *J. Phys. Chem.*
- (3) G. A. Oldershaw and D. A. Porter, *J. Chem. Soc., Faraday Trans. 1*, **68**, 709 (1972).
- (4) H. Rommel and H. I. Schiff, *Int. J. Chem. Kinet.*, **4**, 547 (1972).
- (5) H. G. Schecker and H. Gg. Wagner, *Int. J. Chem. Kinet.*, **1**, 541 (1969).
- (6) H. A. Wiebe, A. R. Knight, O. P. Strausz, and H. E. Gunning, *J. Am. Chem. Soc.*, **87**, 1443 (1965).
- (7) T. L. Pollock, Ph.D. Thesis, University of Alberta, 1971; R. A. Back, *Can. J. Chem.*, **37**, 1834 (1959); R. L. Cvetanovic, "Progress in Reaction Kinetics", Vol. II, G. Porter, Ed., Pergamon Press, New York, N. Y., 1963.
- (8) A. B. Callear and J. C. McGurk, *J. Chem. Soc., Faraday Trans. 2*, **68**, 289 (1972); A. B. Callear and P. M. Wood, *ibid.*, **68**, 302 (1972).
- (9) T. L. Pollock, E. J. Jakubowski, H. E. Gunning, and O. P. Strausz, *Can. J. Chem.*, **47**, 3474 (1969).
- (10) M. J. Kurylo, N. C. Peterson, and W. Braun, *J. Chem. Phys.*, **54**, 943 (1971).
- (11) E. Jakubowski, M. G. Ahmed, E. M. Lown, H. S. Sandhu, R. K. Gosavi, and O. P. Strausz, *J. Am. Chem. Soc.*, **94**, 4094 (1972).
- (12) It may be argued that the  $\text{HgH}$  formed in the primary step of  $\text{H}_2$  decomposition may contribute to  $\text{CO}$  formation via the hypothetical reaction,  $\text{HgH} + \text{COS} \rightarrow \text{Hg} + \text{CO} + \text{SH}$ ,  $\Delta H = +5 \text{ kcal/mol}$ . The activation energy of this reaction can be estimated to be equal to  $E_0(1) + D(\text{HgH}) = 3.9 + 8.6 = 12.6 \text{ kcal/mol}$  with an  $A$  factor of not greater than  $10^9 M^{-1} \text{ sec}^{-1}$ . Thus, the rate of this hypothetical reaction under the experimental conditions employed in this study would be negligibly slow as compared to the unimolecular decomposition of  $\text{HgH}$ .
- (13) S. W. Benson, "Thermochemical Kinetics", Wiley, New York, N. Y., 1968.

# Reaction between Ozone and Hydrogen Sulfide<sup>1</sup>

Sotirios Glavas and Sidney Toby\*

School of Chemistry, Rutgers University, New Brunswick, New Jersey 08903 (Received September 9, 1974)

- ▼ The reaction between O<sub>3</sub> and H<sub>2</sub>S was studied from 25 to 70° over a pressure range of 0.005–0.1 Torr of O<sub>3</sub> and 0.2–5 Torr of H<sub>2</sub>S. Previous work on this reaction employed ozonized oxygen and the stoichiometry was reported as O<sub>3</sub> + H<sub>2</sub>S → SO<sub>2</sub> + H<sub>2</sub>O. We found that O<sub>2</sub> is the most important product of the reaction and that the (O<sub>2</sub> formed)/(O<sub>3</sub> used) ratio approached 1.5. We also found that the H<sub>2</sub>O/SO<sub>2</sub> ratio varied considerably from unity. SO<sub>2</sub>, H<sub>2</sub>O, and H<sub>2</sub>S in the products were determined and good H, O, and S mass balances were obtained. Runs carried out in the presence of added O<sub>2</sub> or CO<sub>2</sub> showed no change in rate, measured as  $-d[O_3]/dt$ . The rate law found was zero order in H<sub>2</sub>S and  $(1.75 \pm 0.25)$  order in O<sub>3</sub>. Taking the rate constant as  $\frac{3}{2}$  order we find  $\log(k/M^{-1/2} \text{ sec}^{-1}) = 5.0 \pm 0.5 - (5000 \pm 700)/2.30RT$ . A free-radical mechanism is proposed which accounts for the observed kinetics and which gives qualitative agreement with the observed product ratios.

## Introduction

Ozone and hydrogen sulfide are two important atmospheric pollutants. They react rapidly at room temperature and the reaction is of considerable kinetic interest. Nevertheless, there are surprisingly few reported studies of the kinetics. Gregor and Martin<sup>2</sup> found that sulfur dioxide and water were formed in equal amounts and postulated the stoichiometry as O<sub>3</sub> + H<sub>2</sub>S → H<sub>2</sub>O + SO<sub>2</sub>. Cadle and Ledford (CL) studied the reaction in a flow system<sup>3</sup> and found the rate of O<sub>3</sub> disappearance was  $\frac{3}{2}$  order in O<sub>3</sub> and zero order in H<sub>2</sub>S. They stated that the reaction was in part heterogeneous. A study by Hales, Wilkes, and York (HWY)<sup>4</sup> was also carried out in a flow system and led to the rate law  $d[SO_2]/dt = k[O_3]^{3/2}[H_2S]^{1/2}$ . They disputed the heterogeneity reported by CL but accepted the simple stoichiometry of the reaction. All of these studies used ozonized oxygen or air as the reactant gas.

There are several puzzling aspects of these results. A concerted molecular rearrangement is clearly most unlikely and would not give rise to the observed rate laws. It is not clear whether or not the rate law reported by CL is consistent with that reported by HWY and in any case no explanation has been put forward for these rate laws. In the study reported here we investigated the reaction between O<sub>3</sub> and H<sub>2</sub>S in the absence of molecular oxygen and we find that the most important product is O<sub>2</sub>. We also find that the H<sub>2</sub>O/SO<sub>2</sub> product ratio is far from unity. Our results show that the reaction H<sub>2</sub>S + O<sub>3</sub> → H<sub>2</sub>O + SO<sub>2</sub> has neither kinetic nor stoichiometric significance and we offer an alternative explanation for this reaction.

## Experimental Section

A conventional high vacuum system was used with traps cooled with Dry Ice to exclude mercury vapor from the quartz reaction vessel. The cylindrical reaction vessel, which was of 21.9 cm length and 460 cm<sup>3</sup> volume, was connected to the reactant inlet and rest of the system by Teflon high vacuum stopcocks. An inlet tube consisting of a "cold finger" of approximately 5 cm<sup>3</sup> volume was attached via a stopcock to the reaction cell. The desired amount of H<sub>2</sub>S was frozen into this inlet tube and allowed to warm before reacting.

The reaction vessel was mounted horizontally in a thermostatted oven ( $\pm 0.8^\circ$ ) with quartz windows at each end.

The ozone concentration was monitored by absorption of 254-nm radiation obtained from an Osram low-pressure mercury lamp and two interference filters. The absorption coefficient of ozone was taken<sup>5</sup> as 134 cm<sup>-1</sup> (1 atm at 273°K)<sup>-1</sup> (base 10) and Beer plots were linear up to about 0.85 Torr of ozone. Ozone pressures were kept below 1 Torr for reasons of safety and also because the reaction rate became too fast to measure with our system. The transmitted light beam was measured with a 1P28 photomultiplier connected to a Keithley 610A electrometer and a recorder.

Products from runs were trapped with liquid nitrogen and the noncondensable gas measured on a gas buret. For several runs this gas was then exposed to pyrophoric lead<sup>6</sup> and was completely absorbed, showing it to be pure oxygen.

Products other than O<sub>2</sub> were analyzed on a Beckman GC4 chromatograph using a 10-ft Poropak Q column at 100°. Erratic results were sometimes obtained in the GC determination of small amounts of H<sub>2</sub>O, presumably because of loss of H<sub>2</sub>O by absorption. A procedure was therefore developed in which, after the more volatile products had been removed, the H<sub>2</sub>O was allowed to evaporate at room temperature and the pressure measured in a calibrated volume on a thermocouple gage which had been calibrated for H<sub>2</sub>O vapor. This was found to give consistent results.

Ozone was generated by passing oxygen (Matheson Ultrapure grade) through a tesla coil. The ozone was condensed at  $-196^\circ$  and the O<sub>2</sub> pumped away. Hydrogen sulfide (Matheson CP grade) was distilled several times before use, rejecting head and tail fractions.

## Results

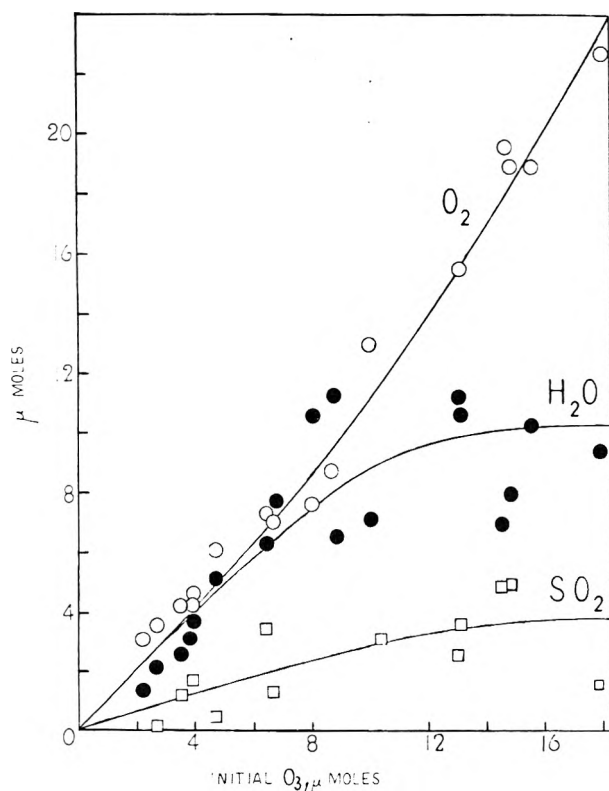
Runs were carried out at approximately 25, 50, and 70° and blanks with pure O<sub>3</sub> showed the reaction to be negligibly slow in the absence of H<sub>2</sub>S. The pressure range for the O<sub>3</sub> was 0.005–0.1 Torr and for H<sub>2</sub>S it was 0.2–5 Torr.

Products. Apart from excess H<sub>2</sub>S, products measured in decreasing order of abundance were O<sub>2</sub>, H<sub>2</sub>O, and SO<sub>2</sub>. In addition, traces of sulfur were deposited as a faint white powder which turned yellow on heating. These deposits were found in tubing cooled to  $-196^\circ$  which was connected to the reaction cell, and the GC sample bulbs.

Product data are given in Table I and plotted as a function of initial ozone in Figure 1. Mass balances for sulfur,

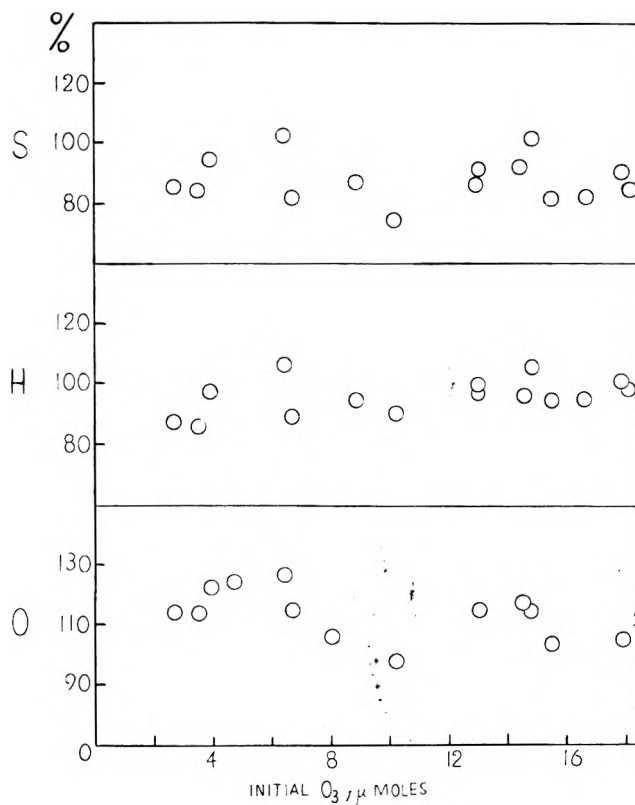
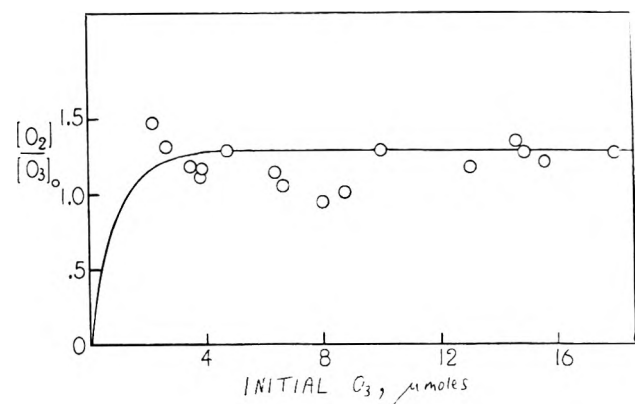
**TABLE I: Products of Reaction between Ozone and Hydrogen Sulfide at 25°**

Reactants, $\mu\text{mol}$		Products, $\mu\text{mol}$			
$\text{O}_3$	$\text{H}_2\text{S}$	$\text{O}_2$	$\text{H}_2\text{O}$	$\text{SO}_2$	$\text{H}_2\text{S}$
2.88	16.9	2.99	2.70	1.70	9.47
4.78	17.0	5.57	4.27	2.57	13.0
10.3	83.8	13.2	7.56	3.13	83.2
6.66	84.2	6.99	7.73	1.18	67.1
13.0	83.8	15.3	10.6	3.62	72.5
3.91	81.8	4.54	3.63	1.64	75.5
2.17	81.5	3.11	1.32		
15.5	83.9	18.8	10.2		68.4
8.76	79.2	8.74	11.2		
3.81	82.2	4.19	3.10		
17.9	81.2	22.7	9.40	1.27	71.8
6.42	82.2	7.34	6.26	3.36	80.8
14.8	81.8	18.8	7.91	4.93	78.0
8.84	83.1		6.53		71.4
8.00	80.3	7.51	10.5		66.5
14.5	81.0	19.5	6.92	4.79	69.7
2.66	81.7	3.47	2.13	0.05	69.0
3.53	83.2	4.17	2.62	1.07	68.3
4.73	80.9	6.05	5.06	0.40	

**Figure 1.** Effect of amount of initial  $\text{O}_3$  on product formation at 25° with initial  $\text{H}_2\text{S} = 80 \mu\text{mol}$ .

hydrogen, and oxygen are shown in Figure 2 as a function of amount of initial ozone. The average mass balances were 86.6% for S, 95.2% for H, and 113% for O. The stoichiometry of ( $\text{O}_2$  formed)/( $\text{O}_3$  used) was measured as a function of initial  $\text{O}_3$  for a fixed value of initial  $\text{H}_2\text{S}$  and the results are shown in Figure 3.

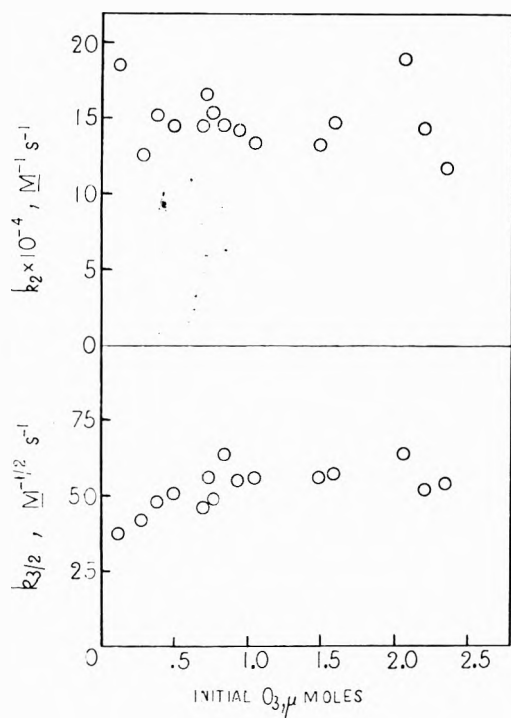
**Kinetics.**<sup>7</sup> The reaction was rapid with a typical half-life

**Figure 2.** Mass balance for sulfur, hydrogen, and oxygen as a function of amount of initial  $\text{O}_3$ .**Figure 3.** Ratio of ( $\text{O}_2$  formed)/( $\text{O}_3$  used) as a function of initial  $\text{O}_3$  at 25° with initial  $\text{H}_2\text{S} = 80 \mu\text{mol}$ .

of  $\sim 2$  sec under the conditions studied. Assuming a rate law of the form  $-\text{d}[\text{O}_3]/\text{d}t = k[\text{O}_3]^m[\text{H}_2\text{S}]^n$  we studied the kinetics in the presence of excess  $\text{H}_2\text{S}$ . Log-log plots gave slopes between 1.5 and 2. We therefore used the integrated equations and made plots corresponding to orders of 1, 1.5, 2, and 2.5. The first- and 2.5-order plots were distinctly curved but the 1.5- and second-order plots were both straight with statistical correlation factors of  $>0.99$  in most cases. The 1.5- and second-order rate constants at 25° were measured over a 20-fold range of initial  $\text{O}_3$  and the results are shown in Figure 4. Within the estimated errors of the data, both 1.5- and second-order constants fit the results equally well over approximately 90% of the reaction. The effect of initial  $\text{H}_2\text{S}$  on the rate constant was studied over a 20-fold range of  $[\text{H}_2\text{S}]$  and no dependence was found, as seen in Table II. On the other hand, plots of rate constants of order of 0.5 or higher in  $\text{H}_2\text{S}$  against  $[\text{H}_2\text{S}]$  showed a

**TABLE II: Effect of Initial H<sub>2</sub>S on Three-Halves Order Rate Constant at 20°**

Initial O <sub>3</sub> , μmol	Initial H <sub>2</sub> S, μmol	k, M <sup>-1/2</sup> sec <sup>-1</sup>
0.76	4.3	49.0
0.75	18.8	53.5
0.90	34.7	63.7
0.82	41.7	62.7
0.72	59.4	56.2
0.68	68.6	45.5
0.75	85.6	46.0

**Figure 4.** Plot of three-halves- and second-order rate constants at 25° as a function of initial O<sub>3</sub>.

clear dependence. We conclude that the rate law is zero order in H<sub>2</sub>S and is given by

$$-d[\text{O}_3]/dt = k[\text{O}_3]^{1.75 \pm 0.25} \quad (1)$$

Experiments were also carried out in the presence of added O<sub>2</sub> and added CO<sub>2</sub>. The presence of more than a 50-fold excess of added gas over O<sub>3</sub> had no effect.

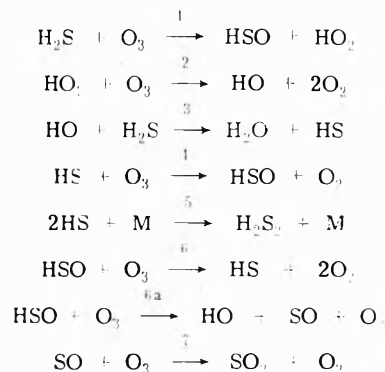
Rate constants were measured at 25, 50, and 70° and the rate constants were plotted as an Arrhenius plot which gave  $\log(k/M^{-1} \text{ sec}^{-1}) = 9.2 \pm 0.8 (5200 \pm 1200)/2.3RT$  for the second-order constant and  $\log(k/M^{-1/2} \text{ sec}^{-1}) = 5.0 \pm 0.5 - (5000 \pm 700)/2.3RT$  for the 1.5-order constant.

## Discussion

As Figure 1 shows, the most abundant product of the reaction between O<sub>3</sub> and H<sub>2</sub>S is O<sub>2</sub>, a fact overlooked by previous investigators. The stoichiometry of (O<sub>2</sub> formed)/(O<sub>3</sub> used) is close to 1.5 as seen in Figure 3, which implies a catalytic decomposition of O<sub>3</sub> with little concomitant consumption of the H<sub>2</sub>S. Similarly a plot of H<sub>2</sub>S used vs. initial O<sub>3</sub>, although extremely scattered because of the large excesses of H<sub>2</sub>S employed shows that as [O<sub>3</sub>]<sub>0</sub> increases the H<sub>2</sub>S used remains constant.

The mass balance average of 95.2% for H probably accounts for all H-containing products within the experimental error. However, the mass balance average of 87.6% for S is slightly low. Sulfur was not deposited in the reaction cell and so was not a direct product of the reaction but a product was formed which later decomposed to give sulfur. The high average mass balance for oxygen of 113% is probably due to systematic errors. It should be noted the O<sub>2</sub> was measured on a thermocouple or McLeod gauge, O<sub>3</sub> was measured by optical absorbance, SO<sub>2</sub> was measured by GC, and H<sub>2</sub>O was measured by pressure with a calibrated thermocouple gauge. Overall, the mass balances show satisfactory product recovery.

We thus have to explain the various product ratios and account for the observed rate law. We therefore postulate mechanism A. Taking steady states in [HO], [HO<sub>2</sub>], [HS], Mechanism A



[SO], and [HSO] and putting M = H<sub>2</sub>S leads to

$$-d[\text{O}_3]/dt = (3 + K)k_1[\text{H}_2\text{S}][\text{O}_3] + (2 + K)k_1^{1/2}k_4k_5^{-1/2}[\text{O}_3]^{3/2} \quad (2)$$

$$-d[\text{H}_2\text{S}]/dt = (2 + K)k_1[\text{H}_2\text{S}][\text{O}_3] + Kk_1^{1/2}k_4k_5^{-1/2}[\text{O}_3]^{3/2} \quad (3)$$

$$d[\text{H}_2\text{O}]/dt = (1 + K)k_1[\text{H}_2\text{S}][\text{O}_3] + Kk_1^{1/2}k_4k_5^{-1/2}[\text{O}_3]^{3/2} \quad (4)$$

$$d[\text{SO}_2]/dt = Kk_1[\text{H}_2\text{S}][\text{O}_3] + Kk_1^{1/2}k_4k_5^{-1/2}[\text{O}_3]^{3/2} \quad (5)$$

where  $K = k_{6a}/(k_6 + k_{6a})$ . Equations 4 and 5 give

$$\frac{[\text{H}_2\text{O}]}{[\text{SO}_2]} = \frac{1 + K + k_1^{-1/2}k_4k_5^{-1/2}K[\text{O}_3]^{1/2}[\text{H}_2\text{S}]^{-1}}{K + k_1^{-1/2}k_4k_5^{-1/2}K[\text{O}_3]^{1/2}[\text{H}_2\text{S}]^{-1}}$$

A plot of [H<sub>2</sub>O]/[SO<sub>2</sub>] should vary from 2 + k<sub>6</sub>/k<sub>6a</sub> to unity as [O<sub>3</sub>]<sub>0</sub> increases from zero. Our results are shown in Figure 5 and although there is considerable scatter, the results are in agreement with expectation.

Equation 3 and 5 give

$$\frac{[\text{H}_2\text{S used}]}{[\text{H}_2\text{O formed}]} = \frac{2 + K + k_1^{-1/2}k_4k_5^{-1/2}K[\text{O}_3]^{1/2}[\text{H}_2\text{S}]^{-1}}{1 + K + k_1^{-1/2}k_4k_5^{-1/2}K[\text{O}_3]^{1/2}[\text{H}_2\text{S}]^{-1}}$$

This function should vary from (2 + K)/(1 + K), which is a number between 1 and 2, to unity as [O<sub>3</sub>]<sub>0</sub> increases from zero. Our results are shown in Figure 6 and, with the exception of two apparently low points, are in good agreement with expectations.

Steps 1 and 2 in the mechanism can be replaced by a sequence involving HSO<sub>2</sub> rather than HO<sub>2</sub>. In addition, HSO<sub>2</sub> may also be formed by the reaction between HSO

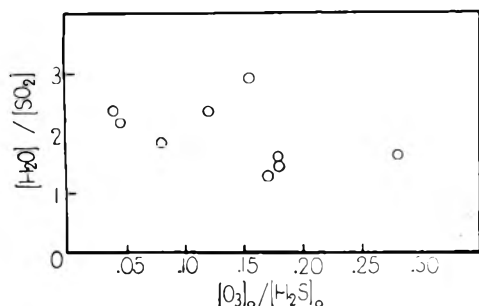


Figure 5. Ratio of  $[H_2O]/[SO_2]$  products as a function of initial reactant ratio.

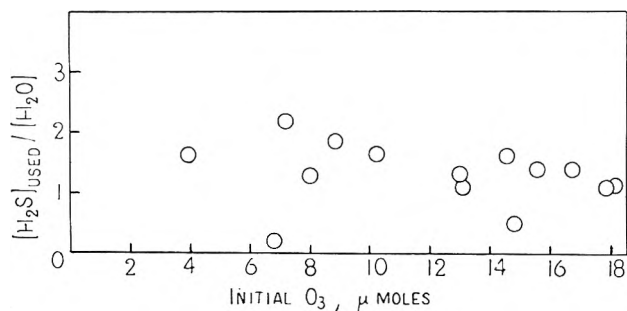
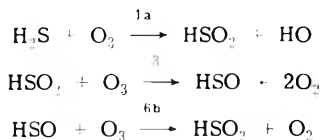


Figure 6. Ratio of  $(H_2S \text{ used})/(H_2O \text{ formed})$  as a function of amount of initial  $O_3$ .

and  $O_3$ . We postulate, as an alternative possibility, mechanism B together with steps 3, 4, 5, 6, 6a, and 7 of mechanism A.

Mechanism B



This gives the same rate law for ozone disappearance and identical expressions for product ratios as does mechanism A. Thus, our data will not distinguish between the two mechanisms.

At the higher values of initial  $O_3$  used a catalytic destruction of  $O_3$  occurred. This requires a chain component of the mechanism. A likely possibility is step 2 along with



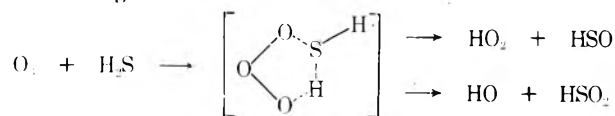
Evidence for the chain decomposition of  $O_3$  resulting from steps 2 and 9 has recently been obtained by DeMore and Tschuikow-Roux.<sup>8</sup> However, other chain sequences are possible, such as steps 6b and 8.

We did not detect  $H_2S_2$  in our GC analyses, but Gunning et al.<sup>9</sup> have reported that this substance readily decomposes:  $H_2S_2 \rightarrow H_2S + S$ . This would account for the sulfur we found deposited and the slightly low mass balance for S. According to Rommel and Schiff,<sup>10</sup> at very low pressures the likely fate for HS radicals is  $2HS \rightarrow H_2S + S$ . However, in the higher pressures of our system step 5 is the most likely reaction.

Neither added  $CO_2$  nor  $O_2$  had any effect on the measured rate constant. The lack of inhibition by  $O_2$  implies that the radical intermediates in the mechanism do not react rapidly with  $O_2$ . This contrasts with what has been found for the reaction of  $O_3$  and unsaturated hydrocarbons.<sup>11</sup>

If the second term on the right in eq 2 predominates over the first then a  $3/2$  order rate law results for the rate of disappearance of ozone. Our observed rate constant is then equal to  $k_1^{1/2}k_4k_5^{-1/2}(2 + K)$ . We compare our rate constant of  $\log(k/M^{-1/2} \text{ sec}^{-1}) = 5.0 \pm 0.5 - (5000 \pm 700)/2.30RT$  and our value of  $k(25^\circ) = 52 \pm 8 M^{-1/2} \text{ sec}^{-1}$  with that of CL who reported<sup>3</sup>  $\log(k/M^{-1/2} \text{ sec}^{-1}) = 6.9 - 8300/2.30RT$  and  $k(25^\circ) = 8.5 \pm 2 M^{-1/2} \text{ sec}^{-1}$ . They used a flow system and found some heterogeneity, and in view of the large differences in experimental methods used, the agreement is encouraging. HWY<sup>4</sup> found  $d[SO_2]/dt = k[H_2S]^{1/2}[O_3]^{3/2}$ . However they studied the system with an air carrier gas. According to our mechanism eq 5 would then become  $d[SO_2]/dt = k[H_2S]^{1/2}[O_3]^{3/2}/[\text{air}]^{1/2}$  and at constant total pressure the rate law found by HWY is then compatible with that found by CL and with the one reported here.

There is no direct evidence for the occurrence of steps 1 or 1a but they presumably take place via a five-membered ozonide ring:



The overall reaction between  $O_3$  and  $H_2S$  is chemiluminescent and Pitts et al.<sup>12</sup> have attributed the emission to  $SO_2^*$ . This is consistent with the high exothermicity (106 kcal) of step 7. A more detailed study<sup>13</sup> of the chemiluminescence found additional bands which were tentatively identified as  $HSO^*$  or  $HSO_2^*$  in accord with our mechanisms.

*Acknowledgment.* We thank the Biomedical Council, Rutgers University, for support of this work. We are grateful to one of the referees for helpful suggestions concerning the mechanism.

*Supplementary Material Available.* Additional kinetic data (Tables III and IV and two additional figures) will appear following these pages in the microfilm edition of this volume of the journal. Photocopies of the supplementary material from this paper only or microfiche (105 × 148 mm, 24× reduction, negatives) containing all of the supplementary material for the papers in this issue may be obtained from the Journals Department, American Chemical Society, 1155 16th St., N.W., Washington, D.C. 20036. Remit check or money order for \$4.00 for photocopy or \$2.50 for microfiche, referring to code number JPC-75-779.

## References and Notes

- Presented at the Physical Chemistry Division, 168th National Meeting of the American Chemical Society, Atlantic City, N.J., Sept 1974.
- I. K. Gregor and R. L. Martin, *Aust. J. Chem.*, **14**, 462 (1961).
- R. D. Cadle and M. Ledford, *Int. J. Air Water Pollut.*, **10**, 25 (1966).
- J. M. Hales, J. O. Wilkes, and J. L. York, *Atmos. Environ.*, **3**, 657 (1969).
- M. Griggs, *J. Chem. Phys.*, **49**, 858 (1968).
- T. M. Gorrie, P. W. Kopf, and S. Toby, *J. Phys. Chem.*, **71**, 3842 (1967).
- Tables of rate data are given in S. Glavas' Ph.D. Thesis, Rutgers University, 1975. See paragraph at end of text regarding supplementary material.
- W. B. DeMore and E. Tschuikow-Roux, *J. Phys. Chem.*, **78**, 1447 (1974).
- P. Fowles, M. DeSorgo, A. J. Yarwood, O. P. Strausz, and H. E. Gunning, *J. Am. Chem. Soc.*, **89**, 1352 (1967).
- H. Rommel and H. I. Schiff, *Int. J. Chem. Kinet.*, **4**, 547 (1972).
- F. S. Toby and S. Toby, *Int. J. Chem. Kinet.*, submitted for publication.
- W. A. Kummer, J. N. Pitts, Jr., and R. P. Steer, *Environ. Sci. Technol.*, **5**, 1045 (1971).
- K. H. Becker, M. Inocencio, and U. Shurath, Abstracts of CODATA Symposium, Warrenton, Va., Sept 1974. To be published in *Int. J. Chem. Kinet.*

# Effects of Solutes, Deuteration, and Annealing on the Production and Decay of Radicals in $\gamma$ -Irradiated 3-Methylpentane Glasses<sup>1</sup>

M. A. Neiss and J. E. Willard\*

Department of Chemistry, University of Wisconsin, Madison, Wisconsin 53706 (Received September 10, 1974)

Publication costs assisted by U.S. Atomic Energy Commission

Understanding of the mechanisms of radical production and decay in  $\gamma$ -irradiated hydrocarbon glasses, and in  $\gamma$ -irradiated and photolyzed solutions of alkyl halides in such glasses, has been extended through studies of yields and decay rates in 3-methylpentane (3MP) and 3MP-*d*<sub>14</sub>, with and without charge scavengers, using ESR as the detection technique. About half of the C<sub>6</sub>H<sub>13</sub> radicals produced by  $\gamma$  irradiation of pure 3MP decay at 77°K by relatively fast intraspur radical-radical reaction with time-dependent first-order kinetics. The remainder decay with second-order kinetics ( $k = 1.6 \times 10^{-25} \text{ cm}^3 \text{ molecule}^{-1} \text{ sec}^{-1}$ ), by reaction following random diffusion ( $D \approx 9.0 \times 10^{-20} \text{ cm}^2 \text{ sec}^{-1}$ ). Changes in resolution of the ESR spectra of trapped C<sub>6</sub>H<sub>13</sub> radicals during decay and during and following photolysis reflect changes in spacing and geometry. The *G* value for radical production (radicals per 100 eV absorbed) in 3MP at 77°K is  $3.0 \pm 0.3$ , while  $G(\text{C}_6\text{D}_{13})$  from the radiolysis of 3MP-*d*<sub>14</sub> is  $2.0 \pm 0.4$ .  $G(\text{C}_6\text{H}_{13})$  in 3MP-*h*<sub>14</sub> and  $G(\text{C}_6\text{D}_{13})$  in 3MP-*d*<sub>14</sub> are lowered by electron scavengers, implying that part of the radical formation in the pure hydrocarbons results from electron capture by cations (unless the additives are unexpectedly effective as energy scavengers). Scavengeable electron yields are higher in C<sub>6</sub>D<sub>14</sub> glass than in C<sub>6</sub>H<sub>14</sub>, which is an unexpected matrix isotope effect.  $G(\text{C}_6\text{H}_{13})$  and  $G(\text{C}_6\text{D}_{13})$  from radiolysis of 3MP-*h*<sub>14</sub> and 3MP-*d*<sub>14</sub> glasses are increased by the presence of 1 mol % hydrogen halide, implying that hot H atoms produced from the halides by dissociative electron capture abstract H (or D) from the matrix. The energetics require capture of electrons with greater than thermal energy. In 3MP-1% HI and 3MP-1% HBr systems, ~70% of the radicals decay by the C<sub>6</sub>H<sub>13</sub> + HX → C<sub>6</sub>H<sub>14</sub> + X reaction, the estimated rate constant and HI diffusion coefficient for the HI system being  $8.5 \times 10^{-5} \text{ M}^{-1} \text{ sec}^{-1}$  and  $1.6 \times 10^{-19} \text{ cm}^2 \text{ sec}^{-1}$ , respectively. HCl forms a stable complex with C<sub>6</sub>H<sub>13</sub> radicals (presumably C<sub>6</sub>H<sub>13</sub>·HCl), which can be photochemically decomposed regenerating the original radicals. Alkyl radicals produced in 3MP-*d*<sub>14</sub> by dissociative electron capture by alkyl chlorides decay faster than identical radicals produced from bromides and iodides, whereas the rates in 3MP-*h*<sub>14</sub> are independent of the geminate halide ion, consistent with recent evidence that the decay mechanisms of CH<sub>3</sub> are different in the two matrices. Photolysis of CH<sub>3</sub>I in 3MP-*h*<sub>14</sub> produces C<sub>6</sub>H<sub>13</sub> (by abstraction of H by hot CH<sub>3</sub>), but no trapped CH<sub>3</sub> radicals. The photolysis of CH<sub>3</sub>I in 3MP-*d*<sub>14</sub> yields  $[\text{CH}_3]/[\text{C}_6\text{D}_{13}] = \sim 0.02$ . CH<sub>3</sub> produced photolytically in 3MP-*d*<sub>14</sub> decays faster than CH<sub>3</sub> produced by dissociative electron capture, implying that geminate recombination with I is faster than with I<sup>-</sup>.

## Introduction

Trapped radicals are readily produced in hydrocarbon glasses at 77°K and below by  $\gamma$  irradiation of the pure matrix. Plausible mechanisms of formation include bond rupture of electronically excited molecules and rupture induced by the energy of recombination of electrons with positive ions. Solutes in the  $\gamma$ -irradiated glasses may yield radicals characteristic of the solute by dissociative electron capture (and possibly by excitation transfer), and additional solvent radicals may be formed when hot solute radicals abstract H from solvent molecules. Photochemical activation of solute molecules also may produce solute radicals, some or all of which abstract H yielding solvent radicals.

The radicals can be detected and identified by their ESR spectra. At sufficiently low temperatures they do not decay. At higher temperatures their decay kinetics can yield information about their spatial distribution, and about their diffusion coefficients and the diffusion coefficients of solutes with which they react. Changes in ESR spectral resolution during decay can be informative of changing interradsical proximity, changing radical geometry, radical isomerization, and proximity of the radicals to other species which share their spin density. Comparisons

of the radical yields in  $\gamma$ -irradiated hydrocarbons with and without charge scavengers present offer the possibility of distinguishing between radical formation by excited molecule decomposition and formation by charge neutralization. Studies of solutes for which the characteristics of electron capture processes in the gas are known (e.g., HCl, HBr, and HI) can yield information on the effect of the glassy state on such processes.

In this paper we report use of each of the above approaches to obtain information on the production and decay dynamics of C<sub>6</sub>H<sub>13</sub> radicals in 3-methylpentane (3MP), a commonly used hydrocarbon glass. To the best of our knowledge no other systematic investigations of this type have been made. Scattered incidental observations which are relevant appear in the literature.<sup>2</sup> These include recent evidence on radical pairs, ESR relaxation times, and saturation concentrations of radicals in  $\gamma$ -irradiated 3MP glass<sup>3</sup> and on carbanion formation ( $\text{R}\cdot + \text{e}^- \rightarrow \text{R}^-$ ) by radicals in 3MP and 3-ethylpentane glasses.<sup>4</sup>

The work reported here includes an extension of earlier work<sup>5-8</sup> on the production and reactions of trapped CH<sub>3</sub> radicals resulting from  $\gamma$  irradiation and photolysis of 3MP-*h*<sub>14</sub> and 3MP-*d*<sub>14</sub> glasses containing methyl halide solutes. The decay characteristics of CH<sub>3</sub> in 3MP-*h*<sub>14</sub>, from

which it can abstract H, and in 3MP- $d_{14}$ , from which it cannot abstract, have been compared. The decay of  $\text{CH}_3$  in 3MP- $d_{14}$  when  $\text{I}^-$  is the geminate partner has been compared with that when I is the partner. The yields of trapped  $\text{CH}_3$  and of hydrogen abstraction by  $\text{CH}_3$  in 3MP- $h_{14}$ - $\text{CH}_3\text{I}$  and 3MP- $d_{14}$ - $\text{CH}_3\text{I}$  glasses have been compared for  $\text{CH}_3$  produced by photolysis and by  $\gamma$  irradiation. Concurrent with these studies, additional information has been obtained on the effects of annealing the glassy matrices on the decay properties of trapped species.

### Experimental Section

**Reagents.** Phillips Pure Grade 3-methylpentane (3MP) was further purified by an initial storage over 13X molecular sieve and passage through a 5 ft column of freshly activated silica gel. The center fraction of the effluent was collected under nitrogen, degassed, and stored under vacuum over Na-K alloy.  $\text{CO}_2$  was removed by pumping on the liquid 3MP. The optical density of the liquid 3MP in a 1-cm cell was  $<0.1$  at 200 nm.

Aldrich  $\text{CH}_3\text{I}$  and Matheson  $\text{CH}_3\text{Cl}$ ,  $\text{CH}_3\text{Br}$ ,  $\text{HCl}$ , and  $\text{HBr}$  were dried by passing the vapors through  $\text{P}_2\text{O}_5$ . The  $\text{CH}_3\text{I}$  was stored over copper in the dark. Anhydrous  $\text{HI}$  was prepared on the vacuum line by allowing frozen 50% aqueous  $\text{HI}$  (Aldrich) to warm in the presence of  $\text{P}_2\text{O}_5$ . The gaseous  $\text{HI}$  was passed through a  $\text{P}_2\text{O}_5$  column and stored in the dark. Eastman White Label biphenyl was used as received.

Deuterated 3-methylpentane (3MP- $d_{14}$ ),  $\text{CD}_3\text{I}$ , and  $\text{C}_3\text{D}_7\text{I}$  were obtained from Merck Sharp and Dohme with stated isotopic purities of  $>98\%$ . Our mass spectrometric analysis of the 3MP- $d_{14}$  and  $\text{CD}_3\text{I}$  showed 99.2 and 99.5 atom % of D, respectively. The 3MP- $d_{14}$  was stored over 13X molecular sieve and the deuterated alkyl iodides were stored over Ag powder in the dark.

**Sample Preparation and Irradiation.** For most ESR studies samples were prepared by distilling metered amounts of 3MP and solute into 2-mm i.d. Suprasil tubes at 77°K under vacuum, and sealing off. For all of the halides the metered amount was 1 or 0.5 mol % of the 3MP. In the case of the hydrogen halides, this equilibrated between the liquid and vapor phases (ca.  $\frac{1}{2}$  volume ratio) when the samples were melted and shaken at room temperature. The samples were frozen to the glass in a manner believed to maintain this equilibrium distribution. For  $\text{HI}$  the ratio of the molarity in liquid 3MP to that in the vapor phase at 22° is 20.<sup>9</sup> The distribution ratio for  $\text{HBr}$  and  $\text{HCl}$  may be assumed to be somewhat lower, but similar. Samples which were to be examined both by ESR and optical spectroscopy were prepared in flat faced 2 × 3 mm i.d. rectangular Suprasil cells.

$\gamma$  Irradiations were made with a  $^{60}\text{Co}$  source at dose rates of ca.  $3 \times 10^{18}$  eV  $\text{g}^{-1}$   $\text{min}^{-1}$  at selected temperatures in the range 67–77°K. The usual dose was  $1.5 \times 10^{19}$  eV  $\text{g}^{-1}$ . Temperatures below 77°K were achieved by pumping on liquid nitrogen in a stainless steel chamber in the irradiation dewar. A Therm-O-Watch device mounted on a mercury column on the attached vacuum line operated a solenoid valve which controlled the vapor pressure above the liquid nitrogen and hence its temperature. Absolute dose rates were determined by Fricke dosimetry on a series of samples irradiated in ESR tubes, the sample height and position relative to the  $^{60}\text{Co}$  source being equivalent to that of the portion of the 3MP glass samples in the ESR cavity. The dose rate over this height was essentially uniform.

$G(\text{Fe}^{3+})$  was taken as 15.5, and the extinction coefficient of  $\text{Fe}^{3+}$  as  $2115 \text{ M}^{-1} \text{ cm}^{-1}$  at 20° at 304 nm with a temperature coefficient of 0.7% per degree between 20 and 30°.<sup>10</sup>

For photolytic radical production the 2-mm i.d. ESR tubes were placed in a quartz dewar which was placed in a Vycor tube at the center of a Suprasil spiral low-pressure mercury vapor lamp which gave an intensity of ca.  $10^{16}$  photons  $\text{sec}^{-1} \text{ cm}^{-1}$  height of tube at 254 nm. A quartz jacketed AH-4 medium-pressure Hg lamp with quartz collimating lens was used for photolysis of  $\gamma$ -irradiated samples.

**Analytical Procedures.** ESR measurements were made with a Varian 4500 X-band spectrometer with a Varian 4531 cavity using 100-kHz modulation and microwave powers of 300–400  $\mu\text{W}$ . The spectrometer sensitivity was monitored by means of the signal at ca. 1850 G of a ruby crystal permanently mounted in the cavity. Samples were transferred under liquid nitrogen at the temperature of irradiation from the dewar used for irradiation into the Varian ESR dewar. For decay studies at 74°K samples were placed in an ESR dewar with enlarged coolant capacity. A flange over the top allowed pumping on the liquid. Temperature control (to  $\pm 0.2^\circ$ ) was achieved as described above for irradiations below 77°K. An iron-constantan thermocouple in the dewar just above the sensitive region of the cavity, coupled with a reference junction at 77°K, monitored the temperature. The liquid nitrogen was cooled to the desired temperature before introduction of the sample. For decay studies below 70°K the sample was cooled by boil-off gas from liquid helium.<sup>11</sup>

To determine the  $G$  value of radical production in pure  $\gamma$ -irradiated 3MP the areas under the ESR absorption curves of samples which had received a known  $\gamma$  dose were compared with the areas from freshly prepared solutions of known concentrations of galvinoxyl, and of diphenylpicrylhydrazyl (DPPH), in benzene in the same tubes. The absorption curves were obtained from the first derivative spectra with an electronic integrator<sup>12</sup> and the relative areas were obtained by weighing cut-out tracings of the spectra. The areas for samples at 77°K to be compared with standards at 298°K were divided by 4 to correct for the temperature effect on the relative spin state populations.  $G$  values of radicals in 3MP glass containing additives were typically determined by comparing the areas under the ESR absorption curves with the area from a sample of pure 3MP ( $G(\text{R}) = 3.0$ ) irradiated simultaneously and measured consecutively. All samples were in calibrated tubes. The microwave powers used in all measurements were 0.4 mW or below and were shown to be below the onset of saturation. Irradiations were performed at 72°K and ESR measurements were made promptly to minimize radical decay. Correction was made for the small decay which occurred.

### Results

**$G$  Value of 3-Methylpentyl Radicals Produced by  $\gamma$  Irradiation of 3MP Glass.** Several determinations of the  $G$  value (radicals produced per 100 eV absorbed) for the formation of radicals by the  $\gamma$  irradiation of 3MP glass at 77°K have been reported. These include  $1.6 \pm 0.3$ <sup>7</sup> which becomes  $3.4 \pm 0.6$  when corrected for saturation,<sup>9</sup>  $2.8 \pm 0.6$ ,<sup>13</sup> and  $3.2 \pm 0.6$ .<sup>9</sup> Determinations in the present work, using DPPH, galvinoxyl, and Varian strong pitch as standards, have reduced the uncertainty limits, giving a value of  $3.0 \pm 0.3$ .



It is known that the  $G$  value at 77°K does not change dramatically up to at least  $5 \times 10^{20}$  eV  $g^{-1}$ ,<sup>13</sup> but that it approaches zero at  $2 \times 10^{21}$  eV  $g^{-1}$ .<sup>13</sup> The radicals are predominately secondary 3-methylpentyl radicals.<sup>14</sup> They have also been observed from  $\gamma$  irradiation of 3MP at 4°K.<sup>15</sup>

Two determinations of  $G(C_6D_{13})$  from the  $\gamma$  irradiation of 3MP- $d_{14}$  at 72°K have yielded values of 2.04 and 2.06<sup>16</sup> in good agreement with the earlier report of  $2.0 \pm 0.4$ .<sup>9</sup> The difference between this and the value of 3.0 for  $G(C_6H_{13})$  in 3MP- $h_{14}$  is one of several indications of unexpected quantitative differences in the radiation chemistry of  $C_6D_{14}$  and  $C_6H_{14}$ .

**Decay of 3-Methylpentyl Radicals in  $\gamma$ -Irradiated 3MP Glass.** Plots of the reciprocal of the concentration of radicals in  $\gamma$ -irradiated 3MP glass at 77°K vs. time after irradiation (Figure 1) indicate two populations with different decay characteristics. About 43% of the radicals decay by a second-order process, indicated by the straight line portions of Figure 1, and 57% by a faster decay. If the concentrations of the "second-order populations" present during the initial period of rapid decay are estimated by extrapolation and are subtracted from the total for each of the samples of Figure 1, the remaining concentrations give plots of  $\log [C_6H_{13}]$  vs. time which are superimposable after normalization for dose (Figure 2), but which show curvature. This time-dependent first-order decay ("composite first order") is consistent with intraspur radical combination processes, while the second-order decay is indicative of combination after random diffusion.

In samples which have been annealed  $\geq 5$  days at 77°K prior to irradiation (decays of  $C_6H_{13}$  at intermediate annealing times were not tested), the initial half-life of the faster decaying radicals is 150 min, independent of dose; in unannealed samples it is ca. 40 min. No differences in the rate of second-order decay have been observed between annealed and unannealed samples, presumably because a major portion of the annealing occurs while the second-order decay is obscured by the first-order process. Irradiations for the 77°K decay experiments of Figure 2 were done at 72°K for the lower dose and 67°K for the higher dose. Corrections were made for the small decay (<2%) which occurred prior to the first 77°K measurement. For the plots of Figures 1 and 2 the radical concentrations were determined from the areas under the ESR absorption curves obtained by integration of the first derivative signal. Curves qualitatively similar to those of Figure 1 have been reported for decay of  $C_6H_{13}$  in 3MP at 77°K following  $\gamma$  doses of  $1 \times 10^{19}$ ,  $5 \times 10^{19}$ , and  $9 \times 10^{19}$  eV  $g^{-1}$ , based on measurements of the peak heights of the first derivative spectra.<sup>17</sup>

**Changes in Resolution of Radical Spectrum in  $\gamma$ -Irradiated 3MP Glass During Decay and During Photolysis.** The ratio of the height of peak 2 from the low-field side of the first derivative ESR spectrum of 3-methylpentyl radicals in  $\gamma$ -irradiated 3MP glass (Figure 3A) to the area under the absorption curve increases as decay proceeds (Figure 4). In unannealed samples the ratio increases by 33% in 80 min, following which no further change occurs. The improvement in resolution with decay is illustrated by the integrated spectra of Figure 3C and 3D. In samples annealed for several days at 77°K prior to  $\gamma$  irradiation the initial spectral resolution is somewhat poorer, and the resolution improvement with time is slower (paralleling the decay).

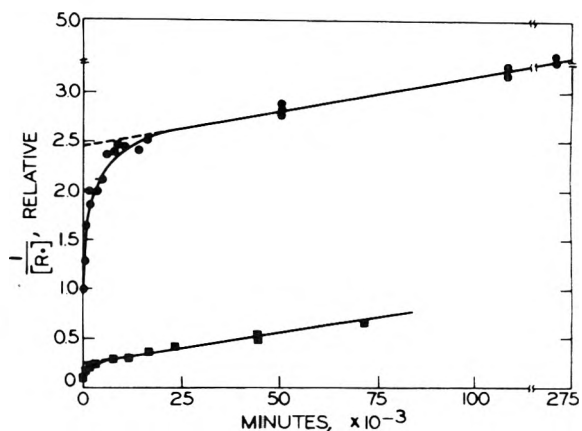


**Figure 1.** Decay of 3-methylpentyl radicals in annealed  $\gamma$ -irradiated 3-methylpentane at 77°K, second-order plot: upper curve,  $\gamma$  dose  $1.5 \times 10^{19}$  eV  $g^{-1}$ , initial radical concentration  $6.5 \times 10^{-4}$  M; lower curve,  $\gamma$  dose  $1.4 \times 10^{20}$  eV  $g^{-1}$ , initial radical concentration  $6.1 \times 10^{-3}$  M.

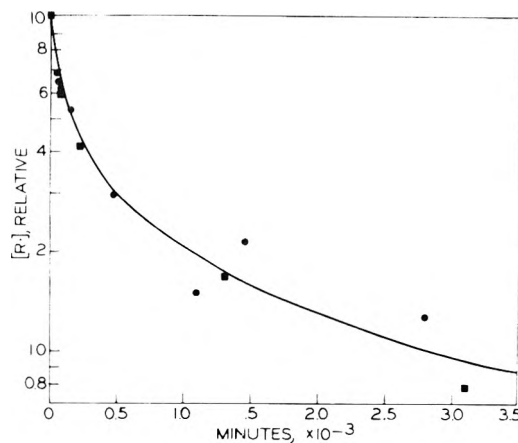


**Figure 2.** Initial (intraspur) decay of 3-methylpentyl radicals in annealed  $\gamma$ -irradiated 3MP at 77°K. Initial radical concentrations were  $6.5 \times 10^{-4}$  M, produced by a  $\gamma$  dose of  $1.5 \times 10^{19}$  eV  $g^{-1}$  (circles), and  $6.1 \times 10^{-3}$  M, produced by a  $\gamma$  dose of  $1.4 \times 10^{20}$  eV  $g^{-1}$  (squares). These data are deduced from the difference in the extrapolated straight line portions and the curved portions of Figure 1.

When 1 mol %  $CH_3I$  is present in the  $\gamma$ -irradiated 3MP, the four lines of the  $CH_3$  spectrum superimpose on the central four peaks of the  $C_6H_{13}$  spectrum. The only source of information on the  $C_6H_{13}$  concentration is the height of lines 1 and 6 of its underlying first derivative spectrum. The initial ratio of  $a$  to  $b$  (Figure 3A) is greater in the presence of  $CH_3I$  than in pure 3MP and appears to remain slightly greater after complete  $CH_3$  decay.

In contrast to peak 2, the height of peak 1 of the  $C_6H_{13}$  radical spectrum in pure  $\gamma$ -irradiated 3MP is proportional to the area under the absorption curve, and hence to the radical concentration, throughout the decay, in agreement with recently published data.<sup>18</sup> Assuming that the same proportionality exists in the 3MP-1%  $CH_3I$  glass, we have determined  $CH_3$  concentrations by subtracting the  $C_6H_{13}$  concentration so determined from the total radical concentration given by the area under absorption curves such as that of Figure 3B.

Figure 5 illustrates the effect on the ESR spectrum of trapped radicals caused by exposure of  $\gamma$ -irradiated 3MP glass at 77°K in the center of the Vycor-filtered mercury arc spiral for 5 min at 15 min after  $\gamma$  irradiation. The ratios

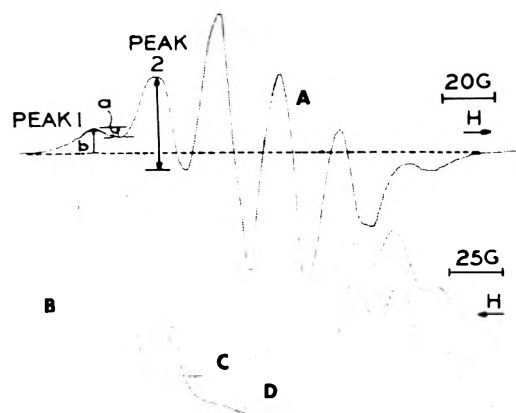


**Figure 3.** (A) First derivative ESR spectrum of 3-methylpentyl radicals in  $\gamma$ -irradiated 3MP glass; (B) integrated spectrum from  $\gamma$ -irradiated 3MP-1%  $\text{CH}_3\text{I}$  glass 3 min after irradiation; (C) integrated spectrum from  $\gamma$ -irradiated 3MP glass 3 min after irradiation; (D) same as C after 24 hr decay. Dose to all samples was  $1.5 \times 10^{19}$   $\text{eV g}^{-1}$ . C measured at a twofold higher sensitivity than B. D measured at a fourfold higher sensitivity than B.

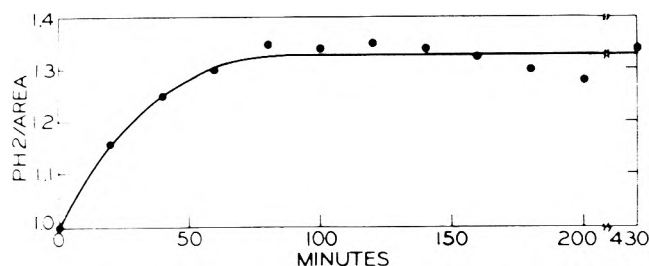


**Figure 4.** The ratio of the height of peak 2 (Figure 3A) of the first derivative ESR spectrum of  $\gamma$ -irradiated 3MP to the area obtained by double integration of the whole spectrum vs. time at  $77^\circ\text{K}$ .

of the heights of lines 2, 3, 4, and 5 to lines 1 and 6 in the first derivative spectrum increased by some threefold. Following illumination the spectrum slowly reverted to its original shape over a period of a few days at  $77^\circ\text{K}$ . Similar changes in the ESR radical spectrum were produced when  $\gamma$ -irradiated 3MP glass was exposed to 2.5 mW at 265 nm from a tunable dye laser for 30 min. Work in progress indicates that the improvement of spectral resolution by photolysis and the reversion on standing do not involve a change in the concentration of unpaired spins; however, the rate of intraspur radical decay is increased by light absorbed by the radicals.

**Radical Concentration as a Function of  $\text{CH}_3$  Decay in 3MP- $\text{CH}_3\text{X}$  Glass.** Reasons have been given for concluding that decay of  $\text{CH}_3$  radicals produced by dissociative electron capture by methyl halides in 3MP at  $77^\circ\text{K}$  does not occur by abstraction of H from the  $\text{C}_6\text{H}_{14}$  matrix molecules.<sup>5,7,8</sup> More recent evidence for such abstraction from polycrystalline  $\text{CH}_3\text{CN}$ ,<sup>19</sup>  $\text{CH}_3\text{NC}$ ,<sup>20</sup> and  $\text{CH}_3\text{OH}$ <sup>21</sup> molecules at  $77^\circ\text{K}$  has led us to further examination of the decay in 3MP.<sup>22</sup> If  $\text{CH}_3$  radicals decay by abstraction from  $\text{C}_6\text{H}_{14}$ ,  $\text{C}_6\text{H}_{13}$  radicals must be produced at the same rate that  $\text{CH}_3$  radicals decay. It is now clear that they are so produced, and that the earlier contrary conclusion<sup>7</sup> resulted from erroneous assumptions as to proportionality of peak heights of the  $\text{C}_6\text{H}_{13}$  first derivative spectrum to the radical concentration during initial decay, coupled with a fortuitous choice of times at which the peaks were measured. The investigations at  $77^\circ\text{K}$  of the changes in  $\text{CH}_3$  concentration, total radical concentration, and peak

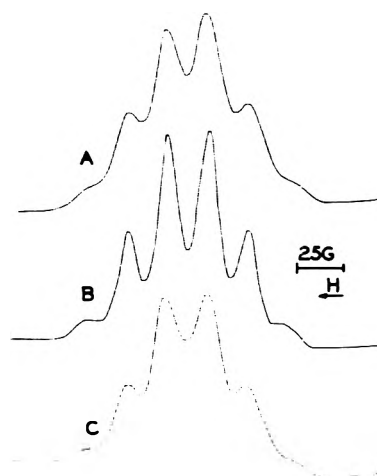


**Figure 5.** Integrated ESR spectra of  $\gamma$ -irradiated 3MP: (A) 15 min after irradiation; (B) after 5-min illumination of A with Hg arc; (C) sample B after standing in the dark for 4 days at  $77^\circ\text{K}$ . The sensitivity of measurement of C was 1.6 times greater than for A and B.

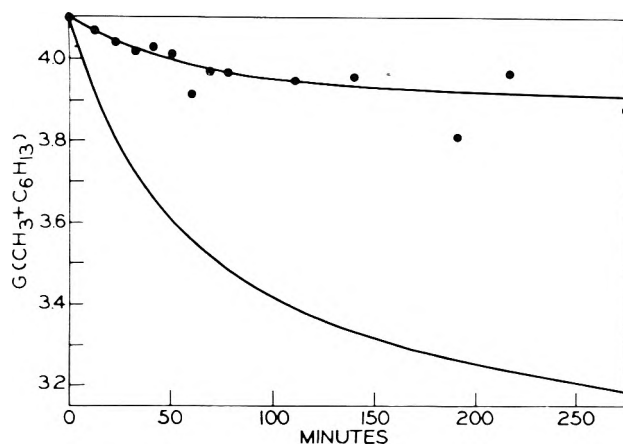


**Figure 6.** Decay of total radical population ( $\text{C}_6\text{H}_{13} + \text{CH}_3$ ) at  $74^\circ\text{K}$  in  $\gamma$ -irradiated annealed sample of  $\text{C}_6\text{H}_{14}$ -1%  $\text{CH}_3\text{Cl}$  (upper curve). Lower curve shows the decay which would have been observed if  $\text{CH}_3$  decayed without generating new  $\text{C}_6\text{H}_{13}$  radicals by H abstraction and no  $\text{C}_6\text{H}_{13}$  decay occurred.

heights on the wings of the  $\text{C}_6\text{H}_{13}$  spectrum following  $\gamma$  irradiation of 3MP-1%  $\text{CH}_3\text{I}$  by Sprague<sup>18</sup> and in our work give essentially the same results. They indicate that each  $\text{CH}_3$  radical which decays is replaced by a  $\text{C}_6\text{H}_{13}$  radical.

The data of Figure 6 show that this also occurs at  $74^\circ\text{K}$ , where the decay of both  $\text{C}_6\text{H}_{13}$  and  $\text{CH}_3$  radicals is much slower than at  $77^\circ\text{K}$ . In a 3MP-1%  $\text{CH}_3\text{Cl}$  sample annealed at  $77^\circ\text{K}$  prior to  $\gamma$  irradiation at  $72^\circ\text{K}$ , the  $\text{CH}_3$  decay at  $74^\circ\text{K}$  was composite first order with 25% occurring in 20 min, 50% in 60 min, and 83% in 270 min. The total radical concentration ( $\text{CH}_3 + \text{C}_6\text{H}_{13}$ ), as measured by the area under the ESR absorption curve, decayed only 5% (attributable to  $\text{C}_6\text{H}_{13}$  decay) during the 270 min. This implies  $\text{CH}_3$  decay by abstraction from the  $\text{C}_6\text{H}_{14}$ , since the area decay due to loss of  $\text{CH}_3$  radicals alone would have been 22% if the  $\text{CH}_3$  was not replaced by  $\text{C}_6\text{H}_{13}$  radicals.

**Effects of Additives on Production and Decay of  $\text{C}_6\text{H}_{13}$  Radicals in  $\gamma$ -Irradiated 3MP Glass.** Table I summarizes determinations of the  $G$  values for production of 3-methylpentyl radicals by  $\gamma$  irradiation of 3MP- $h_{14}$  and 3MP- $d_{14}$  glasses containing seven different additives, and Figures 7 and 8 show the decay of the radicals in the 3MP-biphenyl

**TABLE I: G Values of Radicals from  $\gamma$  Irradiation of 3MP- $h_{14}$  and 3MP- $d_{14}$  Glasses with and without Additives**

	$G(R \cdot$ total)	$G(C_6H_{13}$ or $C_6D_{13})$	$G(CH_3)$
Pure 3MP- $h_{14}$	3.0	3.0	
Pure 3MP- $d_{14}$	2.0	2.0	
3MP- $h_{14}$ -0.1% $Ph_2$		2.4	
3MP- $h_{14}$ -1% $C_3D_7I$	3.3	2.2 <sup>a</sup>	
3MP- $h_{14}$ -1% $CH_3I$	4.1	3.0	1.1
3MP- $d_{14}$ -1% $CH_3I$	3.6	1.3 <sup>b</sup>	2.3
3MP- $h_{14}$ -1% $HCl$	3.8 <sup>c</sup>		
3MP- $h_{14}$ -1% $HI$	3.6 <sup>c</sup>		

<sup>a</sup> Average of only two experiments (2.1 and 2.3). <sup>b</sup>  $G(C_6D_{13total}) = 1.3$  was deduced from the total area under the ESR absorption curve ( $G = 3.6$ ) by subtracting  $G(CH_3trapped) = 2.3$ . Subtraction of  $G(CH_3D_{hot}) = 0.7^{16}$  from the 1.3 yields  $G(C_6D_{13direct}) = 0.6$ , the presumed yield by processes other than hot abstraction. <sup>c</sup> Based on a single comparison of irradiated 3MP with an identical 3MP-HX sample.

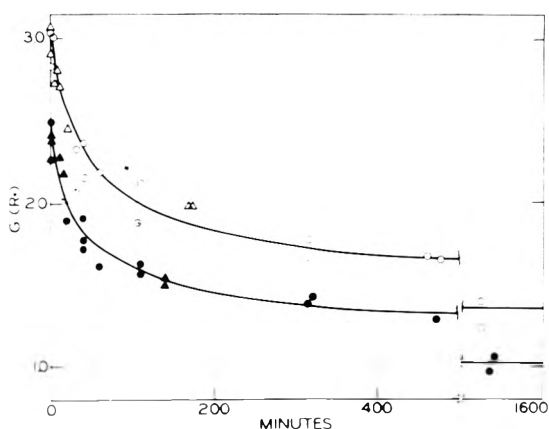


**Figure 7.** Effect of biphenyl on the yield (at 72°K) and decay (at 77°K) of  $C_6H_{13}$  radicals in  $\gamma$ -irradiated annealed 3MP: open points, pure 3MP; closed points, 3MP-0.1%  $Ph_2$ . Data shown by circles obtained from the height of peak 2 of the  $C_6H_{13}$  first derivative ESR spectrum, assuming the changing ratio to radical concentration of Figure 4. Data shown by triangles obtained from the height of peak 1, assuming a constant ratio to the concentration.

( $Ph_2$ ) and 3MP-hydrogen halide glasses. These tests were initiated to determine the effects of charge scavengers on the yield and spatial distribution of the  $C_6H_{13}$  radicals, under conditions similar to those used in the studies of the mechanism of  $CH_3$  decay described in the previous section, but in the absence (in the case of  $HCl$ ,  $HBr$ ,  $HI$ , and 2MP-1) of interference from a solute spectrum, and in the absence (in the case of  $Ph_2$  and  $C_3D_7I$ ) of hot abstraction reactions.

The additives were present at 1 mol % in all cases except  $Ph_2$ , where the concentration was 0.1 mol %. Irradiations and yield measurements were made at 72°K and decay measurements at 77°K. The total dose in each case was  $1.5 \times 10^{19} \text{ eV g}^{-1}$ .

Since the ESR spectrum of  $Ph_2$  overlaps the central lines of the first derivative  $C_6H_{13}$  spectrum, the concentrations of the  $C_6H_{13}$  for Figure 7 were estimated from (a) the height of peak 2 corrected for the changing peak height to area ratio read from Figure 4, and (b) the height of peak 1 assuming the same constant ratio of this line to the value of the double integral observed in pure 3MP.

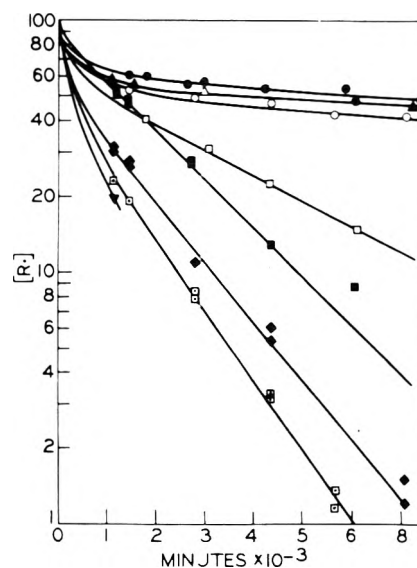


**Figure 8.** Decay at 77°K of  $C_6H_{13}$  radicals in annealed 3MP  $\gamma$ -irradiated at 72°K: 3MP (O); 3MP-1%  $HI$  ( $\square$ ,  $\blacklozenge$ ); 3MP-0.5%  $HI$  ( $\square$ ); 3MP-1%  $HCl$  ( $\blacktriangle$ ); 3MP-1%  $HBr$  ( $\blacktriangledown$ ); 3MP- $d_{14}$  ( $\bullet$ ); and 3MP- $d_{14}$ -1%  $HI$  ( $\blacksquare$ ).

Although the partially saturated ESR singlet of trapped electrons was observed with samples of  $\gamma$ -irradiated pure 3MP at 0.4 mW power, it was not seen with 3MP containing hydrogen halides. Further confirmation that the hydrogen halides act as electron scavengers in the glass was given by a sample of  $\gamma$ -irradiated 3MP-1%  $HCl$  glass which gave no electron signal when examined at a microwave power of 10  $\mu W$ . The electron signal is unsaturated at this power, and in pure 3MP irradiated and measured under the same conditions was several-fold higher than the radical signal.

**Formation of Complexes between  $C_6H_{13}$  and Hydrogen Halides.** Our initial reason for experiments with hydrogen halide solutes in 3MP glass was to determine their effect as electron scavengers, and possible sources of hot H atoms, on the yields of  $C_6H_{13}$  from  $\gamma$  irradiation. Unexpectedly the results have also yielded evidence for complex formation with  $C_6H_{13}$  radicals. This is most dramatic in the case of 3MP- $HCl$  glasses where the typical six-line  $C_6H_{13}$  spectrum (similar to Figure 9B) changes with time after  $\gamma$  irradiation to a broad singlet (Figure 9A), from which the well-resolved spectrum can be regenerated (Figure 9B) by illumination with the AH-4 lamp with a Vycor filter. Concurrent with the changes in the ESR spectrum on standing and bleaching, the changes in uv absorption illustrated in Figure 10 occur. The ESR and optical measurements were made on the same sample in a flat-faced 2 mm  $\times$  3 mm i.d. rectangular Suprasil cell. During the 20 hr between  $\gamma$  irradiation and taking the spectrum of Figure 9A the area under the ESR absorption curve decreased by ca. 50%, which is about the same as the fractional decrease in  $C_6H_{13}$  concentration which occurs in the same time in pure 3MP following  $\gamma$  irradiation. The illumination which regenerated the resolved signal caused a 25% decrease relative to that before illumination, within a time period during which thermal decay would be negligible.

The resolution of the ESR signal in  $\gamma$ -irradiated 3MP- $h_{14}$  containing 1%  $HBr$  or  $HI$  was initially always about the same as that in pure 3MP but did not improve with decay as it does in pure 3MP, nor did a major loss in resolution occur, as in the 3MP- $HCl$  system.

The uv absorption by  $\gamma$ -irradiated 3MP-1%  $HBr$  glass

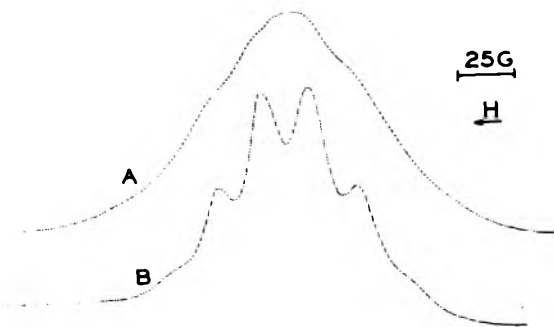


**Figure 9.** ESR absorption curves (integral of first derivative spectrum) of  $\gamma$ -irradiated 3MP containing 1% HCl: (A) after standing 20 hr at 77°K following  $\gamma$  irradiation; (B) same as A but with subsequent 1-hr bleaching with Vycor filtered AH-4 lamp. The spectral resolution immediately following  $\gamma$  irradiation was essentially the same as B.

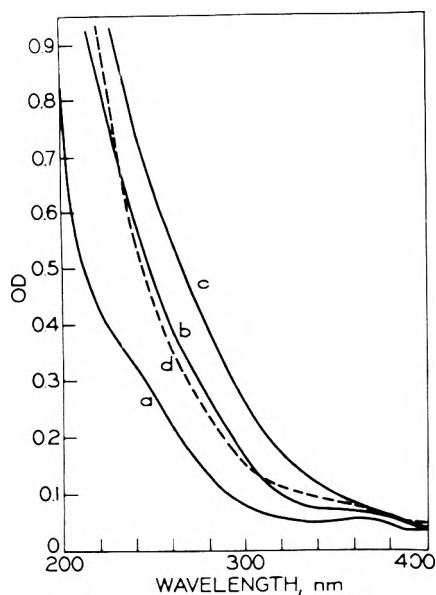


**Figure 10.** Uv spectra of 3MP-1% HCl: (a) before irradiation; (b) following  $\gamma$  dose of  $1.5 \times 10^{19}$  eV g<sup>-1</sup>; (c) after 20 hr in the dark at 77°K; (d) after subsequent 1-hr bleaching with Vycor filtered AH-4 lamp. The temperature was 77°K throughout.

increased on standing at 77°K in a manner similar to that of 3MP-HCl, but with added structure (Figure 11). During the 19-hr standing period represented in Figure 11, the total radical concentration measured by ESR decayed by ca. 80%. Bleaching reduced the remaining concentration by ca. 10%.

**Effects of Matrix Annealing on the Rate of Decay of  $CH_3$  Produced by Dissociative Electron Capture in 3MP- $h_{14}$ .** It is known from earlier work<sup>3,8</sup> and confirmed in the present investigation that methyl radicals formed by dissociative electron capture by 1 mol % methyl halide ( $CH_3X + e^- \rightarrow CH_3 + X^-$ ) in 3MP- $h_{14}$  glass, in samples freshly quenched to 77°K, decay by pure first-order kinetics with a half-life of ca. 16 min. To determine whether the decay process is affected by the extent of annealing of the glass prior to radical formation, we have measured the  $CH_3$  decay rates in samples which have stood at 77°K for periods of up to 10 days prior to initiating the dissociative capture process by  $\gamma$  irradiation. All irradiations were at 72°K, to a dose of  $1.5 \times 10^{19}$  eV g<sup>-1</sup>. Regardless of the nature of the halide ion ( $Cl^-$ ,  $Br^-$ , or  $I^-$ ), an increase in  $t_{1/2}$  from about 16 min to 24 min was observed as a result of preirra-

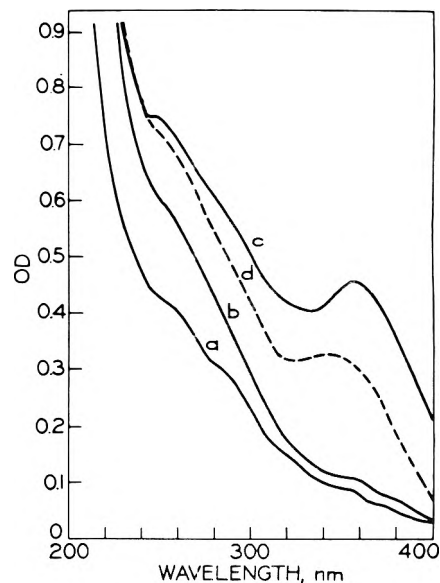


**Figure 11.** Uv spectra of 3MP-1% HBr at 77°K: (a) before irradiation; (b) after  $\gamma$  dose of  $1.5 \times 10^{19}$  eV g<sup>-1</sup>; (c) after subsequent standing for 19 hr; (d) after subsequent 15-min bleaching with AH-4 lamp with Pyrex filter.

diation annealing for >24 hr at 77°K. In all cases the  $CH_3$  decays were very nearly pure first order at 77°K. (In a preceding section it has been shown that the decay at 74°K in an annealed sample is composite first order).

The relative  $CH_3$  concentrations in 3MP- $h_{14}$  were measured using the height of the second peak from the low-field side of the quartet of the first derivative ESR spectrum. In 3MP- $d_{14}$ -1%  $CH_3I$ , where peak 1 does not overlap the underlying  $C_6D_{13}$  spectrum, its shape (width at half-height of the integral spectrum) does not change with decay, and this is assumed to be so for all the lines in the  $CH_3$  spectrum in both matrices. The underlying 3-methylpentyl radical contribution in the 3MP- $h_{14}$  matrix represented only about 15% of the initial total height and was assumed to be constant for the purpose of evaluating the  $CH_3$  radical decay.

**Effects of Matrix Annealing and Halide Partner on the Rates of Decay of  $CH_3$  in 3MP- $d_{14}$ .** Consistent with earlier results,<sup>8</sup> we find the fractional rate of decay of  $CH_3$  formed by dissociative capture by  $CH_3X$  in a 3MP- $d_{14}$  matrix at 77°K to be at least tenfold slower than in 3MP- $h_{14}$ . In 3MP- $d_{14}$  which had been quenched to 77°K just before irradiation, the rate is not pure first order. Plots of  $\log [CH_3]$  vs. time are curved up to 12-24 hr, after which they are linear as illustrated by data for  $CH_3Br$  in Figure 12. After 24-hr decay the half-lives of the  $CH_3$  radicals in the unannealed 3MP- $d_{14}$  samples are equal to those in the annealed samples. The half-life for decay in samples annealed >2 days at 77°K is independent of annealing time and is very nearly pure first order. In an unannealed sample of 3MP- $d_{14}$ -1%  $CH_3Br$  which was deliberately cracked by thermal shock following irradiation (by transfer between 77 and 72°K), the  $CH_3$  decay was first order with a half-life equal to that in an annealed sample of the same composition (Figure 12).

The half-life for  $CH_3$  decay in an unannealed sample of 1%  $CH_3I$  in 3MP- $d_3$  ( $CH_3CH_2CH(CD_3)CH_2CH_3$ ) was ca. 15 min, in close agreement with that in 3MP- $h_{14}$ . The 3-methylpentyl radical ESR spectrum in 3MP- $d_3$  is the same as that in 3MP- $h_{14}$ , consistent with evidence that the radicals

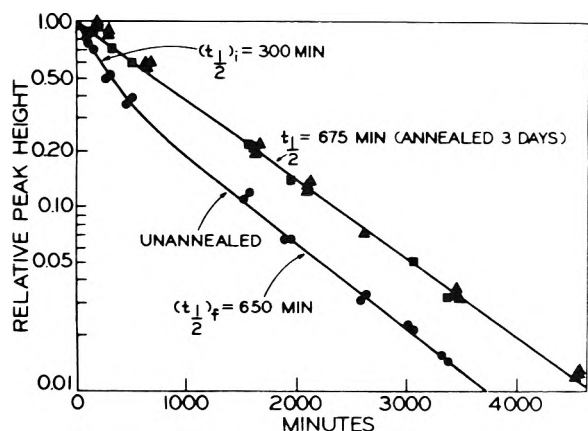


Figure 12. Decay at 77°K of  $\text{CH}_3$  produced in 3MP- $d_{14}$ -1%  $\text{CH}_3\text{Br}$  by  $\gamma$  irradiation: upper curve, triangles represent three different samples annealed for 3 days at 77°K before irradiation; squares represent unannealed sample which was cracked 90 min after irradiation. Lower curve is for unannealed and uncracked sample.

formed by  $\gamma$ -irradiation and by decay of  $\text{CH}_3$  in 3MP- $h_{14}$  are formed by abstraction of a secondary hydrogen.<sup>14,16,18</sup>

Although the rate of decay of  $\text{CH}_3$  radicals in either unannealed or annealed 3MP- $h_{14}$  at 77°K is independent of whether the geminate halide ion is  $\text{Cl}^-$ ,  $\text{Br}^-$ , or  $\text{I}^-$ , in 3MP- $d_{14}$  the half-life is greater for the bromide and iodide than for the chloride in both unannealed and annealed samples (Table II). In unannealed  $\gamma$ -irradiated 3MP- $d_{14}$  at 77°K  $\text{C}_2\text{H}_5$  radicals produced from  $\text{C}_2\text{H}_5\text{Cl}$  decay faster (initial  $t_{1/2} \approx 500$  min) than those produced from  $\text{C}_2\text{H}_5\text{I}$  (initial  $t_{1/2} \approx 2400$  min).

**Effect of Temperature on the Decay of  $\text{CH}_3$  Radicals in 3MP Glass.** Earlier experiments<sup>8</sup> have shown that the half-life of  $\text{CH}_3$  radicals produced by dissociative capture of electrons by  $\text{CH}_3\text{Cl}$  in unannealed 3MP glass decreases rapidly from 16 min to <1 min in the range of 77 to 87°K. Since this is the range just above the glass transition temperature,<sup>23</sup> the changes in rate may result predominately from changes in the rigidity of the matrix rather than from the activation energy of the chemical reaction by which the radicals are lost. In the present work we have determined the decay rates below the glass transition temperature, in the range from 77 to 45°K (Figures 13 and 14). The rates have been measured by the change in the height of peak 2 of the four-line  $\text{CH}_3$  ESR spectrum, corrected for the  $\text{C}_6\text{H}_{13}$  background.

When plotted as  $\log [\text{CH}_3]$  vs. time the data of Figure 13 for temperatures below 77°K show the curvature typical of composite first-order decay, in contrast to the pure first-order decay observed in this and earlier work at 77°K. We have used tangents to the curves of Figure 13 at points of zero decay and 15% decay to compare the rates at different temperatures. The results are shown on the Arrhenius plot of Figure 14. On the basis of limited evidence, the decay rate at temperatures below 77°K appears to be slower in annealed than unannealed samples, as it is at 77°K. The data of Figure 14 indicate that the apparent activation energy of the  $\text{CH}_3$  decay is  $770 \pm 300$  cal/mol at temperatures below 77°K. The earlier data<sup>8</sup> indicate that for the range of 77–87°K it is  $>4$  kcal/mol.

**Radicals Produced by Photolysis of  $\text{CH}_3\text{I}$  in 3MP and 3MP- $d_{14}$ .** Photolysis of alkyl iodides other than  $\text{CH}_3\text{I}$  in 3MP glass at 77°K has been shown to produce trapped 3-methylpentyl radicals but no alkyl radicals characteristic of

TABLE II: Effects of Halide and Annealing on Half-Life for  $\text{CH}_3$  Decay in 3MP- $d_{14}$  at 77°K

Methyl halide <sup>a</sup>	Unannealed samples		Annealed samples <sup>b</sup>
	Initial $t_{1/2}$ , min	Final $t_{1/2}$ , min	
$\text{CH}_3\text{Cl}$	225	375	400
$\text{CH}_3\text{Br}$	300	650	675
$\text{CH}_3\text{I}$	350	650	675

<sup>a</sup> 1 mol % concentration. <sup>b</sup> Samples annealed 3 days at 77°K.

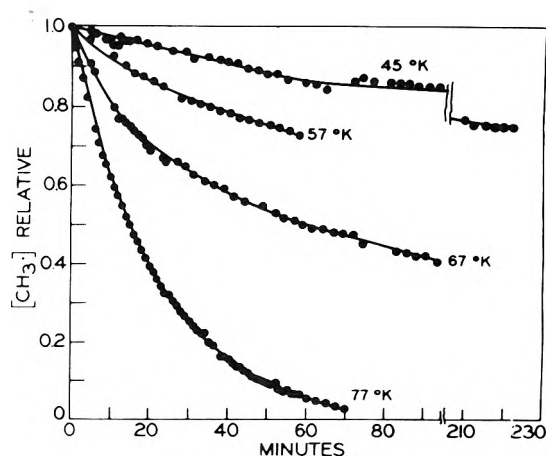


Figure 13. Decay of  $\text{CH}_3$  in  $\gamma$ -irradiated 3MP-1%  $\text{CH}_3\text{I}$  at 77, 67, 57, and 45°K. All samples unannealed. Dose  $1.5 \times 10^{19}$  eV  $\text{g}^{-1}$ .

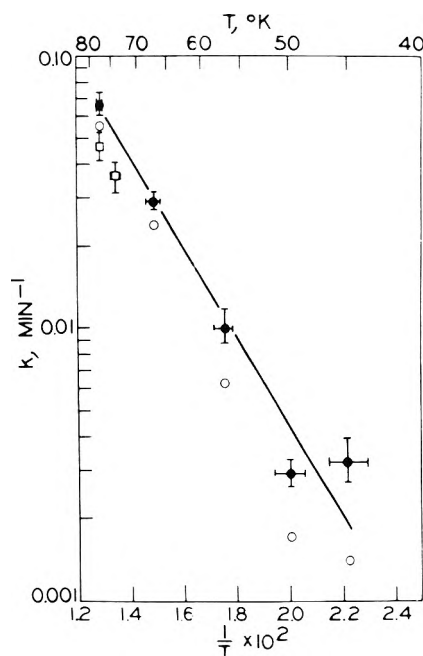


Figure 14. Arrhenius plot of  $\text{CH}_3$  decay rates in  $\gamma$ -irradiated 3MP-1%  $\text{CH}_3\text{I}$ . (●) and (○) represent tangents to the curves of Figure 13 for unannealed samples at 0% decay and 15% decay, respectively. (□) from tangents at 0% decay for annealed samples. Error bars estimated from reproducibility of tangent measurements and temperature fluctuations during decay measurements.

the photolyzed solute.<sup>5,14</sup> This indicates that those radicals which escape geminate recombination with their I atom partner all abstract H from the 3MP. Similarly, all H atoms formed by photolysis of HI in 3MP at 77°K and

below abstract H.<sup>9</sup> In the present work, photolysis of 1 mol % CH<sub>3</sub>I or CD<sub>3</sub>I in 3MP at 77°K with the Vycor filtered medium-pressure lamp or low-pressure mercury lamp has readily produced 3-methylpentyl radicals but no evidence of methyl radicals. Similar illuminations of pure 3MP and of 3MP-1% CH<sub>3</sub>Cl induced no ESR signal. We now believe that the earlier report from our laboratory<sup>9</sup> of trapped CH<sub>3</sub> production from photolysis of CH<sub>3</sub>I in 3MP was in error.

A more sensitive test for production of trapped CH<sub>3</sub> radicals by photolysis of CH<sub>3</sub>I in a hydrocarbon glass was made by using a 3MP-*d*<sub>14</sub>-1% CH<sub>3</sub>I matrix. More radicals might be expected to escape the hot abstraction reaction and be trapped in a medium of C-D bonds than in C<sub>6</sub>H<sub>14</sub>. Furthermore, the sensitivity of detection is increased because the outer lines of the CH<sub>3</sub> ESR quartet are free of overlap from the relatively narrow C<sub>6</sub>D<sub>13</sub> spectrum.

Two identical Suprasil tubes (2 mm i.d., 3 mm o.d.), containing annealed samples of 1 mol % CH<sub>3</sub>I and 1 mol % HI, respectively, in 3MP-*d*<sub>14</sub> were photolyzed for 1 min each at ~72°K in the center of the spiral low-pressure mercury arc with Vycor filter with an intensity of ~10<sup>16</sup> photons sec<sup>-1</sup> cm<sup>-1</sup> height of sample. Since both samples were nearly opaque at 254 nm (optical densities of >2 for a 2-mm path), equal numbers of photons were absorbed. Comparison of the double integrals of the first derivative ESR absorption spectra indicates that the quantum yield for C<sub>6</sub>D<sub>13</sub> production by the 254-nm photolysis of CH<sub>3</sub>I in 3MP-*d*<sub>14</sub> is ~2.4 × 10<sup>-3</sup> assuming a yield<sup>9</sup> of 0.11 for C<sub>6</sub>D<sub>13</sub> from the photolysis of HI in glassy 3MP-*d*<sub>14</sub>. By increasing the illumination of the CH<sub>3</sub>I sample and the ESR sensitivity, a detectable ESR signal for the outer lines of the CH<sub>3</sub> spectrum was obtained. The ratio of trapped CH<sub>3</sub> radicals to C<sub>6</sub>D<sub>13</sub> radicals is estimated to be ~0.02. The result is in dramatic contrast to the CH<sub>3</sub>/C<sub>6</sub>D<sub>13</sub> ratio of 1.8 (Table I) resulting from dissociative electron capture by CH<sub>3</sub>I in 3MP-*d*<sub>14</sub> at 72°K.

The rate of decay of the CH<sub>3</sub> formed by photolysis of CH<sub>3</sub>I in 3MP-*d*<sub>14</sub> was determined at 77°K from the change in line height of the first derivative spectrum as observed at high spectrometer gain. The initial quarter-life was less than 20 min and the initial half-life less than 100 min, as compared to the initial half-life of 675 min (Table II) in annealed γ-irradiated 3MP-*d*<sub>14</sub>-1% CH<sub>3</sub>I samples.

The initial ESR spectrum of the C<sub>6</sub>H<sub>13</sub> radicals formed by photolysis of CH<sub>3</sub>I in 3MP at 77°K was better resolved than that produced by γ radiolysis and the resolution did not change with decay as the latter does. Decay rates measured at 60 mW were the same as those measured at 0.4 mW. The spectral resolution was poorer at 60 mW, but did not change with decay.

The C<sub>6</sub>H<sub>13</sub> radicals produced by photolysis of CH<sub>3</sub>I in 3MP decay more slowly than those produced by photolysis of HI (initial *t*<sub>1/4</sub> and *t*<sub>1/2</sub> = ~8 and ~40 min, respectively, as compared to ~2 and ~10 min, respectively<sup>8</sup>).

## Discussion

**Radical Decay Kinetics, Spectral Resolution, and Spatial Distribution of Radicals.** The dose-independent decay of the first ~57% of the radicals produced by γ irradiation of 3MP-*h*<sub>14</sub> glass (Figure 2) must result from combination and disproportionation between radicals within the parent spur. The fractional rate of decay decreases with time because the average time between intraspur radical encounters becomes longer as the small population of radicals in each spur is decreased by reaction and by diffusion away.

There is evidence that initial radical-radical distances in the spurs may be of the order of 15 Å,<sup>3</sup> and it is plausible to assume that ~3 ± 1 radicals are formed per spur. Approximately 43% of these escape intraspur reaction and react with radicals from other spurs and tracks after random diffusion, giving the second-order portion of Figure 1. Radical pairs have been detected in γ-irradiated 3MP glass at 77°K, but is not yet known whether these result from a mechanism of pair production during irradiation, or only from pair production by diffusive encounters.<sup>3</sup>

The improvement in resolution of the ESR spectra of the radicals produced by γ irradiation of 3MP glass as decay progresses (Figure 3C) is presumed to be due to a decrease in line broadening by electron dipole interactions between closely spaced radicals, as these radicals are removed by intraspur decay. Consistent with this interpretation, the resolution of the spectra of C<sub>6</sub>H<sub>13</sub> radicals formed randomly in 3MP glass by the hot radicals formed in the photolysis of CH<sub>3</sub>I (CH<sub>3</sub>\* + C<sub>6</sub>H<sub>14</sub> → C<sub>6</sub>H<sub>13</sub> + CH<sub>4</sub>) is equivalent to that after prolonged decay in γ-irradiated samples. Also, the initial resolution in γ-irradiated 3MP containing CH<sub>3</sub>I is better than in pure 3MP. In the γ-irradiated system hot CH<sub>3</sub> radicals which can produce C<sub>6</sub>H<sub>13</sub> by abstraction may be produced by dissociative capture of electrons which have escaped<sup>13</sup> some distance from the center of the radical spurs.

The cause of the dramatic and reversible photoinduced change in the ESR spectrum of radicals in γ-irradiated 3MP with no significant change in radical concentration (Figure 5) is not obvious. Speculatively, it may involve rearrangement of the radical to a higher energy configuration in the trap from which it reverts slowly to the most stable configuration. A reversible chemical isomerization must also be considered.

Another example of change in ESR spectral resolution during radical decay has been observed for C<sub>2</sub>H<sub>5</sub> radicals produced from 1% C<sub>2</sub>H<sub>5</sub>Cl or C<sub>2</sub>H<sub>5</sub>I in γ-irradiated 3MP-*d*<sub>14</sub>. The strongest lines of the C<sub>2</sub>H<sub>5</sub> first derivative spectrum become narrower and increase in height by some 25% during the first 70-min decay, during which the radical concentration decreases by 15%.

**Rate Constants and Diffusion Coefficients.** Assuming that the straight line portions of Figure 1 represent the bimolecular decay of 3-methylpentyl radicals which are randomly distributed in 3MP glass at 77°K, the second-order rate constant *k* from the relation  $-\frac{1}{2}(d[C_6H_{13}]/dt) = k(C_6H_{13})^2$  for the sum of the combination and disproportionation processes is 9.5 × 10<sup>-5</sup> M<sup>-1</sup> sec<sup>-1</sup>. Assuming reaction on every radical-radical encounter, the diffusion coefficient of C<sub>6</sub>H<sub>13</sub> may be estimated to be  $D = 9.0 \times 10^{-20}$  cm<sup>2</sup> sec<sup>-1</sup> ( $k = 1.6 \times 10^{-25}$  cm<sup>3</sup> molecule<sup>-1</sup> sec<sup>-1</sup> =  $4\pi d[D_{C_6H_{13}} + D_{C_6H_{13}}]$ ); the diameter (*d*) of the C<sub>6</sub>H<sub>13</sub> radical is taken as 7 Å. Use of the Stokes-Einstein equation,  $D = kT/6\pi\eta r$ , with the viscosity ( $\eta$ ) as 2.2 × 10<sup>12</sup> P<sup>23</sup> and the radius (*r*) as 3.5 Å yields  $D = 7.4 \times 10^{21}$  cm<sup>2</sup> sec<sup>-1</sup>. The latter relation tends to yield values of *D* much below observed values in glassy matrices.<sup>24</sup>

In earlier work of our laboratory,<sup>8</sup> the decay of 3-methylpentyl radicals produced by γ irradiation of 3MP at 77°K was measured at 87°K. All of the radicals observed decayed by a pure second-order process, 85% disappearing in 40 min. The rate constant was reported as 1.7 × 10<sup>-21</sup> cm<sup>3</sup> molecule<sup>-1</sup> sec<sup>-1</sup> and the diffusion coefficients calculated by the Smoluchowski and Stokes-Einstein equations as 2 × 10<sup>-15</sup> and 2 × 10<sup>-16</sup> cm<sup>2</sup> sec<sup>-1</sup>, respectively. At that time it

was thought that  $G(\text{C}_6\text{H}_{13})$  in 3MP at 77°K was 1.6 rather than 3.0, and it was not known that the radicals which decay by intraspur encounter (ca. 57%) are eliminated during warming from 77 to 87°K. Fortunately, these factors compensate for each other, leaving the calculated values of the rate constant and diffusion coefficient essentially unchanged. It is of interest that when our value of the diffusion coefficient at 77°K is used to predict the value of 87°K on the assumption that the coefficient is inversely proportional to the viscosity, it gives  $4 \times 10^{-15} \text{ cm}^2 \text{ sec}^{-1}$  in substantial agreement with the reported<sup>8</sup> value of  $2 \times 10^{-15} \text{ cm}^2 \text{ sec}^{-1}$ . An experiment by Vlatkovic in our laboratory<sup>8</sup> showed that the radicals produced in 3MP by a very large  $\gamma$  dose ( $1.2 \times 10^{21} \text{ eV g}^{-1}$ ) decay by 85% in 100 hr at 77°K by second-order kinetics. This dose (~400 min) was sufficiently long so that the ratio of long-lived radicals to those capable of rapid intraspur decay was high and the latter were obscured.

*Decay of  $\text{C}_6\text{H}_{13}$  and  $\text{C}_6\text{D}_{13}$  in 3MP- $h_{14}$  and 3MP- $d_{14}$  Glasses Containing Hydrogen Halides.* An enlarged plot of the data for the early portions of the decay curves of Figure 8 indicates that the fractional decay rates of  $\text{C}_6\text{H}_{13}$  in 3MP glass and 3MP glasses containing hydrogen halides are all the same, within experimental error, up to ca. 30% decay. After 30% decay, the rates in the glasses containing HI are much faster than those in pure 3MP or 3MP containing HCl, and are first order in the concentration of  $\text{C}_6\text{H}_{13}$  over the tenfold or more decays of Figure 8. The single point for HBr decay suggests that it is similar to the HI decay.

We interpret this to indicate that in the presence of HI reaction of the  $\text{C}_6\text{H}_{13}$  radicals with the HI by the  $\text{C}_6\text{H}_{13} + \text{HI} \rightarrow \text{C}_6\text{H}_{14} + \text{I}$  process predominates over intraspur radical-radical reaction after the first 30% decay, at which point the decay kinetics become pseudo-first order. HCl, unlike HI and HBr, does not increase the rate of decay because the activation energy of the  $\text{C}_6\text{H}_{13} + \text{HCl} \rightarrow \text{C}_6\text{H}_{14} + \text{Cl}$  reaction, which is endothermic by ca. 9 kcal mol<sup>-1</sup>, is too high. The  $\text{C}_6\text{H}_{13}$  ESR spectrum changes to the broad singlet (Figure 9) attributed to a  $\text{C}_6\text{H}_{13} \cdot \text{HCl}$  complex, but the concentration of spins changes no faster than in pure 3MP. The abstractions of hydrogen from HI and HBr by the  $\text{C}_6\text{H}_{13}$  radicals are exothermic and expected to have low activation energies.<sup>25</sup> Further, the activation energy for hydrogen abstraction from HI and HBr by radicals in glasses may be lowered by matrix effects or tunneling, as is the activation energy for abstraction from C-H bonds.<sup>16,18,21,26</sup>

The fraction of the radicals in  $\text{C}_6\text{D}_{14}$ -1% HI for which the decay is not influenced by the HI seems to be less than in  $\text{C}_6\text{H}_{14}$ -1% HI (Figure 8). This implies that there are fewer radicals per spur or greater average interradical distances within the spurs in the deuterated matrices. If  $G$  (total spurs) is the same in the two pure matrices, the number of radicals per spur must be smaller in the deuterated matrix since  $G(\text{radicals}) = 2.0$  in  $\text{C}_6\text{D}_{14}$  and 3.0 in  $\text{C}_6\text{H}_{14}$ . If added HI results in production of  $\text{C}_6\text{D}_{13}$  radicals by the  $\text{C}_6\text{D}_{14} + \text{H}^* \rightarrow \text{C}_6\text{D}_{13} + \text{HD}$  reaction of hot H atoms formed by dissociative electron capture, the radicals so formed may be produced with greater average separation than the radicals formed by excitation and/or charge neutralization events. This is probable since it is known that in pure hydrocarbon glasses electrons migrate faster from the sites of their formation and are trapped in "expanded" spurs compared to the "intrinsic" spurs<sup>3,13</sup> of the radicals. Thus the dissociative electron capture by HI may occur in expanded spurs. The yield of scavengeable electrons is sig-

nificantly higher in  $\text{C}_6\text{D}_{14}$  than  $\text{C}_6\text{H}_{14}$  glass (as discussed later). Thus the proportion of the radicals which are more widely separated than those in the intrinsic spurs is probably greater in  $\text{C}_6\text{D}_{14}$  than  $\text{C}_6\text{H}_{14}$  and may have significant influence on the initial fractional rates of decay in pure and mixed 3MP- $d_{14}$  systems such as shown in Figure 8. The yield of the radicals formed by hot H from HI is equal to the increase in  $G(\text{C}_5\text{D}_{13})$  in the HI system as compared to the yield in pure 3MP- $d_{14}$ , unless HI decreases the intrinsic yield by charge scavenging or energy transfer, as do biphenyl and  $\text{C}_3\text{D}_7\text{I}$  in 3MP- $h_{14}$ , in which case the yield from abstraction by hot H may be much larger.

The rate law for the decay of radicals after 1000 min in the 3MP glasses containing HI and HBr may be written as

$$\frac{-d[\text{C}_6\text{H}_{13}]}{dt} = k[\text{HX}][\text{C}_6\text{H}_{13}] = k'[\text{C}_6\text{H}_{13}]$$

The data of Figure 8 for the systems containing HI give values of  $k$  lying in the range of  $8.7 \pm 1.9 \times 10^{-5} \text{ M}^{-1} \text{ sec}^{-1}$ , assuming the nominal values of 0.5 and 1 mol % (0.05 and 0.1  $M$ ) for [HI], and the measured value of  $8 \times 10^{-4} M$  for  $[\text{C}_6\text{H}_{13}]$ . The sum of the diffusion coefficients  $D_{\text{HI}}$  and  $D_{\text{C}_6\text{H}_{13}}$  may be estimated to be  $2.3 \times 10^{-19} \text{ cm}^2 \text{ sec}^{-1}$  from the relation  $k = 1.5 \times 10^{-25} \text{ cm}^3 \text{ molecule}^{-1} \text{ sec}^{-1} = 4\pi(r_{\text{HI}} + r_{\text{C}_6\text{H}_{13}})(D_{\text{HI}} + D_{\text{C}_6\text{H}_{13}})$ , the radii ( $r$ ) being taken as  $1.6 \times 10^{-8}$  and  $3.5 \times 10^{-8} \text{ cm}$ , respectively. Assuming  $D$  is proportional to  $1/r$ , in accord with the Stokes-Einstein equation ( $D = kT/6\pi\eta r$ ), this sum may be partitioned to give  $D_{\text{HI}} = 1.6 \times 10^{-19} \text{ cm}^2 \text{ sec}^{-1}$ , and  $D_{\text{C}_6\text{H}_{13}} = 7.4 \times 10^{-20} \text{ cm}^2 \text{ sec}^{-1}$ . Alternatively the value of  $9.0 \times 10^{-20} \text{ cm}^2 \text{ sec}^{-1}$  for  $D_{\text{C}_6\text{H}_{13}}$  in pure 3MP (see above) may be substituted, giving a value of  $D_{\text{HI}}$  of  $1.4 \times 10^{-19} \text{ cm}^2 \text{ sec}^{-1}$ .<sup>27</sup>

The results of the diffusion coefficient calculations suggest that clumping of HI molecules when the 3MP-1% HI solutions are cooled to 77°K is not significant. If clumping occurred, the value used for [HI] would have been too large, and the rate constant ( $k = k'/[\text{HI}]$ ) and the value of  $(D_{\text{HI}} + D_{\text{C}_6\text{H}_{13}})$  obtained would have been too small. Partitioning the sum on the basis of the assumed radii would therefore yield a diffusion coefficient for  $\text{C}_6\text{H}_{13}$  lower than that determined in pure 3MP, rather than the agreement observed.

The relatively fast decay of  $\text{C}_6\text{H}_{13}$  radicals produced by abstraction by hot H atoms from the photolysis of HI in  $\text{C}_6\text{H}_{14}$ ,<sup>8,9</sup> compared to those produced by  $\gamma$  radiolysis of 3MP, presumably results from combination of the  $\text{C}_6\text{H}_{13}$  with its sibling I atom.<sup>8,9</sup> The longer half-life of the  $\text{C}_6\text{H}_{13}$  formed by photolysis of  $\text{CH}_3\text{I}$  than by photolysis of HI (see above) suggests that the geometry for the  $\text{C}_6\text{H}_{13} + \text{I}$  sibling reaction is less favorable when  $\text{CH}_4$  is the cage partner than when it is  $\text{H}_2$ .

*$\text{C}_6\text{H}_{13}$ -HX Complexes.* The loss of resolution in the ESR spectrum of  $\text{C}_6\text{H}_{13}$  radicals in  $\text{C}_6\text{H}_{14}$ -1% HCl glasses with time following  $\gamma$  irradiation, and the regeneration of the spectrum on photolysis (Figure 9) indicate formation and photodecomposition of a  $\text{C}_6\text{H}_{13} \cdot \text{HCl}$  complex. The photodecomposition, which resulted in 25% loss of signal in our test, may plausibly be by two routes:  $\text{C}_6\text{H}_{13} \cdot \text{HCl} + h\nu \rightarrow \text{C}_6\text{H}_{14} + \text{Cl}$ , accompanied by<sup>28</sup>  $\text{Cl} + \text{C}_6\text{H}_{14} \rightarrow \text{C}_6\text{H}_{13} + \text{HCl}$ ; and  $\text{C}_6\text{H}_{13} \cdot \text{HCl} + h\nu \rightarrow \text{C}_6\text{H}_{13} + \text{HCl}$ . The net loss may imply some trapping of the Cl atoms produced by route 1. Unlike the complex formed in  $\gamma$ -irradiated 3MP- $\text{Cl}_2$  glasses,<sup>28</sup> which produces a change in the  $\text{C}_6\text{H}_{13}$  ESR signal similar to that of Figure 9, formation of the HCl complex is not accompanied by a uv absorption peak at 260

nm (a maximum may occur below the 200-nm limit of this measurement). It appears that the complexes formed in the HCl and Cl<sub>2</sub> systems are different, but that each involves broadening of the ESR spectrum by interaction with a Cl nucleus. In the HCl system there was no evidence for the Cl<sub>2</sub><sup>-</sup> ESR spectrum on the low-field side of the C<sub>6</sub>H<sub>13</sub> signal which was seen<sup>28</sup> in the Cl<sub>2</sub> work.

Evidence for C<sub>6</sub>H<sub>13</sub>·HX complex formation in the HBr and HI systems is less definite than in the HCl system. It is suggested by the failure of the resolution of the initial C<sub>6</sub>H<sub>13</sub> ESR spectra to improve on decay. Also, the 360-nm peak which grows in the 3MP-HBr glass following radiolysis (Figure 11) and the 395-nm peak reported previously<sup>29</sup> to grow in the 3MP-HI glass may be due to such complexes. The ability of C<sub>6</sub>H<sub>13</sub> radicals to abstract from HI and HBr (C<sub>6</sub>H<sub>13</sub> + HX → C<sub>6</sub>H<sub>14</sub> + X) but not from HCl may explain why a sufficient concentration of complexes to broaden the ESR spectra significantly is not built up in these systems. Past experience indicates that line broadening precludes observation of the ESR signal of I atoms in 3MP glass.<sup>30</sup>

*Effects of Additives on G(C<sub>6</sub>H<sub>13</sub>) in γ-Irradiated 3MP.* The reduction in G(C<sub>6</sub>H<sub>13</sub>) in γ-irradiated 3MP glass from 3.0 to 2.4 by 0.1% biphenyl and by about the same amount by 1% C<sub>3</sub>D<sub>7</sub>I (Table I and Figure 7), both of which scavenge both electrons and positive charge, suggests that charge neutralization of C<sub>6</sub>H<sub>14</sub><sup>+</sup> or C<sub>6</sub>H<sub>15</sub><sup>+</sup> is responsible for at least part of the radical production in pure 3MP. The alternative possibility that the radical production is reduced as a result of excitation transfer to these molecules from excited matrix molecules seems less probable.

Indirect evidence indicates that CH<sub>3</sub>I also reduces the yield of C<sub>6</sub>H<sub>13</sub> from the radiolysis of 3MP, but that this reduction is compensated by production of radicals by abstraction by hot CH<sub>3</sub> radicals (CH<sub>3</sub>\* + C<sub>6</sub>H<sub>14</sub> → CH<sub>4</sub> + C<sub>6</sub>H<sub>13</sub>). G(C<sub>6</sub>H<sub>13</sub>) from the radiolysis of 3MP containing 1 mol % CH<sub>3</sub>I is the same as in pure 3MP (3.0) within the certainty of the measurement based on the height of the outer line. In 3MP-d<sub>14</sub>-1% CH<sub>3</sub>I the hot abstraction reaction (CH<sub>3</sub>\* + C<sub>6</sub>D<sub>14</sub> → CH<sub>3</sub>D + C<sub>6</sub>H<sub>13</sub>) is clearly demonstrated, G(CH<sub>3</sub>D) being 0.7.<sup>16</sup>

HCl, HBr, and HI are not expected to scavenge positive charge in γ-irradiated 3MP, since their ionization potentials are 13.8, 13.2, and 12.8 eV while that of 3MP is 10.1. HI in an argon matrix at 4°K is, however, able to capture electrons produced by photoionization of metals to yield H and I<sup>-</sup>.<sup>31</sup> In the gas phase all three hydrogen halides undergo dissociative electron capture,<sup>32</sup> but for HCl and HBr the process from the ground state is endothermic by 0.88 and 0.44 eV, respectively, and the measured appearance potentials of X<sup>-</sup> at room temperature are 0.64 and 0.11 eV. For HI, the process is essentially thermoneutral and the appearance potential is zero. The cross sections of HCl, HBr, and HI for e<sup>-</sup> capture in the gas phase have been given as 2 × 10<sup>-17</sup>, 3 × 10<sup>-16</sup>, and 2 × 10<sup>-14</sup> cm<sup>2</sup>, respectively.<sup>32</sup> These large differences in properties in the gas phase are in striking contrast to the similarity in the effects of HCl and HI on the G(C<sub>6</sub>H<sub>13</sub>) value in γ-irradiated 3MP glass. Both of the halides appear to increase the value by ca. 20% of that in pure 3MP (from 3.0 to ca. 3.6). The increase in G(C<sub>6</sub>H<sub>13</sub>) seems to require dissociative electron capture (HX + e<sup>-</sup> → H + X<sup>-</sup>) followed by abstraction (H + C<sub>6</sub>H<sub>13</sub> → C<sub>6</sub>H<sub>14</sub> + H<sub>2</sub>), unless energy transfer from the matrix to the HX is unexpectedly efficient. Since it is not known whether the hydrogen halides reduce the "direct" yield of

C<sub>6</sub>H<sub>13</sub> from 3MP, as biphenyl and C<sub>3</sub>D<sub>7</sub>I appear to do, the data leave open the question as to whether the G value of hot abstraction is 3.6 - 3.0 = 0.6 or 3.6 - 2.4 = 1.2. For HCl and HBr the endothermic dissociation process requires capture of electrons of greater than thermal energy. Still higher energy is required to produce hot hydrogen atoms.

It appears possible that the similarity of the electron capture reactions of HCl and HI in 3MP glass as compared to the contrasting reaction parameters in the gas (and similar contrasts for the reactions of CH<sub>3</sub>Cl, CH<sub>3</sub>Br, and CH<sub>3</sub>I) are the result of the high probability of capture of electrons in the subexcitation energy range of the 3MP matrix. The first singlet excitation level of 3MP is expected to be ca. 7-8 eV; triplet levels at 6 and possibly 3 eV have been indicated by thin film studies.<sup>33</sup>

*Effect of Deuteration on Radical Yields.* Differences in radical yields from the γ irradiation of 3MP-d<sub>14</sub> and 3MP-h<sub>14</sub> glasses indicate heretofore unrecognized isotope effects. Thus G(3-methylpentyl radicals) is 2.0 in C<sub>6</sub>D<sub>14</sub> in contrast to 3.0 in C<sub>6</sub>H<sub>14</sub>. In the presence of 1% CH<sub>3</sub>I the total radical yield in 3MP-d<sub>14</sub> is 3.6, of which 2.3 is due to CH<sub>3</sub> radicals. This indicates a lowering of the yield of C<sub>6</sub>D<sub>13</sub> to 1.3 from 2.0 by the presence of the CH<sub>3</sub>I. The yield of CH<sub>3</sub>D, presumed to result from abstraction of D by hot CH<sub>3</sub> radicals, is 0.7.<sup>16</sup> This implies that G(C<sub>6</sub>D<sub>13</sub>) produced directly as a result of the γ irradiation is 1.3 - 0.7 = 0.6 in the 3MP-d<sub>14</sub>-CH<sub>3</sub>I matrix. The reduction of 70% from the value in pure 3MP-d<sub>14</sub> is much greater than the reduction from 3.0 to 2.2-2.4 (~25%) caused by biphenyl and C<sub>3</sub>D<sub>7</sub>I in 3MP-h<sub>14</sub>. Presumably, G(C<sub>6</sub>D<sub>13</sub>) would also be 0.6 in the presence of biphenyl, but the overlapping ESR spectra of the C<sub>6</sub>D<sub>13</sub> radical and the biphenylide ion preclude a satisfactory test of this. It is of significance that the total yield of CH<sub>3</sub> (that which abstracts plus that which is trapped) is 3.0 in C<sub>6</sub>D<sub>14</sub> and only 1.5 in C<sub>6</sub>H<sub>14</sub>. This implies a higher yield of scavengeable electrons from the γ irradiation of C<sub>6</sub>D<sub>14</sub> glass than from C<sub>6</sub>H<sub>14</sub> glass. Other evidence for enhanced charge scavenging is our observation that when 0.1 mol % solutions of biphenyl in 3MP-h<sub>14</sub> glass and 3MP-d<sub>14</sub> glass are given equal γ doses the optical density increase at 410 nm, due to biphenyl anions (with possible contribution from cations) is 50% greater in the deuterated matrix. In related experiments Hager of our laboratory has recently found that 2MP-1 which is known to enhance the G(e<sub>1</sub><sup>-</sup>) in 3MP-h<sub>14</sub> glass,<sup>34,35</sup> presumably by stabilization of positive charge, enhances it much more in 3MP-d<sub>14</sub>. It is important that this matrix isotope effect be investigated further. Whatever the mechanism responsible for the effect, it must be consistent with the evidence that the G values for individual stable hydrocarbon products measured after warm-up of γ-irradiated samples of C<sub>6</sub>H<sub>14</sub> and C<sub>6</sub>D<sub>14</sub> are indistinguishable.<sup>36</sup> There is evidence that hot methyl radicals produced by the photolysis of CH<sub>3</sub>I in hydrocarbon matrices at 77°K abstract with equal probability from C-H and C-D bonds.<sup>37</sup>

*Effect of Temperature on Rate of CH<sub>3</sub> Decay in 3MP Glass.* When first-order decay of CH<sub>3</sub> produced by dissociative capture by methyl halides in 3MP at 77°K was first observed,<sup>5,6</sup> it was reasoned<sup>5</sup> that a mechanism of pseudo-first-order abstraction of H from the C<sub>1</sub>H<sub>4</sub> matrix was precluded by the activation energy, unless the energy required in the glassy state is very much lower than that in the gas. With the evidence that abstraction is indeed the method of decay of CH<sub>3</sub> in C<sub>6</sub>H<sub>14</sub> at 77 and 74°K, it is clear that a low activation energy route (<1 kcal mol<sup>-1</sup>) is available for the



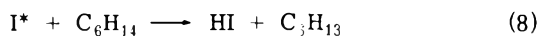
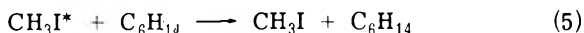
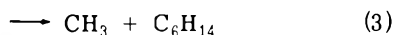
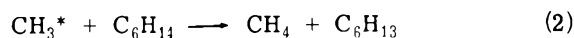
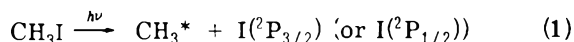
abstraction. There are two alternative explanations for the lowering of the activation energy: (1) the intermolecular constraining forces in the glass distort the molecules in a manner to provide a lower activation energy pathway than is available in the gas; (2) quantum mechanical tunneling occurs. Present knowledge does not allow a decision as to which is correct. The tunneling hypothesis, which has been considered in some detail for abstraction by  $\text{CH}_3$  in polycrystalline  $\text{CH}_3\text{CN}$ ,  $\text{CH}_3\text{NC}$ , and  $\text{CH}_3\text{OH}$ ,<sup>26</sup> is plausible.

The rate of  $\text{CH}_3$  decay in 3MP- $d_{14}$  increases more rapidly with temperature above 77°K (apparent  $E_A \cong 7$  kcal mol<sup>-1</sup>) than the rate in 3MP- $h_{14}$ .<sup>8</sup> This may reflect the differences in decay mechanism observed<sup>16</sup> in the two matrices at 77°K. In 3MP- $h_{14}$   $\text{CH}_3$  decays by abstraction of H from the  $\text{C}_6\text{H}_{14}$ , while in 3MP- $d_{14}$  abstraction does not occur and the decay reaction is apparently  $\text{CH}_3 + \text{I}^- \rightarrow \text{CH}_3\text{I}^-$ .

In  $\text{C}_6\text{D}_{14}$  in which ~1% of the total carbon-hydrogen bonds are C-H rather than C-D, 17% of the  $\text{CH}_3$  radicals abstract to form  $\text{CH}_4$  when they are allowed to decay at 77°K before warm-up, but no  $\text{CH}_4$  is formed when the sample is warmed immediately after irradiation.<sup>16</sup> This suggests that the geminate recombination is more favored by increasing temperature than the C-H abstraction in a glass where diffusion is required for the latter to occur. In 3MP- $h_{14}$  all  $\text{CH}_3$  decay appears to be by abstraction at 77 and 74°K and may be presumed to be so at lower temperature.

**Radical Production by Photolysis of  $\text{CH}_3\text{I}$  in 3MP- $h_{14}$  and 3MP- $d_{14}$ .** Photolysis of  $\text{CH}_3\text{I}$  in the gas phase with 254-nm light produces  $\text{CH}_3$  radicals and I atoms with 59 kcal mol<sup>-1</sup> in excess of the energy required for bond rupture if the I is in the ground state and 39 kcal mol<sup>-1</sup> if it is in the  $\text{I}(^2\text{P}_{1/2})$  state. Because of the mass difference, >90% of this energy is in the translational, vibrational, and rotational degrees of freedom of the  $\text{CH}_3$ . There is evidence<sup>38</sup> that ~80% is translational for photodissociation at 266 nm.

In glassy 3MP and 3MP- $d_{14}$  the following reactions and their  $\text{C}_6\text{D}_{14}$  analogs must be considered:



The low quantum yields for  $\text{C}_6\text{D}_{13}$  ( $\sim 2.4 \times 10^{-3}$ ) and  $\text{CH}_{3\text{tr}}$  ( $\sim 5 \times 10^{-5}$ ) production in  $\text{C}_6\text{D}_{14}$  indicate that reaction 2, reaction 3 followed by reaction 7, and reaction 8 are improvable. Thus most of the activated  $\text{CH}_3\text{I}$  molecules must either be deactivated by (5) or by prompt geminate recombination following (1), or undergo a concerted reaction of the type of (6). The extent of (6) is amenable to test by analysis for the  $\text{C}_6\text{D}_{13}\text{I}$  and  $\text{CH}_3\text{D}$ . Analogous concerted reactions have been observed in the photolysis of HI in 3MP ( $\text{HI}^* + \text{C}_6\text{H}_{14} \rightarrow \text{C}_6\text{H}_{13}\text{I} + \text{H}_2$ ) and of  $\text{Cl}_2$  in  $\text{C}_6\text{H}_{14}$

( $\text{Cl}_2 + \text{C}_6\text{H}_{14} \rightarrow \text{C}_6\text{H}_{13}\text{Cl} + \text{HCl}$ ) with quantum yields of 0.2<sup>9</sup> and 0.5,<sup>28</sup> respectively.

In view of the low radical yields from the photolysis of  $\text{CH}_3\text{I}$  in 3MP- $d_{14}$ , the product yields from the dissociative electron capture process are surprising (i.e.,  $G(\text{CH}_3\text{D}_{\text{hot}}) = 0.7$  and  $G(\text{CH}_{3\text{tr}}) = 2.3$ ). Assuming  $G(e^- \text{ total}) = 4$ , 75% of all the electrons produced in the system are captured by 1%  $\text{CH}_3\text{I}$  to result in either production of  $\text{C}_6\text{H}_{13}$  by abstraction or  $\text{CH}_3$  tapping. By contrast <0.3% of the 254-nm photons absorbed by  $\text{CH}_3\text{I}$  in the photolysis experiments led to either of these products. For the trapped radicals which are produced in the radiolysis, the ratio of  $\text{CH}_3$  to  $\text{C}_6\text{H}_{13}$  is 100-fold higher than in the photolysis. Since the total energy available from the dissociative capture process with thermal electrons is  $\sim 12$  kcal mol<sup>-1</sup>, which is less than that from the photochemical process, it would appear that the difference in effectiveness is the result of a difference in distribution of the energy of the methyl radical between translational and vibrational, unless dissociative capture by electrons of greater than thermal energy is very significant. There is evidence that 254-nm photodissociation of  $\text{CH}_3\text{I}$  may produce  $\text{CH}_3$  with the excess energy predominately as translational.<sup>38-40</sup>

**Effect of Halide Partner on Rate of Decay of Alkyl Radicals Produced by Dissociative Electron Capture.** The present work confirms earlier work<sup>5,8</sup> showing that the rate of decay of  $\text{CH}_3$  radicals produced by the  $\text{CH}_3\text{X} + e^- \rightarrow \text{CH}_3 + \text{X}^-$  process in 3MP- $h_{14}$  at 77°K is independent of whether X is Cl, Br, or I, but shows that in 3MP- $d_{14}$  the half-lives of both  $\text{CH}_3$  and  $\text{C}_2\text{H}_5$  are shorter when the geminate partner is  $\text{Cl}^-$  than when it is  $\text{Br}^-$  or  $\text{I}^-$ . Thus it appears (as is reasonable) that the rate of the  $\text{CH}_3 + \text{C}_6\text{H}_{14} \rightarrow \text{CH}_4 + \text{C}_6\text{H}_{13}$  process, which occurs in the protiated matrix, is unaffected by the nature of the geminate halide ion, whereas the  $\text{CH}_3 + \text{X}^- \rightarrow \text{CH}_3\text{X}^-$  process, reasoned to account for  $\text{CH}_3$  decay in the deuterated matrix, proceeds more rapidly with the smaller halide ion. The much faster decay of  $\text{CH}_3$  formed by photolysis of  $\text{CH}_3\text{I}$  in 3MP- $d_{14}$  than of that formed by dissociative electron capture (half-lives of <100 and 675 min, respectively, in annealed samples) indicates that the geminate recombination with a neutral atom ( $\text{CH}_3 + \text{I} \rightarrow \text{CH}_3\text{I}$ ) proceeds more readily than that with the ion ( $\text{CH}_3 + \text{I}^- \rightarrow \text{CH}_3\text{I}^-$ ). It is probable that for both mechanisms the radical must rearrange from the planar to tetrahedral form. For the iodide ion an added limitation may arise related to the polarized solvent surroundings or to the size.

**Annealing Effects.** The results reported here include the first evidence of which we are aware that the rate of radical decay in a hydrocarbon matrix is dependent upon the time of annealing of the matrix near the glass transition temperature. For samples of 3MP- $h_{14}$  annealed for >2 days at 77°K in 2-mm i.d. ESR tubes the initial quarter-life at 77°K of  $\text{C}_6\text{H}_{13}$  is 150 min, as compared to 40 min for samples irradiated immediately after quench cooling. The quarter-life of  $\text{CH}_3$  radicals produced by dissociative capture by methyl halides in annealed samples is 12 min as compared to 8 min for unannealed samples. Results for methyl radicals from dissociative capture in 3MP- $d_{14}$  are given in Table II and illustrated in Figure 12. Thus annealing affects the rate of intraspur radical-radical reaction in 3MP, the rate of  $\text{CH}_3$  decay by hydrogen abstraction in 3MP- $h_{14}$  and the rate of  $\text{CH}_3$  decay in 3MP- $d_{14}$  where decay is presumed to be by combination with the geminate halide partner. It is not possible to determine the effect of

annealing on the random second-order radical-radical combination (Figure 1) because the major portion of the annealing in a 2-m.m i.d. ESR tube is complete before the second-order process is resolved from the intraspur decay. Figure 12 shows the effect observed when annealing occurs on a time scale similar to the decay half-life. In the annealed sample the decay follows a linear log  $[CH_3]$  vs. time plot (pure first order). In the unannealed sample the initial decay is faster but approaches the slope of the annealed sample as annealing progresses.

In studies of the effect of annealing on trapped electron decay rates, the rate at which complete annealing is approached in 3MP held at 77°K is critically dependent on the shape as well as the size of the sample.<sup>41</sup> Presumably this is also true for radical decay. Annealing of 3MP glass has been independently studied by a physical method.<sup>42</sup> When samples of 3MP which have been annealed at 77°K for various times are warmed in a differential thermal analysis apparatus, an endothermic peak at 83°K, representing the  $\Delta H$  of the change in free volume which occurs during annealing, grows with time of annealing. It approaches its limiting value at the same rate that the half-life for decay of electrons approaches its limit. Presumably the effect of matrix annealing on the rate of radical decay is related to increase in the macroscopic and microscopic viscosity of the medium.

*Acknowledgment.* We have appreciated the opportunity to discuss this work with Dr. E.D. Sprague during part of its progress, while collaborating with him on a related study.<sup>16</sup>

## References and Notes

- (1) This work has been supported in part by the U.S. Atomic Energy Commission under Contract No. AT(11-1)-1715 and by the W.F. Vilas Trust of the University of Wisconsin.
- (2) Past work on trapped radicals in organic glasses is discussed and references are given in: J. E. Willard in "Fundamental Processes in Radiation Chemistry", P. Ausloos, Ed., Interscience, New York, N.Y., 1968, pp 599-649; J. E. Willard, *Science*, **180**, 553 (1973); J. E. Willard, *Intl. J. Radiat. Phys. Chem.*, **6**, 325 (1974).

- (3) D. P. Lin and J. E. Willard, *J. Phys. Chem.*, **78**, 2233 (1974).
- (4) D. P. Lin and J. E. Willard, *J. Phys. Chem.*, **78**, 1135 (1974).
- (5) R. F. C. Claridge and J. E. Willard, *J. Am. Chem. Soc.*, **87**, 4992 (1965).
- (6) D. W. Skelly, R. G. Hayes, and W. H. Hamill, *J. Chem. Phys.*, **43**, 2795 (1965).
- (7) M. Shrom and J. E. Willard, *J. Phys. Chem.*, **72**, 1702 (1968).
- (8) W. G. French and J. E. Willard, *J. Phys. Chem.*, **72**, 4604 (1968).
- (9) L. Perkey and J. E. Willard, *J. Chem. Phys.*, **60**, 2732 (1974).
- (10) R. H. Schuler and A. O. Allen, *J. Chem. Phys.*, **24**, 56 (1956).
- (11) D. Timm and J. E. Willard, *Rev. Sci. Instrum.*, **40**, 848 (1969).
- (12) P. J. Ogren, Ph.D. Thesis, University of Wisconsin—Madison, 1968.
- (13) D. P. Lin and L. Kevan, *J. Chem. Phys.*, **55**, 2629 (1971).
- (14) D. J. Henderson and J. E. Willard, *J. Am. Chem. Soc.*, **91**, 3014 (1969).
- (15) D. Timm and J. E. Willard, *J. Phys. Chem.*, **73**, 2403 (1969).
- (16) M. A. Neiss, E. D. Sprague, and J. E. Willard, unpublished.
- (17) Wing Kun Kam, M.S. Thesis, University of Wisconsin—Madison, 1970.
- (18) E. D. Sprague, *J. Phys. Chem.*, **77**, 2066 (1973).
- (19) E. D. Sprague and F. Williams, *J. Am. Chem. Soc.*, **93**, 787 (1971).
- (20) J. T. Wang and F. Williams, *J. Am. Chem. Soc.*, **94**, 2930 (1972).
- (21) A. Campion and F. Williams, *J. Am. Chem. Soc.*, **94**, 7633 (1972).
- (22) During this work we learned of a concurrent similar investigation by Sprague.<sup>18</sup>
- (23) A. C. Ling and J. E. Willard, *J. Phys. Chem.*, **72**, 3349 (1968).
- (24) R. H. Doremus in "Modern Aspects of the Vitreous State", Vol. 2, J. D. Mackenzie, Ed., Butterworths, Washington, D.C., 1962, Chapter 1.
- (25) The activation energies for the  $CH_3 + HBr \rightarrow CH_4 + Br$  and  $CH_3 + HI \rightarrow CH_4 + I$  reactions in the gas phase have been reported as  $< 1.5$  kcal  $mol^{-1}$ . H. C. Anderson and G. B. Kistiakowsky, *J. Chem. Phys.*, **11**, 6 (1943); R. R. Williams and R. A. Ogg, *ibid.*, **15**, 896 (1947).
- (26) R. J. LeRoy, E. D. Sprague, and F. Williams, *J. Phys. Chem.*, **76**, 546 (1972).
- (27) Values of  $D_{Cl_2}$  and  $D_{O_2}$  estimated earlier<sup>28</sup> from the rates of reaction of dissolved  $Cl_2$  and  $O_2$  with trapped radicals in 3MP glass are much larger than would be predicted from the value of  $D_H$  determined here on the basis of relative radii. The higher values may be due in part to less well developed methods of measuring changes in radical concentration, but the magnitude of the difference implies that physical or chemical factors are also involved.
- (28) R. Arce-Quintero and J. E. Willard, *J. Phys. Chem.*, **76**, 1800 (1972).
- (29) R. F. C. Claridge and J. E. Willard, *J. Am. Chem. Soc.*, **89**, 510 (1967).
- (30) S. Aditya and J. E. Willard, *J. Chem. Phys.*, **44**, 833 (1966).
- (31) P. H. Kasai, *Acc. Chem. Res.*, **4**, 329 (1971).
- (32) L. G. Christophorou, R. N. Compton, and H. W. Dickson, *J. Chem. Phys.*, **48**, 1949 (1968).
- (33) K. Hiraoka and W. H. Hamill, *J. Chem. Phys.*, **59**, 5749 (1973).
- (34) J. P. Guarino and W. H. Hamill, *J. Am. Chem. Soc.*, **86**, 777 (1964); J. B. Gullivan and W. H. Hamill, *J. Chem. Phys.*, **44**, 2378 (1966).
- (35) A. Ekstrom and J. E. Willard, *J. Phys. Chem.*, **72**, 4599 (1968).
- (36) D. D. Mainwaring and J. E. Willard, *J. Phys. Chem.*, **77**, 2974 (1973).
- (37) R. Rebbert and P. Ausloos, *J. Chem. Phys.*, **48**, 306 (1968).
- (38) S. J. Riley and K. R. Wilson, *Discuss. Faraday Soc.*, **53**, 132 (1972).
- (39) G. M. Harris and J. E. Willard, *J. Am. Chem. Soc.*, **76**, 4678 (1954).
- (40) F. P. Hudson, R. R. Williams, Jr., and W. H. Hamill, *J. Chem. Phys.*, **21**, 1894 (1953).
- (41) D. Shooter and J. E. Willard, *J. Phys. Chem.*, **76**, 3167 (1972).
- (42) S. L. Hager, Ph.D. Thesis, University of Wisconsin—Madison, 1975.

# Temperature Dependence of the Heat Capacities of Activation for the Aquations of Bromo- and Sulfatopentaamminecobalt(III) Ions in Acidic Aqueous Solution<sup>1</sup>

Anthony M. Newton and Thomas W. Swaddle\*

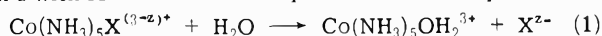
Department of Chemistry The University of Calgary, Calgary, Alberta, Canada, T2N 1N4 (Received August 26, 1974)

The heat capacities of activation  $\Delta C_p^*$  for the hydrogen-ion-independent aquation pathways of  $\text{Co}(\text{NH}_3)_5\text{Br}^{2+}$  and  $\text{Co}(\text{NH}_3)_5\text{SO}_4^+$  in 0.1 M  $\text{HClO}_4$  are strongly temperature dependent, with pronounced maxima near 35°, the range of  $\Delta C_p^*$  values being about twice as great for the latter complex as for the former. It is shown that this effect cannot be due to ion pairing between perchlorate ion and the complex cations, but may be explained semiquantitatively with the aid of a modified version of the Leung-Grunwald theory, in terms of solvational changes occurring during the activation process.

## Introduction

We have been engaged over the past decade in attempts to identify and interpret patterns in the activation parameters of substitution reactions of cationic octahedral complexes in solution.<sup>2</sup> In order to make valid comparisons of the enthalpies  $\Delta H^*$  and entropies  $\Delta S^*$  of activation within a series of related reactions, it is necessary to establish that the temperature dependence of these parameters (which is governed by the heat capacity of activation  $\Delta C_p^* = (\partial\Delta H^*/\partial T)_p$ ) is not numerically large, since kinetic measurements may have to be made over different temperature ranges for different complexes. Furthermore,  $\Delta C_p^*$  has proved to be a parameter of considerable intrinsic interest in relation to organic solvolysis reactions;<sup>3-5</sup> for example, for the solvolysis of alkyl halides in water,  $\Delta C_p^*$  may serve as a mechanistic criterion, being typically on the order of  $-50 \text{ cal deg}^{-1} \text{ mol}^{-1}$  for  $\text{SN}_2$  reactions and about  $-90$  for  $\text{SN}_1$ .<sup>4</sup> However,  $\Delta C_p^*$  for inorganic reactions has received very little attention to date (Table I).

We have therefore attempted to measure  $\Delta C_p^*$  for reaction 1 with  $\text{X}^{2-} = \text{Br}^-$  and  $\text{SO}_4^{2-}$  in 0.1 M  $\text{HClO}_4$ .



These reactions were chosen because their mechanisms are well established (dissociative interchange,  $I_d$ ),<sup>2,6</sup> they proceed at convenient rates over a wide range of temperatures, and because they were expected to yield information on the effect on  $\Delta C_p^*$  of reaction charge type (i.e., of  $z$ ). The relatively high concentration of  $\text{HClO}_4$  was necessary to maintain constant ionic strength as the reactions proceeded, and to suppress the decomposition of the product  $\text{Co}(\text{NH}_3)_5\text{OH}_2^{3+}$  at the higher temperatures.<sup>7</sup> When  $\text{X}^{2-}$  was sulfate, this high acidity helped ensure that reaction 1 went to effective completion, since the  $\text{p}K_a$  of  $\text{HSO}_4^-$  is about 2 at 25° and higher at higher temperatures; the small contribution of a pathway first order in  $[\text{H}^+]$  to the equation rate<sup>8,9</sup> can readily be allowed for.

## Experimental Section

Distilled water was passed through fresh Barnstead deionizer and organic removal cartridges before use. All chemicals were analytical reagent grade. Throughout this article, concentrations are given on the molar scale as if at 25°.

*Bromopentaamminecobalt(III) perchlorate* was made by heating 10 g of carbonatopentaamminecobalt(III) per-

chlorate<sup>10</sup> with excess  $\text{HBr}$  on the steambath for 2 hr, dissolving the crystals recovered from the cooled reaction mixture in water at 0°, and filtering the solution into 100 ml of 70%  $\text{HClO}_4$  at 0°. The feathery crystalline product was filtered, washed successively with water, ethanol, and ether, and dried in vacuo. Anal. Calcd for  $[\text{Co}(\text{NH}_3)_5\text{Br}](\text{ClO}_4)_2$ : N, 16.56; H, 3.58. Found: N, 16.44; H, 3.62. The absorption maximum of the aqueous complex at 253 nm ( $\epsilon 18,100 \text{ M}^{-1} \text{ cm}^{-1}$ ) was in reasonable agreement with that reported by Jorgensen.<sup>11</sup>

*Sulfatopentaamminecobalt(III) perchlorate*, free of the aquopentaammine salt and other such impurities, was made from the acid sulfate<sup>12</sup> by cation exchange chromatography on Dowex 50W-X8 resin ( $\text{Na}^+$  form) using 0.4 M  $\text{NaClO}_4$  as eluant. The eluate was kept at 0° overnight, and the crystalline product was washed and dried as above. Anal. Calcd for  $[\text{Co}(\text{NH}_3)_5\text{SO}_4](\text{ClO}_4)$ : N, 20.62; H, 4.45. Found: N, 20.47; H, 4.63. The absorption maxima at 516 ( $\epsilon 62.2$ ) and 355 nm ( $\epsilon 50.3 \text{ M}^{-1} \text{ cm}^{-1}$ ) agreed well with those reported by several authors,<sup>13-16</sup> although Po and Jordan<sup>16</sup> recorded  $\epsilon 34.8 \text{ M}^{-1} \text{ cm}^{-1}$  for their maximum at 357 nm.

*Kinetic Measurements.* The conductimetric method, normally preferred for  $\Delta C_p^*$  measurements on ionogenic reactions,<sup>4,5</sup> was inapplicable because of the need to maintain high  $\text{HClO}_4$  concentrations. Instead, a method was devised for following the more rapid reactions spectrophotometrically in situ with high precision, using Cary Model 15 or 16 spectrophotometers (with equal accuracy, in practice). The apparatus (Figure 1), based on Robertson's design,<sup>17</sup> consisted of a darkened, stirred reaction vessel surrounded by a thermostated, insulated water jacket. The stirring forced a stream of the reaction solution rapidly through the optical cell. This cell was held in a thermally insulating wooden mount which permitted the cell to be moved in or out of the spectrophotometer light beam as desired, to eliminate the possibility of photolysis between readings, and to allow the spectrophotometer baseline to be zeroed, air against air, before each measurement. A null method, whereby the absorbance of the reaction solution was matched by adding a measured amount of a standard solution from a microburet to a vessel with windows in the reference beam, was tried as an alternative to direct measurement of the absorbance of the reaction solution, but the spectrophotometer slidewire calibration was sufficiently good that any gain in precision obtained in the null method was outweighed by the additional operational com-

TABLE I:  $\Delta C_p^*$  for Aquation of Cobalt(III) Complexes

Complex	Temp range, °C	$\Delta C_p^*$ , cal deg <sup>-1</sup> mol <sup>-1</sup>
$[\text{Co}(\text{NH}_3)_5\text{NO}_3](\text{ClO}_4)_2$	0–59	–20 <sup>a</sup>
$[\text{Co}(\text{NH}_3)_5\text{Cl}](\text{ClO}_4)_2$	20–70	–49 <sup>b</sup>
<i>cis</i> - $[\text{Co}(\text{en})_2\text{NH}_2\text{Cl}](\text{ClO}_4)_2$	20–80	–50 <sup>b</sup>
<i>cis</i> - $[\text{Co}(\text{trien})\text{NH}_2\text{Cl}](\text{ClO}_4)_2$	30–80	–49 <sup>b</sup>
<i>cis</i> - $[\text{Co}(\text{en})_2\text{N}_3\text{Cl}]_2\text{S}_2\text{O}_3$		–29 <sup>c</sup>
<i>cis</i> - $[\text{Co}(\text{en})_2(\text{CN})\text{Cl}]\text{Cl}$		–17 <sup>c</sup>

<sup>a</sup> T. W. Swaddle, R. B. Jordan, and W. E. Jones, *Inorg. Chem.*, **8**, 2504 (1969). <sup>b</sup> S. C. Chan, *J. Chem. Soc. A*, 291 (1967). <sup>c</sup> D. M. Parboe and R. E. Robertson, private communication.

plexity. Prior to a kinetic run, the reaction medium was thoroughly thermostated ( $\pm 0.01^\circ$ ) in the apparatus of Figure 1, using circulating water from an external thermostat bath controlled by a Fisher proportional controller. To start a kinetic run, a weighed sample of the solid cobalt(III) complex was dissolved in a 5-ml portion of the thermostated solvent, and flushed quickly into the reaction vessel using a syringe with a Teflon needle, thereby minimizing temperature fluctuations and premature aquation.

The aquations of  $\text{Co}(\text{NH}_3)_5\text{Br}^{2+}$  at 0–30°, and of  $\text{Co}(\text{NH}_3)_5\text{SO}_4^+$  at 5–40°, were rather too slow to permit use of the above technique. Instead, the reaction solution, contained in a darkened Pyrex flask, was thermostated in a Sargent-Welch Thermonitor-controlled water bath ( $\pm 0.01^\circ$  or better) fitted with a coil which was supplied with coolant from a Lauda Model K-2/R refrigerated circulator as required. Aliquots of solution were withdrawn as required and quenched at 0°, and brought quickly to 25° when ready for absorbance measurements. Duplicate measurements, comparing this and the *in situ* methods, showed that the results obtained by the two techniques were identical within the experimental uncertainty. This observation confirms that surface effects did not contribute to the measured reaction rates, since the surface-to-volume ratio was different in each method and was in any event small, and furthermore the complex concentrations used were too high ( $\sim 6 \times 10^{-4} M$ ) to be significantly affected by surface absorption. Runs at 0° were made using well-mixed ice-water slushes in dewar vessels as the thermostat bath.

Bath temperatures were measured, with appropriate precautions,<sup>18</sup> using precision mercury-in-glass thermometers which were calibrated against a platinum resistance thermometer having standardization traceable to NBS. The temperature of the solution in the reaction vessel (Figure 1) was measured with an Atkins thermistor thermometer, the probes of which were calibrated during every run against the precision mercury thermometers. Temperature measurements were accurate to  $\pm 0.05^\circ$  at worst.

## Results

In every case, the absorbance  $A_t$  at time  $t$  was measured at 313 ( $X^{2-} = \text{Br}^-$ ) or 274 nm ( $X^{2-} = \text{SO}_4^{2-}$ ) at intervals over at least the first 80% reaction, and followed pseudo-first-order kinetics (rate coefficient  $k_{\text{obsd}}$ ) to well within the experimental uncertainty of  $\pm 0.002$  in  $A_t$ , according to both graphical and least-squares numerical analysis.

$$k_{\text{obsd}} t = \ln [(A_0 - A_\infty)/(A_t - A_\infty)] \quad (2)$$

The final absorbances  $A_\infty$  showed that reaction 1 was ef-

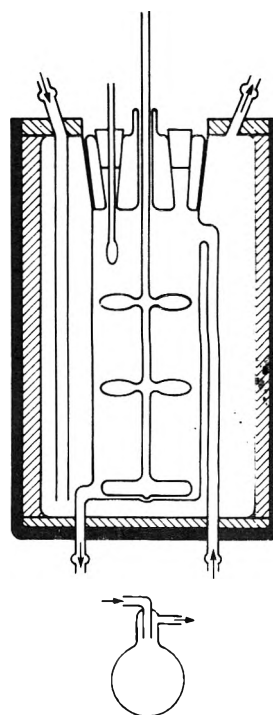


Figure 1. Stirred thermostated reaction vessel, feeding optical cell (below).

fectively complete in all cases, and isoshestic points were strictly maintained throughout the reactions. No changes were observed in the visible spectrum of  $\text{Co}(\text{NH}_3)_5\text{OH}_2^{3+}$  in the presence of an equimolar amount of  $\text{Br}^-$  in 0.1 *M*  $\text{HClO}_4$  at 73° over several days, and extrapolation of the spontaneous decomposition rate of  $\text{Co}(\text{NH}_3)_5\text{OH}_2^{3+}$  from higher temperatures<sup>7</sup> showed that this reaction is some  $10^5$  times slower than reaction 1 ( $X^{2-} = \text{Br}^-, \text{SO}_4^{2-}$ ) at 70°. Thus, reaction 1 occurs to the exclusion of secondary processes, under the conditions employed in this study.

However, for  $X^{2-} = \text{SO}_4^{2-}$ , values of  $k_{\text{obsd}}$  obtained at the higher temperatures must be corrected for a small contribution from an acid-dependent equation pathway (rate coefficient  $k_a$ ).

$$k_{\text{obsd}} = k + k_a[\text{H}^+] \quad (3)$$

Fortunately, values of  $k_a$  can be computed with ample accuracy from the data of Monacelli,<sup>9</sup> despite a difference in ionic strength, and this was verified by direct measurements of the aquation rate of  $\text{Co}(\text{NH}_3)_5\text{SO}_4^+$  in 0.10 *M*  $\text{HClO}_4$  and 0.01 *M*  $\text{HClO}_4$ –0.09 *M*  $\text{LiClO}_4$ . Values of  $k_{\text{obsd}}$  ( $=k$ ) for  $\text{Co}(\text{NH}_3)_5\text{Br}^{2+}$ , and of  $k_{\text{obsd}}$  and  $k$  for  $\text{Co}(\text{NH}_3)_5\text{SO}_4^+$ , are collected in Tables II and III, respectively.

The precision in  $k$  was  $\pm 0.5\%$  at worst, so that the major source of experimental uncertainty in calculating  $\Delta C_p^*$  was temperature measurement, especially where thermistors were used, since the possible error of  $\pm 0.05^\circ$  corresponds to about  $\pm 0.6\%$  in  $k_{\text{obsd}}$  for the experiments described here. This limitation was anticipated, and the experiments were planned accordingly to cover as wide a range of temperature as possible without loss of accuracy in the measurement of  $k_{\text{obsd}}$ , so as to minimize the impact of the uncertainty in the temperature  $T$  on the derived value of  $\Delta C_p^*$ , which was naively expected to be approximately constant over the experimental temperature range. Furthermore, Wold and Ahlberg<sup>19</sup> have pointed out that equations such

**TABLE II: Rate Constants for the Aquation of  $\text{Co}(\text{NH}_3)_5\text{Br}^{2+}$  in 0.1 M  $\text{HClO}_4^a$** 

Temp, °C	$10^6 k_{\text{obsd}}, \text{sec}^{-1}$	Temp, °C	$10^6 k_{\text{obsd}}, \text{sec}^{-1}$
0.00	0.1210 <sup>b</sup>	45.18	70.64 ± 0.15 <sup>c</sup>
5.14	0.2818 ± 0.0012 <sup>c</sup>	50.35	130.4 ± 0.1 <sup>c</sup>
10.02	0.6086 ± 0.0013 <sup>c</sup>	55.17	221.7 ± 0.7 <sup>c</sup>
15.07	1.334 ± 0.002 <sup>c</sup>	60.07	375.8 <sup>b</sup>
19.99	2.770 ± 0.014 <sup>c</sup>	60.09	376.5 ± 1.0 <sup>d</sup>
25.93	6.081 ± 0.015 <sup>c</sup>	64.89	611.4 <sup>b</sup>
30.02	10.59 ± 0.03 <sup>c</sup>	64.90	605.9 <sup>b</sup>
34.92	20.26 ± 0.00 <sup>d</sup>	70.17	1000 ± 5 <sup>d</sup>
35.00	20.42 <sup>b</sup>	70.19	998.7 <sup>b</sup>
40.16	38.91 ± 0.12 <sup>c</sup>		

<sup>a</sup> Complex concentration  $\sim 6 \times 10^{-4}$  M. <sup>b</sup> Single runs. <sup>c</sup> Triplicate runs. <sup>d</sup> Duplicate runs.

**TABLE III: Rate Constants for the Aquation of  $\text{Co}(\text{NH}_3)_5\text{SO}_4^+$  in 0.1 M  $\text{HClO}_4^a$** 

Temp, °C	$10^7 k_{\text{obsd}}, \text{sec}^{-1}$	$10^7 k, \text{sec}^{-1}$
5.27	0.6673 ± 0.0102 <sup>c</sup>	0.6370 ± 0.0102
10.03	1.585 ± 0.009 <sup>d</sup>	1.512 ± 0.009
14.94	3.182 ± 0.012 <sup>d</sup>	3.006 ± 0.012
20.15	6.670 ± 0.036 <sup>d</sup>	6.238 ± 0.036
25.02	12.49 ± 0.03 <sup>d</sup>	11.52 ± 0.03
29.98	22.93 ± 0.04 <sup>d</sup>	20.76 ± 0.04
34.76	41.60 ± 0.20 <sup>d</sup>	37.02 ± 0.20
39.77	81.09 ± 0.19 <sup>d</sup>	71.31 ± 0.19
44.95	141.2 ± 0.2 <sup>c</sup>	120.2 ± 0.2
45.02	142.0 <sup>b</sup>	120.8
50.32	259.2 <sup>b</sup>	214.4
50.36	260.9 <sup>b</sup>	215.8
55.14	441.7 <sup>b</sup>	354.6
55.15	442.3 <sup>b</sup>	355.1
60.06	752.6 <sup>b</sup>	584.5
60.10	751.5 <sup>b</sup>	582.6
65.25	1291 ± 3 <sup>c</sup>	961.6 ± 3.6
70.03	2126 <sup>b</sup>	1524

<sup>a</sup> Complex concentration  $\sim 6 \times 10^{-4}$  M. <sup>b</sup> Single run. <sup>c</sup> Duplicate runs. <sup>d</sup> Triplicate runs.

as that of Hyne and Robertson<sup>20</sup> (eq 4), which are widely used for the calculation of  $\Delta C_p^*$ , become numerically unstable and highly sensitive to the experimental uncertainty when  $\Delta T/T$  is small ( $\Delta T$  is the temperature range with median temperature  $T$ ).

$$\log k = A/T + B \log T + C \quad (4)$$

where  $A = (T_0 \Delta C_p^* - \Delta H_0^*)/2.303R$ ,  $B = \Delta C_p^*/R + 1$ ,  $C = \log \kappa/h + (\Delta S_0^* - \Delta C_p^*)/2.303R - (\Delta C_p^*/R) \log T_0$ , and  $\Delta H_0^*$ ,  $\Delta S_0^*$  refer to a reference temperature  $T_0$ , here taken as 298.16 K.

We therefore made measurements of  $k_{\text{obsd}}$  over temperature ranges of over 60°, for which an accuracy as poor as ±3% in  $k$ , or a corresponding uncertainty in  $T$ , would be entirely adequate for a reliable computation of  $\Delta C_p^*$  if this were effectively temperature independent.<sup>19</sup> However, as data accumulated, it became clear that the apparent value of  $\Delta C_p^*$ , calculated by fitting  $k$  and  $T$  data to eq 4 using a

**TABLE IV: Activation Parameters for the Aquation of  $\text{Co}(\text{NH}_3)_5\text{Br}^{2+}$  in 0.1 M  $\text{HClO}_4$** 

Temp range, °C	Av temp, °C	$\Delta H^*, \text{cal mol}^{-1}$	$\Delta S^*, \text{cal deg}^{-1} \text{mol}^{-1}$	$\Delta C_p^*, \text{cal deg}^{-1} \text{mol}^{-1}$
0-60	31.78	23,704 ± 11	-3.1 ± 0.0	-26.0 ± 1.2
0-70	36.10	23,690 ± 29	-3.2 ± 0.1	-36.2 ± 2.2
20-70	44.54	24,649 ± 2	-1.1 ± 0.2	-63.0 ± 2.7
25-70	47.09	24,292 ± 84	-1.2 ± 0.3	-60.1 ± 3.7
0-40	21.74	23,636 ± 49	-3.3 ± 0.2	-36.4 ± 7.0
5-45	25.15	23,648 ± 34	-3.3 ± 0.1	-35.1 ± 6.0
10-50	31.18	23,634 ± 44	-3.4 ± 0.2	-22.7 ± 6.2
15-55	35.19	23,478 ± 58	-3.9 ± 0.2	-11.4 ± 5.3
20-60	40.19	23,451 ± 88	-4.0 ± 0.3	-13.2 ± 5.7
25-65	44.43	24,077 ± 70	-1.9 ± 0.2	-46.6 ± 3.6
30-70	49.53	24,419 ± 119	-0.8 ± 0.4	-64.6 ± 4.8
0-25	14.27	23,195 ± 222	-4.8 ± 0.8	-74.9 ± 18.9
5-31	17.69	23,200 ± 130	-4.8 ± 0.4	-84.8 ± 15.4
10-35	22.65	23,535 ± 94	-3.7 ± 0.3	-49.5 ± 20.4
15-40	27.68	23,455 ± 70	-4.0 ± 0.2	-8.6 ± 16.3
20-45	32.69	23,240 ± 129	-4.7 ± 0.4	+16.0 ± 15.6
25-50	37.75	23,947 ± 116	-2.3 ± 0.4	-37.0 ± 8.8
30-55	42.63	23,917 ± 150	-2.4 ± 0.5	-36.6 ± 8.5
35-60	47.64	23,675 ± 177	-3.2 ± 0.6	-26.9 ± 7.9
40-64	51.91	24,577 ± 307	-0.3 ± 1.0	-64.1 ± 11.4
45-70	57.20	26,316 ± 251	-5.3 ± 0.8	-121.7 ± 7.7

<sup>a</sup> Values at 25°.

**TABLE V: Activation Parameters for the Hydrogen-Ion Independent Aquation of  $\text{Co}(\text{NH}_3)_5\text{SO}_4^+$  in 0.1 M Perchlorate Media**

Temp range, °C	Av temp, °C	$\Delta H^*, \text{cal mol}^{-1}$	$\Delta S^*, \text{cal deg}^{-1} \text{mol}^{-1}$	$\Delta C_p^*, \text{cal deg}^{-1} \text{mol}^{-1}$
5-60	30.47	21,818 ± 34	12.6 ± 0.1	-13.6 ± 3.2
5-70	33.50	21,822 ± 32	12.6 ± 0.1	-15.1 ± 2.2
20-70	41.31	21,604 ± 40	13.2 ± 0.1	-9.6 ± 2.3
5-45	24.98	21,813 ± 47	12.6 ± 0.2	-18.6 ± 8.6
10-50	29.20	21,808 ± 30	12.6 ± 0.1	-7.3 ± 4.7
15-55	33.58	21,763 ± 35	12.8 ± 0.1	-4.1 ± 3.3
20-60	38.12	21,571 ± 50	13.4 ± 0.2	-4.8 ± 3.5
25-65	42.72	21,719 ± 122	12.9 ± 0.4	-10.2 ± 6.3
30-70	46.66	22,240 ± 25	11.2 ± 0.1	-33.1 ± 1.2
5-30	17.56	21,143 ± 45	14.8 ± 0.2	-204.8 ± 6.1
10-35	22.47	21,587 ± 69	13.3 ± 0.2	-69.0 ± 15.0
15-40	27.43	21,847 ± 142	12.5 ± 0.5	+55.1 ± 34.2
20-45	32.43	21,095 ± 79	15.0 ± 0.3	+54.5 ± 9.5
25-50	36.71	21,167 ± 176	14.7 ± 0.6	+38.0 ± 14.0
30-55	41.20	22,186 ± 21	11.4 ± 0.1	-30.1 ± 1.2
35-60	45.97	22,293 ± 51	11.0 ± 0.2	-35.1 ± 2.4
40-65	51.12	19,127 ± 598	21.2 ± 1.9	+68.3 ± 22.2
45-70	55.54	21,692 ± 175	13.0 ± 0.6	-12.3 ± 5.6

<sup>a</sup> Values at 25°.

non-linear least-squares program on an IBM 360/50 computer, varied strongly and systematically with both  $T$  and  $\Delta T/T$ .

This is illustrated for  $\text{Co}(\text{NH}_3)_5\text{Br}^{2+}$  in Table IV, in which apparent  $\Delta C_p^*$  values computed over 25°, 40°, and larger intervals are listed. The standard deviations of  $\Delta C_p^*$  suggest that the calculations verge on numerical instability for 25° intervals, and smaller  $\Delta T$  values were not used. For

$\Delta T = 25$  and  $40^\circ$  alike, a clearly defined maximum in  $\Delta C_p^*$  occurs near  $35^\circ$ ,  $\Delta C_p^*$  being near zero at the maximum and strongly negative above and below it. The actual numerical values of  $\Delta C_p^*$  have only limited significance, since an excessively wide choice of  $\Delta T$  will result in incorrect averaging of the nonlinear dependence of  $\Delta C_p^*$  on  $T$ ; in particular,  $\Delta C_p^*$  values based on  $\Delta T = 40^\circ$  are unreliable because they inevitably include data from *both* sides of the maximum. The data based on  $\Delta T = 25^\circ$  suggest a limiting value of  $\Delta C_p^*$  of about  $-80 \text{ cal deg}^{-1} \text{ mol}^{-1}$  near  $0^\circ$ , with the maximum some  $100 \text{ cal deg}^{-1} \text{ mol}^{-1}$  above this. There is also a suggestion of a second maximum near  $50^\circ$ .

The corresponding data for  $\text{Co}(\text{NH}_3)_5\text{SO}_4^+$  (Table V) show the same general phenomena, with a maximum over  $200 \text{ cal deg}^{-1} \text{ mol}^{-1}$  high (relative to low temperatures) near  $30^\circ$  and a suggestion of a second maximum near  $50^\circ$ . The mean values of  $\Delta H^*$  and  $\Delta S^*$  at the higher temperatures are close to those reported by Monacelli<sup>9</sup> for a higher ionic strength ( $1.0 M$ ) over the range  $55\text{--}84^\circ$ .

## Discussion

The temperature dependence of  $\Delta C_p^*$  for reaction 1 is too strong to permit much significance to be attached to the apparent values of this parameter calculated as above, and, although the functional form of the temperature dependence of  $\Delta C_p^*$  is not known, it is clear that at least two further parameters in addition to  $\Delta H_0^*$ ,  $\Delta S_0^*$ , and  $\Delta C_{p0}^*$  at a reference temperature  $T_0$  would be involved, and it is doubtful whether the accuracy of the measured  $k$  and  $T$  values warrant a five-parameter fit.

Nevertheless, some useful conclusions can be drawn from the data of Tables IV and V. First, because the mean  $\Delta C_p^*$  values are not numerically large in the region  $25\text{--}50^\circ$  (which is near the middle of the temperatures ranges commonly used to obtain activation parameters for reaction 1), it is reasonable to disregard the temperature dependence of  $\Delta H^*$  and  $\Delta S^*$  when seeking correlations involving these parameters for reaction 1 within a series in which  $X^{z-}$  is changed.<sup>2</sup> However, data obtained at the extremes of the normal liquid range of water should be regarded with caution. Secondly, comparison of the data of Tables I, IV, and V shows that  $\Delta C_p^*$  values calculated over the  $0\text{--}60^\circ$  range for  $X^{z-} = \text{SO}_4^{2-}$ ,  $\text{NO}_3^-$ , and  $\text{Br}^-$  are not significantly different; for the  $20\text{--}70^\circ$  range,  $\Delta C_p^*$  is similar for  $X^{z-} = \text{Br}^-$  and  $\text{Cl}^-$ , but here the sulfato complex is anomalous. These considerations suggest that  $\Delta C_p^*$  values for reaction 1 may be similar for a given charge type at a given temperature, although calculation of  $\Delta C_p^*$  over such wide  $\Delta T$  intervals obviously conceals important temperature dependence effects.

Most importantly, maxima in  $\Delta C_p^*$  at least  $100$  ( $X^{z-} = \text{Br}^-$ ) and  $200$  ( $X^{z-} = \text{SO}_4^{2-}$ )  $\text{cal deg}^{-1} \text{ mol}^{-1}$  high, relative to low-temperature values, occur near  $35^\circ$ , and this effect requires an explanation. We have taken care to demonstrate that the maxima cannot be artifacts arising from side reactions or the experimental methodology, and there is no evidence for a gross change in reaction mechanism as the temperature is varied. For organic solvolyses in water, the reported values of  $\Delta C_p^*$  have in general been based on measurements over small temperature intervals  $\Delta T$ , and with some exceptions<sup>20,21</sup> the possible temperature dependence of  $\Delta C_p^*$  has not been considered important. However, Wold<sup>22</sup> has reanalyzed the reported rate coefficients of 60 organic solvolysis reactions and has concluded that  $\Delta C_p^*$  for these reactions typically passes through a rela-

tively shallow but distinct *minimum* near  $35^\circ$ . We have recalculated  $\Delta C_p^*$  values over  $25$  and  $40^\circ$  intervals from data obtained by Robertson<sup>23</sup> for the hydrolysis of aqueous methyl *p*-methylbenzenesulfonate over a wide temperature range, and have found a distinct minimum near  $45^\circ$ ; however, the range in  $\Delta C_p^*$  was much smaller (about  $-10$  to  $-50 \text{ cal deg}^{-1} \text{ mol}^{-1}$ ) than for reaction 1 and most values lay in a narrow range ( $-30$  to  $-40 \text{ cal deg}^{-1} \text{ mol}^{-1}$ ). Thus, the existence of extrema in  $\Delta C_p^*$  as a function of temperature seems to be not only a real effect but also a rather general one.

Similar extrema have been observed in the heat capacities of ionization  $\Delta C_p^0$  of several aqueous acids<sup>24-28</sup> and of water itself,<sup>27,28</sup> as a function of temperature. Indeed, the partial molal heat capacities  $\bar{C}_p^0$  of typical electrolytes in water generally rise sharply from strongly negative values at  $0^\circ$  and in most cases pass through a *maximum* within the normal liquid range of water, especially for 2:1 and 3:1 electrolytes, as the temperature is increased.<sup>29</sup> The latter fact provides an empirical explanation for the maxima in  $\Delta C_p^*$  for reaction 1, in which extra electrolyte is in effect generated as the reaction proceeds from the initial state  $\text{Co}(\text{NH}_3)_5\text{X}^{(3-z)+}$  to the transition state  $[\text{Co}(\text{NH}_3)_5^{3+}, \text{X}^{z-}]$ . However, this encouraging observation does not constitute a theoretical basis for understanding the phenomenon of extrema in  $\Delta C_p^*$ .

Leung and Grunwald<sup>27</sup> have shown that, for a formal solute which exists in two forms A and B, in equilibrium but differing in enthalpy,  $\bar{C}_p$  will exhibit a maximum. If  $x$  is the fraction of solute molecules belonging to form B, then, for the formal solute

$$\bar{C}_p^0 \text{ formal} = \bar{C}_p^0 \text{ A} + [x(1-x)(\Delta H')^2/RT^2] \quad (5)$$

where  $\Delta H'$  is the excess in molar enthalpy of B over A and is assumed to be independent of temperature.  $\bar{C}_p^0 \text{ A}$  may be expected to increase slowly with rising temperature, but the second term on the right will pass through a maximum at a temperature  $T_{\text{max}}$  at which  $x = 1/2 - (RT_{\text{max}}/\Delta H')$ , the height of the maximum being governed by  $\Delta H'$ .

Leung and Grunwald<sup>27</sup> applied eq 5 to explain the maximum in  $\Delta C_p^0$  for the ionization of water; here,  $\bar{C}_p^0$  for the formal solute  $[\text{H}^+ + \text{OH}^-]$  governs the temperature dependence of  $\Delta C_p^0$ , since  $\bar{C}_p^0$  for un-ionized water is almost independent of temperature. A recent reevaluation of the thermodynamic data for the ionization of water<sup>28</sup> indicates that Leung and Grunwald's  $\Delta C_p^0$  values are somewhat in error, the maximum of about  $-40 \text{ cal deg}^{-1} \text{ mol}^{-1}$  occurring near  $70^\circ$  rather than  $30^\circ$ , but it is nevertheless clear that  $\Delta H'$  would have to be on the order of  $7\text{--}10 \text{ kcal mol}^{-1}$  to produce a  $\Delta C_p^0$  maximum of the magnitude observed. Because the data considered by Leung and Grunwald referred to simple ions in solution at infinite dilution, the difference between their postulated species A and B would almost certainly be one of mode of solvation, and it is therefore reasonable to suppose that solvational phenomena can also account for the maximum  $\Delta C_p^*$  for reaction 1 on the basis of the Leung-Grunwald theory. Indeed, for organic solvolyses in water,  $\Delta C_p^*$  itself is generally believed to reflect solvational effects, probably through disruption of the solvation sheath of the initial state as the system moves to solvate the newly formed ions.<sup>4</sup>

However, because reaction 1 was studied in  $0.1 M$  aqueous perchlorate, one must first consider the possibility that the distinction between species A and B might originate in ion pairing by perchlorate.<sup>30</sup> The ion-pair formation con-

stant would then be  $10 M^{-1}$  near  $T_{\max}$  when the free-ion form A and the perchlorate ion-pair B are present in equal amounts. Since the Co-N bond length in typical species  $\text{Co}(\text{NH}_3)_5\text{X}^{(3-z)+}$  is about 0.200 nm,<sup>31</sup> one can use values of the ionic radii<sup>32</sup> of  $\text{Co}^{3+}$ ,  $\text{O}^{2-}$ , and  $\text{Cl}^{7+}$  to estimate that the closest approach of the  $\text{Co}(\text{NH}_3)_5\text{X}^{(3-z)+}$  and  $\text{ClO}_4^-$  ion centers will be not less than 0.6 nm, and following Anderegg<sup>33</sup> one can calculate theoretical upper limits for the ion-pair formation constant of  $6.4 M^{-1}$  and for the associated enthalpy change ( $=\Delta H'$ ) of  $0.5 \text{ kcal mol}^{-1}$  for a cationic charge of 2 (the bromo complex), or  $1.9 M^{-1}$ ,  $0.3 \text{ kcal mol}^{-1}$  for a cationic charge of 1 (the sulfato complex). This calculation and experimental data<sup>34-36</sup> suggest that the required formation constant of  $10 M^{-1}$  is not impossibly high, though Johansson's recent critical review<sup>37</sup> gives cause for skepticism, but the calculated enthalpy changes are too small by a factor of 10 or more to permit identification with  $\Delta H'$  (unfortunately, experimental enthalpy data for perchlorate ion pairing are not available).

In any event, the question is not how ion pairing might affect  $\bar{C}_p^i$  for the initial state  $[\text{Co}(\text{NH}_3)_5\text{X}^{(3-z)+}\text{aq}]$  or  $\bar{C}_p^*$  for the transition state  $[\text{Co}(\text{NH}_3)_5\text{X}^{3+}\text{aq}]^*$ , but rather how it might influence  $\Delta C_p^*$ , which is  $\bar{C}_p^*$  for formal -  $\bar{C}_p^i$  for formal. From the standpoint of their tendency to pair with  $\text{ClO}_4^-$ , both the initial and transition states are in effect cations of charge  $(3-z)^+$ , and so their perchlorate ion pair formation constants, and the associated enthalpy changes, will not be significantly different. Thus, the observed temperature dependence of  $\Delta C_p^*$  for reaction 1 cannot be attributed to ion pairing with perchlorate. Furthermore, ion pairing of this type is not relevant to the organic solvolyses, which nevertheless also show significant (albeit different and smaller) temperature dependences of  $\Delta C_p^*$ .<sup>22</sup>

We should therefore seek to explain the temperature dependence of  $\Delta C_p^*$  in terms of a hypothetical Leung-Grunwald distribution of the formal ionic species between two different modes of solvation. Complex ions such as  $\text{Co}(\text{NH}_3)_5\text{X}^{(3-z)+}$  in aqueous solution may be considered to be surrounded by a "second coordination sphere" (region I) of solvating water molecules with their oxygen atoms oriented toward the central ion, and probably hydrogen bonded to each other and (in the complexes considered here) to the ammine ligand protons. Beyond the "ordered" region, a second region (II) containing "disordered" water molecules is believed to exist, in which the tendency of these water molecules to hydrogen bond into bulk solvent "structure" is nullified by the proximity of the central ion.<sup>30,38</sup> At the low temperature limit, presumably corresponding to the homogeneously frozen solution, region II would be completely depopulated, and the complex ion plus the extended region I may then be identified with the Leung-Grunwald species A. At sufficiently high temperatures, thermal disordering will depopulate region I completely, and the complex ion surrounded by region II alone can be identified with the Leung-Grunwald species B. Since the transfer of  $n$  water molecules from region I to region II will proceed stepwise as the temperature rises, the generalized Leung-Grunwald eq 6 is more appropriate than eq 5; Leung and Grunwald's preference<sup>27</sup> for the latter was based on a fit of  $\Delta C_p^0$  data for the ionization of water which are probably in error.<sup>28</sup>

$$\bar{C}_p^0 \text{ formal} = \bar{C}_p^0 \text{ A} + [nx'(1-x')(\Delta H'')^2/RT^2] \quad (6)$$

Here,  $\Delta H''$  is the enthalpy (assumed to be independent of  $T$ ) required to release one molecule of water from the

presumably hydrogen-bonded environment of region I to the non-hydrogen-bonded region II.  $\Delta H''$  can therefore be expected to be on the order of  $5 \text{ kcal mol}^{-1}$  (equivalent to the breaking of two hydrogen bonds per water molecule in bulk water<sup>39</sup>). We can write

$$\begin{aligned} \Delta C_p^* &= \bar{C}_p^* \text{ formal} - \bar{C}_p^i \text{ formal} \\ &= C_p^* \text{ A} - C_p^i \text{ A} + [nx'(1-x') - nx'(1-x')] (\Delta H'')^2/RT^2 \quad (7) \end{aligned}$$

where  $n^*$  and  $n$  are the time-averaged numbers of water molecules solvating the transition and initial states, respectively. Writing  $\Delta n$  for  $(n^* - n)$ , the change in the number of solvating water molecules on going from the initial to the transition state, and putting  $x'^*$  equal to  $x'$  as an arbitrary simplification, we obtain

$$\Delta C_p^* = \Delta C_{pA} + \Delta nx'(1-x')(\Delta H'')^2/RT^2 \quad (8)$$

High-pressure studies<sup>40</sup> indicate  $\Delta n \sim 4$  for  $\text{Co}(\text{NH}_3)_5\text{Br}^{2+}$  and  $\sim 8$  for  $\text{Co}(\text{NH}_3)_5\text{SO}_4^+$  in reaction 1, and with  $\Delta H'' \sim 5 \text{ kcal mol}^{-1}$  the last term of eq 8 generates maxima  $\sim 120$  and  $\sim 250 \text{ cal deg}^{-1} \text{ mol}^{-1}$  high in  $\Delta C_p^*$  for these respective complexes at  $35^\circ$ , in good agreement with our experimental observations.

In view of the gross assumptions made in deriving eq 8, and the large uncertainties in our  $\Delta C_p^*$  values based on small intervals  $\Delta T$ , it is enough simply to observe that we have identified a mechanism which could generate  $\Delta C_p^*$  maxima of the magnitude observed. The possibility that more than one maximum may exist in the temperature profile of  $\Delta C_p^*$  can be accommodated by noting that assumptions such as  $x'^* = x'$  are probably not strictly valid. The occurrence of minima in  $\Delta C_p^*$  as a function of temperature for several organic solvolyses in water could probably be explained as above if it is recognized that the mode of solvation of neutral organic solutes in water is qualitatively different from that of inorganic cationic complexes.<sup>4</sup> As Leung and Grunwald showed,<sup>27</sup> their theory can accommodate either maxima or minima in  $\Delta \bar{C}_p^0$  for the ionization of aqueous acids, and presumably the same will hold true of  $\Delta C_p^*$  for solvolysis reactions.

## References and Notes

- (1) This work forms part of the thesis presented by A.M. Newton in partial fulfillment of the requirements of the Ph.D. Degree. The University of Calgary, 1974. We thank the National Research Council of Canada for financial assistance, and Drs. R.E. Robertson and L.G. Hepler for advice and discussions.
- (2) T. W. Swaddle, *Coord. Chem. Rev.*, **14**, 217 (1974).
- (3) J. R. Hulett, *Quart. Rev. Chem. Soc.*, **18**, 227 (1964).
- (4) R. E. Robertson, *Prog. Phys. Org. Chem.*, **4**, 213 (1967).
- (5) G. Kohnstam, *Adv. Phys. Org. Chem.*, **5**, 121 (1967).
- (6) C. H. Langford in "Ionic Interactions", Vol. 2, S. Petrucci, Ed., Academic Press, New York, N.Y., 1971, p. 1.
- (7) A. M. Newton and T. W. Swaddle, *Can. J. Chem.*, **52**, 2751 (1974).
- (8) H. Taube and F. Posey, *J. Am. Chem. Soc.*, **75**, 1465 (1953).
- (9) F. Monacelli, *Inorg. Chim. Acta*, **7**, 65 (1973).
- (10) D. R. Stranks, *Trans. Faraday Soc.*, **51**, 505 (1955).
- (11) C. K. Jorgensen, *Adv. Chem. Phys.*, **5**, 95 (1963).
- (12) S. M. Jorgensen, *Z. Anorg. Chem.*, **17**, 455 (1898).
- (13) R. A. Sutula and J. B. Hunt, *Inorg. Chem.*, **11**, 1879 (1972).
- (14) W. E. Jones, Ph.D. Thesis, The University of Calgary, 197C.
- (15) J. P. Candlin, J. Halpern, and D. L. Trimm, *J. Am. Chem. Soc.*, **86**, 1019 (1964).
- (16) L. L. Po and R. B. Jordan, *Inorg. Chem.*, **7**, 526 (1968).
- (17) B. N. Hendy, W. A. Redmond, and R. E. Robertson, *Can. J. Chem.*, **45**, 2071 (1967).
- (18) J. F. Swindells, *Nat. Bur. Stand. Monogr.*, No. 90 (1965).
- (19) S. Wold and P. Ahlberg, *Acta Chem. Scand.*, **24**, 618 (1970).
- (20) J. B. Hyne and R. E. Robertson, *Can. J. Chem.*, **33**, 1544 (1955).
- (21) E. A. Moelwyn-Hughes, *Proc. Roy. Soc., Ser. A*, **220**, 386 (1953).
- (22) S. Wold, *J. Phys. Chem.*, **76**, 369 (1972).
- (23) R. E. Robertson, *Can. J. Chem.*, **33**, 1536 (1955).
- (24) F. S. Feates and D. J. G. Ives, *J. Chem. Soc.*, 2798 (1956).

- (25) D. J. G. Ives and P. D. Marsden, *J. Chem. Soc.*, 649 (1965).  
 (26) J. M. Readnour and J. W. Cobble, *Inorg. Chem.*, **8**, 2174 (1969).  
 (27) C. S. Leung and E. Grunwald, *J. Phys. Chem.*, **74**, 687 (1970).  
 (28) G. Olofsson and L. G. Hepler, forthcoming publication.  
 (29) W. L. Gardner, E. C. Jekel, and J. W. Cobble, *J. Phys. Chem.*, **73**, 2017 (1969).  
 (30) M. Eigen and E. Wicke, *J. Phys. Chem.*, **58**, 702 (1954).  
 (31) E. B. Fleischer and R. Frost, *J. Am. Chem. Soc.*, **87**, 3598 (1965).  
 (32) J. P. Jesson and E. L. Muetterties, "Chemists' Guide", Marcel Dekker, New York, N.Y., 1969, pp 4-5.  
 (33) G. Anderegg, *Chimia*, **22**, 477 (1968).  
 (34) L. Heck, *Inorg. Nucl. Chem. Lett.*, **7**, 701 (1971).  
 (35) S. Katayama and R. Tamamushi, *Bull. Chem. Soc. Jpn.*, **41**, 606 (1968).  
 (36) D. W. Archer, D. A. East, and C. B. Monk, *J. Chem. Soc.*, 720 (1965).  
 (37) L. Johansson, *Coord. Chem. Rev.*, **12**, 241 (1974).  
 (38) H. S. Frank and W.-Y. Wen, *Discuss. Faraday Soc.*, **24**, 133 (1957).  
 (39) D. Eisenberg and W. Kauzmann, "The Structure and Properties of Water", Oxford University Press, New York, N.Y., 1969, p 179.  
 (40) W. E. Jones, L. R. Carey, and T. W. Swaddle, *Can. J. Chem.*, **50**, 2739 (1972).

## The Use of the Enthalpy of Transfer of Slightly Soluble Salts in the Study of Water-Nonelectrolyte Structural Interactions. The *tert*-Butyl Alcohol-, Dioxane-, and Urea-Water Systems

Linford L. Bright and John R. Jezorek\*

Department of Chemistry, The University of North Carolina at Greensboro, Greensboro, North Carolina 27412

(Received April 15, 1974; Revised Manuscript Received January 23, 1975)

Publication costs assisted by the Petroleum Research Fund

The enthalpies of precipitation of AgI, silver tetraphenylborate (AgTPB), tetraphenylarsonium tetraphenylborate (TPAsTPB), and tetrabutylammonium tetraphenylborate (Bu<sub>4</sub>NTPB) were measured in *t*-BuOH-H<sub>2</sub>O mixtures, of AgI and Bu<sub>4</sub>NTPB in dioxane-H<sub>2</sub>O mixtures, and of Bu<sub>4</sub>NTPB in urea-H<sub>2</sub>O mixtures via the calorimetric titration technique. From these data the enthalpy of transfer from pure water to the aqueous mixtures was obtained as an indication of water-Nonelectrolyte structural interactions. Results indicate that sparingly soluble salts (such as the TPAsTPB and Bu<sub>4</sub>NTPB) containing two highly structure-altering ions are effective probes of these structural interactions, the enthalpies of transfer for each from pure water to about 5 mol % *t*-BuOH being about 25 kcal/mol. In all three solvent systems studied structure-promoting probe salts exhibited endothermic transfer enthalpies from pure water to the highly aqueous mixtures, while the structure disrupting AgI had an endothermic transfer enthalpy in the water-*t*-BuOH system and exothermic in the water-dioxane system. Results are discussed in terms of solute-water and solute-Nonelectrolyte interactions. The entropy of precipitation of the four salts in pure water is given and discussed in terms of the solvent structural changes occurring upon reaction.

### Introduction

While extensive studies still need to be performed on water-electrolyte interactions, understanding of these systems appears to have reached a level of respectability. This might even be claimed to be true for the interaction of water with Nonelectrolytes containing large hydrophobic moieties, such as the alcohols and amines.<sup>2,3</sup> However, the situation is not so favorable for water-hydrophilic Nonelectrolyte systems. Clearly all these types of interactions must rest on firm footing if bodily processes and interactions in natural aqueous systems are to be understood. We therefore decided to begin studies of water interactions with hydrophilic Nonelectrolytes such as carbohydrates and simple proteins, and we chose initially to utilize a technique which had proven to be very valuable in explaining many water-Nonelectrolyte interactions,<sup>3,4</sup> the enthalpy of transfer of some structurally sensitive probe species from water to a mixture of water with the Nonelectrolyte in question. As our equipment holdings included several titration calorimeters we wanted to utilize a titration procedure to obtain

the enthalpy data of the probe species. In measuring the heat of precipitation of sparingly soluble salts we are able to obtain enthalpies of transfer for probes containing two highly structure-altering ions. In this way we felt we ought to realize enhanced transfer enthalpies compared to those for soluble salts, in that most soluble salts that have been used in the past have contained only one highly structure-altering ion, such as the tetraphenylborate (TPB) ion of sodium tetraphenylborate.<sup>3</sup> The heats of precipitation of the sparingly soluble salts reported here are essentially the same as would be obtained from heat of solution measurements (with opposite sign, of course), could these experiments be done.

Before this approach could be applied, for example, to water-carbohydrate mixtures to investigate the interaction of the Nonelectrolyte with water, it had to be tested in water-Nonelectrolyte mixtures for which data were available from other probes. We wanted to study both structure promoting and disrupting probe species in water-Nonelectrolyte systems of both enhanced and decreased structure

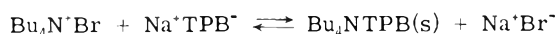
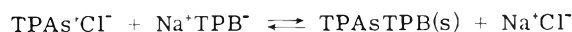
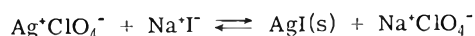


compared to pure water. The purpose of our initial investigations, then, was to determine if, indeed, sparingly soluble salts could be effective probe species, or if problems in the precipitation process would render them inefficient for this use. Additionally, we wished to see if, as expected, enhanced heats of transfer would be obtained using salts containing two structurally sensitive ions. Further, even though water-Nonelectrolyte systems that had received previous study would be utilized, additional clarification of the interactions of structure promoting and disrupting ions in these mixtures might be realized.

With these purposes in mind we chose the *tert*-butyl alcohol-water system as the structure enhanced aqueous mixture in which to test our probe reactions, because this system exhibits large structural changes with small amounts of added cosolvent.<sup>2,3</sup> It was felt that the relative sensitivity of the probe reactions ought to be apparent in this system. Two species were chosen as examples of structure-disrupting nonelectrolytes, urea and dioxane. Urea is thought to be a structure breaker of a "statistical" type, in that it appears to dissolve preferentially in the nonlattice component of water, thereby shifting the equilibrium from lattice to nonlattice and destroying some long-range order.<sup>5,6</sup> Dioxane also appears to disrupt the long-range order of water. Viscosity studies of dioxane-water mixtures<sup>7</sup> and the presence of a negative structural component of the temperature-of-maximum-density shift<sup>8</sup> seem to offer clear evidence for the structure-breaking properties of this nonelectrolyte.

The sparingly soluble salt probes chosen for this investigation are silver iodide (AgI), silver tetraphenylborate (Ag(C<sub>6</sub>H<sub>5</sub>)<sub>4</sub>B), tetraphenylarsonium tetraphenylborate ((C<sub>6</sub>H<sub>5</sub>)<sub>4</sub>As(C<sub>6</sub>H<sub>5</sub>)<sub>4</sub>B), and tetra-*n*-butylammonium tetraphenylborate ((C<sub>4</sub>H<sub>9</sub>)<sub>4</sub>N(C<sub>6</sub>H<sub>5</sub>)<sub>4</sub>B). The iodide ion is known to be fairly strongly structure breaking;<sup>7,9</sup> silver(I) probably does not influence structure significantly, although like most ions it is an overall structure breaker. While there is still some uncertainty concerning the phenyl-containing ion, most researchers now agree that these species are strong hydrophobic structure promoters,<sup>10</sup> as is the tetrabutylammonium<sup>7</sup> ion.

The precipitation reactions utilized in this study are



The titrate concentrations were all approximately millimolar and hence the enthalpy results can be considered to be equivalent to those at infinite dilution. The perchlorate anion was chosen to minimize ion-pairing difficulties,<sup>11</sup> which in any case are expected to be minimal at these concentration levels.

## Experimental Section

**Chemicals and Solutions.** The water used in this study was taken from the lab tap water system, deionized with a mixed-bed ion-exchange resin, and then distilled from an all-glass apparatus. The water was collected, stored in, and used from a closed polyethylene container. Its conductivity was about  $1.2 \times 10^{-6} \text{ ohm}^{-1} \text{ cm}^{-1}$ .

*tert*-Butyl alcohol (Fisher Certified Reagent) was puri-

fied after the method of DeVries and Soffer.<sup>12</sup> It was first dried over calcium hydroxide (100 g/l. of alcohol) for at least 12 hr, and then fractionally distilled under nitrogen. The middle 80%, boiling at 79.5–80.5°, was collected and stored under nitrogen and over Type 4A molecular sieves at about 30° to prevent freezing. The water content of the TBA (Karl Fischer method) prepared and stored in this way was less than 0.01% by weight.

Dioxane (Fisher Certified Reagent) was refluxed over sodium metal for 24 hr<sup>7</sup> under a dry nitrogen atmosphere in an all-glass system, and distilled immediately before use. The middle 80% was taken. Any purified solvent not needed for a water-dioxane mixture was stored frozen, under nitrogen, in an all-glass container. The dioxane prepared in this manner had a uv cutoff of 220 nm (Beckman DK-2A).

Both *tert*-butyl alcohol- and dioxane-water mixtures were prepared by weight. Dioxane-water mixtures were stored in a refrigerator.

Urea (Fisher Certified ACS grade), used as received, was dried in an oven for 1–2 hr at 110°, then at 70° in a vacuum oven for 24 hr.

Tris(hydroxymethyl)ammimethane (THAM) (Fisher Certified ACS grade, 99.97%), silver nitrate (Mallinckrodt Chemical Works ACS grade), and sodium hydroxide (Fisher Certified ACS grade, 50% (wt/wt) solution) were used as received as calorimetric standards. Hydrochloric acid (Fisher ACS grade) was used as the calorimetric titrant for these reagents.

Sodium iodide (Fisher Certified) and sodium tetraphenylborate (Fisher Certified ACS grade, 99.9%) were used as received. Silver perchlorate (G. F. Smith Chemical Co., anhydrous), the titrant for these reagents, was also used without purification.

Tetraphenylarsonium chloride (TPAsCl) was prepared from the hydrochloride (Eastman Organic Chemicals) using an ion-exchange procedure suggested by Bolleter and Baczuk.<sup>13</sup> These authors gave few details of the procedure, which therefore had to be developed independently. A strong base anion exchanger (Rexyn 201, Fisher Scientific, 65 g) in the chloride and sulfate form was first converted to the hydroxide cycle by passing 3 l. of 25% (wt/wt) NaOH solution through the column. An acidified silver nitrate test was applied to be sure all the Cl<sup>-</sup> and SO<sub>4</sub><sup>2-</sup> were removed. The TPAsCl · HCl (10 g) was dissolved in a minimum of warm water, placed on the column, and eluted with water. To prevent solidification during the exchange the column was maintained at about 40–50° with electrical heating tape. The presence or absence of TPAsOH in the effluent was determined by adding excess dilute perchloric acid to several drops of eluent. When the TPAs ion was present, a white precipitate of TPAsClO<sub>4</sub> formed. This precipitate was centrifuged and the supernatant liquid checked for the presence of chloride with silver nitrate to determine if any TPAsCl · HCl had not exchanged. A direct test on the eluent for chloride was not possible as it was found that nitrate ion produces a white precipitate of TPAsNO<sub>3</sub>, indistinguishable from silver chloride. Of course, silver perchlorate exhibits the same problem, forming TPAsClO<sub>4</sub>. These tests were never positive for chloride ion, indicating complete exchange with the hydroxide. About 500 ml of water was used to elute the TPAsOH, with nearly all of the salt being present in the middle 300 ml. The TPAsOH was then converted to TPAsCl by neutralizing to pH 7.00 with dilute hydrochloric acid. As the TPAsOH eluent was dissolved in rather strong sodium hydroxide solution, neutralization

also yielded a fairly concentrated sodium hydroxide solution. Because of the fairly large solubility difference between TPAsCl and sodium chloride (9.75 g/100 ml water<sup>14</sup> vs. 35.7 g/100 ml,<sup>15</sup> respectively), pure TPAsCl crystallized out of solution when the volume was reduced to 40–50 ml. The crystals, reported to be TPAsCl · 2H<sub>2</sub>O by Faithful and Wallwork,<sup>16</sup> were dried and the melting point was found to be 254–257° (258–260° lit.<sup>17</sup>). The slight melting point depression probably was due to residual water or a small amount of coprecipitated sodium chloride, neither of which were considered to be serious problems in the thermometric titration to be run using the TPAsCl as titrant. Therefore, no further purification was performed. About 80% of the TPAsCl was recovered by this procedure.

Tetrabutylammonium bromide (Bu<sub>4</sub>NBr) (Eastman Co.) was dissolved in acetone (Fisher Certified), filtered, precipitated with diethyl ether<sup>18</sup> (Fisher reagent grade), and dried under vacuum at 60° for several hours. This Bu<sub>4</sub>NBr was used as a "primary standard". In the urea-water system the Bu<sub>4</sub>NBr was used as received, but the concentration of these solutions was determined by the AgBr method. Bu<sub>4</sub>NBr and all other solid reagents were stored in a desiccator over indicating Drierite. Calorimetric titrants were generally about 0.1–0.25 *M*, depending on the enthalpy of the reaction. Sample solutions to be titrated calorimetrically were generally millimolar, and stock solutions of all except NaTPB were prepared. To prevent possible hydrolysis of the TPB ion, only that amount of solution required for one titration was prepared, and it was used immediately.

*Instrumentation.* Three titration calorimeters were utilized in this study. A medium precision differential calorimetric titration apparatus (system no. 1) (patterned after that described by Tyson, McCurdy, and Bricker)<sup>19</sup> was constructed for a portion of this study. The differential system was chosen to minimize common heat effects such as those produced by stirring and self-heating of thermistor temperature probes, and to eliminate the necessity for making corrections for heats of titrant dilution, which occur in both cells and hence are cancelled out. The cell system was not thermostated as this original apparatus was not envisioned as a high precision system and the small changes in reaction enthalpies which might occur over the range of room temperatures (23–27°) were expected to be within the limits of error of the apparatus.

Titrant delivery was effected with a Sage syringe pump (Model 234-2) and dual 2-ml glass syringes. The pair of syringes used had rates of 0.01053 and 0.01056 ml/sec. The titration cells were 90-ml capacity, polyethylene containers. With the titration cells in place, a large piece of styrofoam insulation was raised into place so that the entire cell assembly was insulated from room air currents. Stirring was effected with internal magnetic stirring bars, driven from below, at a rate of 600 rpm.

A second differential titration apparatus was later constructed (system no. 2) which had much better precision than the one described above. This apparatus utilized twin 25-ml silvered dewar reaction vessels. The entire cell assembly, as well as a length of titrant delivery tube containing sufficient titrant for at least two titrations, was thermostated in a water bath at 25 ± 0.003° (Haake Model E 52 controller). Titrant delivery rates (Sage pump, Model 234-2, 2-ml syringes) were 0.01040 and 0.01041 ml/sec. The cell assembly was constructed of a block of 1-in. thick polyethylene. Circular grooves were milled into the underside of

this block into which were glued gaskets of polyethylene foam. Into two other blocks of polyethylene were cut beveled holes to fit the bottom of each dewar cell. A system of springs attached between this bottom block and the top one held the reaction cells tightly against the polyethylene gaskets.

Stirring for this system was accomplished with internal, egg-shaped, 1-in. stirring bars. The external drive system operated at 480 rpm.

The third titration calorimeter used was a Tronac Model 450 single cell system, with Model 1040 temperature controller. Specifications for this system can be obtained from the vendor (Sanda, Inc.). The cell supplied with this system was a 50-ml capacity, thin-walled dewar similar to that described by Christensen et al.<sup>20</sup> The rate of titrant delivery for this apparatus was 0.00658 ml/sec. Temperature control was about ±0.001°.

*Circuitry.* The calibration heating circuit of system no. 1 was powered by a Kepco constant current dc power supply, Model PAT 15-1.5R. In the usual way the current was obtained by measuring the voltage across a standard resistor. (ESI, RC4R 1.0 ohm (±0.01%)). The sample cell heating coil wire (Evanohm 83 ohm/ft No. 40, Wilber B. Driver Co.) was enamel-coated to protect it from corrosion.

The temperature sensing circuitry used was similar to that of Tyson et al.<sup>19</sup> The temperature differential of the two cells was monitored with a Wheatstone bridge circuit, two arms of which contained pairs of the temperature sensing probes, while the other two arms contained fixed 15-kohm resistors. A pair of thermistors was used in each cell in order to balance out sudden heat gradients in the solutions. It was found that much decreased noise was obtained in this way. The thermistors used were 2-in. glass probe type, 30 kohm (±20%) at 25°, temperature coefficient of resistance -4.5%/deg, from Victory Engineering Co., Type A43R. The bridge power was provided by two 1.45-V mercury cells wired in series. In series with the Wheatstone bridge measuring circuit was a bridge-type buckout circuit used to bring the recorder pen on scale.

The circuitry of system no. 2 was similar to that of no. 1, with a few exceptions. The heater circuit was powered by a Heathkit regulated low-voltage power supply, Model IP-27, and the standard resistor was 10.0 ohm (±0.01%), from the same vendor as above. The bridge was not a Wheatstone type, but rather was constructed with a 1.45-V mercury cell in each of two arms, while the remaining two arms each contained a thermistor pair. This bridge configuration provides a more linear resistance vs. temperature response.<sup>21</sup> The voltage of the temperature sensing bridge of this, as well as the other two systems was monitored with a Leeds and Northrup Speedomax XL, 600 series, strip chart recorder. The standard resistor and heating coil voltages of all three systems were measured by one of three digital multimeters, a Weston Model 1240, a Data Precision Model 245, or a Digitec 275A.

*Procedure.* Two or three heating calibration runs were performed for each titration with all three instrumentation systems to ensure a reliable heat capacity determination. Calculation of enthalpy values was effected using the procedure of Tyson et al.,<sup>19</sup> direct comparison of the average heating run slope with the titration slope. At least four titration runs were performed for each enthalpy value reported. Because system no. 1 had only moderate adiabaticity heating and titration slopes were somewhat curved, and thus the "initial slope method" was used to determine

the slope values.<sup>22</sup> This necessitated using a correction based only on the pretitration or preheating drifts.

The very good adiabaticity of the other two titration systems ensured much more linear slopes. Generally, the slope was measured near the midpoint of the titration and corrections were made (for the Newton cooling effect) based on pre- and post-titration baseline drifts and the post-end point baseline, and for the effect of titrant temperature (which normally is different than the cell content's temperature) on the titration slope. A final correction for the heat capacity change resulting from addition of titrant was also made. Heat of dilution corrections were found to be very small for the reactions employed, and were not made for titrations using the Tronac system. Of course, these effects are cancelled out by the differential systems.

For both system no. 2 and the Tronac system the Newton cooling correction at point "p" at which the titration slope was measured was calculated by assuming a linear cooling effect over the small temperature ranges experienced, and a simple interpolation was performed using the pre- and post-titration baselines. For the differential system the effect of the titrant on the system is a function only of the difference in temperature of the two cells, and the baseline drift at any point is a measure of this difference. Knowing this drift at the end of the titration (titrant off) and the overall slope after the end point (titrant still on) permits the calculation of this titrant effect for the temperature differential existing at the end point. A simple proportion, using the Newton cooling effect at the end point (post-titration baseline) and at point "p" permits the calculation of the titrant effect at point "p", knowing what it is at the end point. For the Tronac system the titrant effect at point "p" was assumed to be the same as that at the end point of the titration.

For both system no. 2 and the Tronac system the heating curve slope at the midpoint was calculated by extrapolating the pre- and post-heating drifts, measuring the time of heating as the distance between perpendiculars drawn at the point of intersection of the extrapolation lines and the heating slope line, and measuring the temperature rise as the height of the line drawn vertically between the extrapolation lines at the point where the heating slope was desired. The final heating slope then was simply the height divided by the time.

Calibration of system no. 1 was performed using the reaction of hydrochloric acid titrant with sodium hydroxide, THAM, and silver nitrate, reactions for which accurate literature values are known. In general, internal precision of the results (for at least five runs) was moderately good (between 1 and 2% relative average deviation ( $\pm 0.2$ – $0.3$  kcal/mol)), while the accuracy was better, usually about 1% or slightly larger. System no. 2 and the Tronac system were calibrated using the hydrochloric acid-THAM reaction. The internal precision was about  $\pm 0.15$  and  $\pm 0.10$  kcal/mol (average deviation), respectively. Agreement with the literature value ( $11.33$  kcal/mol)<sup>22</sup> was good,  $11.24$  and  $11.32$  kcal/mol, respectively, at  $25^\circ$ . In general for these as well as the precipitation reactions titration times were between 30 and 60 sec.

## Results

All the precipitation reactions studied had fast kinetics and exhibited sharp end points. The only exception to this was for  $\text{Bu}_4\text{NTPB}$  at 0.15 mole fraction dioxane. Here somewhat slower kinetics was observed, but still rapid

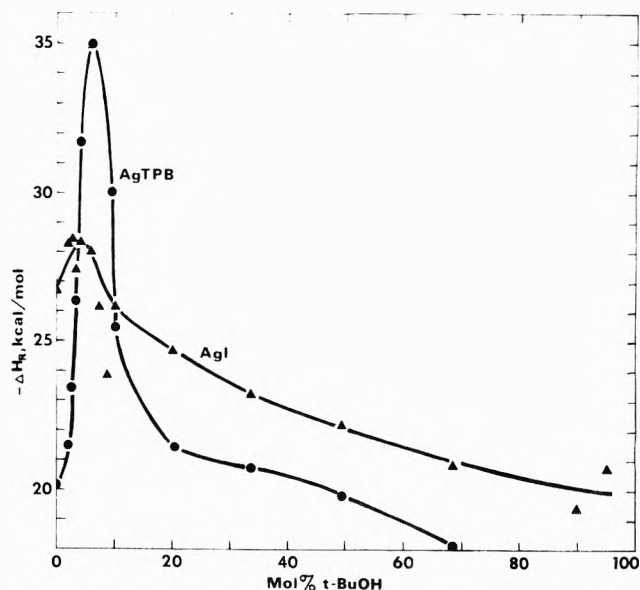


Figure 1. The overall enthalpy of reaction for AgI and AgTPB precipitation as a function of TBA concentration. Silver titrant was about  $0.1$  M and titrate was about  $0.001$  M.

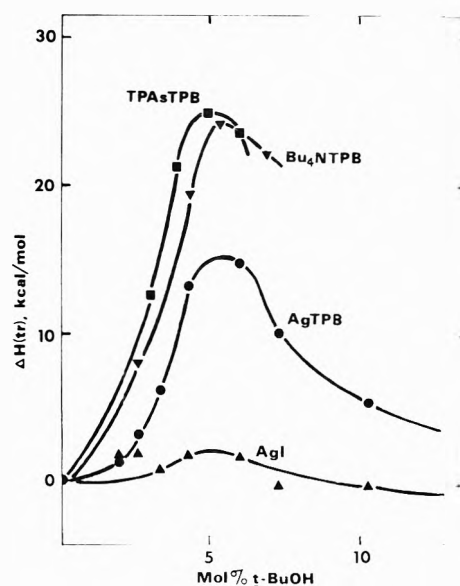


Figure 2. The enthalpy of transfer of some sparingly soluble salts from water to water-TBA mixtures as a function of TBA concentration in the highly aqueous region.

enough to yield a titration curve that could be analyzed in the straightforward manner described above. Data for  $\text{Bu}_4\text{NTPB}$  in 0.20 mole fraction dioxane could not be obtained because of extremely slow kinetics of precipitation. Indications are that this problem can be overcome by using a seed crystal of  $\text{Bu}_4\text{NTPB}$  in the reaction vessel, but this technique was not fully explored.

The enthalpy of precipitation of AgI, AgTPB, and TPA5TPB in TBA-water mixtures was obtained with system no. 1. The only exception is that for TPA5TPB in pure water, for which system no. 2 was used. All the remaining data were taken on the Tronac system except for  $\text{Bu}_4\text{NTPB}$  in pure water, 0.0451 mole fraction TBA and 0.0299 and 0.0627 mole fraction urea solutions, for which system no. 2 was used.

TABLE I: Enthalpy of Precipitation ( $\Delta H(R)$ ) of Some Sparingly Soluble Salts in the Water-*t*-BuOH System and the Enthalpy of Transfer ( $\Delta H(tr)$ ) from Water to the Mixtures

Mole fraction <i>t</i> -BuOH	$-\Delta H(R)$ , kcal/mol	$\Delta H(tr)$ , kcal/mol	No. of runs	Mole fraction <i>t</i> -BuOH	$-\Delta H(R)$ , kcal/mol	$\Delta H(tr)$ , kcal/mol	No. of runs
AgI							
0	26.70 ± 0.24		5	0.103	26.20 ± 0.30	-0.50	6
0.0201	28.31 ± 0.23	1.61	6	0.205	24.72 ± 0.18	-1.98	6
0.0265	28.48 ± 0.26	1.78	6	0.337	23.29 ± 0.25	-3.41	8
0.0341	27.41 ± 0.46	0.71	5	0.496	22.23 ± 0.22	-4.47	6
0.0433	28.41 ± 0.26	1.71	5	0.685	20.90 ± 0.18	-5.80	5
0.0607	28.09 ± 0.39	1.39	6	0.900	19.42 ± 0.23	-7.28	6
0.0746	26.18 ± 0.31	-0.52	7	0.954	20.78 ± 0.85	-5.92	5
0.0887	23.89 ± 0.29	-2.81	5				
AgTPB							
0	20.16 ± 0.24		6	0.103	25.50 ± 0.30	5.34	5
0.0201	21.50 ± 0.35	1.34	5	0.205	21.44 ± 0.27	1.28	6
0.0265	23.46 ± 0.35	3.30	5	0.337	20.27 ± 0.20	0.11	7
0.0341	26.35 ± 0.27	6.19	5	0.496	19.80 ± 0.15	-0.36	5
0.0433	31.73 ± 0.42	11.57	6	0.685	18.15 ± 0.17	-2.01	5
0.0607	34.98 ± 0.20	14.82	4	0.900	13.10 ± 0.14	-7.06	5
0.0746	30.05 ± 0.22	9.89	6	0.954	11.45 ± 0.14	-8.71	6
TPAsTPB							
0		7.54 ± 0.23					7
0.0311		20.04 ± 0.27			12.60		3
0.0400		28.75 ± 0.41			21.31		3
0.0504		32.39 ± 0.42			24.95		3
0.0612		31.01 ± 0.32			23.57		3
Bu <sub>4</sub> NTPB, at 25°							
0		5.76 ± 0.12					5
0.0267		13.65 ± 0.21			7.89		6
0.0451		23.05 ± 0.25			19.29		5
0.0552		29.77 ± 1.1			24.01		6
0.0702		27.89 ± 0.22			22.13		4

The enthalpy of transfer of a salt from pure water to an aqueous mixture was calculated as

$$\Delta H(tr) = \Delta H(R, H_2O) - \Delta H(R, \text{mix})$$

where  $\Delta H(R, \text{mix})$  is the overall reaction enthalpy in the water-nonelectrolyte mixture and  $\Delta H(R, H_2O)$  is the reaction enthalpy in pure water. The calculation has been performed in such a manner as to obtain transfer enthalpies of the same sign as would be obtained from heat of solution data. Of the four reactions studied a reliable literature value is available only for AgI in pure water.<sup>19</sup> The literature value for TPAsTPB in pure water is in gross disagreement with ours.<sup>23</sup> To our knowledge the enthalpy of precipitation of AgTPB and Bu<sub>4</sub>NTPB has not been previously determined. The enthalpies of precipitation and transfer of the four salts in the three solvent systems studied are given in Tables I-III. The overall reaction enthalpy for AgI and AgTPB in TBA-water mixtures as a function of solvent composition is shown in Figure 1. It can be seen that for AgI a "shotgun pattern" was obtained in the highly aque-

ous region, and reproducibility was very poor. This was also found to be true to a lesser extent for AgI in dioxane-water mixtures. In the more highly nonaqueous regions reproducibility was much better (this seems to be true for all the systems studied), and the particles of AgI appeared much more crystalline. The difficulty in the highly aqueous regions is probably due to the colloidal nature of the AgI precipitate although the exact cause was not determined. The precision of the results for precipitation reactions is generally poorer than for titrations where a soluble product is formed, but scatter is still small enough that trends in  $\Delta H(tr)$  are not obscured. The enthalpy of transfer of the four salts as a function of TBA concentration, of Bu<sub>4</sub>NTPB as a function of urea concentration, and of Bu<sub>4</sub>NTPB and AgI as a function of dioxane concentration is shown in Figures 2, 3, and 4, respectively.

It can be seen from Figures 1 and 2 that all four reactions studied have enthalpy vs. TBA concentration extrema at about 4-5% alcohol, in agreement with other probes used previously in this solvent system.<sup>2,3</sup> The sensitivity of the

**TABLE II: Enthalpy of Precipitation ( $\Delta H(R)$ ) of  $Bu_4NTPB$  in the Water-Urea System and the Enthalpy of Transfer ( $\Delta H(tr)$ ) from Water to the Mixtures at 25°**

Mole fraction urea	$-\Delta H(R)$ , kcal/mol	$\Delta H(tr)$ , kcal/mol	No. of runs
0	$5.76 \pm 0.12$		5
0.0134	$6.21 \pm 0.16$	0.45	5
0.0299	$6.73 \pm 0.17$	0.97	4
0.0627	$8.17 \pm 0.10$	2.41	4

**TABLE III: Enthalpy of Precipitation ( $\Delta H(R)$ ) of  $Bu_4NTPB$  and  $AgI$  in the Water-Dioxane System and the Enthalpy of Transfer ( $\Delta H(tr)$ ) from Water to the Mixtures at 25°**

Mole fraction dioxane	$-\Delta H(R)$ , kcal/mol	$\Delta H(tr)$ , kcal/mol	No. of runs
$Bu_4NTPB$			
0	$5.76 \pm 0.12$		5
0.0204	$9.68 \pm 0.13$	3.92	6
0.0400	$11.99 \pm 0.17$	6.23	5
0.0600	$13.20 \pm 0.25$	7.44	4
0.100	$13.40 \pm 0.14$	7.64	4
0.150	$12.43 \pm 0.08$	6.67	4
$AgI$			
0	$26.70 \pm 0.24$		5
0.0200	$24.68 \pm 0.42$	-2.02	4
0.0400	$24.88 \pm 0.32$	-1.82	5
0.0600	$24.31 \pm 0.10$	-2.39	5

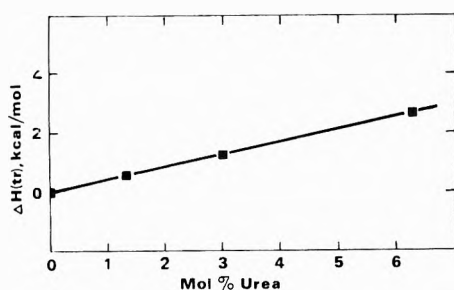


**Figure 3.** The enthalpy of transfer of  $Bu_4NTPB$  from water to water-urea mixtures as a function of urea concentration at 25°.

salts as probes of solution structure changes is  $AgI \ll AgTPB < TPAsTPB \approx Bu_4NTPB$ , the enthalpy of transfer from pure water to the extremum being about 1.7, 15, 25, and 24 kcal/mol, respectively. It would appear that both  $TPAsTPB$  and  $Bu_4NTPB$  are sensitive structure-promoting probes of water-Nonelectrolyte structural interactions. Given the expense of  $TPAsCl$ , however,  $Bu_4NTPB$  seems to be the preferred probe of this type. While  $AgI$  is not sensitive compared to the hydrocarbon-containing salts, and reproducibility is not as good, still it seems to be the most convenient of the structure-disrupting salts. It appears also that probes containing two structure-affecting ions are indeed more sensitive than those with only one.  $Bu_4NTPB$  and  $TPAsTPB$  yield transfer enthalpies about 10 kcal/mol

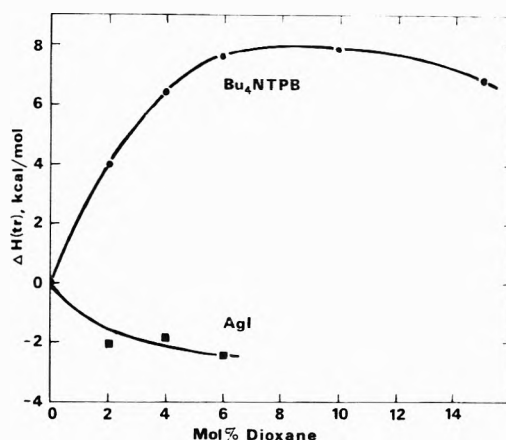


**Figure 4.** The enthalpy of transfer of  $AgI$  and  $Bu_4NTPB$  from water to water-dioxane mixtures as a function of dioxane concentration at 25°.

greater than  $NaTPB$  in  $TBA$ -water mixtures (25 vs. 15 kcal/mol)<sup>3</sup>.

### Discussion

Some comments on the contributions to the overall heat of the precipitation reactions seems to be in order here. The enthalpy of these reactions can be conceptually broken up into its "stepwise" components, reflecting the stripping of the solvation sphere totally or partially away from the cation ( $M$ ) and anion ( $A$ ), the coming together of the "bare" ions to form the molecule  $MA$ , possibly partially solvated, and the final solvation sphere stripping as several, then many,  $MA$  molecules come together to form the crystalline  $MA(s)$ . These effects may all be grouped under a so-called electrostatic category. All other solute-solvent effects can be thought of as nonelectrostatic or structural.<sup>24</sup>

$$\Delta H(R) = \Delta H(A \text{ desolv}) + \Delta H(M \text{ desolv}) + \Delta H(MA \text{ form}) + \Delta H(MA(s) \text{ form}) + \Delta H(st)$$

where  $\Delta H(R)$  is the overall reaction enthalpy,  $\Delta H(A \text{ desolv})$  and  $\Delta H(M \text{ desolv})$  are the enthalpy of desolvating the anion and cation, respectively,  $\Delta H(MA \text{ form})$  is the enthalpy of formation of the individual  $MA$  molecules,  $\Delta H(MA(s) \text{ form})$  is the enthalpy of  $MA$  solid formation, and  $\Delta H(st)$  is the enthalpy of any solvent reorganization which takes place upon removal of the  $M$  and  $A$  from solution. It almost goes without saying that the old "sphere-in-a-continuum", Born-charging approach is inadequate to account for specific solute-solvent interactions.<sup>24,25</sup>

If the enthalpy of transfer of these sparingly soluble salts is to be an effective probe of water-Nonelectrolyte structural interactions, obviously it is the last term of the series above ( $\Delta H(st)$ ) for which maximum changes are desired as the nature of the solvent is changed. In many water-Nonelectrolyte solvents it is probably a fairly safe approximation that the cation and anion solvation shells in the highly aqueous region of these mixtures closely resemble those in pure water, i.e.,  $\Delta H(\text{desolv}) \approx \Delta H(\text{dehydration})$ . Quist and Marshall have shown that in mixtures of water with "inert" solvents, such as dioxane, which do not solvate ions because of their low dipole moments, hydration numbers of most ions are the same as in pure water.<sup>26</sup> This is so despite the greatly altered dielectric constant of the solvent mixture. In other solvent systems, of course, the situation may not be the same; indeed, these authors found some intrusion of

methanol and acetone, more polar molecules, into the solvation sphere of the ions. In the TBA-water system the bulkiness of the alcohol molecule probably inhibits its entrance to any significant extent into the solvation sphere of the ions in the highly aqueous regions. Of course, as the fraction of nonelectrolyte ( $X_2$ ) becomes greater, the solvation shell undoubtedly becomes mixed. If the above approximation holds true, and because  $\Delta H(\text{MA form})$  and  $\Delta H(\text{MA(s) form})$  are constants (approximating the lattice energy) as long as the same crystal form exists as in pure water,  $\Delta H(\text{tr})$  ought to reflect the change in the desired  $\Delta H(\text{st})$  with changing  $X_2$ ; and the more "specific" the solvation of ions by water, the better this reflection becomes. That is, in the calculation of  $\Delta H(\text{tr})$  all terms cancel, or nearly so, save the  $\Delta H(\text{st})$ , so that

$$\Delta H(\text{tr}) \approx \Delta H(\text{st}, \text{H}_2\text{O}) - \Delta H(\text{st}, \text{mix})$$

and the  $\Delta H(\text{tr})$  of the salt can be used as a probe of the change in the structure of the water caused by the added nonelectrolyte.

As stated above, one of the purposes of this investigation was to determine whether precipitation of sparingly soluble salts could be an effective method of obtaining transfer enthalpy data. The results appear to indicate the affirmative. Besides this information, however, the data present an opportunity for further consideration of solute-solvent interactions in these ternary systems. It can be seen (Tables I-III) that the transfer of a structure-enforcing salt ( $\text{Bu}_4\text{NTPB}$ ) from water to the mixtures yields an enthalpy that is in the same direction whether the nonelectrolyte-water mixture is more or less structured than pure water.

In TBA-, urea-, and dioxane-water mixtures the transfer enthalpy is endothermic in the highly aqueous regions where solvent structure is changing but where three-dimensional water structure still exists. As stated earlier, TBA is a highly structure-enforcing nonelectrolyte, while urea and dioxane are considered to be disruptive of water structure, although possibly by different types of interactions. Contrasting with the behavior of  $\text{Bu}_4\text{NTPB}$  is that of  $\text{AgI}$ . This structure-breaking salt exhibits a  $\Delta H(\text{tr})$  that is endothermic in the TBA-water system (at high water concentrations) but exothermic in the structure-disrupted dioxane-water mixtures.

A reasonable explanation of this behavior can be arrived at by examining the interaction of structure-disrupting and -enforcing ions in the water-nonelectrolyte systems involved. In the structure-enforced TBA-water system structure-breaking ions,  $\text{Ag}^+$  and  $\text{I}^-$ , are more effective than in pure water, disrupting more structure because there is more to disrupt.<sup>3</sup> The structure-breaking ions apparently can "undo" what the structure-enforcing TBA molecules have done. Electrostrictive solvation of the ions by nonlattice water necessitates a shift of the water lattice = nonlattice equilibrium to the right, resulting in a less hydrogen-bonded system. However since there is less nonlattice water in the TBA-water mixture than in pure water, relatively more disruption is necessary to adequately solvate the ions. In terms of the precipitation process, an exothermic reorganization of the structure disrupted by the ions occurs upon precipitation. This exothermic term increases as the extent of structure disruption increases up to the TBA-water structural maximum, and hence  $\Delta H(\text{R})$  is greater in the highly aqueous mixture than in pure water.

For structure-enforcing ions, on the other hand, interactions in an *opposite* sense to those of structure-disrupting

ones lead to a  $\Delta H(\text{tr})$  in the *same* direction. As stated by Arnett,<sup>3</sup> in a water-nonelectrolyte solution more structured than pure water (such as TBA-water) added structure-enforcing nonelectrolyte must compete with the cosolvent for the available "structure promotability" of the water. This apparently follows as well for structure promoting salts, and these are therefore less effective as structure enforcers than in pure water. When these salts are precipitated from pure water endothermic collapse occurs of the structure they had promoted. In the solvent mixture, however, this endothermic term is smaller because less ordering was effected by the ions. Therefore,  $\Delta H(\text{R})$  is more exothermic (a less endothermic  $\Delta H(\text{st})$  term) than in pure water.

Similar reasoning for the case of structure-breaking ions in the dioxane-water system leads to the conclusion that the ions ( $\text{Ag}^+$ ,  $\text{I}^-$ ) are *less* effective in this structure-disrupted solution than in pure water. They are in essence competing with the structure-disrupting cosolvent (dioxane) for the available "structure disruptability" of the water. Because these ions are less disrupting, the extent of exothermic solvent reorganization upon precipitation is less than in pure water,  $\Delta H(\text{R})$  is less exothermic, and  $\Delta H(\text{tr})$  of the salt is exothermic. A similar situation has been observed for  $\text{NaCl}$  transfer from water to water-urea mixtures.<sup>27</sup>

As stated above, while structure-breaking salts exhibit transfer enthalpies of opposite sign in structure-enforced and structure-disrupted water-nonelectrolyte systems, structure-promoting salts, as shown by  $\text{Bu}_4\text{NTPB}$ , exhibit an endothermic transfer from water to the mixture in both types of systems. This result indicates that structure-promoting salts such as this are *less* effective in all these solvent systems than in pure water, but for different reasons. In the TBA-water system the  $\text{Bu}_4\text{NTPB}$  was competing with the alcohol. This cannot be the case in the urea- and dioxane-water systems.  $\text{Bu}_4\text{NTPB}$  apparently cannot "undo" what the urea and dioxane have done. The salt is a less effective promoter than in pure water, perhaps because there is less three-dimensional structure present with which it can interact hydrophobically. This situation may be clearer if it is viewed from the perspective of the structure-disrupting nonelectrolyte rather than that of the  $\text{Bu}_4\text{NTPB}$ . Analogous to the water-TBA- $\text{AgI}$  system, the urea and dioxane can be considered to be more effective structure breakers in the water- $\text{Bu}_4\text{NTPB}$  system than in pure water. If there is more disruption than in pure water, there must, in effect, be less promotion (by the  $\text{Bu}_4\text{NTPB}$ ). In any case, the net result is a  $\Delta H(\text{R})$  for  $\text{Bu}_4\text{NTPB}$  in urea- and dioxane-water systems that is more exothermic than in pure water, because not as much endothermic structure collapse occurs upon precipitation. Similar results have been observed for transfer of  $\text{Bu}_4\text{NBr}$  from water to urea-water mixtures.<sup>28</sup> Likewise, Kay and Broadwater found a similar increase in the Walden product of  $\text{Bu}_4\text{N}^+$  in both ethanol- and dioxane-water mixtures, and attributed this result to a "hydrophobic dehydration" of the  $\text{Bu}_4\text{N}^+$  ion in dioxane.<sup>7</sup> Mohanty and Ahluwalia<sup>29</sup> attributed the decrease in the excess partial molal heat capacity of  $\text{Bu}_4\text{NBr}$  in dioxane-water compared to pure water to interference by dioxane with hydrophobic enforcement of water structure by the hydrophobic side chains of  $\text{Bu}_4\text{NBr}$ .

The "competition effect" explanation of, e.g.,  $\text{Bu}_4\text{NTPB}$  in TBA-water mixtures is able to account satisfactorily for  $\Delta H(\text{tr})$  of the salt from pure water to the mixtures, but

**TABLE IV: Thermodynamic Parameters for Sparingly Soluble Salt Precipitation in Pure Water at 25°**

Salt	$pK_{sp}^a$	$\Delta G$ , kcal/mol	$\Delta H(\bar{R})$ , kcal/mol	$\Delta S(\bar{R})$ , cal deg <sup>-1</sup> mol <sup>-1</sup>
AgI	16.0 <sup>c</sup>	-21.82	-26.70	-16.4
AgTPB	17.2 <sup>b</sup>	-23.46	-20.16	-11.1
TPAsTPB	16.7 <sup>c</sup>	-22.77	-7.54	+51.1
<i>n</i> -Bu <sub>4</sub> NTPB	13.0 <sup>c</sup>	-17.73	-5.76	+40.2

<sup>a</sup> L. G. Sillen and A. E. Martell, "Stability Constants of Metal Ion Complexes", The Chemical Society, London, 1964. <sup>b</sup> I. M. Kolthoff and M. K. Chantooni, *Anal. Chem.*, **44**, 194 (1971). <sup>c</sup> R. Alexander and A. J. Parker, *J. Am. Chem. Soc.*, **89**, 5549 (1967).

cannot account for the increase in partial molal heat capacity of Bu<sub>4</sub>NBr on transfer from water to TBA-water mixtures.<sup>30</sup> If competition were the only effect present, a decrease in heat capacity would be expected. However, it has been pointed out that a second type of interaction must be considered, namely, solute-solute hydrophobic overlap interactions between the salt and cosolvent.<sup>31-33</sup> At lower temperatures the competition effect seems to predominate. Both the hydrophobic nonelectrolyte and the hydrophobic salt seek water lattice cavities in which to reside, and must compete for those that are available. At higher temperatures the number of cavities decreases and the salt and cosolvent solvation cospheres may overlap in micelle-like configurations. The overlap theory predicts that hydrophobic (structure-making) solutes will have an endothermic  $\Delta H(\text{tr})$  from water to TBA-water mixtures and dioxane-water mixtures in the high water regions,<sup>31</sup> as is confirmed by our results, and that the partial molal heat capacity will increase. Nevertheless, the situation is still such that, clearly, more systems need to be studied before a sensible picture of interactions in these ternary systems emerges. Whatever the interactions are, however, the effects can be summarized as below for water-nonelectrolyte mixtures in general and specifically in terms of the effect on  $\Delta H(\bar{R})$ .

(1) In mixtures more structured than pure water: (a) structure-disrupting ions are more effective than in pure water, and  $\Delta H(\bar{R})$  is more exothermic because exothermic solvent reorganization occurs to a greater extent; (b) structure-promoting ions are less effective than in pure water, and  $\Delta H(\bar{R})$  is more exothermic because endothermic structure collapse occurs to a lesser extent.

(2) In mixtures less structured than pure water: (a) structure-disrupting ions are less effective than in pure water, and  $\Delta H(\bar{R})$  is more endothermic because exothermic solvent reorganization occurs to a lesser extent; (b) structure-promoting ions are less effective than in pure water, and  $\Delta H(\bar{R})$  is more exothermic because endothermic structure collapse occurs to a lesser extent.

Beyond the structural maximum in the TBA-water system, even with further added structure-enforcing TBA, structure collapse occurs due to the presence of more foreign species (TBA) than the water structure can tolerate.<sup>2</sup> At this point the amount of nonlattice water begins to increase, the ions are probably more strongly solvated, and  $\Delta H(\text{desolv})$ , and hence  $\Delta H(\bar{R})$ , begin to become more endothermic. In the dioxane- and urea-water systems this situation probably exists with the introduction of even a small amount of structure-disrupting nonelectrolyte, and

increases in extent as the nonelectrolyte concentration increases.

Just as, for a series of structure-promoting alcohols, the structure-enforcing NaTPB probe was able to be used to determine relative orders of structure-making ability, the same situation ought to obtain for a series of known structure-disrupting nonelectrolytes. As our data show that Bu<sub>4</sub>NTPB is a very sensitive probe of structural changes relative to pure water, the transfer enthalpy of this salt should be a good probe to magnify small structure-altering differences between structure-disturbing nonelectrolytes. An indication of this is seen in the limited results obtained for the urea- and dioxane-water mixtures. Urea is thought to only slightly disturb the water structure. Bower and Robinson found only a slight deviation from unity in the activity coefficient of urea in fairly concentrated solutions.<sup>34</sup> The rather small and linear concentration dependence of  $\Delta H(\text{tr})$  shown by our results reflects the slight, statistical, structure-breaking tendencies of this species. It breaks water structure, but does not compensate with electrostrictive structure promotion. In dioxane-water mixtures larger  $\Delta H(\text{tr})$  values are observed, reflecting the more extensive structure disruption by dioxane.<sup>35</sup> Further studies are under way in this laboratory with Bu<sub>4</sub>NTPB in water-carbohydrate mixtures, where differences in the extent of structure alteration are expected to be slight.<sup>36</sup>

The ideas expressed above concerning structural reorganization of the solvent upon precipitation of the salts are given further credence by the entropy of precipitation in pure water. Using literature values for the solubility product constants for the sparingly soluble salts involved the entropy is easily calculated using our measured enthalpy values and the relationships given below.

$$\Delta G = -RT \ln K$$

$$\Delta G = \Delta H - T\Delta S$$

The overall loss in entropy (Table IV) for the AgI precipitation is consistent with the structure-disrupting tendencies of the iodide and the silver ion. The reorganization of the water which takes place upon precipitation is an entropy losing process. The +28 eu change on replacing the iodide by the TPB and the additional +40 eu change on replacing the silver of the AgTPB by TPAs are both consistent with structure-promoting tendencies of these phenyl-containing ions. The water structure promoted by these ions collapses on precipitation, an entropy gaining process. The gain in entropy for Bu<sub>4</sub>NTPB precipitation results from the same process of collapse. While these entropy values do contain the lattice entropy, an unknown factor, they are consistent with the interpretation we and others<sup>3</sup> have given these precipitation and solution processes.

*Acknowledgment.* Acknowledgment is made to the Donors of the Petroleum Research Fund, administered by the American Chemical Society, for partial support of this research, and also to the UNC-G Research Council for partial support. Thanks also go to Mr. Dick Greenwood for performing some of the calorimetric titrations, and to Dr. J.E. Desnoyers for helpful comments.

## References and Notes

- (1) (a) Taken in part from the M.S. Thesis of L. L. Bright, Jr., The University of North Carolina at Greensboro, June 1973. (b) Presented before the Division of Physical Chemistry, 25th Southeastern Regional Meeting of the American Chemical Society, Charleston, S.C., Nov 7-9, 1973.
- (2) F. Franks and D. J. G. Ives, *Quart. Rev. Chem. Soc.*, **20**, 1 (1966)

- (3) E. M. Arnett in "Physico-Chemical Processes in Mixed Aqueous Solvents", F. Franks, Ed., American Elsevier, New York, N.Y., 1967, Chapter 6
- (4) J. H. Stern and J. M. Nobilone, *J. Phys. Chem.*, **72**, 3937 (1963).
- (5) H. S. Frank and F. Franks, *J. Chem. Phys.*, **48**, 4746 (1968)
- (6) E. G. Finer, F. Franks, and M. J. Tait, *J. Am. Chem. Soc.*, **94**, 4424 (1972).
- (7) R. L. Kay and T. L. Broadwater, *Electrochim. Acta*, **16**, 667 (1971)
- (8) G. Wada and S. Umeda, *Bull. Chem. Soc. Jpn.*, **35**, 646, 1797 (1962).
- (9) H. S. Frank and M. G. Evans, *J. Chem. Phys.*, **13**, 507 (1945)
- (10) R. K. Mohanty and J. C. Ahluwalia, *J. Chem. Thermodyn.*, **4**, 53 (1972).
- (11) J. C. Synnott and J. N. Butler, *J. Phys. Chem.*, **73**, 1470 (1969)
- (12) T. DeVries and H. Soffer, *J. Phys. Chem.*, **55**, 406 (1951)
- (13) W. T. Bolleter and R. J. Baczuk, *Anal. Chem.*, **39**, 93 (1967)
- (14) P. W. Carr and J. Jordan, *Anal. Chem.*, **44**, 1278 (1972)
- (15) R. C. Weast, Ed., "Handbook of Chemistry and Physics", 51st ed., Chemical Rubber Co., Cleveland, Ohio, 1970-1971.
- (16) B. D. Faithful and S. C. Wallwork, *Acta Crystallogr. Sect. B*, **28**, 2301 (1972).
- (17) P. G. Stecher, M. Windholz, and D. S. Leahy, Ed., "The Merck Index", Merck and Co., Inc., Rahway, N.J., 1968.
- (18) A. K. R. Unni, L. Elias, and H. I. Schiff, *J. Phys. Chem.*, **67**, 1216 (1963).
- (19) B. C. Tyson, Jr., W. H. McCurdy, Jr., and C. E. Bricker, *Anal. Chem.*, **33**, 1640 (1961).
- (20) J. J. Christensen, R. M. Izatt, and L. D. Hansen, *Rev. Sci. Instrum.*, **36**, 779 (1965)
- (21) "Philbrick Applications Manual", 2nd ed., G. A. Philbrick Researches, Inc., Dedham, Mass., 1966, p 102.
- (22) P. W. Carr, *Crit. Rev. Anal. Chem.*, **10**, 491 (1972)
- (23) G. Choux and R. L. Benoit, *J. Am. Chem. Soc.*, **91**, 6221 (1969).
- (24) R. G. Bates, *J. Electroanal. Chem.*, **29**, 1 (1971)
- (25) R. L. Kay, G. P. Cunningham, and D. F. Evans in "Hydrogen-Bonded Solvent Systems", A. K. Covington and P. Jones, Ed., Taylor and Francis, London, 1968, pp 249-260.
- (26) A. S. Quist and W. L. Marshall, *J. Phys. Chem.*, **72**, 1536 (1968).
- (27) J. H. Stern and J. D. Kulluk, *J. Phys. Chem.*, **73**, 2795 (1969).
- (28) T. S. Sarma and J. C. Ahluwalia, *J. Phys. Chem.*, **76**, 1366 (1972)
- (29) R. K. Mohanty and J. C. Ahluwalia, *J. Solution Chem.*, **1**, 531 (1972).
- (30) R. K. Mohanty, S. Sundar, and J. C. Ahluwalia, *J. Phys. Chem.*, **76**, 2577 (1972).
- (31) W. Y. Wen and J. H. Hung, *J. Phys. Chem.*, **74**, 170 (1970)
- (32) J. E. Desnoyers, M. Arel, G. Perron, and C. Jolicœur, *J. Phys. Chem.*, **73**, 3346 (1969)
- (33) F. Franks and D. S. Reid in "Water: A Comprehensive Treatise", Vol. II, F. Franks, Ed., Plenum Press, New York, N.Y., 1973, pp 375-377.
- (34) V. E. Bower and R. A. Robinson, *J. Phys. Chem.*, **67**, 1524 (1963).
- (35) F. Franks, in ref 33, p 21.
- (36) Reference 33, p 350

## Electrochemistry of Chemisorbed Molecules. III. Determination of the Oxidation State of Halides Chemisorbed on Platinum. Reactivity and Catalytic Properties of Adsorbed Species

Ross F. Lane and Arthur T. Hubbard\*

Department of Chemistry, University of Hawaii, Honolulu, Hawaii 96822

(Received July 26, 1974; Revised Manuscript Received December 6, 1974)

Publication costs assisted by the National Science Foundation and the Petroleum Research Fund

Thin layer voltammetric data for Pt electrodes indicate that  $F^-$ ,  $Cl^-$ ,  $Br^-$ , and  $I^-$  form chemisorbed layers which withstand rinsing with typical aqueous electrolytes. The chemisorbed halides are much less reactive toward electrochemical oxidation than the corresponding dissolved ions. Aqueous  $I^-$  reacts with the Pt surface to form an uncharged adsorbed species, whereas  $F^-$ ,  $Cl^-$ , and  $Br^-$  are adsorbed in anionic form. Accordingly,  $F^-$ ,  $Cl^-$ , and  $Br^-$ , but not  $I^-$ , induce the adsorption of  $Fe^{2+}$  in a 2:1 ratio of halide to iron. The influence of adsorbed halide on electrode reactions of metal ions such as Pt(II), Pt(IV), Sb(III), and Sb(V) can be understood simply in terms of electrostatic interaction between the reactant and the electrode surface. Chemisorbed  $F^-$ ,  $Cl^-$ , and  $Br^-$  cause the surface to be less positively charged, whereas chemisorbed  $I^-$  has the opposite effect. In the irreversibly chemisorbed form, halide does not serve as an electron transfer bridge in the oxidation of Pt(II) or Sb(III).

### Introduction

A great variety of organic and inorganic ions and molecules chemisorb on Pt surfaces<sup>1,2</sup> and when adsorbed profoundly influence the reactivity of electrodes<sup>3,4</sup> and catalysts.<sup>5</sup> In particular, the halides and isoelectronic anions such as  $SCN^-$  and  $S^{2-}$  are strongly adsorbed, and when present appear to be intimately involved in electron transfer reactions, such as those of transition metal complexes.<sup>4,6-8</sup> Their involvement is of a fundamental sort and is expectable for all types of reactants.<sup>5</sup> Pt and Hg surfaces differ in some important respects in their behavior as adsorbents. For instance, adsorption of halides and olefins is considerably stronger on Pt than on Hg and the adsorbed layers are formed irreversibly; that is, they are not removed

when the surface is subsequently rinsed with a solution of the pure solvent.<sup>3,9</sup> The fact that the charge of the adsorbed species does not necessarily correspond to its dissolved form, and thus the reactivity and influence may also be unexpected,<sup>3,4,6</sup> combined with the fact that the charge and valency of species adsorbed at Pt surfaces have not been determined prompted the studies reported here.

The negative shift in the "rest" potential of a Pt electrode observed when KI is added to the aqueous electrolytic cell has been interpreted by Bagotsky *et al.*<sup>10</sup> as due to specific adsorption of  $I^-$ , in anionic form, and the correctness of their conclusions rests on the appropriateness of this assumption; there is considerable evidence to the contrary, however, that upon chemisorption the  $I^-$  is convert-



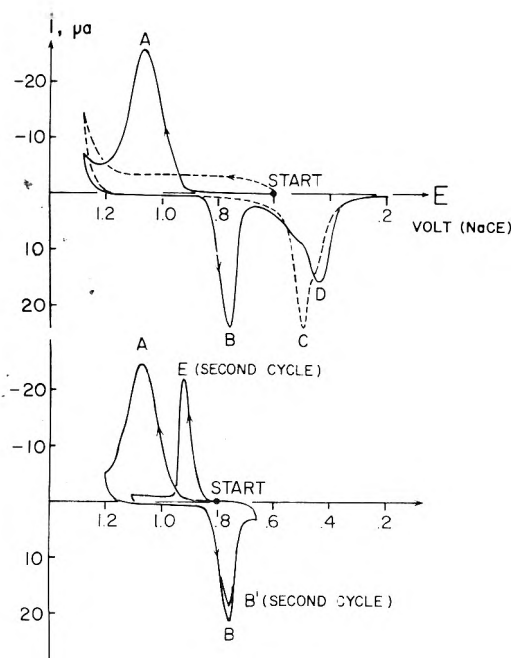


**Figure 1.** Cyclic thin layer current-potential curves for clean and iodide-treated platinum electrodes: (---) clean electrodes; (—) electrodes containing chemisorbed iodine. The experimental conditions were as follows. The thin layer electrode was cleaned prior to each trial as described in the Experimental Section. Chemisorption of iodide occurred during exposure of the clean electrode to a 1 M aqueous solution of KI for 3 min, at open circuit. The electrode was then rinsed thoroughly with the pure supporting electrolyte, 1 F HClO<sub>4</sub>, to remove the excess, nonchemisorbed iodide from the solution layer; thus, only chemisorbed material was present at the onset of the current-potential curves. Thin layer volume,  $V = 3.88 \mu\text{l}$ ; platinum electrode area,  $A = 1.15 \text{ cm}^2$ ; average solution layer thickness,  $l = 33.7 \mu\text{m}$ ; rate of potential sweep,  $\dot{V} = 2.00 \text{ mV sec}^{-1}$ ; solution temperature,  $T = 23 \pm 1^\circ$ .

ed to a neutral species<sup>3,4,6,11</sup> which displaces adsorbed anions and thus shifts the potential,  $\phi_2$ , at the outer Helmholtz plane to values more positive than would otherwise be observed. The observed shift in "rest" potential results, instead, simply from the fact that  $\text{I}^-$  is an effective reducing agent.

Enhancement of the electrooxidation of  $\text{SbCl}_4^-$  in 2 F HCl solutions at Pt electrodes resulting from pretreatment of the electrodes with KI has been interpreted as evidence that the chemisorbed species acts as an electron-transfer bridge between the electrode and the Sb(III) reactant.<sup>12</sup> Electrostatic double layer effects were excluded as a possible cause of the enhancement on the premise that  $\text{I}^-$  adsorbs on Pt as the simple anion. However, the results could have been explained equally well by saying that adsorption increased  $\phi_2$ , and in turn the effective reactant concentration, leading to the observed increase in rate in a manner identical with that already demonstrated for Pt complexes.<sup>4,6,11</sup>

At issue, therefore, in the present work is the charge carried by species adsorbed from  $\text{I}^-$  solutions on Pt, and the role played by the adsorbed species in electron transfer reactions.  $\text{F}^-$ ,  $\text{Cl}^-$ , and  $\text{Br}^-$  have been investigated similarly to allow comparison.

## Results and Discussion

**1. Interfacial Excess and Reactivity of Chemisorbed Halides. i. Iodide.** Thin layer current-potential curves for clean electrodes and ones containing a layer of chemisorbed

I appear in Figure 1. Oxidation of chemisorbed I commences at potentials about 500 mV more positive than the standard potential of the  $\text{I}_2/\text{I}^-$  couple in the initial, positive-going potential scan (curve A), indicating that the chemisorbed material is hindered thermodynamically and/or kinetically from reacting. The oxidation products are nonchemisorbed  $\text{IO}_3^-$ <sup>13</sup> and adsorbed oxygen, as evidenced by peaks corresponding to reduction of  $\text{IO}_3^-$  to  $\text{I}_2$  (curve B, peak potential,  $E_p = 0.76 \text{ V NaCE}$ ) and the onset of reduction of the surface layer (curve C) in the subsequent negative-going scan. Following reduction of  $\text{IO}_3^-$  to  $\text{I}_2$  at the oxidized surface, concomitant reduction of  $\text{I}_2$  with the surface layer occurs (curve D), such that the layer of chemisorbed I is reestablished, as evidenced by the fact that subsequent scans are identical with the first one. That the chemisorbed oxygen layer formed during the initial, positive-going scan effectively prevents halide adsorption can be seen from the current-potential curve obtained when the scan direction is reversed following  $\text{IO}_3^-$  reduction, curve B, but prior to oxygen-layer reduction (curves C and D), in which a new curve E appears corresponding in area and position to oxidation of dissolved  $\text{I}_2$  to  $\text{IO}_3^-$ , and from which curve A due to oxidation of chemisorbed material is absent. Rinsing the electrode with pure solvent just after the scan had passed curve B ( $E = 0.70 \text{ V NaCE}$ ) completely removed the  $\text{I}_2$  from the cell, confirming that it was not present in an irreversibly chemisorbed state.

Since current-potential curves for chemisorbed I obtained previously were not analyzed quantitatively to confirm their adherence to the particular form of the experimental equations dictated by the assumed mechanism,<sup>13</sup> it seemed appropriate to do so here. The appropriate experimental equations were derived, tested,<sup>3</sup> and reviewed,<sup>14</sup> earlier. The thin layer current-potential curve for oxidation of an individual, chemisorbed halogenic species in an electrochemically irreversible process is expected to follow eq 1-3. Please refer to the Appendix for definitions of sym-

$${}_a i = nFA^*k^0_1\gamma_R\Gamma_R^0 \exp\left\{\frac{(1-\alpha)F}{RT}(E-E^0) - \frac{RT^*b^0_1\gamma_R}{(1-\alpha)F\gamma} \exp\left[\frac{(1-\alpha)F}{RT}(E-E^0)\right]\right\} \quad (1)$$

$${}_a i_p = \frac{(1-\alpha)nF^2Ar\Gamma_R^0}{(e)RT} \quad (2)$$

$${}_a E_p = E^0 + \frac{RT}{(1-\alpha)F} \ln \frac{RT_1\gamma_R^*k^1}{(1-\alpha)F\gamma} \quad (3)$$

bols employed. For the purpose of comparing experiment with theory, it is convenient to rewrite eq 1 in terms of the peak current and peak potential, as follows:

$${}_a i = (e)_a i_p \exp\left\{\frac{(-{}_a i_p)e}{nFAr\Gamma_R^0}(E - {}_a E_p) - \exp\left[\frac{(-{}_a i_p)e}{nFAr\Gamma_R^0}(E - {}_a E_p)\right]\right\} \quad (4)$$

Graphs of eq 4 and of the experimental data (corrected for contribution to the current due to background reactions as described in ref 3) appear in Figure 2. The agreement between experiment and theory is evidence for the correctness of the above interpretation. In plotting eq 4, it was assumed that the reaction involves a net transfer of five electrons ( $n = 5$ ; oxidation of zero-valent I to  $\text{IO}_3^-$ ); direct determination of  $n$  was carried out to substantiate this assumption, as described below. The initial coverage was de-

**TABLE I: Thin Layer Coulometric Determination of the Number of Electrons Required for Oxidative Desorption of Chemisorbed I<sup>a</sup>**

$Q - Q_b, \mu\text{C}^b$ (oxidation)	$Q - Q_b, \mu\text{C}^c$ (reduction)	$10^9 \Gamma_1^0, \text{mol cm}^{-2}$ , from eq 6	$n$ , Faraday mol <sup>-1</sup> , from eq 6
220.5	203.5	0.37	5.4
284.1	288.3	0.52	4.9
347.7	373.1	0.67	4.7
657.9	623.3	1.12 <sup>d</sup>	5.3
652.3	625.0	1.13 <sup>d</sup>	5.2
648.9	642.4	1.16 <sup>d</sup>	5.0
	1060.0	1.91 <sup>e</sup>	
	1123.6	2.03 <sup>e</sup>	

<sup>a</sup> The experimental conditions were as follows. The supporting electrolyte was 1 F HClO<sub>4</sub>; thin layer volume,  $V = 3.88 \mu\text{l}$ ; electrode area,  $A = 1.15 \text{ cm}^2$ ; average solution layer thickness,  $l = 33.7 \mu\text{m}$ . <sup>b</sup> The potential step was 0.400 to 1.040 V NaCE. <sup>c</sup> Values resulting from reduction of dissolved IO<sub>3</sub><sup>-</sup>, immediately following the potential step *b*. The potential step was 1.040 to 0.700 V NaCE. <sup>d</sup> Saturation value, obtained as in Figure 1. <sup>e</sup> These values resulted from rinsing the electrode with 1 mF I<sub>2</sub> for 3 min, at open circuit. I<sub>2</sub> solutions were prepared as described in ref 13.

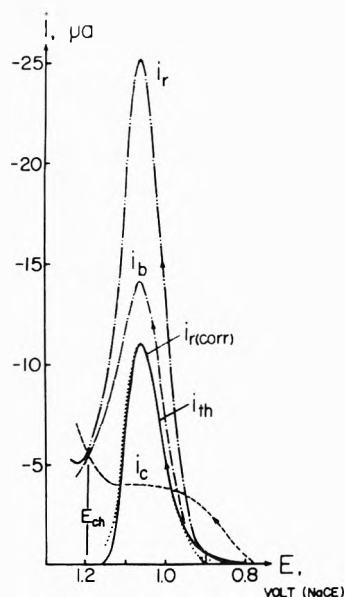


**Figure 2.** Theoretical thin layer current-potential curves for electro-oxidation of chemisorbed I (eq 4): (---) observed anodic current,  $i_r$ , for electrode containing chemisorbed I; (—) theoretical current,  $i_{th}$ , for electrode containing chemisorbed I, graph of eq 4; (· · ·) observed current for iodide-coated electrode,  $i(ccrr)$ , after correction for background current as explained in ref 3; (- - -) background current,  $i_c$ , for clean electrode; (- - - -) theoretical background current,  $i_b$ , for a coated electrode. The following values were employed in preparing the plots:  $a i_p = 25.2 \mu\text{A}$ ;  $a E_p = 1.07 \text{ V}$ ;  $\Gamma_1 = 1.12 \times 10^{-9} \text{ mol cm}^{-2}$  (Table I);  $n = 5$ . Other parameters and experimental conditions were as in Figure 1.

terminated by means of thin layer coulometry, again based upon  $n = 5$ .

Pt surfaces containing analytically known quantities of chemisorbed I were prepared for use in determination of the  $n$  value for chemisorbed I oxidation by taking advantage of the fact that the adsorption process is quantitative and irreversible<sup>13</sup> and that it is a simple matter by means of the thin layer electrode to expose the surface to a known volume of solution. Since, for a Pt surface not fully saturat-

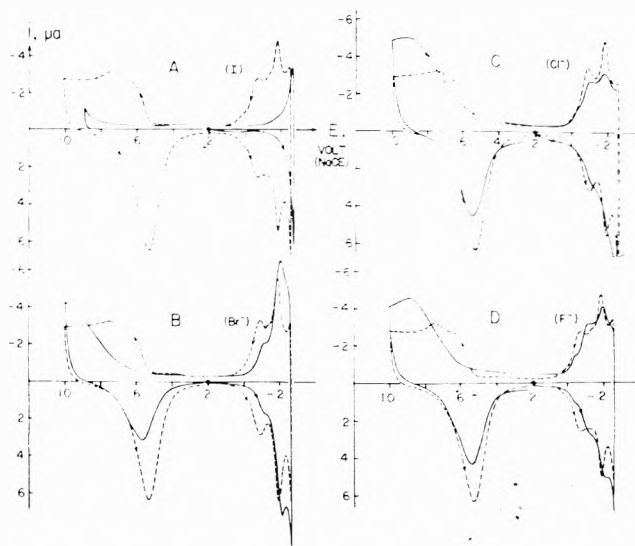


**Figure 3.** Thin layer current-potential curves for clean and halide-treated Pt surfaces: (---) clean electrodes; (—) electrodes rinsed with aqueous sodium halide: (A) iodide, (B) bromide, (C) chloride, (D) fluoride. The experimental conditions were as follows. The electrode, cleaned as described in the Experimental Section, was exposed for 3 min at open circuit to 1 mF aqueous NaX (X = I, Br, Cl, or F), followed by thorough rinsing with water and with pure supporting electrolyte. Current-potential curves for the clean surface were obtained by an exactly identical procedure in which pure H<sub>2</sub>O was substituted for the halide solution. The supporting electrolyte was 1 F H<sub>2</sub>SO<sub>4</sub>. Other experimental conditions were as in Figure 1.

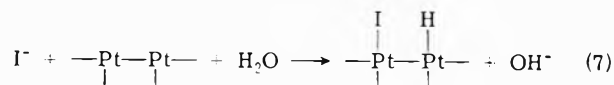
ed with chemisorbed I, essentially all of the I<sup>-</sup> introduced into the solution layer will become adsorbed, the interfacial excess resulting from filling the thin layer cavity with a total volume,  $V$ , of I<sup>-</sup> solution of initial concentration,  $C^0$ , will be given by eq 5. The quantity,  $n$ , in eq 4 is related to

$$\Gamma^0 = C^0 V/A \quad (5)$$

the measured coulometric charge, corrected for a contribution from background reactions, by the Faraday law, eq 6.

$$Q - Q_b = nFA\Gamma^0 \quad (6)$$

Equation 6 can be applied to the coulometric charge for reduction of IO<sub>3</sub><sup>-</sup> ( $n = 5$ ) produced by oxidative desorption of I, as a test of the analytical accuracy of the above determination of  $n$ . The results appear in Table I, from which it is clear that oxidation of adsorbed I to IO<sub>3</sub><sup>-</sup> is a five-electron process.  $\Gamma^0$  approaches a limiting value of about  $1 \times 10^{-9} \text{ mol cm}^{-2}$  as compared with approximately  $2 \times 10^{-9} \text{ mol cm}^{-2}$  of surface Pt atoms based upon geometric considerations, implying one adsorbed I per two Pt surface atoms. A possible explanation of this observation is that adsorption from I<sup>-</sup> solutions involves the formation of a mixed deposit of I and H, eq 7. It is surprising that ad-



sorbed H, if present, is not electrochemically oxidized at potentials as positive as 1.0 V NaCE, although adsorption of H on Pt, in a form functionally distinct from that derived from reduction of H<sub>2</sub>O, upon chemisorption of hydrocarbons, has been reported.<sup>15</sup> Adsorption of I from solutions of I<sub>2</sub> was also studied. The results, Table I, indicate that when I<sub>2</sub> is the surfactant, the saturation coverage ap-

proaches one I per Pt in the surface layer, as would be expected if  $I_2$  is adsorbed without the necessity of sharing the surface equally with adsorbed H. However, the purpose of the present section is to describe the reactivity of the chemisorbed halides; the charge of the adsorbed species has been investigated more directly through experiments described below.

*ii. Bromide, Chloride, and Fluoride.* Current-potential curves obtained for clean Pt electrodes and ones exposed briefly to microliter volumes of dilute aqueous solutions of NaBr, NaCl, or NaF appear in Figure 3. Peaks related to reversible H deposition-dissolution appear in the current-potential curves for clean electrodes and may be taken as evidence that the surface is relatively clean,<sup>15,16</sup> although determination of the origins of these peaks evidently must await the results of experiments upon electrodes of precisely known surface atomic structure and composition. Similarly, positive-going scans exhibit several indistinct peaks in the oxygen-adsorption region which are associated with surface cleanliness.<sup>17</sup> The influence of chemisorbed halide on the H and O adsorption regions of the current-potential curves is apparent for all of the halogens, but most dramatic for I. Exposing the Pt surface to 1 mF aqueous NaI completely prevents H and O electrodeposition over the normal ranges of potential characteristic of the clean surface. Similarly, treatment of the surface with aqueous  $Br^-$ ,  $Cl^-$ , or  $F^-$  suppresses H and O electrodeposition, although not as dramatically as I. The degree of influence is in the order  $I > Br^- > Cl^- > F^-$ .

Halide adsorption has the effect of decreasing the amount of H deposited at a given magnitude of the electrode potential, as has been pointed out in many articles, listed in ref 16, and shifts the current peaks to less reversible potentials, as can be seen from Figure 3. Previous studies have not made clear the fact that chemisorption of each of the halides on Pt surfaces occurs irreversibly; that is, the chemisorbed halide is not removed by rinsing with inert electrolyte apart from extremely positive electrode potentials within a practicable length of time. Once the surface is exposed to halide it remains coated until cleaned. The characteristics of the Pt-halide bond in the chemisorbed layer are thus reminiscent of the nonlabile coordination compounds formed between halide ions and Pt(II) or Pt(IV).<sup>18</sup> Studies of the Pt-halide bond in adsorption situations and coordination compounds are in progress and will be reported elsewhere.<sup>19</sup>

Irreversibly chemisorbed halide layers on Pt have escaped detection at least in part because the adsorbed material is difficultly reactive, giving no appreciable faradaic current in the range of electrode potentials in which the "dissolved" halides react freely.<sup>13,20</sup> Comparison of the current-potential curves in Figure 3, obtained when only chemisorbed halide was present, with those obtained with halide in the solution, Figure 4, illustrates this situation.  $I^-$ ,  $Br^-$ , and  $Cl^-$  solutions all exhibit well-defined, reversible current-potential curves at the thin layer electrode.  $F^-$  being masked by oxidation of the solvent, but the chemisorbed layers betray their presence only by suppressing the reactions of other species. Quantitative evidence has been presented for the unreactivity of I chemisorbed at Pt,<sup>13</sup> based upon experiments in which the clean thin layer electrode was supplied with only enough liquid to fill the thin layer cavity; due to the unreactivity of the chemisorbed material, the Faraday law takes the form of eq 8, resulting

$$Q - Q_b = nFVC^0 - nFAI^{(0)} \quad (8)$$

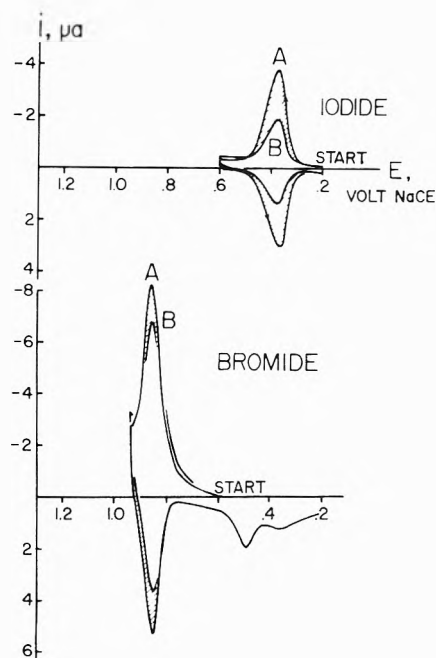


**Figure 4.** Thin layer current-potential curves illustrating the unreactivity of halide when chemisorbed on Pt: (curves A) electrode treated with large excess of halide solution; (curves B) electrode supplied with exactly  $3.88 \times 10^{-3} \text{ cm}^3$  of 0.5 mF NaX. The solution contained 0.5 mF NaX ( $X = I, Br$ ) in 1 F  $H_2SO_4$ . Other experimental conditions were as in Figure 1. Shaded area designates decrease in total charge caused by chemisorption in unreactive form.

in an area under the current peak ( $nFVC^0 - nFAI^{(0)}$ ) of less than that expected under normal circumstances ( $nFVC^0$ ), achieved in the present case by rinsing the surface with an excess of the halide solution. The results appear in Figure 4. The difference in area between pairs of curves (shaded) indicates that  $I^{(0)}$  equals about  $10^{-9} \text{ mol cm}^{-2}$  for the conditions employed. Note that this is the maximum not the equilibrium value corresponding to the given concentration. However, owing to the large contribution to the measured charge resulting from background reactions, and the difficulty of properly assigning this charge, this procedure was not employed for quantitative estimation of  $I^{(0)}$ . Instead, after  $Br^-$ ,  $Cl^-$ , or  $F^-$  had been allowed to adsorb, the coated surface was exposed to an exact volume of a solution of NaI in 1 F  $HClO_4$ , and the excess  $I^-$  determined coulometrically, taking advantage of the circumstance that the adsorption process is irreversible, that I adsorption is quantitative and that adsorbed  $Br^-$ ,  $Cl^-$ , and  $F^-$  do not interfere with the determination of  $I^-$ . Typical current-potential data resulting from this procedure appear in Figure 5. Each curve represents a separate experiment. Curve A, obtained in the absence of adsorbed  $Br^-$ , indicates the amount of  $I^-$  remaining after saturation of the initially clean surface with I (eq 8). Curve B shows that less  $I^-$  is removed from solution by a surface pretreated with  $Br^-$  and curve C shows that no further  $I^-$  uptake is possible once the surface has been saturated with I. Curve D was obtained for an electrode containing only chemisorbed I. Curves having a similar appearance were obtained for surfaces treated with  $Cl^-$  or  $F^-$ . In analyzing the resulting data it was assumed that chemisorbed I occupied all sites not occupied by  $Br^-$ , in a ratio of two Pt surface atoms per I atom adsorbed and one Pt surface atom per  $Br^-$  adsorbed (eq 9), where  $\Gamma_1^{(0)}(\text{satd})$  and  $\Gamma_1^{(0)}$  refer to the maximum (satu-

TABLE II: Interfacial Excess Data for I<sup>-</sup>, Br<sup>-</sup>, Cl<sup>-</sup>, and F<sup>-</sup> Chemisorbed on Pt<sup>a</sup>

Halide X	Iodide concn. mF	Q, $\mu\text{C}$	Q <sub>b</sub> , $\mu\text{C}$	FA $\Gamma_{\text{I}^-}$ <sup>0</sup> , $\mu\text{C}$ , from eq 8	10 <sup>10</sup> $\Gamma_{\text{X}^-}$ <sup>0</sup> , mol cm <sup>-2</sup> from eq 9
I	1.0	274.0 ± 2.3	23.9 ± 1.0	124.3 ± 3.3	11.2 ± 0.3
Br <sup>-</sup>	1.0	350.3 ± 6.6	28.1 ± 1.2	52.2 ± 7.8	13.0 ± 0.9
Cl <sup>-</sup>	1.0	317.4 ± 4.2	24.0 ± 1.6	81.0 ± 5.8	7.8 ± 0.7
F <sup>-</sup>	1.0	308.0 ± 7.1	23.5 ± 0.9	89.9 ± 8.0	6.2 ± 0.9

<sup>a</sup> Chemisorption of Br<sup>-</sup>, Cl<sup>-</sup>, and F<sup>-</sup> was effected as in Figure 3. Exactly 3.88 × 10<sup>-3</sup> cm<sup>3</sup> of 1.0 mF NaI in 1 F HClO<sub>4</sub> was then added. Each entry represents the average of several trials with the reproducibility shown. Electrode area, A = 1.15 cm<sup>2</sup>; initial potential, 0.200 V NaCE; final potential, 0.550 V NaCE.

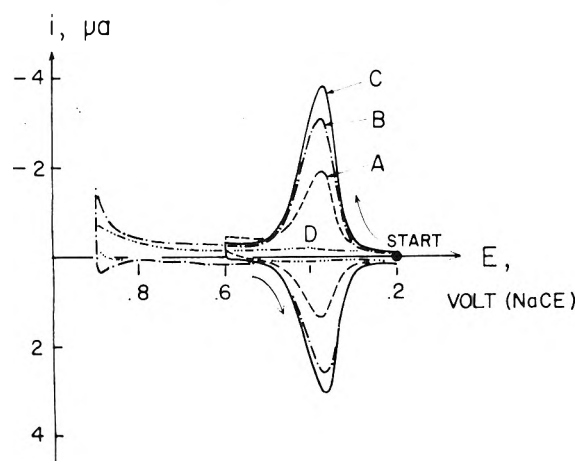


Figure 5. Thin layer current-potential curves for Pt electrodes containing mixed deposits of chemisorbed Br<sup>-</sup> and I<sup>-</sup>: (curve A) clean electrode with 3.88 × 10<sup>-3</sup> cm<sup>3</sup> of 0.5 mF NaI, in 1 F HClO<sub>4</sub>, added; (curve B) electrode was rinsed with 1 mF NaBr for 3.0 min; 3.88 × 10<sup>-3</sup> cm<sup>3</sup> of 0.5 mF NaI in 1 F HClO<sub>4</sub> was then introduced; (curve C) electrode was rinsed with 0.5 mF NaI for 3.0 min; 3.88 × 10<sup>-3</sup> cm<sup>3</sup> of 0.5 mF NaI in 1 F HClO<sub>4</sub> was then introduced; (curve D) electrode was rinsed with 0.5 mF NaI for 3.0 min; 3.88 × 10<sup>-3</sup> cm<sup>3</sup> of 1 F HClO<sub>4</sub> was then introduced. Other experimental conditions were as in Figure 1.

$$\Gamma_{\text{Br}^-} = 2[\Gamma_{\text{I}^-}(\text{satd}) - \Gamma_{\text{I}^-}] \quad (9)$$

ration) and observed (after Br<sup>-</sup> pretreatment) interfacial excesses, respectively. Equation 9 was also employed for Cl<sup>-</sup> and F<sup>-</sup>. That I<sup>-</sup> does not dislodge chemisorbed Br<sup>-</sup> from the surface is indicated by the absence of a peak for oxidation of dissolved Br<sup>-</sup> (Figure 5, curve B). The results are summarized in Tables II and III.

2 Adsorption of Fe<sup>2+</sup> Induced by Halide. Kinetic evidence was presented in ref 4 and 6 that aqueous I<sup>-</sup> solutions react with Pt surfaces to form neutral chemisorbed species. Thermodynamic evidence in support of this hypothesis has now been obtained, also, by taking advantage of the fact that when a thin layer electrode is rinsed and filled with a solution of a species which adsorbs in an electroactive form the adsorbed amount is directly and accurately indicated by the coulometric charge,<sup>8,11,21</sup> eq 10. In

$$Q - Q_b = nFVC^0 + nF\Gamma^0 \quad (10)$$

particular, when a Pt thin layer electrode is rinsed with a solution of FeI<sub>2</sub> in H<sub>2</sub>O the surface acquires a layer of adsorbed halogenic species, and Fe<sup>2+</sup> ions will be retained at the interface to preserve electroneutrality if the adsorbed halogenic species is negatively charged, but will be swept away into the bulk solution if the adsorbed halogen is uncharged; accordingly, observation of an interfacial excess of Fe<sup>2+</sup> would be indicative of halide adsorption in anionic

TABLE III: Interfacial Excess Data for Fe<sup>2+</sup> at Halide-Coated Pt Surfaces<sup>a</sup>

Halide X	Halide concn, mF	Q, $\mu\text{C}$	Q <sub>b</sub> , $\mu\text{C}$	10 <sup>10</sup> $\Gamma_{\text{Fe}^{2+}}$ <sup>0</sup> , mol cm <sup>-2</sup> , from eq 6
I	1.0	23.3 ± 1.5	22.0 ± 1.1	0.1 ± 0.2
Br <sup>-</sup>	1.0	98.4 ± 2.7	31.8 ± 1.4	6.0 ± 0.4
Cl <sup>-</sup>	1.0	70.1 ± 3.1	35.7 ± 1.8	3.1 ± 0.5
F <sup>-</sup>	1.0	69.2 ± 3.0	41.4 ± 2.0	2.5 ± 0.5

<sup>a</sup> Experimental conditions as in Table II, except C<sub>Fe<sup>2+</sup></sub><sup>0</sup> = 0.5 mF; initial potential, 0.200 V NaCE; final potential, 0.520 V NaCE.

form, and, conversely, the absence of an interfacial excess would argue against the presence of anionic adsorbates. That is, the electrode electronic charge, q, must be equal and opposite to the sum of the ionic charges, q<sub>i</sub>,<sup>9</sup> eq 11. Ne-

$$q = -\sum_i q_i = -FA \sum_i Z_i \int_0^\infty C_i dx = -FA \sum_i Z_i \Gamma_i^{*0} \quad (11)$$

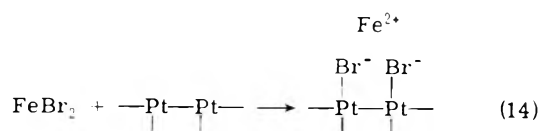
glecting the charge due to H<sup>+</sup> and OH<sup>-</sup> for C<sub>Fe<sup>2+</sup></sub> ≥ 10<sup>-4</sup> F leads to eq 12. Thus, 2 $\Gamma_{\text{Fe}^{2+}}$ <sup>0</sup> and  $\Gamma_{\text{X}^-}$ <sup>0</sup> differ by an amount

$$q = -FA \int_0^\infty [2C_{\text{Fe}^{2+}} - C_{\text{X}^-}] dx = -FA[2\Gamma_{\text{Fe}^{2+}}^{*0} - \Gamma_{\text{X}^-}^{*0}] \quad (12)$$

equal to q, of course, but this difference is not sufficiently large to invalidate the qualitative result because the halide ionic charge excess, FA $\Gamma_{\text{X}^-}$ <sup>0</sup>, is very large in comparison with q, at least for X = I, Br, Cl, and F. Thus, to preserve electroneutrality solely by equating q to FA $\Gamma_{\text{X}^-}$ <sup>0</sup> would require unreasonably large electrode potential, capacitance, and/or zero charge potential. For instance, if  $\Gamma_{\text{X}^-}$ <sup>0</sup> is taken to be 10<sup>-9</sup> mol cm<sup>-2</sup>, then the departure of electrode potential, E, from the zero charge potential, E<sub>z</sub>, predicted by means of eq 13 for electrode double layer capacitance, C,

$$q = \int_{E_z}^E C dE = FA\Gamma_{\text{X}^-}^{*0} \quad (13)$$

on the order of 25  $\mu\text{F cm}^{-2}$ ,<sup>22,23</sup> would have to be about E - E<sub>z</sub> = 4 V! Instead, it seems very likely that preservation of electroneutrality is formation of a mixed layer either as stated in eq 7, or in eq 14. Fe(II) exists primarily as the



simple aquo dication, Fe(H<sub>2</sub>O)<sub>6</sub><sup>2+</sup>, in its dilute halide solutions at slightly acidic pH.<sup>24</sup> Determination of Fe<sup>2+</sup> was carried out by means of thin layer coulometric experiments

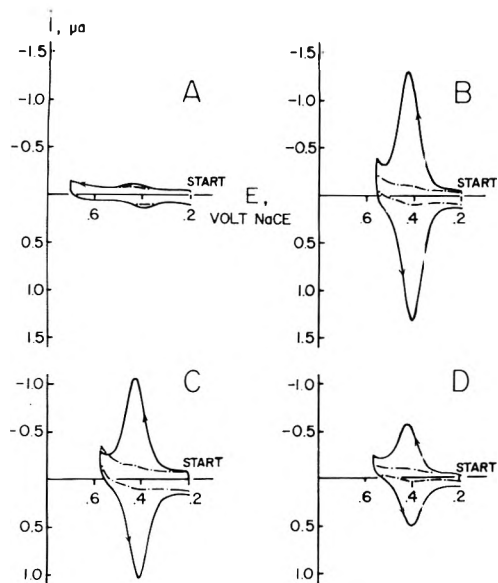


**Figure 6.** Current-potential curves of Pt thin layer electrodes rinsed with aqueous  $\text{FeX}_2$ : (—) reactant solution; (---) background; (A)  $\text{FeI}_2$ , (B)  $\text{FeBr}_2$ , (C)  $\text{FeCl}_2$ , (D)  $\text{FeF}_2$ . The experimental conditions were as follows. Prior to recording each current-potential curve the clean electrode was rinsed with an excess of 0.5 mF  $\text{FeX}_2$  in pure water at pH 6.5, freed of excess solution by application of pressurized inert gas and filled with exactly  $3.88 \times 10^{-3} \text{ cm}^3$  of 1 F  $\text{HClO}_4$ . NaX was employed in place of  $\text{FeX}_2$  in recording the background curves. Other conditions were as in Figure 1.

in which it was ascertained that the excess of  $\text{FeX}_2$  solution could be expelled from the thin layer cavity by application of pressurized inert gas, retaining only a thin film having a negligible volume, and that the cell could be subsequently filled with an aliquot of 1 F  $\text{HClO}_4$  by release of the inert gas pressure without loss of the adsorbed material. Thus, the measured coulometric charge corresponded solely to the adsorbed  $\text{Fe}^{2+}$  and background reactions (eq 6).

Current-potential curves for Pt electrodes treated at open circuit with aqueous  $\text{FeI}_2$ ,  $\text{FeBr}_2$ ,  $\text{FeCl}_2$ , or  $\text{FeF}_2$ , freed of excess solution ( $E = 0.200 \text{ V}$ ) and filled with 1 F  $\text{HClO}_4$  appear in Figure 6, and values of  $\Gamma_{\text{Fe}^{2+}}$  are compiled in Table III, from which it can be seen that halide ions induce the adsorption of  $\text{Fe}^{2+}$  in the order  $\text{Br}^- > \text{Cl}^- > \text{F}^-$  and that  $\text{FeI}_2$  does not lead to  $\text{Fe}^{2+}$  adsorption, within the sensitivity of the method, a few per cent of a monolayer. This substantiates the claim that  $\text{I}^-$  forms a neutral chemisorbed species on Pt.

3. The Question of Electron Transfer Bridging by Chemisorbed Halide. i. Electrochemical Interconversion of Pt(II) and Pt(IV) Compounds. Previous studies have detailed the influence of chemisorbed I on the electrode reactions of Pt(II) and Pt(IV) complexes.<sup>4,6,11,14</sup> By comparison with various other surfactants, charged and neutral, it is apparent that chemisorbed I limits the adsorption of other anions, rendering the potential,  $\phi_z$ , at the reaction plane more positive than it would otherwise be, leading to an increase in the effective concentration of anionic reactants at the reaction plane and to an increase in reaction rate, or to a decrease in concentration and reaction rate of positively charged species, with little or no effect being observed for neutral reactants.<sup>4</sup> The kinetic influence of chemisorbed I and other surfactants not reacting chemically with the Pt(II) and Pt(IV) complexes is preponderantly of electrostatic origin and depends only on the ionic charges of the reactant and surfactant for a wide variety of structural and

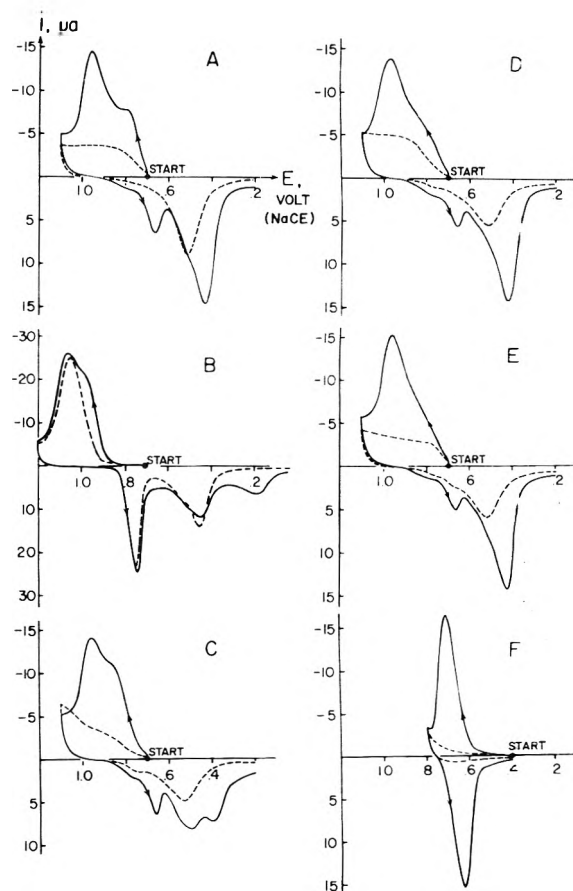
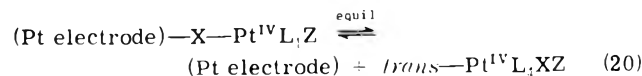
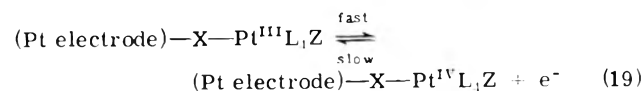
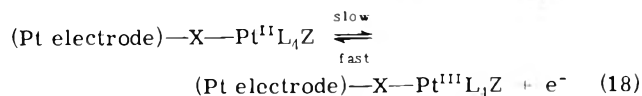
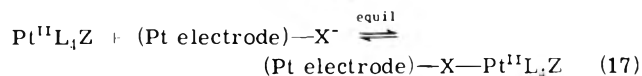
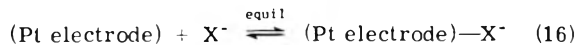


**Figure 7.** Thin layer current-potential curves for  $\text{Pt}((\text{NO}_2)(\text{NH}_3))_2$  at clean and halide-coated platinum electrodes: (—) reactant solution; (---) blank; (A) clean electrode, (B) chemisorbed I, (C) chemisorbed  $\text{Br}^-$ , (D) chemisorbed  $\text{Cl}^-$ , (E) chemisorbed  $\text{F}^-$ , (F) solution contains 1 mF  $\text{Cl}^-$ . The solution initially contained 1 mF  $\text{Pt(II)}$  and 1 F  $\text{HClO}_4$ . Other conditions were as in Figure 1.

charge types. The remaining factors, steric hindrance and conformation, are important only at very high coverages or when reactant-surfactant chemical bonding<sup>3</sup> is present.

Further, the chemisorbed halide layer (the material not removed by rinsing and not electrochemically reactive at the reversible potential) does not serve as an electron transfer bridge in Pt(II)-Pt(IV) interconversion. That is, an electrode known to contain chemisorbed halide does not oxidize Pt(II) in halide-free solution by way of the characteristic halide-bridged path<sup>4,6,7,11,25,26</sup> eq 15-20 (where  $\text{X}^-$



=  $\text{Cl}^-$ ,  $\text{Br}^-$ , or  $\text{I}^-$ ,  $\text{L} = \text{X}^-$ ,  $\text{SCN}^-$ ,  $\text{CN}^-$ ,  $\text{NO}_2^-$ ,  $\text{NH}_3$ ,  $\text{NR}_3$ , or  $\text{H}_2\text{O}$ , in any combination, and  $\text{Z} = \text{L}$  or  $\text{X}^-$ , as illustrated by typical data in Figure 7. Thus, apparently, halide in its irreversibly chemisorbed state on Pt is not nearly as effective in promoting the electron-transfer process,<sup>24</sup> eq 17 and 18, as halide present in a reversibly adsorbed state, or as the "free" ion. Comparison of experimental activation energies with values calculated by means of an extended-Hückel molecular orbital method has indicated that the strength of the electronic interaction between the bridging halide and the Pt(II) complex is of primary importance in determining the reaction rate.<sup>26</sup> Since the bond between the Pt surface and the bridging halide is at least as strong for chemisorbed halide as for reversibly adsorbed or "free" halide, it must be a weakening of the interaction between the bridge and the Pt(II) complex that accounts for the ineffectiveness of chemisorbed halide. Thus, these experiments must be viewed in the context of two distinct states of adsorbed halide, halide in the chemisorbed state being less capable of interacting with the Pt(II) complex (eq 17) and/or of conducting electron density from Pt(II) to the electrode within the transition state complex (eq 18). Indeed, from the standpoint of electronic structure one would not expect species having such different surface chemical characteristics to behave similarly toward electron transfer.

*ii. Oxidation of Sb(III) at Pt Electrodes in Aqueous HCl Solutions.* By analogy with the behavior of Pt complexes, the reported facilitation by adsorbed I of the oxidation of Sb(III) in 2 F HCl at Pt electrodes is not necessarily due to electron transfer bridging by the chemisorbed I, as was suggested,<sup>12</sup> but may instead be due to the fact that adsorbed I causes  $\phi_2$  to have more positive values than otherwise with a corresponding increase in the surface concentration of Sb(III), present primarily as the anion,  $\text{SbCl}_4^-$ ,<sup>27,28</sup> which would account for the observed increase in rate. In order to clarify this point the electrochemical oxidation of Sb(III) was studied under conditions identical with those employed by the previous workers, except that thin layer electrodes were used. In addition, the reaction was carried out at electrodes coated with ionizable substituted olefins capable of substantially altering the potential  $\phi_2$  but incapable of acting as effective electron transfer bridges.<sup>4</sup> The results are illustrated in Figure 8. Chemisorbed I facilitates the oxidation of Sb(III) (curves A and B) but the products are a mixture of species (curve B) and not simply  $\text{SbCl}_6^-$ , as previously reported.<sup>12</sup> Of greater significance, however, is the fact that allylamine, allylacetic acid, and acrylic acid form chemisorbed layers on the Pt surface which facilitate the oxidation of Sb(III) in the same manner as chemisorbed I (curves C-E), yet the structures of these species preclude effective electron transfer through them and their influence on the electrode rates of Pt(II) and Pt(IV) complexes of various structural and charge types is fully accounted for by their tendency to inhibit  $\text{Cl}^-$  adsorption and to block access of the reactant to the electrode. Since similar rates are observed at similar coverage or  $\phi_2$  value, it is evident that nonspecific electrostatic effects account for the influence of all of the surfactants, including chemisorbed I, and no occasion remains for postulating bridging by chemisorbed I in this instance.

### Experimental Section

Electrode rate measurements by means of thin layer electrodes have been described in papers dealing with the electrochemistry of Pt complexes<sup>3,4,6,11,25</sup> and reviewed,<sup>14</sup>

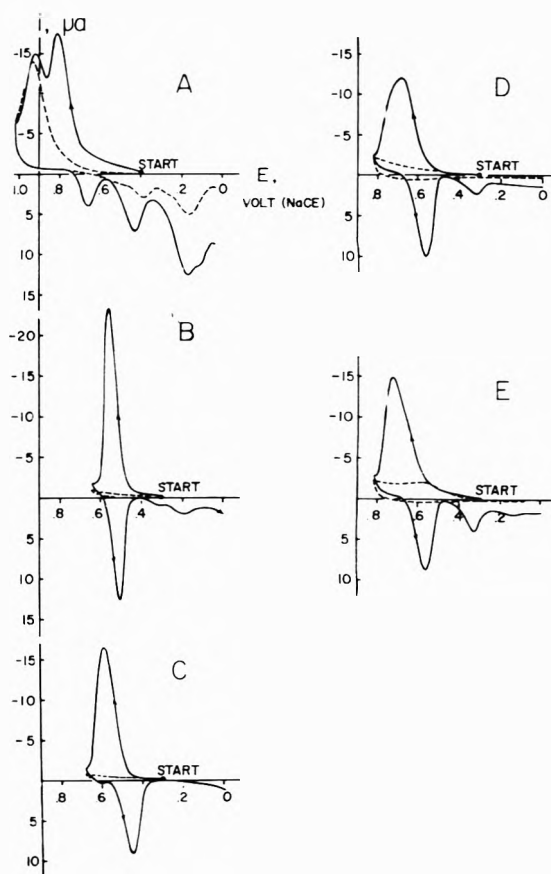


**Figure 8.** Current-potential curves for  $\text{SbCl}_4^-$  at clean and surfactant-treated Pt thin layer electrodes: (—) reactant solutions; (---) background; (A) clean electrode; other electrodes treated with (B) iodide; (C) allylamine; (D) allylacetic acid; (E) acrylic acid. The experimental conditions were as follows. The electrode was cleaned and surfactant pretreated as described in the Experimental Section. Reactant solutions initially contained 1 M  $\text{Sb}_2\text{O}_3$  and 2 F HCl. Surfactant coverages, in units of  $10^{-10}$  mol  $\text{cm}^{-2}$ , were as follows: curve A, none; B, 11.2; C, 9.1; D, 6.3; E, 6.0. Other experimental conditions were as in Figure 1.

recently. The thin layer electrode design employed for this work, a platinum rod positioned concentrically within a close-fitting precision Pyrex glass capillary, was described in ref 25.

Electrode pretreatment is crucial in studies such as this and is rendered particularly difficult by the fact that chemisorbed layers were made to form on the surface. Highly reproducible surfaces free of spurious properties and exhibiting the characteristics commonly attributed to the so-called "clean" Pt surface were obtained as follows: heating in an oxidizing gas-oxygen flame, with intermittent quenching in 11 N  $\text{HClO}_4$ , was followed by cooling for a few seconds in air and insertion into the precision glass capillary. A cyclic current-potential curve, recorded at 2  $\text{mV sec}^{-1}$  in deaerated 1 F  $\text{HClO}_4$  from 0.4 to 1.3 to -0.3 and finally to 0.4 V (NaCE), served both to remove the last traces of adsorbed organic materials and to confirm the purity of the surface. The resulting surface was undoubtedly complex; experiments with single crystal surfaces, cleaned, annealed, and characterized in ultra-high vacuum, will be reported elsewhere.<sup>29</sup> Prior to each experimental trial, or sequence, the electrode was further pretreated by alternate potentiostatic oxidation (1.2 V) and reduction (0.0 V), followed by equilibration at 0.4 V (NaCE) in 1 F  $\text{HClO}_4$  for a

minimum of 120 sec, with thorough rinsing at each potential.

In order to obtain reproducible surface coverage in various trials with the same surfactants, the clean electrode was exposed for exactly 180 sec to an excess of a deaerated, freshly prepared solution of the surfactant in pure H<sub>2</sub>O. The electrode was then rinsed with H<sub>2</sub>O and with supporting electrolyte, after which the current-potential curve was obtained.

All solutions were prepared from reagent grade or specially prepurified chemicals and triply distilled H<sub>2</sub>O. The temperature was 24 ± 1°. Solutions were deaerated with nitrogen. Potentials were measured relative to a calomel half-cell, prepared with 1 *F* NaCl, and denoted NaCE.

*Acknowledgments.* Acknowledgment is made to the donors of the Petroleum Research Fund, administered by the American Chemical Society, and to the National Science Foundation (Grant No. GP19747) for support of this research.

#### Appendix. Notation

$A$	=	electrode area, cm <sup>2</sup>
$a_j$	=	activity of species <i>j</i> adsorbed in the compact layer, mol cm <sup>-3</sup>
$\alpha$	=	charge transfer coefficient, apparent value
$C$	=	differential double layer capacitance, Farad
$C_j^0$	=	initial concentration of species <i>j</i> , mol cm <sup>-3</sup>
$C_j$	=	concentration of species <i>j</i>
$E$	=	electrode potential, V
$E^0$	=	formal standard electrode potential
$E_p$	=	potential at which anodic peak current occurred
$e$	=	2.718
$F$	=	Faraday constant, C equiv <sup>-1</sup>
$\Gamma_j^0$	=	interfacial excess of species <i>j</i> , mol cm <sup>-2</sup>
$\Gamma_j$	=	$\Gamma_j^0/\Gamma_j$
$i$	=	anodic component of current, A
$i_p$	=	anodic component of current, peak value
$k^{(1)}$	=	apparent standard electrochemical rate constant, cm sec <sup>-1</sup>
$n$	=	number of electrons transferred per molecule
$Q$	=	coulometric charge required for the reactant solution, C

$Q_0$	=	coulometric charge required for the blank solution
$q$	=	electrode electronic charge, C
$q_j$	=	ionic charge due to species <i>j</i>
$R$	=	gas constant, J mol <sup>-1</sup> °K <sup>-1</sup>
$r$	=	rate of potential scan, dE/dt, V sec <sup>-1</sup>
$T$	=	temperature, °K
$x$	=	perpendicular distance from the electrode surface, cm
$V$	=	volume of thin layer cavity, cm <sup>3</sup>
$Z_j$	=	ionic valence of species <i>j</i>
NaCE	=	calomel reference half-cell prepared with 1 <i>F</i> NaCl

#### References and Notes

- (1) N. A. Balashova and V. E. Kazarinov, *Russ. Chem. Rev. [Engl. Transl.]*, **34**, 730 (1965).
- (2) E. Gileadi, "Electrosorption", Plenum Press, New York, N.Y., 1967.
- (3) R. F. Lane and A. T. Hubbard, *J. Phys. Chem.*, **77**, 1401 (1973).
- (4) R. F. Lane and A. T. Hubbard, *J. Phys. Chem.*, **77**, 1411 (1973).
- (5) G. C. Bond, "Catalysis by Metals", Academic Press, New York, N.Y., 1962.
- (6) J. R. Cushing and A. T. Hubbard, *J. Electroanal. Chem.*, **23**, 183 (1969).
- (7) W. R. Mason and R. C. Johnson, *J. Electroanal. Chem.*, **14**, 345 (1967).
- (8) A. T. Hubbard and F. C. Anson, *Anal. Chem.*, **38**, 1601 (1966).
- (9) P. Delahay, "Double Layer and Electrode Kinetics", Interscience, New York, N.Y., 1965.
- (10) V. S. Bagotsky, Yu. B. Vassilyev, J. Weber, and J. N. Pirtskhalava, *J. Electroanal. Chem.*, **27**, 31 (1970).
- (11) A. L. Y. Lau and A. T. Hubbard, *J. Electroanal. Chem.*, **33**, 77 (1971).
- (12) R. J. Davenport and D. C. Johnson, *Anal. Chem.*, **45**, 1755 (1973).
- (13) A. T. Hubbard, R. A. Osteryoung, and F. C. Anson, *Anal. Chem.*, **38**, 692 (1966).
- (14) A. T. Hubbard, *Crit. Rev. Anal. Chem.*, **3**, 201 (1973).
- (15) B. E. Conway, B. MacDougall, and H. A. Kozłowska, *J. Chem. Soc., Faraday Trans. 1*, **68**, 1566 (1972).
- (16) M. Breiter, *Electrochim. Acta*, **8**, 925 (1963).
- (17) H. A. Kozłowska, B. E. Conway, and W. B. A. Sharp, *J. Electroanal. Chem.*, **43**, 9 (1973).
- (18) F. R. Hartley, "The Chemistry of Platinum and Palladium", Applied Science Publishers, London, 1973.
- (19) M. A. Leban and A. T. Hubbard, *Inorg. Chem.*, to be submitted for publication.
- (20) D. C. Johnson and S. H. Bruckenstein, *J. Electrochem. Soc.*, **117**, 460 (1970).
- (21) A. T. Hubbard and F. C. Anson, *J. Electroanal. Chem.*, **9**, 165 (1966).
- (22) M. Breiter, *Electrochim. Acta*, **8**, 925 (1963).
- (23) M. A. V. Devanathan and K. Ramakrishnaiah, *Electrochim. Acta*, **18**, 259 (1973).
- (24) J. Bjerrum, L. G. Sillen, and A. E. Martell, "Stability Constants of Metal-Ion Complexes", 2nd ed, Chemical Society, London, 1964.
- (25) C. N. Lai and A. T. Hubbard, *Inorg. Chem.*, **11**, 2081 (1972).
- (26) C. N. Lai and A. T. Hubbard, *Inorg. Chem.*, **13**, 1199 (1974).
- (27) G. P. Haight, Jr., *J. Am. Chem. Soc.*, **75**, 3848 (1953).
- (28) M. V. Vojnovic and D. B. Sepa, *J. Electroanal. Chem.*, **31**, 413 (1971).
- (29) R. M. Ishikawa and A. T. Hubbard, *J. Electroanal. Chem.*, to be submitted for publication.

## Dissolution Rates of Aqueous Silver Halide Dispersions<sup>1</sup>

D. D. F. Shiao,\* L. J. Fortmiller, and A. H. Herz

Research Laboratories, Eastman Kodak Company, Rochester, New York 14650 (Received September 5, 1974)

Publication costs assisted by Eastman Kodak Company

The dissolution rates of silver halides dispersed in alkaline gelatin solutions containing excess ligands for  $\text{Ag}^+$ , such as, ethanolamines, glycine, thiosulfate, or sulfite, were determined at constant ionic strength and temperature as a function of substrate variables and solution composition. The initial dissolution rates,  $r_i$ , were insensitive to variations of AgX crystal habit but they increased in direct proportion to (1) the effective surface area,  $A$ , of the silver halide, (2) its apparent solubility product,  $K_{sp}$ , and (3) for ligands of equal charge, the product of the total ligand concentration squared,  $L_0^2$ , and the stability constant of its  $\text{Ag}^+$  complex,  $\beta_2$ . Thus,  $r_i = \alpha(A\beta_2L_0^2K_{sp})$ , where  $\alpha$  is a constant that depends on factors such as ionic strength, halide excess, and ionic charge of the ligand. The latter proved to be particularly important as shown by the decrease in dissolution rates with the number of negative ligand charges. Thus, for a given AgBr dispersion at pBr 3, the relative values for  $\alpha$  varied from 500 for uncharged alkylamines to about 30 and 3 for glycine (-1) and sulfite (-2), respectively. An activation energy of 6.4 kcal/mol was obtained for AgBr dissolution in thiosulfate; these results are interpreted in terms of a model involving the formation of charged  $\text{Ag}^+$  complex ions at the charged silver halide/water interface and a rate-determining process whereby the complexed  $\text{Ag}^+$  diffuses from the AgX surface into the bulk of the solution.

### Introduction

The dissolution rates of sparingly soluble compounds have apparently received limited attention; recent work in this field has been reported by Lang and Lieser<sup>2a</sup> and Potashnikov et al.<sup>2b</sup> In the field of photographic science, the dissolution of undeveloped silver halide in conventional photography has been studied in connection with thiosulfate fixation. Despite the large amount of information on the behavior of thiosulfate,<sup>3</sup> even with that much-studied silver ligand, no agreement has been reached on whether the rate of the silver halide dissolution reaction is controlled by formation of the silver thiosulfate complex, as proposed by Jaenicke,<sup>4</sup> or if diffusion of thiosulfate is the rate-limiting step, as is consistent with the 4–5 kcal/mol activation energy obtained by Sahyun.<sup>5</sup> Other silver halide solvents have been investigated by James and Vanselow, who devised a method for determining dissolution rates in developers containing ligands, such as, thiosulfate, sulfite, thiocyanate, or ammonia.<sup>6</sup> Their activation energies of 15–20 kcal/mol were higher than those associated with pure diffusion processes.

In the present work we obtained dissolution data in order to establish the role of variables such as the silver halide crystal habit, its size and composition, as well as variations in the concentration, structure, and  $\text{Ag}^+$  affinity of the silver halide solvent. It also seemed desirable to avoid indirect measurements of dissolution and to eliminate bulk diffusion gradients, which previous experimenters may have encountered in their gelatin coatings. Accordingly, all our experiments were carried out in agitated liquid silver halide dispersions where AgX dissolution was measured directly by monitoring the time-dependent formation of the soluble  $\text{Ag}^+$ -ligand complex. For this purpose, a polarographic technique was employed that had been originated in these Laboratories by E. Przybylowicz; applications of this technique have been described previously.<sup>7</sup>

### Experimental Section

**Silver Halide Substrates.** Dispersions in dilute gelatin

(isoionic point, pH 4.9) of crystallographically defined silver halides were obtained by conventional procedures.<sup>3</sup> These substrates had a narrow dispersity and their surface areas were determined electron micrographically (Figure 1). An in situ spectral technique previously described by Herz et al.<sup>8</sup> was also employed to determine the surface areas of some dispersions. Good agreement was achieved with these independent methods.

**Potentiometry.** The apparatus used for the potentiometric measurements of silver-ion activity consists of a thermostated reaction vessel, a silver billet electrode, a reference electrode, a glass electrode, and a digital potentiometer. The reference electrode was a custom-designed Leeds and Northrup double-junction electrode with an  $\text{Ag}|\text{AgCl}$ , 1.9 N KCl internal cell and a bridge compartment containing 0.5 N  $\text{KNO}_3$ . Combination of the three electrodes allowed the simultaneous determination of both the  $\text{Ag}^+$  potentials and the  $\text{H}^+$  concentrations. The response of the glass electrode was not corrected for any salt effects; apparent  $\text{OH}^-$  concentrations did not exceed pH 11.5.

An automatic buret system from the London Co., Cleveland, Ohio, was employed to deliver the titrant; the volume of the titrant added was accurate to  $\pm 0.01$  ml.

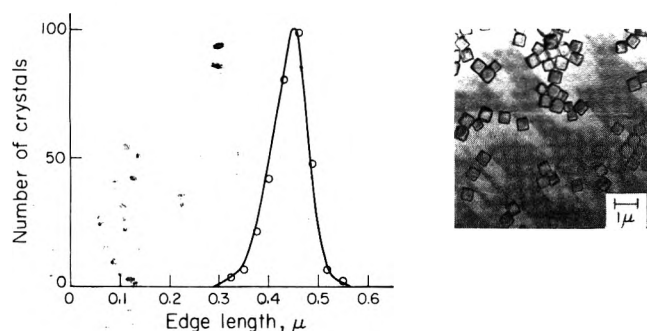
The electrode system was calibrated with known concentrations of silver nitrate with reproducible potentials of  $\pm 1$  mV and was shown to obey the Nernst equation with 59 mV per one pAg unit.

The ligands used in this study to determine dissolution rates of AgX dispersion included thiosulfate, sulfite, ethanolamine, diethanolamine, triethanolamine, and glycine in an alkaline environment (pH between 11.2 and 11.5) at an ionic strength of one. The stability constants of the  $\text{Ag}^+$  complexes of these ligands were measured in a similar medium (pH 11, 1 M  $\text{KNO}_3$ ). The computational method for obtaining these values from potentiometric measurements was adopted from Leden,<sup>9</sup> and led to the constants of Table I; they are significantly different from values obtained at low ionic strength.<sup>10</sup> This was to be expected



**TABLE I: Stability Constants of Ag<sup>+</sup> Complexes at pH 11.0 in Aqueous 1 M KNO<sub>3</sub>, 25°**

Ligand	log β <sub>1</sub> (±0.2)	log β <sub>2</sub> (±0.2)	log β <sub>3</sub> (±0.4)
H <sub>2</sub> NCH <sub>2</sub> CH <sub>2</sub> OH	3.4	6.8	
HN(CH <sub>2</sub> CH <sub>2</sub> OH) <sub>2</sub>	2.5	5.1	
N(CH <sub>2</sub> CH <sub>2</sub> OH) <sub>3</sub>	1.6	3.3	
H <sub>2</sub> NCH <sub>2</sub> CO <sub>2</sub> H	3.5	6.4	
Na <sub>2</sub> SO <sub>3</sub>	4.3	7.4	10.1

**Figure 1.** Size frequency of a cubic AgBr dispersion.

since the stability constants are defined in terms of concentrations rather than activities.

**Polarography.** To facilitate agitation of the AgX dispersion during dissolution measurements, a streaming Hg<sup>0</sup> electrode was employed.<sup>11</sup> The main component of the polarographic unit was purchased from Heath Co. (Model EUA-19-2). A Leeds and Northrup double-junction electrode (see description in the preceding section) was used as a reference to replace the original calomel electrode. The polarographic current was recorded by a Houston Omni-graphic 2000 recorder as a function either of time or of applied voltage. The AgX dispersion was kept at a constant temperature in a thermostated reaction vessel and stirred with a magnetic stirrer to ensure homogeneous mixing.

In relating the polarographic current to the concentration of soluble Ag<sup>+</sup> complexes, knowledge of  $E_{1/2}$  values and reversibility of electrode reactions was not required; it was only necessary to calibrate the system for a given ligand over a wide range of concentrations in the pH range under consideration. This was done by determining the diffusion current at a fixed voltage as a function of known Ag<sup>+</sup> complex concentration. A suitable potential was chosen to keep this current insensitive to small variations in voltage.

The diffusion current of Ag<sup>+</sup> complexes in contact with Hg<sup>0</sup> may sometimes be time dependent. In the case of the Ag<sup>+</sup>/CN<sup>-</sup>/Hg<sup>0</sup> system, it is known that Hg<sup>0</sup> reduces Ag<sup>+</sup> slowly but spontaneously;<sup>12</sup> this kind of reaction may produce time-dependent diffusion currents. In our Ag<sup>+</sup>/SO<sub>3</sub><sup>2-</sup>/Hg<sup>0</sup> system, such a time dependence was indeed observed. In order to correct for this effect, the following equation was established empirically without theoretical justification:

$$I/I_0 = 0.64 + 0.36 \times 10^{-0.105t}$$

where  $I$  = the current observed at any time,  $t$ , and  $I_0$  = the corrected current.

**Procedures for Measuring Dissolution Rate.** In a typical experiment, a solution of 150 ml of 0.5% gelatin + 0.133 M Na<sub>2</sub>CO<sub>3</sub> + 10<sup>-3</sup> M NaBr was introduced into a thermo-

stated vessel and was deaerated by bubbling nitrogen. Then Na<sub>2</sub>SO<sub>3</sub> was added giving a 0.2 M sulfite solution at a pH of 11.2. The solution was further deaerated before addition of a known amount of AgX dispersion. The dispersion was usually diluted by a known volume of 2% gelatin and 10<sup>-3</sup> M NaBr; it was stirred continuously at 40° before being pipetted at zero time into the sulfite solution at 25°. The concentration of AgX used was about 1 mM so that sulfite was present in a 200-fold molar excess.

A potential of -0.5 V was applied to the streaming mercury electrode with respect to the reference electrode. The current was recorded as a function of time and yielded plots such as those of Figure 2, which were used with the calibrations to calculate the concentration of silver complex resulting from dissolution of the AgX. From knowledge of the total concentration of silver complex produced at equilibrium, the initial rate of dissolution ( $r_i$ ) was expressed in terms of percent dissolved AgX per second. This rate, which was obtained graphically with an error not exceeding 10%, was shown to be independent of the amount of AgX used in the experiment.

For other ligands, the choice of potential, the amount of added halide, and inert ion, etc., varied but the procedure for determining dissolution rates was the same as that described above.

A typical time vs. diffusion current curve is shown in Figure 2. The slight increase in current at long reaction times is due to slow reduction of the silver sulfite complex by Hg<sup>0</sup>. With application of the previously given correction, this current becomes independent of time when AgX dissolution is completed.

## Results

It was expected that dissolution rates would be influenced by changes involving the silver halide substrate and the ligand structure, concentration, and environment. Some of these variables were examined and the results are summarized below.

**Dissolution Kinetics.** It was of immediate interest to learn if the dissolution process could be expressed by appropriate rate laws. Thus, the log of undissolved AgBr was plotted (see Figure 3) as a function of dissolution time in alkaline sulfite. The results indicate that this dissolution process can be described by an apparent first-order rate equation. Analysis of other experiments shows the generality of this conclusion, which is also in accordance with the observation that the initial dissolution rate of AgX is directly proportional to its total surface area (Figure 4).

**Silver Halide Surface Area.** The initial dissolution rate ( $r_i$ ) of a series of cubic AgBr grains in alkaline sulfite was studied as a function of their surface area ( $A$ ). The average grain sizes of these dispersions ranged between 0.05 and 2.3 μm. The experimental precision achieved in dissolution-rate measurements was estimated to be ±10%. The results are summarized in a plot of log  $r_i$  vs. surface area as shown in Figure 4. The line drawn through the experimental points has a slope of unity; it shows that in alkaline sulfite the initial rate of dissolution of AgX grains is directly proportional to their average surface area. The same conclusion was reached by Battaglia<sup>13</sup> with thiosulfate and the results are consistent with those obtained by James and Vanselow.<sup>6</sup>

**Silver Halide Solubility Products.** Considerations of the solubilities of AgCl, AgBr, and AgI led to the expectation that their dissolution rates in a given solvent should de-

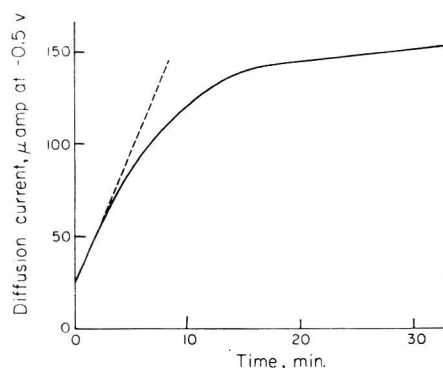


**Figure 2.** Rate of formation of  $\text{Ag}(\text{SO}_3)_2^{3-}$  from the dissolution of a cubic  $\text{AgBr}$  dispersion ( $390 \text{ m}^2/\text{mol}$ ) at  $25^\circ$  in water containing  $0.2 \text{ M Na}_2\text{SO}_3$ ,  $0.13 \text{ M Na}_2\text{CO}_3$ ,  $0.007 \text{ M NaBr}$ , and  $0.5\%$  gelatin. Dashed line is the initial rate.

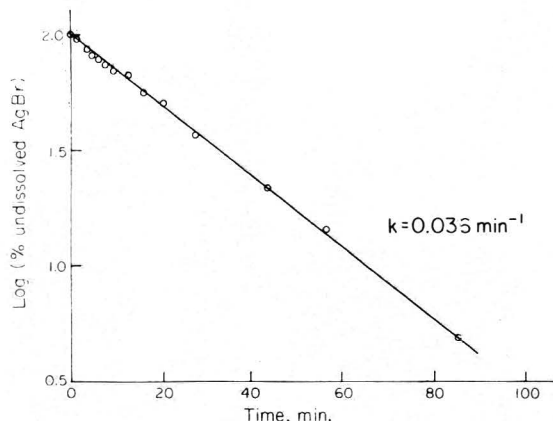


**Figure 3.** An apparent first-order plot for the rate of dissolution of an  $\text{AgBr}$  dispersion ( $76 \text{ m}^2/\text{mol}$ ). Solution conditions as in Figure 2.

crease in the order  $\text{AgCl} > \text{AgBr} > \text{AgI}$ . Accordingly, a series of cubic  $\text{AgCl}$ ,  $\text{AgBr}$ , and  $\text{AgI}$  dispersions was studied to establish the relation between dissolution rates and solubility products of these salts in alkaline sulfite. The dispersions had different areas but the resulting dissolution rates were normalized to a common surface area of  $130 \text{ m}^2/\text{mol}$  of  $\text{AgX}$ . Since the dissolution rates were measured at an ionic strength of 1, the apparent solubility products of the silver halides were also determined at that ionic strength. Moreover, the initial rates were measured under conditions where they proved to be insensitive to small changes of initial halide concentrations, i.e., at a halide excess of  $0.01 \text{ M}$  with  $\text{AgCl}$  and  $\text{AgBr}$  and at a  $0.001 \text{ M}$   $\text{KI}$  excess with  $\text{AgI}$ .

The results, which are illustrated by Figure 5, demonstrate direct proportionality between the apparent solubility product of the silver halide and its dissolution rate in alkaline sulfite.

**Silver Halide Crystal Habit.** Reproducible methods are available for controlling silver halide morphology and the preparation of cubic [100] and octahedral [111]  $\text{AgBr}$  has been discussed in detail.<sup>3</sup> The results given in Table II demonstrate that dissolution rates in alkaline sulfite are not sensitive to variations of  $\text{AgBr}$  crystal habit.

**Bromide Ion Concentration.** Since under equilibrium conditions the reaction between a ligand for  $\text{Ag}^+$  and  $\text{AgBr}$  will lead to increased  $\text{Br}^-$  concentration, the effect of  $\text{Br}^-$  on the reaction rate is observed most meaningfully in the initial reaction period. Accordingly, initial  $\text{AgBr}$  dissolution

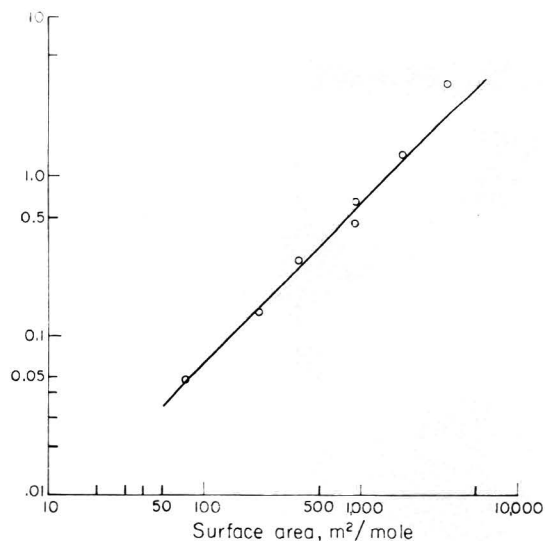


**Figure 4.** Effect of surface area on the rate of dissolution of  $\text{AgBr}$  dispersion. Solution conditions as in Figure 2.

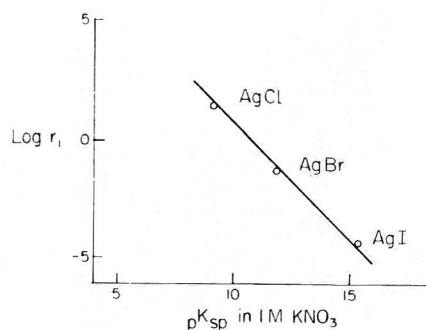


**Figure 5.** Effect of  $\text{AgX}$  composition on the rate of dissolution of a  $\text{AgX}$  dispersion ( $180 \text{ m}^2/\text{mol}$ ). Solution conditions as in Figure 2; see text for discussion on the level of halide ion used in these experiments.

rates in sulfite were examined as a function of initial  $\text{Br}^-$  concentrations in the solvent, i.e., the initial  $\text{pBr}$ .

The results are plotted in Figure 6; they show that the rates are essentially independent of  $\text{Br}^-$  levels between  $\text{pBr}$  3.5 and 2.5. This behavior is consistent with previous observations.<sup>6</sup> That the decrease in the rate shown in Figure 6 has a slope, not of unity but of 0.57, suggests that the  $\text{Br}^-$  adsorbed on the  $\text{AgBr}$  surface rather than its solution concentration affects the rate of dissolution. In fact, the region of  $\text{Br}^-$  independence ( $\text{pBr} > 2.5$ ), corresponds approximately to the previously determined saturation coverage of  $\text{AgBr}$  by adsorbed  $\text{Br}^-$ .<sup>14</sup>

**Adsorbates.** Early studies established that  $\text{AgBr}$  dissolution rates in thiosulfate and in sulfite could be accelerated by quaternary ammonium salts.<sup>6,15</sup> In agreement with these observations, it was noted in these experiments that quaternary pyridinium and quinolinium salts, whose adsorption behavior in silver halide-gelatin dispersion is already known,<sup>16</sup> accelerated  $\text{AgBr}$  dissolution in approximate proportion to their free energy of adsorption. By way of contrast, addition to the  $\text{AgBr}$  dispersion of 2,2'-cyanines or thiocarbocyanines diminished the dissolution rate. This decreased rate did not depend on the cyanine charge but is considered to be a consequence of essentially irreversible dye adsorption,<sup>16</sup> which effectively decreases the silver halide surface that is available for the reaction with

**TABLE II: Dependence of Dissolution Rate in Alkaline Sulfite on AgBr Morphology<sup>a</sup>**

Surface area, m <sup>2</sup> /mol	Initial rate of dissolution, % sec <sup>-1</sup>		
	Cubes	Octahedra	Spheres
580	0.43	0.39	
390	0.28	0.26	
225	0.16		0.14

<sup>a</sup> Solvent: 0.2 M Na<sub>2</sub>SO<sub>3</sub>, 0.13 M Na<sub>2</sub>CO<sub>3</sub>, 0.67 × 10<sup>-3</sup> M NaBr, 0.5% Gelatin.

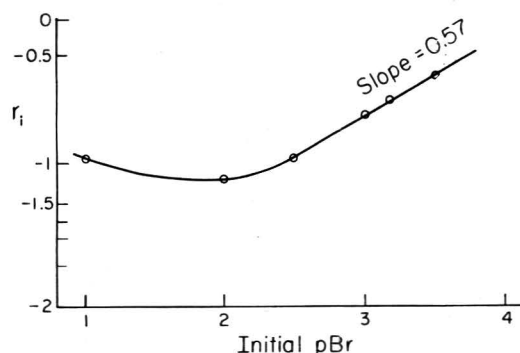


**Figure 6.** Effect of bromide-ion concentration on the rate of dissolution of a cubic AgBr dispersion (390 m<sup>2</sup>/mol). Except for bromide, solution conditions as in Figure 2.

the ligand. It is noteworthy that AgBr recrystallization rates were also oppositely influenced by simple cationic pyridinium salts and irreversibly adsorbed cationic cyanines.<sup>17</sup>

**Stability Constants of Ag<sup>+</sup> Complexes.** The experimental results discussed so far were obtained using alkaline sulfite as the ligand for Ag<sup>+</sup>. To examine the effect of the stability of Ag<sup>+</sup>-ligand complexes on the dissolution rates of AgX grains, we used a series of amines of the same charge but with different stability constants,  $\beta_2$  (see Table I). For comparison, the same 0.4- $\mu$  cubic AgBr dispersion was used but the ligand and its concentration,  $L_0$ , were varied independently in the range of 0.1 to 0.4 M. The initial dissolution rates,  $r_i$ , when plotted against  $\beta_2 L_0^2$ , yielded a line with a slope of unity (Figure 7). From this direct dependence of the rate on  $\beta_2 L_0^2$ , it is concluded that under the given conditions,  $\beta_2$  rather than  $\beta_1$  is the important stability parameter. However, further experiments indicated that in addition to the magnitude of  $\beta_2$  and the ligand concentration, the ligand charge is a significant variable for determining the rates of silver halide dissolution.

**Ligand Charge.** This effect is illustrated in Figure 8, which shows that AgBr dissolves in sulfite and in glycine at rates that are again proportional to  $\beta_2 L_0^2$ . However, under identical conditions, the rates for glycine are about 25-fold smaller for this singly negatively charged amine than they are for an uncharged analog such as hydroxyethylamine.

The preceding measurements showed that the initial dissolution rates,  $r_i$ , are proportional to the silver halide's available surface area ( $A$ ), its apparent solubility product in solution ( $K_{sp}$ ) and, for ligands of equal charge, the cumulative stability constant of the Ag<sup>+</sup> complex ( $\beta_2$ ) and the square of the ligand concentration ( $L_0^2$ ). Hence

$$r_i = \alpha (AK_{sp}\beta_2 L_0^2) \quad (1)$$

where  $\alpha$  is a proportionality constant that depends on ha-

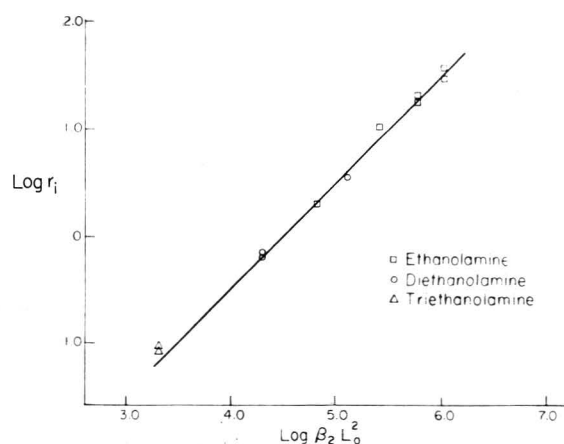


**Figure 7.** Effect of amine structure, total concentration ( $L_0$ ), and stability constants of the Ag<sup>+</sup> complexes ( $\beta_2$ ) on the AgBr dissolution rates at 25°. In addition to the amines, the aqueous solutions contained 0.2 M Na<sub>2</sub>CO<sub>3</sub>, 0.4 M KNO<sub>3</sub>, 0.001 M NaBr, and 0.1% gelatin at pH 11.4 ± 0.3.

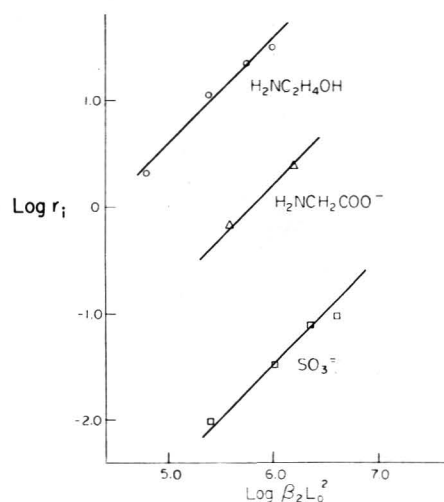


**Figure 8.** Effect of ligand variables on AgBr dissolution rates in 0.1% gelatin, pBr 3, pH 11.4, 25°. The AgBr substrate for the amine ligands had an area of 390 m<sup>2</sup>/mol of AgBr; that for sulfite was 76 m<sup>2</sup>/mol of AgBr. The ionic strength was 1.0 and 2.0 for the amines and sulfite, respectively.

lide ion concentration at the AgX/water interface, ionic strength, and ligand charge. By using a cubic AgBr dispersion at constant temperature, ionic strength, pH, and pBr, the contribution to the value of  $\alpha$  by the charge of the ligand could be determined. The results are plotted in Figure 9; they show that dissolution rates decrease with the number of anionic charges. Thus, the relative values for  $\alpha$  varied from 500 for the uncharged amine to about 30 and 3 for glycine (-1 charge) and sulfite (-2 charges), respectively. This observed dependence of AgBr dissolution rates on the charge of the ligand is in agreement with the previously noted relative behavior of ammonia and sulfite as silver halide solvents.<sup>6</sup>

**Temperature Dependence.** The variation with temperature of the initial dissolution rate of a cubic AgBr dispersion in 0.01 M thiosulfate yielded an activation energy of 6.4 kcal/mol (Figure 10). This value is in reasonable agreement with the 4-5 kcal/mol observed for the thiosulfate dissolution of AgBr coatings.<sup>5</sup> An activation energy of 5 kcal/mol for AgCl dissolution in water was previously argued to be consistent with a diffusion process in solution.<sup>18</sup>

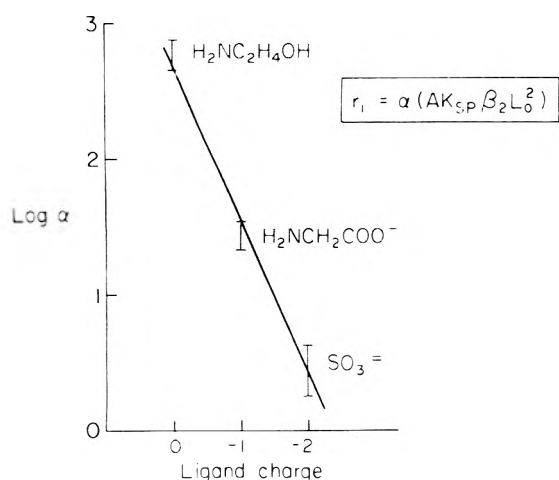


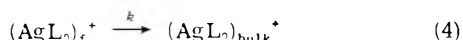
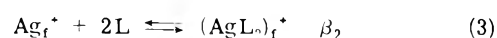
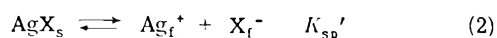
**Figure 9.** Effect of ligand charge on the rate of dissolution of an AgBr dispersion ( $390 \text{ m}^2/\text{mol}$ ) in 0.1% gelatin at ionic strength of 1.0, pH 11.4, pBr 3, and  $25^\circ$ . See text for explanation.

This argument should not be generalized, however, since according to eq 1, the enthalpy contributions to  $K_{sp}$  and  $\beta_2$  should also be considered in order to interpret correctly the activation energy of dissolution of AgX dispersions.<sup>19</sup>

### Discussion

Under the cited conditions it was found that initial silver halide dissolution rates,  $r_i$ , were related to the indicated variables by eq 1.

In order to rationalize this experimental observation, a model is proposed that can be described by



where  $s$  refers to the solid state,  $f$  signifies the AgX/solution interface, and  $K_{sp}'$  represents the apparent solubility product of AgX at the interface. The rate-determining process is considered to involve diffusion of complexed  $\text{Ag}^+$  from the surface into the bulk of the solution; this step is defined by the rate constant  $k$ . Nernst's dissolution law<sup>22</sup> and eq 4 lead to

$$\text{dissolution rate} = -dA/dt = kA\theta \quad (5)$$

where  $\theta$  is defined as the surface coverage by  $(\text{AgL}_2)_f^+$ . Combination of eq 2, 3, and 5 yields

$$\begin{aligned} -dA/dt &= kE' A \beta_2 L^2 K_{sp}' \frac{1}{[\text{X}_f^-]} \\ &= kE' A \beta_2 L_0^2 K_{sp}' \frac{1}{[\text{X}_f^-]} \end{aligned} \quad (6)$$

Here  $L$  is replaced by  $L_0$ , the total ligand concentration, because the amount of ligand removed by complexation is negligible and  $K_{sp}$  refers to the apparent solubility product of AgX in solution. Because with these substrates the charges at the solid/solution interface are ill-defined due to adsorbed gelatin, we do not attempt to apply the Gouy-Chapman treatment to distribution of ions in the double layer; instead, the variable  $E$  is introduced to account for coulombic effects associated with ligand and silver halide surface charges and contains factors relating the various macroscopic constants to the phenomenon taking place at

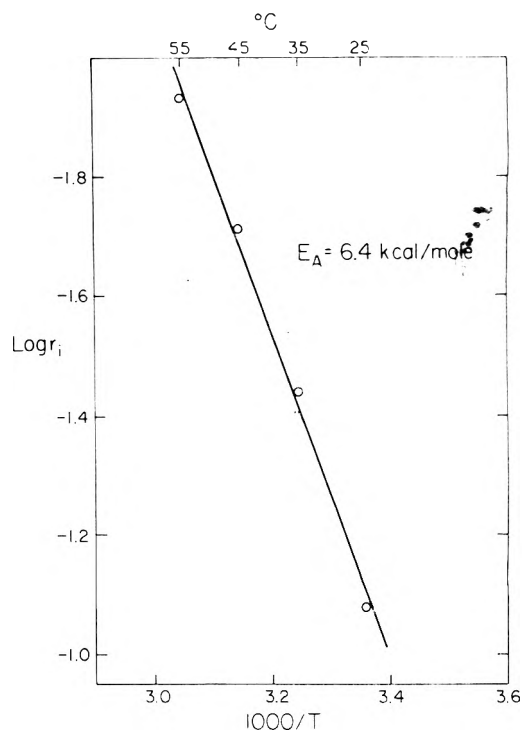


**Figure 10.** Effect of temperature on the rate of dissolution of a cubic AgBr dispersion ( $390 \text{ m}^2/\text{mol}$ ) in water containing 0.01 M  $\text{Na}_2\text{S}_2\text{O}_3$ , 0.001 M NaBr, and 0.5% gelatin at pH 10.

the AgX/water interface. Based on the definition of  $r_i$ , eq 6 can be transformed to eq 7, which is equivalent to the empirical relation of eq 1.

$$r_i = kE \lim_{t \rightarrow 0} \frac{1}{[\text{X}_f^-]} (A \beta_2 L_0^2 K_{sp}') \quad (7)$$

Equation 7 is based on a model that involves the formation of charged  $\text{Ag}^+$  complex ions at the charged silver halide/water interface and a rate-determining process whereby the complexed  $\text{Ag}^+$  diffuses from the AgX surface into the bulk of the solution; this model leads to several predictions some of which have already been tested.

(1) Since  $r_i$  is inversely proportional to the surface concentration of halide at the AgX/water interface, dissolution rates should diminish with increasing halide adsorption. This effect was demonstrated in Figure 6.

(2) At elevated  $\text{X}^-$  concentrations where the AgX/water interface is negatively charged, the magnitude of  $E$  should decrease with the number of anionic ligand charges. This conclusion is borne out by Figure 9, which shows that dissolution rates decrease in the order  $\text{H}_2\text{NCH}_2\text{CH}_2\text{OH} > \text{H}_2\text{NCH}_2\text{CO}_2^- > \text{SO}_3^{2-}$ . Moreover, in agreement with these charge considerations, reversibly adsorbed additives that decrease the negative charge density at the AgX/ $\text{X}^-$  interface, e.g., cationic surfactants,<sup>23</sup> enhance AgBr dissolution rates in sulfite and thiosulfate.

(3) Based on electrical double-layer considerations, the significance of coulombic contributions to the term  $E$  should diminish with salt concentration. Indeed, it was observed that dissolution of AgBr/ $\text{Br}^-$  in sulfite was accelerated with growing ionic strength in the range from 1 to 3.5. However, since changes of  $\beta_2$  with ionic strength remain to be determined, it is uncertain if the observed acceleration can be related to a modification of  $E$ .

(4) Since  $r_i$  is related to the surface concentration of

$AgL_2$ , the dissolution rate should become independent of  $L_0$  at sufficiently high ligand concentrations. This prediction also remains to be verified in detail although it is consistent with the observation that the clearing time of AgX films can become independent of thiosulfate concentration at a sufficiently high level of that ligand.<sup>3</sup>

(5) The dependence of  $r_1$  on the available surface area  $A$  demands that irreversibly adsorbed additives that diminish  $A$  should also diminish the dissolution rate. This effect was produced by strongly adsorbed cyanines in the AgBr systems examined and also accounts for the retardation by eosin of AgCl dissolution.<sup>24</sup>

**Acknowledgments.** We wish to express our gratitude to E. Przybylowicz for sharing with us his original polarographic method that was used in these determinations and to C. Battaglia, D. Cross, P. Hartman, and J. Helling for their early dissolution-rate measurements. Progress was facilitated by R. Daubendiek, who prepared and characterized the AgI dispersions, and by E. Brown's assistance with the polarographic instrumentation.

## References and Notes

- (1) Presented in part at the 167th National Meeting of the American Chemical Society, Los Angeles, Calif., April 4, 1974.
- (2) (a) A. Lang and K. H. Lieser, *Z. Phys. Chem. (Frankfurt am Main)*, **86**, 143 (1973); (b) Y. M. Potashnikov, M. V. Mokhoshev, and O. I. Kovalerkski, *Russ. J. Inorg. Chem.*, **18**, 4621 (1973).
- (3) "The Theory of the Photographic Process", C. E. K. Mees and T. H. James, Ed., 3rd ed. Macmillan, New York, N.Y., 1966, p 400.
- (4) W. Jaenicke, *Z. Phys. Chem.*, **195**, 88 (1950).
- (5) M. R. V. Sahyun, *Photogr. Sci. Eng.*, **17**, 171, 174 (1973).
- (6) T. H. James and W. Vanselow, *Photogr. Sci. Tech.*, [II] **2**, 135 (1955); **3**, 69 (1956); *J. Phys. Chem.*, **62**, 1189 (1958).
- (7) L. E. Oppenheimer and T. H. James, *Photogr. Sci. Eng.*, **13**, 242 (1969); D. C. Shuman and T. H. James, *ibid.*, **15**, 119 (1971).
- (8) A. H. Herz, R. P. Danner, and G. A. Janusonis, *Adv. Chem. Ser.*, **No. 79** (1968).
- (9) L. Leden, *Z. Phys. Chem.*, **188A**, 160 (1941).
- (10) "Stability of Metal-Ion Complexes", compiled by L. G. Sillens and A. E. Martell, The Chemical Society, London, 1964.
- (11) W. Ruby, Research Laboratories, Eastman Kodak Co., private communications.
- (12) R. F. Large and E. P. Przybylowicz, *Anal. Chem.*, **36**, 1642 (1964).
- (13) C. Battaglia, Research Laboratories, Eastman Kodak Co., private communication.
- (14) A. H. Herz and J. O. Helling, *J. Colloid Sci.*, **17**, 293 (1962).
- (15) M. Aribat and J. Pouradier in "Science and Applications of Photography" (Proceedings of the International Centenary Conference, London, 1953), Royal Photographic Society, London, 1955, p 177.
- (16) A. H. Herz and J. O. Helling, *J. Colloid Sci.*, **22**, 391 (1966).
- (17) L. Oppenheimer, T. James, and A. H. Herz in "Particle Growth in Suspensions", A. L. Smith, Ed., Academic Press, London, 1973, p 159.
- (18) J. Howard, G. Nancollas, and N. Purdie, *Trans. Faraday Soc.*, **56**, 278 (1960).
- (19) For the case of thiosulfate, the overall enthalpy changes from  $K_{sp}$  and  $\beta_2$  cancel each other.<sup>20,21</sup>
- (20) W. Jaenicke, *Z. Naturforsch.*, **4**, 353 (1949).
- (21) E. Klein, *Z. Elektrochem.*, **60**, 1003 (1956).
- (22) W. Nernst, *Z. Phys. Chem.*, **47**, 52 (1904).
- (23) G. Weiss, R. Ericson, and A. Herz, *J. Colloid Interface Sci.*, **23**, 277 (1967).
- (24) C. Davies and G. Nancollas, *Trans. Faraday Soc.*, **51**, 823 (1955).

## Vibrational Spectra of Liquid Crystals. IX. Calculation of Infrared and Raman Active Lattice Vibration Frequencies of 4,4'-Azoxydianisole

Dolores Grunbaum<sup>1</sup> and Bernard J. Bulkin\*

Hunter College of the City University of New York, New York, New York 10021 (Received August 1, 1974)

Publication costs assisted by the American Cancer Society

The 21 infrared and Raman active lattice vibrations of 4,4'-azoxydianisole (PAA) have been calculated using a combined potential of atom-atom and dipole-dipole terms. The parameters in the potential function are not adjusted but are transferred directly from other calculations. The results reproduce the observed infrared and Raman spectra quite well. They are discussed in terms of the intermolecular interactions responsible for the crystal lattice energy as well as contrasted to the structure and dynamics of the nematic and isotropic phases of PAA.

## Introduction

Infrared and Raman spectra of nematogenic crystals in the lattice vibration region of the spectrum ( $10\text{--}100\text{ cm}^{-1}$ ) have yielded information about the intermolecular interactions in these materials as well as in the nematic phases themselves.<sup>2-9</sup> To date, only qualitative discussions of the spectra have appeared. This is not surprising in view of the complexity of the molecular crystals involved. For example, 4,4'-azoxydianisole (PAA), the subject of several investigations, including the one reported herein, is a 33 atom molecule which crystallizes in a structure containing four mole-

cules per unit cell. Analysis of its intermolecular forces is further complicated by the presence of eight aromatic C-H bonds, two OCH<sub>3</sub> groups, and an NNO unit in each molecule.

A number of interesting qualitative aspects have been noted from the spectra.<sup>2,7</sup> First, it has been pointed out that the most intense infrared active lattice vibration modes are at higher frequency than the Raman active modes. This trend carries over in the nematic phase, where pseudo-lattice (intermolecular) vibrations appear at  $100\text{--}150\text{ cm}^{-1}$  in the infrared and  $50\text{--}75\text{ cm}^{-1}$  in the Raman. Second, infrared spectra of aligned nematics have indicated

that the absorption band observed in the nematic phase far-infrared spectrum is probably of rotatory rather than translatory origin. Third, while it is true that the highest and lowest frequency modes in the spectra were seen only in the infrared and Raman, respectively, other lattice vibrations were near coincidence in the two sets of spectra. Whether this was accidental or a consequence of weak intermolecular coupling was unclear.

The far-infrared spectra of solid PAA which have been reported were only obtained on polycrystalline samples. The Raman spectra of oriented single crystals of PAA have been published, however.<sup>2</sup> From these it was possible to separate lattice modes according to symmetry species. It was found that many near coincidences existed between species. Again, it was speculated that these were due to modes arising from closely related symmetry coordinates, e.g., hindered translations along the same axis. Bulkin and Prochaska suggested assignments for certain modes based on qualitative arguments.

Finally, it was proposed that one mode in the lattice vibration region of the spectrum near 70 cm<sup>-1</sup> behaved as a "soft mode" in the crystalline phase as the crystal-nematic transition was approached. No assignment of this mode to a particular symmetry coordinate was possible.

In this paper we present methodology and results of a calculation of the lattice vibration frequencies, both infrared and Raman active, for PAA crystals in the  $k = 0$  rigid body approximation. These results provide answers to many of the questions raised in previous papers. They also give other information about the intermolecular interactions in this nematogenic crystal.

### Methodology

There have been a number of attempts to compute lattice vibration frequencies. Without reviewing these here in any detail, one can say that they may be divided into two classes. In one, a limited number of force constants are permitted to take on nonzero values. These are adjusted to give the best fit to the observed frequencies. Usually, this has been carried out in cases where only infrared or Raman data are available, and the normal modes are factored by symmetry. Among the molecules treated in this fashion are pyrazine,<sup>10</sup> uracil,<sup>11</sup> diketopiperazine,<sup>11</sup> cyanuric acid,<sup>11</sup> cyanamide,<sup>12</sup> and benzene.<sup>13</sup> In the second approach, a potential function has been determined, often semiempirically, using the physical properties of the crystal such as heat of sublimation and equilibrium structure. In principle, this treatment should give more information about the intermolecular forces responsible for the lattice vibrations. It is considered to be a more laborious approach, as one must derive analytical expressions for the force constants by hand. In addition, there have been some problems with the theory, or, again, with the lack of sufficient experimental information, or both. Benzene,<sup>14-16</sup> Cl<sub>2</sub>,<sup>17</sup> hexachlorobenzene,<sup>17</sup> cyanogen,<sup>18</sup> and carbon dioxide<sup>18</sup> are among the cases treated by this method. Two comprehensive reviews, with extensive references, have been published.<sup>19,20</sup>

In this work a version of the second method described above has been used. We have relied, to a certain extent, on the experimentally determined static crystal structure to determine the "goodness" of a particular intermolecular potential. The procedure has also been used to test qualitative ideas extant in the literature regarding intermolecular forces in nematogenic crystals. Certain details of the methodology which apparently have not been widely recognized

are discussed in the Appendix, in which the coordinate system is defined using the symmetrical parameters.

### Intermolecular Potentials

Many authors and texts have stressed the importance of dipolar interactions in stabilizing nematic phases.<sup>23</sup> As the crystalline arrangement of molecules closely approximates that believed to be present in the nematic phase, an initial attempt was made to approximate the crystal lattice as a set of oriented dipoles. Each PAA molecule contains three such dipoles, two OCH<sub>3</sub> groups, and an NNO group.

The dipolar potential may be written as

$$V_{\text{di-dip}} = \frac{\mu\mu'}{r^3} (\cos \epsilon - 3 \cos \theta \cos \theta') \quad (1)$$

where  $\mu$  and  $\mu'$  are the magnitude of the dipoles,  $r$  the distance, and  $\cos \epsilon$  is defined as usual in terms of the direction cosines of the dipoles  $\mu$  and  $\mu'$  as  $\cos \epsilon = ll' + mm' + nn'$ . In this system

$$\cos \theta = \frac{1}{r} [l(x - x') + m(y - y') + n(z - z')]$$

and

$$\cos \theta' = \frac{1}{r'} [l'(x - x') + m'(y - y') + n'(z - z')]$$

To perform calculations using this potential the molecules were considered as a collection of oriented dipoles of values R-O-CH<sub>3</sub> equal to 1.35 D (R-O-C angle of 125°)<sup>24</sup> and N → O equal to 1.705 D.<sup>25</sup> Interdipole distances within a 7 Å radius were generated using ORTEP.<sup>26</sup> The calculation of the direction cosines is straightforward.<sup>27</sup>

Assuming the dipole-dipole potential to be the only one operative in the crystal, a lattice energy was calculated. It is 1.13 kcal/mol. To our knowledge the heat of sublimation of PAA has never been measured. However, considering the mass of the molecule it is clear that this value is much too small. Kitaigorodskii<sup>15</sup> has pointed out that the energy due to interacting dipoles in a crystal ranges between 5.0 and -2.5 kcal/mol. These energies are not small enough to be neglected, but they are not big enough to explain the crystal stability either.

The calculated first derivatives of the dipolar potential with respect to the  $x$ ,  $y$ , and  $z$  axes show that there exist minima at the equilibrium geometry along the first two axes but none along the  $z$  axis. Thus the potential is clearly unsuitable on the two conditions one can set down for a trial potential: value of the heat of sublimation and existence of an energy minimum at the equilibrium crystal geometry.

Consider now the more commonly used potential expressed as a pairwise sum of all nonbonded atom-atom interactions. The assumption of such a potential is not justified theoretically, especially when delocalized electrons are present. Some authors have suggested considering interactions between electrons in delocalized  $\pi$  states as if they were also atom-atom in nature.<sup>28</sup>

The potential used is designated in its most general form as

$$V_n = -\frac{A}{r^6} + \frac{Be^{-cr}}{r^d} \quad (2)$$

for the  $n$ th atom-atom interaction, where  $r$  is the distance between two nonbonded atoms. Note that the first term represents attractive or long-range forces corresponding to instantaneous dipole-dipole polarization, as distinct from

the interaction of permanent dipoles described above. The repulsive or short-range force is expressed by the second term of the potential. The common forms used,  $Be^{-cr}$  and  $B/r^{12}$ , are clearly oversimplifications. In this work, we have fixed the parameter  $d = 0$  for all interactions.

In Table I is collected a number of different values for these parameters which are extant in the literature. They are not really applicable to PAA for the interactions with nitrogen atoms; those shown are from the peptide literature. Only one term poses any particular problems, the C-CH<sub>3</sub> interaction. An expression proposed by DeSantis et al.<sup>30</sup>

$$V_{\text{C-CH}_3} = \frac{(-1.235 \times 10^3)}{r^6} + (2.879 \times 10^5 e^{-1.67r}) \quad (3)$$

was found to give anomalously high values for certain rotation-translation interaction force constants. Instead, we have successfully used the parameters shown in Table I, which are obtained from a geometric average of the C-C and CH<sub>3</sub>-CH<sub>3</sub> parameters. This procedure has previously been used by Williams<sup>14</sup> to obtain a C-H potential from C-C and H-H. An arithmetic average gives similar results.

A number of combinations of the listed parameters have been tried for calculation of lattice energy and equilibrium geometry. It is interesting, and somewhat surprising, to note that almost all combinations of the listed parameters give an energy minimum at the equilibrium crystal geometry. This fact has been previously noted by Mason,<sup>31</sup> who points out that choice of a potential function based on equilibrium structure data is not a particularly sensitive method, especially when the potential is represented by a single form of the Buckingham type. For the calculations described below, we have used the parameters of Kitaigorodskii<sup>15</sup> for C-C, Williams<sup>14</sup> for C-H and H-H, and Liquori<sup>29</sup> for N-N and O-H. All interactions within a 7-Å radius are included. This combination of parameters is selected on the sole arbitrary criterion of giving the deepest minimum. The lattice energy thus obtained is a reasonable value of -59.00 kcal/mol.

To conclude the section, we wish to make the point that the calculation is performed with a completely transferred set of atom-atom interactions, including one obtained by the geometric averaging procedure. None of the parameters was allowed to vary so as to obtain better geometry, lattice energy fits, or frequencies, procedures which have been quite common in the past. The ability to adequately reproduce experimental data using the transferred parameters is one of the points of this work.

### Force Constant Calculations

The **F** matrix is, in the case of PAA, a 24 × 24 symmetric matrix. The C<sub>2h</sub><sup>5</sup> factor group symmetry, 4 molecules/unit cell, imposes the following relations on the elements of **F**

$$f_{ij}^{11} = f_{ij}^{22} = f_{ij}^{33} = f_{ij}^{44}$$

$$f_{ij}^{12} = f_{ij}^{34} \quad f_{ij}^{13} = f_{ij}^{21} \quad f_{ij}^{14} = f_{ij}^{23}$$

where  $i$  and  $j$  represent any of the coordinates  $x, y, z, \xi, \eta$ , or  $\zeta$ , and the superscripts refer to pairs of molecules in the unit cell.<sup>38</sup>

The matrix **G**<sup>-1</sup> is diagonal for the translations, with elements equal to the molecular mass. Because the Cartesian molecular frame used does not coincide with the principal axes of inertia of the molecule, **G**<sup>-1</sup> for the rotations is not diagonal. It is necessary to have **G**<sup>-1</sup> expressed in diagonal

TABLE I: Parameters in the Atom-Atom Potentials

Atom pair	A, kcal/mol Å <sup>6</sup>	B, kcal/mol	C, Å <sup>-1</sup>	Ref
H-H	36	4,000	3.74	14
	57	42,000	4.86	15
C-C	358	42,000	3.58	15
	535	74,500	3.60	14
C-H	39	9,400	3.67	14
	154	42,000	4.12	15
O-H	99.2	28,100	4.32	29
	497.61	19,820	3.84	30
N-H	99.2	28,100	4.32	29
N-N	200	186,400	4.55	29
	125.1	105,700	4.61	30
N-O	200	186,400	4.55	29
C-O	244	212,100	4.44	
C-N	244	212,100	4.44	
O-O	200	186,400	4.55	
CH <sub>3</sub> -CH <sub>3</sub>	2942	273,900	3.33	30
H-CH <sub>3</sub>	2089	31,905	3.20	30
C-CH <sub>3</sub>	1026	107,270	3.45	See text

form in order to calculate **G**<sup>1/2</sup>. This is achieved by simply diagonalizing **G**<sup>-1</sup> with a matrix **D**

$$\mathbf{D}^t \mathbf{G}^{-1} \mathbf{D} = \mathbf{G}_D^{-1}$$

This same transformation must be applied to **F**.

The 24 symmetry coordinates are constructed in the usual way, with S<sub>6</sub>, S<sub>10</sub>, and S<sub>11</sub> representing the acoustical modes. This **U** matrix is used to factor the (**G**<sub>D</sub><sup>1/2</sup> **D**<sup>t</sup> **F** **D** **G**<sub>D</sub><sup>1/2</sup>) matrix into the A<sub>g</sub>, B<sub>g</sub>, A<sub>u</sub>, and B<sub>u</sub> blocks. As usual it is most useful to write this in the form

$$\mathbf{G}_D^{1/2} \mathbf{D}^t (\mathbf{U} \mathbf{F} \mathbf{U}^t) \mathbf{D} \mathbf{G}_D^{1/2}$$

so as to maintain the general form of the elements of (**U****F****U**<sup>t</sup>) independent of the numerical value of the force constants.

Using the potential discussed above, the (**U****F****U**<sup>t</sup>) matrix can be calculated. The results for the atom-atom interactions are shown in Table II. It is important to note the large values of many off-diagonal elements in this force constant matrix. There is clearly considerable mixing of certain modes, in particular some of the rotatory oscillations. Analysis of the individual terms of the force constant expressions reveals that certain intermolecular interactions are consistently strong (molecules 1-3, 1-4, 2-3, and 2-4) while others are very weak (1-2, 3-4). Note also that the 1-3 terms are generally greater than 1-4, and 2-4 > 2-3.

As noted above, calculations of eigenvalues and frequencies have been performed using a variety of parameters in the potential. In Table III, we summarize the frequencies obtained from the potential we believe to be most suitable, i.e., the one using the parameters specified above plus the contribution from static dipole-dipole terms. Omission of the latter has the effect of reducing the spread of the frequencies without affecting the lattice energy greatly. Thus the indication is that the dipolar terms have some importance in the intermolecular interactions, as their inclusion causes a greater splitting of different symmetry coordinates composed of related molecular displacement coordinates. The results of calculations involving other potentials are available in ref 27.

Also included in Table III are our assignments of ob-

TABLE II: The UFU<sup>+</sup> Matrix<sup>a</sup>

The A <sub>g</sub> Block					
25.28	-13.66	-14.44	2.81	-76.6	60.87
	67.88	-1.39	29.58	-89.2	-73.08
		80.59	-173.5	-43.1	77.54
			2746.0	-1344.0	-2816.1
				6557.0	-302.5
					4831.0
The A <sub>u</sub> block					
72.70	-13.95	0.0	-212.6	-42.42	296.3
	143.2	0.0	299.6	248.3	-347.3
		0.0	0.0	0.0	0.0
			5691.0	-1324.1	-4372.0
				10630.0	-739.6
					8591.0
The B <sub>g</sub> block					
54.1	10.38	-34.82	-65.62	97.38	137.9
	85.44	-17.66	-13.83	6.6	-49.8
		98.2	-111.9	-163.3	44.2
			3227.0	-2215.0	-3233.1
				8908.0	740.0
					5203.0
The B <sub>u</sub> block					
0.0	0.0	0.0	0.0	0.0	0.0
	0.0	0.0	0.0	0.0	0.0
		98.6	-110.5	58.9	-22.7
			5210.0	-450.5	-3954.0
				8272.0	-1783.0
					8221.0

<sup>a</sup> Elements of the matrix are force constants, calculated from the potential function as described in the text, combined according to the symmetry operations of C<sub>2h</sub> so as to factor the matrix in the usual way. In each 6 × 6 block of elements a<sub>ij</sub>, when i, j = 1, 2, or 3, the elements are combinations of translations, when i, j = 4, 5, or 6 they are rotations; and when i = 1, 2, or 3 and j = 4, 5, or 6 they are translation-rotation interactions. The sequence of coordinates in numbering the elements is x, y, z, ξ, η, ζ. (See Appendix for definition of rotatory coordinates.) Thus, the a<sub>11</sub> elements of the blocks are

$$\begin{aligned} A_g: & f_{xx}^{11} + f_{xx}^{12} + f_{xx}^{13} + f_{xx}^{14} \\ A_u: & f_{xx}^{11} + f_{xx}^{12} - f_{xx}^{13} - f_{xx}^{14} \\ B_g: & f_{xx}^{11} - f_{xx}^{12} + f_{xx}^{13} - f_{xx}^{14} \\ B_u: & f_{xx}^{11} - f_{xx}^{12} - f_{xx}^{13} + f_{xx}^{14} \end{aligned}$$

where the superscripts refer to force constants between molecules exchanged under E(11), C<sub>2</sub>(12), i(13), and σ<sub>h</sub>(14) operations of the group. Notice that the a<sub>ij</sub> elements of the blocks have different units. When i and j = 1, 2 and 3 the units are kcal/mol Å<sup>2</sup>. When i = 1, 2 and 3 and j = 4, 5 and 6 or i = 4, 5 and 6 and j = 1, 2 and 3 the units are kcal/mol Å. When i and j = 4, 5, and 6 the units are kcal/mol.

served experimental data to the calculated frequencies. The Raman frequencies<sup>2</sup> are assigned to A<sub>g</sub> or B<sub>g</sub> modes based on the available single crystal data. For the A<sub>u</sub> and B<sub>u</sub> modes, however, the less complete far-infrared data were used. Consequently there is no basis in experiment for assuming that particular frequency maxima in the spectrum do indeed arise from several vibrational modes. However, the calculations predict such groupings and the assignments have been made accordingly.

## Discussion

Before turning to a discussion of the frequencies and assignments, certain aspects of the calculations and potential are worth noting. It has been general practice, in the calculation of force constants for internal vibrations, to develop methods where a good transferability of force constants is possible. To attempt such a procedure for lattice vibration force constants would be absurd, as the diversity of crystal geometries, molecular shapes, intermolecular interactions, and intermode coupling is too great. For internal vibrations this problem is solved by use of internal coordinate force constants as starting parameters for a refinement. It seems

reasonable on the basis of the calculation presented herein to assume that atom-atom interactions, perhaps modified by other terms (e.g., dipole-dipole, coulombic, etc.) in the potential for particular cases, will prove to be a viable approach. More work, particularly more complete sets of experimental data on complex crystals, is necessary to test this.

In this paper we have not dwelt on the many assumptions of the calculation as it was performed. The molecules have been assumed to be rigid bodies executing small oscillations about their equilibrium positions. All interactions between lattice vibrations and internal vibrations have been neglected. This assumption has recently been the subject of discussions by Borgen and others,<sup>32</sup> who have attempted corrections for it in a few cases where particularly complete sets of data are available. PAA should be a poor case for these assumptions to hold, as it is a large molecule with low frequency internal vibrations. The experimental data for PAA are contradictory on this point, however. On one hand there are changes in the infrared and Raman spectra between crystal and solution phases, indicative of some coupling between lattice modes and internal modes.<sup>33</sup>



**TABLE III: Observed<sup>a</sup> and Calculated Lattice Vibration Frequencies**

Symmetry species	Translatory <sup>b</sup>			Rotatory <sup>b</sup>		
A <sub>g</sub>						
Obsd	30	52	70	16	74	91
Calcd	28	55	62	20	69	94
B <sub>g</sub>						
Obsd	30,37	52	70	16	74,90	95
Calcd	37	60	69	25	82	101
A <sub>u</sub>						
Obsd	50	70		135,150	84	50?
Calcd	51	69	0 <sup>c</sup>	130	89	55
B <sub>u</sub>						
Obsd			70?	115	84?	50?
Calcd	0 <sup>c</sup>	0 <sup>c</sup>	67	119	78	52

<sup>a</sup> Raman data (A<sub>g</sub>, B<sub>g</sub>) from ref 2, single crystal frequencies at -90°. Far-infrared (A<sub>u</sub>, B<sub>u</sub>) data from ref 7, polycrystalline sample at 25°. <sup>b</sup> Modes are primarily rotatory or translatory in nature, however, the translation-rotation interaction force constants are not negligible. <sup>c</sup> Acoustical modes.

By contrast, however, one finds that the selection rules for the internal modes are those of a C<sub>1</sub> symmetry molecule—the infrared and Raman spectra are virtually identical.<sup>4</sup> In the external mode region this is not the case. Here C<sub>2h</sub> selection rules are being obeyed. The isolated molecules have C<sub>1</sub> symmetry and this is also the site symmetry for all four molecules in the unit cell. There is no systematic doubling or quadrupling of internal modes between molecules. It is on these bases that we justify the assumption that while low-lying internal modes exist there is a reasonable factoring of the potential energy between these modes and the external modes of vibration.

Several points need to be made concerning the approximate intermolecular potential. First, it is not unique, in the sense that one can prove that this is *the* intermolecular potential for a PAA crystal. Quite the contrary, the potential parameters can be varied slightly, certain terms such as the static dipolar terms can even be omitted, and a reasonable fit to the observed data can still be obtained. Calculations have been carried out in this way with five different potential functions.<sup>27</sup> The results indicate that several of them will reproduce the crystal geometry and give positive eigenvalues for all motions. However, the difference between these potentials is small. A "best" potential could readily be obtained from an iterative procedure using the experimental data. This has not been done, because it was felt that this would not yield any particularly new information. Rather, one point of this calculation is to show that it can be reasonably carried out with transferred potential parameters. Of the potentials which have been shown to successfully reproduce the experimental crystal geometry and approximated lattice energy, all predict the same assignments of the vibrational frequencies. It is only the error in observed vs. calculated values which changes slightly. Second, many discussions of nematic liquid crystals in the literature have emphasized the importance of dipolar interactions in stabilizing the nematic phase.<sup>23</sup> Indeed, some have even stated that the molecules are held parallel to each other in long chains by end-to-end dipolar interactions. This is clearly not the case. To our knowledge, no calculation of the intermolecular potential has been attempted in the past, other than the one reported here for crystalline

PAA. One notes that the individual dipolar terms in the potential are large, but there are simply not very many of them. In determining the total lattice energy, and the energy surface for the unit cell, the large number of van der Waals terms dominate the potential. We have examined the eigenvalues to see if certain ones are particularly influenced by the dipolar contribution. This is not the case. If the potential is calculated without the static dipole-dipole interaction terms the frequencies all change slightly. This change is such that the lowest frequencies move up, and the highest frequencies move down. This means that there is less interaction between the molecules of the unit cell, but the extent of the change is small (5%). Thus in the crystal the dipolar terms play only a minor role in composing the total lattice energy. This result is quite independent of which atom-atom interaction parameters are used.

In the equilibrium crystal geometry, the interatomic distances are quite short. At one time it was believed that there was a considerable volume increase at the crystal-nematic transition.<sup>34</sup> However the best data now available indicate that this is not the case.<sup>35</sup> This is important, as the dipolar terms have a 1/r<sup>3</sup> dependence on distance, while the Buckingham potential terms decrease as 1/r<sup>6</sup>. If there was a substantial volume increase, one might expect that the dipolar terms would assume a relatively greater importance. Since this does not appear to happen, one can conclude that even in the nematic phase the dipolar terms are playing only a minor role in the intermolecular potential. Finally, we note that at least one nematic material, quinquephenyl, exists which has no permanent dipoles in the molecule.

Turn now to a discussion of the results shown in Table III. Although the table does give some indication of the modes as translatory or rotatory in nature, with indication of the axes about which this motion takes place, we again caution that the large off-diagonal force constants do not allow these designations to be taken too literally.

The results of the calculation as shown in this table should be viewed by column, as the calculated numbers in each column represent different combinations of the same motion under the different transformations of the U matrix. These transformations are noted in a footnote to Table II. The difference between calculated values in the same column gives information about the extent of intermolecular interaction along that coordinate. This comes about in the following way. In the absence of intermolecular forces, the predicted translatory and rotatory modes would reduce to four. The translations would all be determined by the molecular mass, and would be degenerate along all axes. The rotatory oscillations would be determined by the moments of inertia; thus three such modes would be observed.

As the intermolecular forces increase, the splitting of translatory and rotatory modes increases. For strong intermolecular interaction, some modes will be higher in frequency, some lower, as is always the case with interacting energy levels. In Table III, when the numbers in the same column are similar, this indicates a small intermolecular coupling with respect to the particular coordinate. In viewing the experimental data without calculations, one has no way of knowing whether modes occurring close together in frequency are the result of small intermolecular interaction about the same coordinate or are simply accidentally degenerate or near degenerate as a result of strong coupling from different coordinates. Indeed, both situations are

shown to exist from the calculations. For example, bands are predicted at 50–60  $\text{cm}^{-1}$  in the Raman and infrared arising from three different types of motion, one rotatory and the others translatory. In one case strong interactions are involved, in the others weak coupling. The calculations are useful in sorting out accidental degeneracy from degeneracy in the potential, and in this way illuminating which coordinates are strongly and which are weakly coupled. This is quite relevant to the quantitation of the idea of the crystal–nematic transition as one in which some intermolecular forces are maintained and others are lost.

The cases in which intermolecular coupling is weak are particularly significant with respect to formation of the nematic phase. It is these intermolecular interactions which presumably determine the point at which the crystalline phase will form a liquid crystal. Weak coupling is most evident for translations along  $z$  ( $24^\circ$  tilt from crystallographic  $c$ ) and rotations about  $\eta$  (approximately equivalent to  $y$  or crystallographic  $b$ ; see Appendix). Note that those motions might be expected to behave similarly as they both involve atomic displacements along the same direction. Further both modes are predicted to occur in the  $\sim 70$ – $80\text{-cm}^{-1}$  range. This point will be discussed further below.

The result of small intermolecular coupling is somewhat less true for the other translatory modes. Strikingly different results are found for the other two rotatory modes. The rotations about  $\zeta$  are noteworthy in that this is the only set of modes for which the Raman is predicted give rise to substantially higher frequencies than the infrared. The calculations show that one should avoid generalizations for complex molecules as to whether the symmetric or asymmetric component of a particular type of motion occurs at higher frequency. Such generalizations are tempting because of their utility in internal vibration theory. In addition, there is apparently little use for generalizations as to the relative magnitudes expected for translational vs. rotational modes, which some authors have proposed in the past.<sup>37</sup> Finally, at least for an anisotropic crystal such as PAA it is not possible to assign rotatory modes based on moments of inertia alone as is often attempted. One sees that the rotatory modes about the  $\xi$  (crystallographic  $a$ ) axis are predicted to be both the highest and lowest frequency lattice modes observed in the spectrum.

This prediction of strong intermolecular coupling with respect to rotation about two axes is of importance to understanding the existence of the nematic phase. It is, we believe, a new way of viewing the restrictions on the degrees of freedom which are present in this phase. In particular, most qualitative discussions of motion in nematic phases have focused on translatory rather than rotatory interactions.

It has been previously mentioned (see Introduction) that examination of the temperature dependence of the Raman spectrum of PAA<sup>2</sup> indicated the presence of pretransition effects at the crystal–nematic phase transition, manifested by what appeared to be a soft mode in the 70– $80\text{-cm}^{-1}$  region in the Raman spectrum. The qualitative idea of this mode is that it is a hindered rotation or translation which becomes free as the phase transition is approached. From Table III one can see that the Raman active modes which are predicted to occur in this region of the spectrum are those for which intermolecular coupling is weak. These are the ones which might be expected to show the “soft mode” behavior. The calculation thus confirms the general idea

that in a nematogenic material certain intermolecular interactions will be easily lost while others are maintained.

The calculations also reinforce the assignment<sup>7</sup> of the strong intermolecular absorption observed in the  $100\text{-cm}^{-1}$  region of the far-infrared nematic and isotropic phase spectra as being due to a rotatory oscillation. In turn, this lends weight to a similar claim with respect to polar liquids by Van der Elsken.<sup>36</sup> Of passing interest is the confirmation of the assignment of the Raman active modes in the 30– $40\text{-cm}^{-1}$  region to hindered translations primarily along  $x$ , made on the basis of qualitative arguments previously.<sup>2</sup>

*Acknowledgments.* We thank Professor David Beveridge for assistance in the use of ORTEP. The support of the American Cancer Society (Grant No. BC 21-c) is gratefully acknowledged.

## Appendix

Shimanouchi et al.<sup>21</sup> have extended the well-known GF method of Wilson for the calculation of internal vibrations to the calculation of the vibrations of a lattice. This extension is relatively straightforward and will not be reviewed here. Suffice to say that the  $\mathbf{F}$  matrix of elements  $f_{ij} = f_{ji}$  is a matrix of force constants with values determined by analytical expressions computed from the second derivatives of the intermolecular potentials. To solve the secular equation, it is convenient to write it in the form

$$\{\mathbf{G}^{1/2}\mathbf{F}\mathbf{G}^{1/2} - \lambda\mathbf{E}\} = 0$$

The eigenvalues of  $\mathbf{G}^{1/2}\mathbf{F}\mathbf{G}^{1/2}$  give the lattice frequencies, including the zeros corresponding to acoustical modes, by the usual  $\lambda:\nu$  relationship.

To describe the translations of the molecules, it is very convenient to use cartesian axes. The  $\mathbf{G}^{-1}$  matrix only has elements along its diagonal then for translations.

Computation of the  $\mathbf{G}^{-1}$  matrix elements for hindered rotations is not so simple. Some further considerations of this problem are necessary. The most common set of parameters used in the literature are, of course, the eulerian angles ( $\theta, \phi, \psi$ ).

The new coordinates of a point after a rotation,  $X, Y$ , and  $Z$ , are obtained from the old coordinates, before rotation ( $x, y$ , and  $z$ ) by means of three successive rotations performed in a specific sequence.<sup>22</sup> Thus

$$\begin{aligned} X &= x(\cos \phi \cos \theta \cos \psi - \sin \phi \sin \psi) - \\ &\quad y(\cos \phi \cos \theta \sin \psi + \sin \phi \cos \psi) + \\ &\quad\quad\quad z(\cos \phi \sin \theta) \\ Y &= x(\sin \phi \cos \theta \cos \psi + \cos \phi \sin \psi) + \\ &\quad y(\cos \phi \cos \psi - \sin \phi \cos \theta \sin \psi) + z(\sin \psi \sin \theta) \\ Z &= x(-\sin \theta \cos \psi) + y(\sin \theta \sin \psi) + z \cos \theta \quad (\text{A1}) \end{aligned}$$

The kinetic energy of the body is given by the following equation:

$$2T = I_1\omega_x^2 + I_2\omega_y^2 + I_3\omega_z^2 \quad (\text{A2})$$

where  $I_1, I_2$ , and  $I_3$  are the principal moments of inertia, and  $\omega_x, \omega_y$ , and  $\omega_z$  are the components of the angular velocity of the body about  $x, y$ , and  $z$ , respectively.

The angular velocity can be expressed in terms of the Euler angles as:

$$\begin{aligned} \omega_x &= \dot{\theta} \sin \psi - \dot{\phi} \sin \theta \cos \psi \\ \omega_y &= \dot{\theta} \cos \psi - \dot{\phi} \sin \theta \sin \psi \\ \omega_z &= \dot{\psi} + \dot{\phi} \cos \theta \quad (\text{A3}) \end{aligned}$$

If the expressions (A3) are used in eq A2 one obtains

$$T = \frac{1}{2} [I_1(\dot{\theta} \sin \psi - \dot{\phi} \sin \theta \cos \omega)^2 + I_2(\dot{\theta} \cos \psi - \dot{\phi} \sin \theta \sin \psi)^2 + I_3(\dot{\psi} + \dot{\phi} \cos \theta)^2] \quad (\text{A4})$$

The elements of the  $\mathbf{G}^{-1}$  matrix are calculated as

$$M_{ij} = \left. \frac{\partial^2 T}{\partial \theta \partial \theta} \right|_0, \quad M_{ii} = \left. \frac{\partial^2 T}{\partial \theta^2} \right|_0, \text{ etc.}$$

These derivatives are evaluated at the equilibrium position, i.e., when  $\theta = \phi = \psi = 0$  or when  $x, y, z$  and  $X, Y, Z$  axes coincide. The  $\mathbf{G}^{-1}$  obtained is

$$\mathbf{G}^{-1} = \begin{bmatrix} I_2 & & \\ & I_3 & I_2 \\ & I_3 & I_3 \end{bmatrix}$$

It is important to note the following facts about the matrix.

(1) No element is a function of  $I_1$ . (2) Its determinant is zero, therefore, it is not an invertible matrix. (3) Of the three possible eigenvalues, at least one is zero. However,  $T$  by definition is positive, its determinant and the principal minors of every order of its determinant are positive, which is contradictory.

For these reasons, one should not use the normal Euler angles for this problem. This has been recognized before in the literature. To be sure, Euler realized that the so-called Euler angles are a special case of the parameters used to treat such a problem. In the dynamics literature, Whittaker<sup>22</sup> instructs on the use of "symmetrical" parameters for treatment of problems similar to the one described here. Some reference to these parameters is also mentioned in one of the review articles referred to earlier.<sup>19</sup> Nonetheless, authors treating lattice vibrations of molecular crystals do not seem to have adopted the symmetrical parameters.

If a rigid body is rotated through an angle about a line through the fixed origin, whose direction angles are  $\alpha, \beta, \gamma$ , the coordinates  $X, Y, Z$  of the new position of any point whose original coordinates were  $x, y, z$  are given by the equation<sup>22</sup>

$$\begin{aligned} X &= x - 2 \sin^2 \frac{1}{2} \omega (x \sin^2 \alpha - y \cos \alpha \cos \beta - \\ &\quad z \cos \alpha \cos \gamma) + 2 \sin \frac{1}{2} \omega \cos \frac{1}{2} \omega (z \cos \beta - \\ &\quad y \cos \gamma) \\ Y &= y - 2 \sin^2 \frac{1}{2} \omega (y \sin^2 \beta - z \cos \beta \cos \gamma - \\ &\quad x \cos \beta \cos \alpha) + 2 \sin \frac{1}{2} \omega \cos \frac{1}{2} \omega (x \cos \gamma - \\ &\quad z \cos \alpha) \\ Z &= z - 2 \sin^2 \frac{1}{2} \omega (z \sin^2 \gamma - x \cos \alpha \cos \gamma - \\ &\quad y \cos \gamma \cos \beta) + 2 \sin \frac{1}{2} \omega \cos \frac{1}{2} \omega (y \cos \alpha - \\ &\quad x \cos \beta) \quad (\text{A5}) \end{aligned}$$

Let us introduce new parameters  $\xi, \eta, \zeta, \chi$ , symmetrical parameters, defined by the equation

$$\begin{aligned} \xi &= \cos \alpha \sin \frac{1}{2} \omega \\ \eta &= \cos \beta \sin \frac{1}{2} \omega \\ \zeta &= \cos \gamma \sin \frac{1}{2} \omega \\ \chi &= \cos \frac{1}{2} \omega \end{aligned} \quad (\text{A6})$$

which satisfy the relation

$$\xi^2 + \eta^2 + \zeta^2 + \chi^2 = 1 \quad (\text{A7})$$

Using them in eq A5 one obtains

$$\begin{aligned} X &= (\xi^2 - \eta^2 - \zeta^2 + \chi^2)x + 2(\xi\eta - \zeta\chi)y + \\ &\quad 2(\xi\zeta + \eta\chi)z \\ Y &= 2(\xi\eta + \zeta\chi)x + (-\xi^2 + \eta^2 - \zeta^2 + \chi^2)y + \\ &\quad 2(\eta\zeta - \eta\chi)z \\ Z &= 2(\xi\zeta - \eta\chi)x + 2(\eta\zeta + \eta\chi)y + \\ &\quad (-\xi^2 - \eta^2 + \zeta^2 + \chi^2)z \quad (\text{A8}) \end{aligned}$$

The angular velocity components  $\omega_x, \omega_y, \omega_z$ , can be expressed in terms of the symmetrical parameters as

$$\begin{aligned} \omega_x &= 2(\chi\dot{\xi} + \zeta\dot{\eta} - \eta\dot{\zeta} - \xi\dot{\chi}) \\ \omega_y &= 2(-\xi\dot{\xi} + \chi\dot{\eta} + \xi\dot{\zeta} - \eta\dot{\chi}) \\ \omega_z &= 2(\eta\dot{\xi} - \zeta\dot{\eta} + \chi\dot{\zeta} - \zeta\dot{\chi}) \quad (\text{A9}) \end{aligned}$$

If expressions (A9) are used in eq A2, one obtains

$$T = 2I_1(\chi\dot{\xi} + \zeta\dot{\eta} - \eta\dot{\zeta} - \xi\dot{\chi})^2 + 2I_2(-\xi\dot{\xi} + \chi\dot{\eta} - \xi\dot{\zeta} - \eta\dot{\chi})^2 + 2I_3(\eta\dot{\xi} - \zeta\dot{\eta} + \chi\dot{\zeta} - \zeta\dot{\chi})^2 \quad (\text{A10})$$

The equilibrium position corresponds to  $\omega = 0$ . From eq A6 it can be seen that at that position  $\xi = \eta = \zeta = 0$  and  $\chi = 1$ . If the elements of the  $\mathbf{G}^{-1}$  matrix are calculated, as before, one obtains

$$\mathbf{G}^{-1} = 4 \begin{bmatrix} I_2 & 0 & 0 \\ 0 & I_3 & 0 \\ 0 & 0 & I_3 \end{bmatrix}$$

This  $\mathbf{G}^{-1}$  is well-behaved. The three principal moments of inertia are present. It is an invertible matrix, and the three eigenvalues are positive.

## References and Notes

- Submitted by D. Grunbaum in partial fulfillment of the requirements for the degree of Doctor of Philosophy at the City University of New York, 1974.
- B. J. Bulkin and F. T. Prochaska, *J. Chem. Phys.*, **54**, 635 (1971).
- N. M. Amer, Y. R. Shen, and H. Rosen, *Phys. Rev. Lett.*, **24**, 718 (1970).
- N. M. Amer and Y. R. Shen, *J. Chem. Phys.*, **56**, 2654 (1972).
- W. J. Borer, S. S. Mitra, and C. W. Brown, *Phys. Rev. Lett.*, **27**, 379 (1971).
- J. M. Schnur, M. Hass, and W. L. Adair, *Phys. Lett.*, **41A**, 326 (1972).
- B. J. Bulkin and W. B. Lok, *J. Phys. Chem.*, **77**, 326 (1973).
- B. J. Bulkin in "Applications of the Newer Techniques of Analysis", G. Ewing, Ed., Plenum Press, New York, N.Y., 1973, pp 1-12.
- J. Billard, M. Delhaye, J.-C. Merline, and G. Vergoten, *C. R. Acad. Sci., Ser. B*, **273**, 1105 (1971).
- M. Ito and T. Shigeoka, *J. Chem. Phys.*, **44**, 100 (1966).
- T. Shimanouchi and I. Harada, *J. Chem. Phys.*, **41**, 2651 (1964).
- J. Durig, M. Walker, and F. Baglin, *J. Chem. Phys.*, **48**, 4670 (1968).
- I. Harada and T. Shimanouchi, *J. Chem. Phys.*, **44**, 2016 (1966).
- D. Williams, *J. Chem. Phys.*, **45**, 3770 (1966).
- A. Kitaigorodskii, *J. Chim. Phys.*, **63**, 6 (1966).
- G. Pawley, *Phys. Status Solidi*, **20**, 347 (1967).
- J. B. Bates and W. R. Busing, paper M2, 28th Symposium on Molecular Structure and Spectroscopy, Columbus, Ohio, 1973.
- P. Richardson and E. Nixon, *J. Chem. Phys.*, **49**, 4276 (1963).
- G. Venkataraman and V. Sahni, *Rev. Mod. Phys.*, **42**, 409 (1970).
- G. Taddie and S. Califoro, *Rev. Nuovo Cimento*, **1**, 547 (1969).
- T. Shimanouchi, M. Tsuboi, and T. Miyazawa, *J. Chem. Phys.*, **35**, 1597 (1961).
- E. T. Whittaker, "A Treatise on the Analytical Dynamics of Particles and Rigid Bodies", Cambridge University Press, New York, N.Y., 1965.
- D. B. DuPré, E. T. Samulski, and A. V. Tobolsky, "Polymer Science and Materials", in A. V. Tobolsky and H. F. Mark, Ed., Wiley, New York, N.Y., 1971, pp 123-160.
- C. P. Smyth, "Dielectric Behavior and Structure", McGraw-Hill, New York, N.Y., 1955.
- J. W. Smith, "Electric Dipole Moments", Butterworths, London, 1955.

- (26) C. K. Johnson, "ORTEP, a Fortran Thermal Ellipsoid Plot Program for Crystal Structure Illustrations", USAEC Report ORNL-3794, Oak Ridge National Laboratory, Oak Ridge, Tenn., 1965.
- (27) D. Grunbaum, Ph.D. Thesis, City University of New York, 1973.
- (28) H. C. Longuet-Higgins, *Discuss. Faraday Soc.*, **40**, 7 (1965).
- (29) A. M. Liquori in "Symmetry and Function of Biological Systems at the Macromolecular Level", A. Engstrom and B. Standberg, Ed., Wiley-Interscience, New York, N.Y., 1969.
- (30) A. DeSantis, E. Giglio, A. M. Liquori, and A. Ripamonti, *Nature (London)*, **206**, 456 (1965).
- (31) R. Mason in "Perspectives in Structural Chemistry III", C. D. Dunitz and J. A. Ibers, Ed., Wiley, New York, N.Y., 1967.
- (32) O. S. Borgen, D. Frenstad, B. Mestvedt, and O. Ra, *Acta Chem. Scand.*, **26**, 2577 (1972).
- (33) B. J. Bulkin, D. Grunbaum, and A. Santoro, *J. Chem. Phys.*, **51**, 1602 (1969).
- (34) H. Arnold, *Z. Phys. Chem.*, **226**, 146 (1964).
- (35) R. Porter and J. Johnson, *J. Appl. Phys.*, **34**, 51 (1963).
- (36) S. G. Kroon and J. Van der Elsken, *Chem. Phys. Lett.*, **1**, 2 85 (1967).
- (37) See, for example, S. Bhagavantam and K. Venkatarayudu, "Theory of Groups and Its Application to Physical Problems", 3rd ed, Andhra University Press, Waltair, 1962.
- (38) W. R. Krigbaum, Y. Chatani, and P. G. Barber, *Acta Crystallogr., Sect. B*, **26**, 97 (1970).

## Spectrophotometric Study of the Vapors of Iron(III) Chloride and of Mixtures of Iron(III) Chloride and Aluminum(III) Chloride. Evidence for Formation of Mixed Metal Dimer Molecules

Chyi-Feng Shieh and N. W. Gregory\*

Department of Chemistry, University of Washington, Seattle, Washington 98195 (Received October 22, 1974)

Publication costs assisted by the National Science Foundation

Molar absorptivities in the wavelength interval 220–400 m $\mu$  have been estimated for FeCl<sub>3</sub>, Fe<sub>2</sub>Cl<sub>6</sub>, and FeAlCl<sub>6</sub> molecules in the vapor phase. The equilibrium constant for the reaction Fe<sub>2</sub>Cl<sub>6</sub>(g) + Al<sub>2</sub>Cl<sub>6</sub>(g)  $\rightarrow$  2FeAlCl<sub>6</sub>(g) has been evaluated from spectrophotometric data and found to be of the order of 1.6 with no marked dependence on temperature. Properties indicated for the mixed metal dimer molecule are discussed.

### Introduction

It has been well established that the dimeric species Fe<sub>2</sub>Cl<sub>6</sub> and Al<sub>2</sub>Cl<sub>6</sub> are the principal molecular components in vapors at equilibrium with condensed phases of iron(III) chloride and aluminum(III) chloride, respectively, at temperatures below 300°. The two species appear to have very similar chlorine-bridged structures with the metal atoms in a fourfold coordination environment. Mixtures of these substances are of considerable interest in certain metallurgical and chemical processes. The phase diagram of the FeCl<sub>3</sub>-AlCl<sub>3</sub> system has been discussed by Morozov et al.<sup>1</sup> and by Semenenko and associates.<sup>2</sup> The latter workers also report observing mass spectrometric evidence for the existence of the mixed metal dimer molecule FeAlCl<sub>6</sub> in vapors above melts containing 30 and 50% FeCl<sub>3</sub>. Formation of such a species is not unexpected; however a systematic study of its properties and conclusions concerning its relative importance in such mixtures has not been found in the literature. Reports of somewhat similar complexes of AlCl<sub>3</sub> with PdCl<sub>2</sub><sup>3</sup> and with UCl<sub>4</sub> and UCl<sub>5</sub><sup>4</sup> have been published recently and haloaluminate complexes in general have been studied widely.<sup>5</sup>

We have made a spectrophotometric study of the equilibrium vapor phase generated by mixtures of aluminum chloride and ferric chloride, with chlorine added to repress the dissociation of ferric chloride. Aluminum chloride does not absorb light appreciably in the wavelength range 200–500 m $\mu$ . A preliminary study of the vapor phase absorption

of ferric chloride made earlier in this laboratory by Christian<sup>6</sup> showed two strong absorption bands, centered around 245 and 360 m $\mu$ . This work has been extended in the present study and molar absorptivities assigned to the species Fe<sub>2</sub>Cl<sub>6</sub> and FeCl<sub>3</sub>, and from a subsequent study of AlCl<sub>3</sub>-FeCl<sub>3</sub> mixtures apparent values also assigned for FeAlCl<sub>6</sub>. Spectrophotometric data have been used to derive equilibrium constants for the reaction



and the properties indicated for the mixed metal dimer molecule are discussed.

### Experimental Section

Vapor phase absorbances were measured with a Cary 14H recording spectrophotometer. Samples were introduced into quartz cells by sublimation in a Pyrex high vacuum system. A sample was finally isolated in a cell by an oxygen-gas flame seal-off of the Pyrex side of a quartz-Pyrex graded seal. The furnace assembly used to heat the cells has been described by Hilden.<sup>7</sup> Thermocouples, calibrated at the melting points of tin and lead, were used to measure temperatures. Cell windows were kept approximately 2° above the temperature of the cell side arm in which the condensed phase collected during the study of vaporization equilibria.

Samples of ferric chloride were prepared either by reaction (in the vacuum system) of iron wire (Merck reagent grade) and chlorine, generated by thermal decomposition

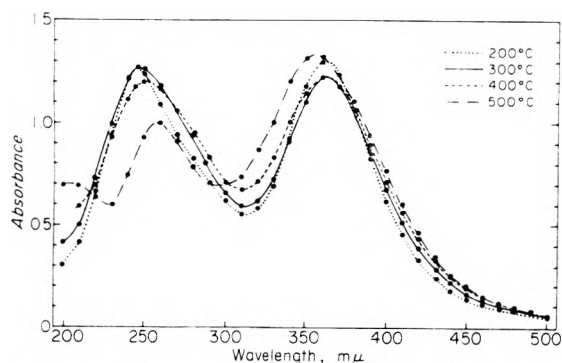


Figure 1. Absorbance vs. wavelength at various temperatures for superheated vapor of iron(III) chloride, sample ES5. The contribution of the excess chlorine present has been subtracted.

of cupric chloride (the latter also served as the source of excess chlorine), or by repetitive vacuum sublimations of Eastman's reagent grade anhydrous ferric chloride. Results did not appear to depend on the sample source. It was found that a reasonable approximation to the desired amount of ferric chloride in the cell could be made by observing the intensity of the color of the partially vaporized sample; rapid cooling left an appropriate amount in the cell and the excess could be sealed off after condensation in an extension of the side arm. The actual amount finally isolated in the cell was determined following the absorbance measurements by colorimetric determination of the iron as the 1,10-phenanthroline complex.<sup>8,9</sup> The quantity of free chlorine in the cell was determined from absorbance measurements at room temperature, using molar absorptivities reported by Gibson and Bayliss.<sup>10</sup>

$\text{AlCl}_3$  was prepared by reaction of hydrogen chloride with analytical grade aluminum wire in the vacuum system. In one instance material resublimed from reagent grade anhydrous  $\text{AlCl}_3$  was used. Samples of aluminum halide were isolated in sealed Pyrex capsules until needed. Thin walled capillary extensions on these capsules were broken inside the vacuum system by dropping a glass enclosed weight when samples were to be transferred by vacuum sublimation into the absorption cells. The total quantity of aluminum in the cell was determined following absorbance measurements by colorimetric determination as the tris(8-quinolino)aluminum(III) ion.<sup>8,9</sup>

### Iron(III) Chloride

The vapor phase absorbances of five independent samples of ferric chloride were observed as a function of temperature in the range 200–500  $m\mu$ . At temperatures below ca. 200° the vapors were in equilibrium with the solid phase. Three of the samples, CS5, ES5, and GS2 (the numbers designate the path length of the absorption cell) were small enough to vaporize completely, as evidenced by a marked change in the variation of the absorbance with temperature, in the temperature range of the study. These samples were also studied as superheated vapors at temperatures up to 550°. The other two samples, AV2.5 and BV5, could only be studied with the solid phase present.

The variation of absorbance with wavelength at various temperatures for sample ES5 as a superheated vapor is shown in Figure 1. The spectrum is characterized by two maxima, centered at 200° around 245 and 360  $m\mu$ ; considerable change in the appearance of the spectrum with temperature is observed. As the temperature increases, disso-

TABLE I: Total Absorbances  $A_t$  of Iron(III) Chloride Vapor Samples and Estimated Molar Absorptivities of  $\text{FeCl}_3(\text{g})^a$

$T, ^\circ\text{C}$	$\alpha$	245 $m\mu$		260 $m\mu$		360 $m\mu$	
		$A_t$	$\epsilon_1$	$A_t$	$\epsilon_1$	$A_t$	$\epsilon_1$
CS5 $C_0 = 3.327 \times 10^{-5}$ ; $C_{\text{Cl}_2} = 9.04 \times 10^{-4} M$							
200	0.0008	1.820		1.572		1.798	
250	0.0056	1.795		1.582		1.735	
300	0.0351	1.739		1.593		1.667	
350	0.0593	1.638		1.531		1.628	
400	0.1109	1.598	3056	1.599	4426	1.655	
450	0.3288	1.467	3826	1.524	4704	1.700	7264
500	0.4920	1.260	3151	1.443	4340	1.777	7056
ES5 $C_0 = 2.441 \times 10^{-5}$ ; $C_{\text{Cl}_2} = 2.206 \times 10^{-4} M$							
200	0.0009	1.318		1.145		1.302	
250	0.0066	1.295		1.164		1.255	
300	0.0412	1.267		1.174		1.229	
350	0.0693	1.201		1.140		1.203	
400	0.1283	1.175	3018	1.167		1.225	8456
450	0.3727	1.089	3611	1.147	4549	1.288	6976
500	0.5467	0.900	2704	1.053	3924	1.343	6728
550	0.6893	1.006	3866	1.004	3859	1.419	6792
GS2 $C_0 = 2.508 \times 10^{-5}$ ; $C_{\text{Cl}_2} = 1.318 \times 10^{-3} M$							
200	0.0009	0.570		0.500		0.537	
250	0.0065	0.560		0.506		0.523	
300	0.0406	0.542		0.489		0.509	
350	0.0683	0.525		0.501		0.501	
400	0.1268	0.502	4598	0.502	6492	0.502	8448
450	0.3686	0.518	5595	0.540	6494	0.540	7350
500	0.5406	0.558	6273	0.489	5029	0.597	7672
550	0.6873	0.425	4050	0.527	5563	0.624	7418

<sup>a</sup> Contribution of excess chlorine deducted.

ciation of dimer to monomer is expected to increase; at higher temperatures the maximum around 245  $m\mu$  was observed to shift to slightly longer wavelengths whereas the peak at 360  $m\mu$  shifted by a comparable amount toward shorter wavelengths.

Several studies of the ferric chloride monomer-dimer equilibrium have been reported; results are summarized conveniently in the JANAF tables.<sup>11</sup> At the vapor concentrations used in this work the degree of dissociation of the dimer is very small below 300°. The absorbance maxima between 200 and 300° are observed to decrease with increasing temperature and this behavior is assumed to characterize  $\text{Fe}_2\text{Cl}_6$ . On the other hand, at 550° for sample GS2, for example, the calculated degree of dissociation of dimer to monomer is nearly 70% and the absorbance of the monomer is expected to be of major importance. Molar absorptivities of the two species were estimated in the following way.

From data in the JANAF tables<sup>11</sup> the concentration of chlorine introduced into the various cells may be shown to prevent significant dissociation of  $\text{FeCl}_3$  to iron(II) chloride. Possible intermediates such as  $\text{Fe}_2\text{Cl}_5$ <sup>12</sup> were also assumed unimportant under these conditions. The contribution of chlorine to the total absorbance, based on measurement of its absorbance at room temperature and the results of Gibson and Bayliss,<sup>10</sup> was subtracted and the remainder attributed to the contributions of  $\text{FeCl}_3(\text{g})$  and  $\text{Fe}_2\text{Cl}_6(\text{g})$ .

**TABLE II: Apparent Pressures of Fe<sub>2</sub>Cl<sub>6</sub>(g) in Equilibrium with FeCl<sub>3</sub>(s)**

T, °K	A (360 mμ)	P, Torr	T, °K	A (360 mμ)	P, Torr
	AV2.5			BV5	
467.4	0.860	0.912	447.4	0.397	0.98
472.7	1.272	1.369	466.0	1.602	0.846
474.4	1.472	1.593	455.0	0.718	0.367
471.0	1.108	1.187	449.0	0.452	0.227
477.6	1.770	1.932	459.2	0.975	0.504
			459.7	1.01	0.523
			465.7	1.56	0.823
	CS5		463.6	1.325	0.694
459.5	0.955	0.495	464.0	1.393	0.731
463.1	1.252	0.655	443.2	0.292	0.144
451.3	0.535	0.270	466.0	1.612	0.851
	ES5			GS2	
455.8	0.822	0.421	458.0	0.363	0.468
456.7	0.878	0.451			
458.2	0.954	0.492			
456.7	0.873	0.448			
461.8	1.243	0.648			

Molar absorptivities of the latter ( $\epsilon_2$ ) were assigned by assuming that all of the iron in the cell was in the form Fe<sub>2</sub>Cl<sub>6</sub> between 200 and 300°. The values at the wavelengths of the maxima and their temperature dependence in this range are approximated by the equations

$$\epsilon_2 \text{ (ca. } 245 \text{ m}\mu) = 12050 - 4.25t \quad (2)$$

$$\epsilon_2 \text{ (ca. } 360 \text{ m}\mu) = 12650 - 8.5t \quad (3)$$

where  $t$  is the temperature in °C.

If eq 2 and 3 are assumed valid at higher temperatures, the Beer-Lambert law for binary mixtures may be used to estimate the molar absorptivity of FeCl<sub>3</sub>.

$$A/b = \epsilon_1 C_1 + \epsilon_2 C_2 = C_0 (1 - \alpha)\epsilon_2 + 2C_0\alpha\epsilon_1 \quad (4)$$

where  $b$  represents the cell path length in cm, subscripts 1 and 2, respectively, indicate monomer and dimer,  $C$  represents the concentration in moles/liter (with  $C_0$  the concentration equivalent of the total number of gram atoms of iron present as either monomer or dimer),  $\epsilon$  the molar absorptivity, and  $\alpha$  the degree of dissociation of the dimer.<sup>11</sup> Results are summarized in Table I. Two maxima, centered around 260 and 360 mμ, respectively, also appear in a plot of  $\epsilon_1$  vs. wavelength with the peak at 250 approximately half the height of that at 360. The values derived for FeCl<sub>3</sub> are subject to a rather large uncertainty; however other than the differences noted, the general shape of its spectrum appears quite similar to that of the dimer.

A plot ( $\log A(360 \text{ m}\mu)/b$  vs.  $1/T$ ) of the total absorbance, after subtracting the contribution of chlorine, is shown in Figure 2. Marked changes at the temperatures where the solid phases have completely vaporized are clearly apparent for samples CS5, ES5, and GS2. When the assigned molar absorptivities of Fe<sub>2</sub>Cl<sub>6</sub> are used to calculate apparent equilibrium vapor pressures above the solid, i.e.,  $P = CRT = ART/\epsilon_2 b$ , values are found to be between 30 and 40% larger than those calculated from the equation based on transpiration and diaphragm gauge data given by Wilson and Gregory.<sup>13</sup> Least-squares analysis of the data (Table II, the data listed in the order measured) for sam-

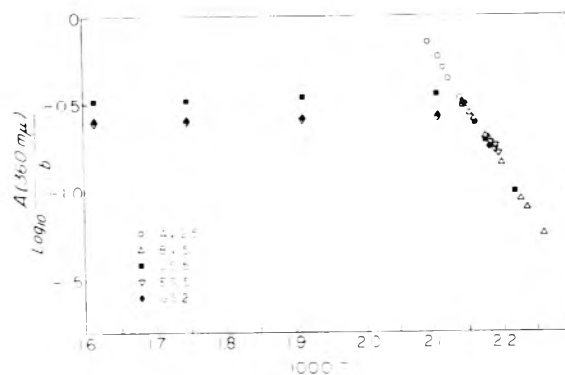


**Figure 2.** Temperature dependence of the absorbance at 360 mμ of the vapors generated by samples of iron(III) chloride, excluding the contribution of excess chlorine.

ples A and B gives the equation  $\log P(\text{Torr}) = 14.907 - 6982T^{-1}$  with a standard deviation of 0.0056. The indicated enthalpy of sublimation, 31.9 kcal for the mean temperature 460 K, does not differ significantly more than the combined experimental uncertainties from Wilson's value (32.6 kcal). The vanishingly small solid samples used in the present study may be partially responsible for the higher apparent vapor pressure although the magnitude of the difference seems larger than might be expected from surface effects alone.

#### The Mixed Metal Dimer FeAlCl<sub>6</sub>

Vapor phase absorbances were measured for nine different mixtures of FeCl<sub>3</sub> and AlCl<sub>3</sub>. Samples C, G, and J were too large to vaporize completely in the range of the measurements and only the absorbance of the saturated vapor in equilibrium with a solid phase (or phases) was observed. Sample K was very small and a condensed phase did not appear to be present except perhaps at the lowest temperature at which the absorbance was measured. With samples D, E, F, H, and I vapor phase absorbances were studied over temperature intervals in which (a) only a homogeneous gas phase was present and (b) a condensed phase (or phases) was also present. A display of  $\log A(360 \text{ m}\mu)/b$  vs.  $1/T$  for all samples is shown in Figure 3. Chlorine was also added to these samples to reduce the concentration of iron(II) species to a negligible value;<sup>11,14,15</sup> the absorbances shown in Figure 3 do not include the small contribution of chlorine. The observed behavior led to the following conclusions.

Below ca. 200° the rapid increase of the total absorbance with increasing temperature indicates that the concentrations of the absorbing vapor species are controlled by equilibrium with a condensed phase. The abrupt change in the temperature dependence observed for D, E, F, H, and I in the vicinity of 200° is attributed to complete vaporization of the sample. In the range where a condensed phase is present, the total absorbance in all cases is substantially greater (by factors in the range 2 to 10) than that of the vapor in equilibrium with pure FeCl<sub>3</sub>(s) (solid line, Figure 3). This indicates clearly the presence of an additional absorbing molecular species in the vapor phase. Since AlCl<sub>3</sub> and similar compounds of aluminum do not absorb at the wavelengths used, the new absorbing species has been assumed to contain iron and to be the mixed dimer FeAlCl<sub>6</sub>. As indicated previously concentrations of FeCl<sub>3</sub>(g) are expected to be negligible at temperatures below 300°. As will be seen the results can be reasonably well explained with-

**TABLE III: Apparent Molar Absorptivities of FeAlCl<sub>6</sub>(g)**

T, °C	E-1				K-5	
	D-2 ε(360)	ε(245)	ε(360)	F-1 ε(360)	ε(245)	ε(360)
200	5630	7310	5640	5750	7520	5520
250	5490	7050	5410	5540		5430
300	5340	8910	5210		7200	5210
350					7000	5040

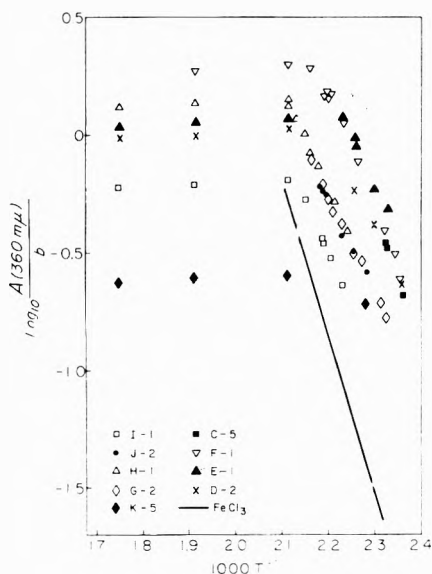


**Figure 3.** Temperature dependence of absorbance at 360 mμ of the vapors generated by the various mixtures of aluminum(III) chloride and iron(III) chloride, excluding the contribution of the excess chlorine.

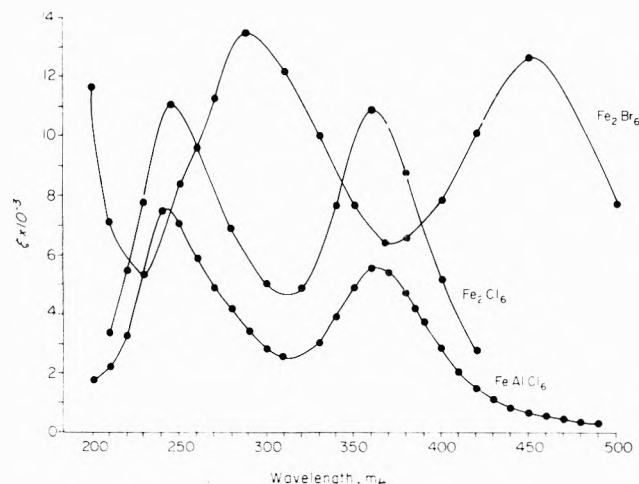


**Figure 4.** Variation of molar absorptivities with wavelength for Fe<sub>2</sub>Cl<sub>6</sub>, FeAlCl<sub>6</sub>, and Fe<sub>2</sub>Br<sub>6</sub> at 200°.

out the need to assume the presence of additional or more complex intermediates.

A sufficiently large excess of aluminum chloride is present in samples D, E, F, and K so that an equilibrium constant for (1) of the order of unity expected from simple statistical considerations would predict the contribution of Fe<sub>2</sub>Cl<sub>6</sub> to the absorbance in the homogeneous gas region to be only a few percent or less of the total. Hence in these

cases virtually all the iron in the cell should be in the form FeAlCl<sub>6</sub>; this assumption permits molar absorptivities of this species to be assigned. The appearance of the spectrum for these samples is very similar to that of Fe<sub>2</sub>Cl<sub>6</sub>. The positions of the two maxima are not significantly different, although the height of the peak at 245 mμ relative to that at 360 mμ is greater for FeAlCl<sub>6</sub> than the Fe<sub>2</sub>Cl<sub>6</sub>. Molar absorptivities assigned to FeAlCl<sub>6</sub> (ε<sub>M</sub>) are shown in Table III. The temperature dependence of ε<sub>M</sub> in the range 200–300° is reasonably well approximated by the equations

$$\epsilon_M \text{ (ca. 245 m}\mu\text{)} = 8100 - 4.0t \quad (5)$$

$$\epsilon_M \text{ (ca. 360 m}\mu\text{)} = 6430 - 3.9t \quad (6)$$

where *t* is the temperature in degrees centigrade. Molar absorptivities derived for Fe<sub>2</sub>Cl<sub>6</sub>, FeAlCl<sub>6</sub>, and values reported for Fe<sub>2</sub>Br<sub>6</sub><sup>6</sup> are compared in Figure 4.

The relative amounts of FeCl<sub>3</sub> and AlCl<sub>3</sub> in samples H and I were such as to give concentrations of Fe<sub>2</sub>Cl<sub>6</sub> and FeAlCl<sub>6</sub> of comparable magnitude when these samples were completely vaporized. Absorbance data in these cases were used to derive values for the equilibrium constant for reaction 1. The molar absorptivity of FeAlCl<sub>6</sub> at 360 mμ is very nearly one-half the value for Fe<sub>2</sub>Cl<sub>6</sub> and the total absorbance at this wavelength is relatively insensitive to the ratio of the two concentrations; A(360) thus serves, in effect, only to indicate the total concentration of iron atoms in the vapor phase. However, the difference in molar absorptivities is greater at 245 mμ and absorbances at this wavelength together with the known amount of iron and aluminum present were used for the homogenous gas samples to derive the *K*<sub>1</sub> values shown in parentheses in Table IV by solution of the following equations.

$$A/h = \epsilon_F C_F + \epsilon_M C_M$$

$$C_{Fe} = 2C_F + C_M$$

$$C_{Al} = 2C_A + C_M$$

$$K_1 = C_M^2 / C_F C_A$$

where ε<sub>F</sub> and ε<sub>M</sub> represent the molar absorptivities of Fe<sub>2</sub>Cl<sub>6</sub> and FeAlCl<sub>6</sub>; C<sub>F</sub>, C<sub>M</sub>, and C<sub>A</sub> the concentrations of Fe<sub>2</sub>Cl<sub>6</sub>, FeAlCl<sub>6</sub>, and Al<sub>2</sub>Cl<sub>6</sub>; and C<sub>Fe</sub> and C<sub>Al</sub> the concentration equivalents of the number of gram atoms of iron and aluminum, respectively, in the cell. Absorbance data at 360 mμ combined similarly with C<sub>Fe</sub> and C<sub>Al</sub>, and alternatively comparison of absorbance data at the two different wavelengths without reference to C<sub>Fe</sub> gave equilibrium constants of comparable magnitude but with considerably greater scatter (range 0.7–3).

No systematic variation of *K*<sub>1</sub> with temperature is indicated; hence Δ*H*<sup>o</sup> for (1) appears to be zero within an uncertainty estimated as ±1 kcal. Thus the equilibrium constant is not greatly different from that expected if the entropy change of (1) is only that associated with a reduction of the molecular symmetry number by a factor of 2. With allowance for this difference the thermodynamic properties of mixed metal dimer molecule appear to be essentially an average of those of Fe<sub>2</sub>Cl<sub>6</sub> and Al<sub>2</sub>Cl<sub>6</sub>.

The behavior observed for the various samples when condensed phases were present proved more difficult to correlate. The absorbances were observed to change slowly with time when temperatures were changed in the low temperature range and, while values were not recorded until the rate of change appeared negligible, some doubt still remains as to whether equilibrium in the solid state had been

TABLE IV: Vapor Phase Absorbance Data for Mixtures of FeCl<sub>3</sub> and AlCl<sub>3</sub> and Apparent Values of  $K_1$ 

Sample	°K	A <sub>360</sub> <sup>a</sup>	$K^a$	Sample	°K	A <sub>360</sub> <sup>a</sup>	$K^a$
C-5				F-1			
$C_{Fe} = 9.22 \times 10^{-5} M$	424	1.042	0.71		448	1.130	1.00
$C_{Al} = 3.0 \times 10^{-3} M$	431	1.720	1.05		453	1.417	1.04
$C_{Cl_2} = 7.0 \times 10^{-4} M$	429	1.647	1.06		455	1.512	1.04
D-2					442	0.772	0.80
	425	0.475		$C_{Fe} = 3.42 \times 10^{-4} M$	454	1.416	1.01
	444	1.170		$C_{Al} = 8.65 \times 10^{-3} M$	455	1.440	1.00
$C_{Fe} = 1.79 \times 10^{-4} M$	436	0.827		$C_{Cl_2} = 1.5 \times 10^{-4} M$	464	1.930	0.81
$C_{Al} = 2.72 \times 10^{-2} M$	473 <sup>b</sup>	2.017			425	0.245	0.21
$C_{Cl_2} = 8.3 \times 10^{-4} M$	523 <sup>b</sup>	1.965			428	0.313	0.34
	573 <sup>b</sup>	1.913			431	0.390	0.26
	673 <sup>b</sup>	1.770			473 <sup>b</sup>	1.964	
	723 <sup>b</sup>	1.690			532 <sup>b</sup>	1.892	
					673 <sup>b</sup>	1.705	
E-1				G-2			
	443	0.989	2.07		440	0.580	2.21
	436	0.600	1.51		449	0.835	2.22
$C_{Fe} = 2.10 \times 10^{-4} M$	448	1.185	2.37		454	1.070	2.24
$C_{Al} = 4.75 \times 10^{-3} M$	444	0.972	2.37		457	1.232	2.41
$C_{Cl_2} = 5.5 \times 10^{-3} M$	429	0.382	0.86	$C_{Fe} = 1.425 \times 10^{-3} M$	457	1.232	2.41
	473 <sup>b</sup>	1.183(1.535)		$C_{Al} = 4.21 \times 10^{-4} M$	432	0.385	1.86
	523 <sup>b</sup>	1.137(1.480)		$C_{Cl_2} = 7.1 \times 10^{-3} M$	463	1.565	2.14
	573 <sup>b</sup>	1.095(1.452)			444	0.630	1.85
H-1					430	0.335	1.62
	466	0.978	1.20		453	0.924	1.97
	459	0.738	1.38	J-2			
	463	0.840	1.07		459	1.200	1.86
	469	1.161	1.22	$C_{Fe} = 1.323 \times 10^{-4} M$	456	1.120	2.32
$C_{Fe} = 2.51 \times 10^{-4} M$	473	1.325	1.15	$C_{Al} = 4.09 \times 10^{-4} M$	449	0.735	1.57
$C_{Al} = 9.14 \times 10^{-4} M$	446	0.390	1.11	$C_{Cl_2} = 1.33 \times 10^{-3} M$	444	0.635	1.95
$C_{Cl_2} = 8.3 \times 10^{-4} M$	452	0.517	1.15		439	0.520	1.98
	473 <sup>b</sup>	1.405(1.683)	(1.55)		457	1.157	2.03
	523 <sup>b</sup>	1.360(1.641)	(1.59)	K-5			
	573 <sup>b</sup>	1.305(1.593)	(1.53)		439	0.952	
	623 <sup>b</sup>	1.255(1.557)	(1.43)	$C_{Fe} = 4.55 \times 10^{-5} M$	473 <sup>b</sup>	1.255(1.710)	
	477 <sup>b</sup>	1.415		$C_{Al} = 4.02 \times 10^{-2} M$	523 <sup>b</sup>	1.235	
I-1					573 <sup>b</sup>	1.185(1.635)	
	464	0.520	0.73		623 <sup>b</sup>	1.145(1.590)	
	457	0.360	1.16				
$C_{Fe} = 1.13 \times 10^{-4} M$	448	0.230	1.13				
$C_{Al} = 1.67 \times 10^{-4} M$	453	0.300	1.22				
$C_{Cl_2} = 4.7 \times 10^{-4} M$	456	0.345	1.21				
	473 <sup>b</sup>	0.632(0.72)	(1.47)				
	523 <sup>b</sup>	0.606(0.699)	(1.24)				
	573 <sup>b</sup>	0.593(0.695)	(2.08)				

<sup>a</sup> Values in parentheses represent data obtained at 245 m $\mu$ . <sup>b</sup> Solid phase not present at these temperatures. Data above 600°K off scale for Figure 3.

fully realized, particularly at temperatures below ca. 160° (it will be noted, Table IV, that the calculated  $K_1$  values appear abnormally low at these temperatures; it is also possible that an AlCl<sub>3</sub> rich phase may have condensed which would make the  $K$  calculated without proper allowance for this abnormally small).

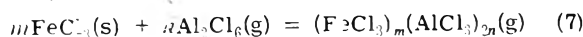
Samples E, G, and J have relatively large amounts of FeCl<sub>3</sub> and it is clear from the magnitude of the absorbance that a substantial amount of the iron remains in the solid phase at low temperatures. If it is assumed for these samples that the solid phase is virtually pure FeCl<sub>3</sub>(s), i.e., that the mole fraction of aluminum in the solid is negligibly small, the concentration of Fe<sub>2</sub>Cl<sub>6</sub> vapor is then known; the additional absorbance (over that expected for Fe<sub>2</sub>Cl<sub>6</sub>) then

gives the concentration of FeAlCl<sub>6</sub>. In this case absorbances at 360 m $\mu$ , which could be measured more accurately than at 245 m $\mu$  because of difficulties in base line calibration for the latter, were used. The concentration of FeAlCl<sub>6</sub> and the value of  $C_{Al}$  then establishes the concentration of Al<sub>2</sub>Cl<sub>6</sub> (dissociation into AlCl<sub>3</sub>(g) is negligible) and values of  $K_1$  were derived (see Table IV; data listed in order temperature was varied). These values of  $K_1$  appear on the average slightly higher than values derived from the homogeneous gas phase data for samples H and I. When a similar treatment is applied to samples C, F, H, and I in the temperature range where condensed phases are present, calculated values of  $K_1$  (shown in Table IV) are substantially less and average close to unity. In these cases the relative amount of



iron is less and solid solution effects may be expected to be more important as the concentration of the  $\text{Al}_2\text{Cl}_6$  vapor increases. If it is assumed that the solid phases contain significant mole fractions of aluminum, the calculated values of  $K_1$  are increased. However, it was not found possible to improve the overall correlation of all the data by assuming formation of ideal solid solutions or by assuming various values of a Henry's law constant for the mixed metal dimer in such solutions. Sample D has such a large amount of  $\text{AlCl}_3$  present that condensation of an aluminum chloride phase (with iron chloride dissolved in it) is expected at lower temperatures rather than an iron chloride rich phase. Absorbance data for D did not give reasonable values of  $K_1$  when the latter was assumed. We conclude therefore that while the interpretation provided when a solid phase is present is generally correct, it seems likely that nonideal solid solutions are formed when partial pressure of aluminum chloride are sufficiently high. This is also indicated in preliminary studies of the phase diagram of the  $\text{AlCl}_3$ - $\text{FeCl}_3$  system.<sup>1,2</sup>

The overall consistency of the values of  $K_1$  derived for the various samples (Table IV) gives substantial support to the accuracy of the stoichiometry represented by eq 1. It may be noted that in the various samples the ratios  $C_{\text{Al}_2\text{Cl}_6}/C_{\text{Fe}_2\text{Cl}_6}$  in the vapor phase differ by factors as large as 200;  $C_{\text{FeAlCl}_6}/C_{\text{Fe}_2\text{Cl}_6}$  varies by as much as a factor of 7. As pointed out by one of the reviewers, a direct test for the number of aluminum atoms in the principal complex species can be made by comparison of absorbances in two samples such as E and J which have significantly different  $\text{Al}_2\text{Cl}_6$  pressures and in which the solid phases appear to be reasonably pure  $\text{FeCl}_3$ . We may write in this case



and  $K_7 = P_{\text{complex}}/P_{\text{Al}_2\text{Cl}_6}^n$ . The absorbance/cm of the complex ( $A_t - A_{\text{Fe}_2\text{Cl}_6}(\text{sat})$ ) for samples E and J, respectively, is found to be 1.14 and 0.34 at 450 K and these values are proportional to  $P_{\text{complex}}$ . Since the concentration of the complex is small compared to that of  $\text{Al}_2\text{Cl}_6$ , the ratio of  $(P_{\text{Al}_2\text{Cl}_6})_E/(P_{\text{Al}_2\text{Cl}_6})_J$  is close to the ratio of the  $C_{\text{Al}}$  values, 47.5/4.09. Hence  $1.14/(47.5)^n = 0.34/(4.09)^n$  from which  $n = 0.495$ , remarkably close to 0.5.

The absorption spectra of  $\text{Fe}_2\text{Cl}_6$ ,  $\text{FeAlCl}_6$ ,  $\text{FeCl}_3$ , and  $\text{Fe}_2\text{Br}_6$  vapors appear very similar in the visible-ultraviolet range (Figure 4). It seems likely that the two peaks are associated with charge-transfer transitions involving the basic Fe-Cl bond rather than reflecting the behavior of bonds with the halogen atoms in different environments

(bridge and nonbridge) since both peaks, although slightly shifted, also appear for the monomer. The substitution of an aluminum atom for one of the atoms of iron in the dimer  $\text{Fe}_2\text{Cl}_6$  has only a minor effect on shape of the spectrum; the reduction of the molar absorptivity by a factor of approximately 2 suggests that the total absorbance is basically related to the number of iron-chlorine bonds in the molecule. The solution spectrum of tetraethylammonium tetrachloroferrate(III) has been reported to show two similar bands with maxima at 248 and 367  $m\mu$ , and similar spectra have been obtained from solutions of iron(III) chloride in other solvents.<sup>16-19</sup>

While the thermodynamic properties of  $\text{FeAlCl}_6$  are such as to give values of  $K_1$  around 1.6, not very large, nonetheless formation of the mixed metal dimer has the effect of considerably increasing the amount of iron in the vapor phase above solid  $\text{FeCl}_3$  when aluminum chloride vapor is present at substantial concentrations.  $\text{FeAlCl}_6$  is appreciably more volatile than  $\text{Fe}_2\text{Cl}_6$  and its formation may be expected to increase the difficulty of separation of iron as an impurity in aluminum chloride and vice versa by fractional sublimation.

*Acknowledgment.* This work was supported in part by a grant from the National Science Foundation, GP 37033X.

## References and Notes

- (1) G. G. Urazov and I. S. Morozov, *Tr. Gos. Inst. Prikl. Khim.*, **No. 20**, 1 (1934); I. S. Morozov, *Zh. Neorg. Khim.*, **1**, No. 2, 2792 (1956).
- (2) K. N. Semenenko, T. N. Naumova, L. N. Gorokhov, G. A. Semenova, and A. V. Novoselova, *Dokl. Akad. Nauk SSSR*, **154**, 169 (1964).
- (3) G. N. Papatheodorou, *J. Phys. Chem.*, **77**, 472 (1973).
- (4) D. M. Gruen and R. L. McBeth, *Inorg. Chem.*, **8**, 2625 (1969).
- (5) C. R. Boston in "Advances in Molten Salt Chemistry", J. Brauntein, G. Mamantov, and G. P. Smith, Ed., Plenum Press, New York, N.Y., 1971, Chapter 3.
- (6) J. D. Christian and N. W. Gregory, *J. Phys. Chem.*, **71**, 1573 (1967).
- (7) D. L. Hilden and N. W. Gregory, *J. Phys. Chem.*, **76**, 1632 (1972).
- (8) E. B. Sandell, "Colorimetric Metal Analysis", 3rd ed., Interscience, New York, N.Y., 1959.
- (9) W. Sprain and C. V. Banks, *Anal. Chim. Acta*, **6**, 363 (1952).
- (10) G. E. Gibson and N. S. Bayliss, *Phys. Rev.*, **44**, 188 (1933).
- (11) "JANAF Thermochemical Data", Thermal Laboratory, Dow Chemical Co., Midland, Mich.
- (12) O. G. Polyachenok and O. N. Komshilova, *Obshch. Prikl. Khim.*, No. 1, 109 (1969).
- (13) L. E. Wilson and N. W. Gregory, *J. Phys. Chem.*, **62**, 433 (1958).
- (14) B. G. Korshunov, G. A. Lovetskaya, and A. A. Palant, *Zh. Neorg. Khim.*, **12**, (1967).
- (15) R. F. Belt and H. Scott, *Inorg. Chem.*, **3**, 1785 (1964).
- (16) H. L. Friedman, *J. Am. Chem. Soc.*, **74**, 5 (1952).
- (17) A. P. Ginsberg and M. B. Robin, *Inorg. Chem.*, **2**, 817 (1963).
- (18) R. S. Drago, D. M. Hart, and R. L. Carlson, *J. Am. Chem. Soc.*, **87**, 1900 (1965).
- (19) R. S. Drago, R. L. Carlson, and K. F. Purcell, *Inorg. Chem.*, **4**, 15 (1965).

# Electron Spin Resonance Study of the Sulfide Radical Adducts to Unsaturated Compounds<sup>1</sup>

Yutaka Kirino and Richard W. Fessenden\*

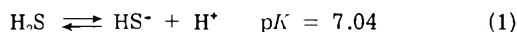
Radiation Research Laboratories, Center for Special Studies and Department of Chemistry, Mellon Institute of Science, Carnegie-Mellon University, Pittsburgh, Pennsylvania 15213 (Received September 23, 1974)

Publication costs assisted by Carnegie-Mellon University and the U.S. Atomic Energy Commission

Addition of the sulfur-containing intermediate produced by OH reaction with sulfide to a number of unsaturated compounds has been studied by means of ESR spectroscopy. Eight types of compounds were used: aliphatic compounds containing C=C (olefinic compounds and enols), C≡C, C=N (oximes and an imine), or C=S bonds, benzenes, furans, pyrroles, and thiophenes. Adduct radicals containing sulfur were detected only in the case of some olefinic compounds and oximes. The lack of detectable lines in the other cases is most likely the result of slow reaction of the intermediate. Values of the p*K* for dissociation of the sulfhydryl proton in three β-mercaptoalkyl radicals were determined. The values are for HSCH<sub>2</sub>CHCO<sub>2</sub><sup>-</sup>, 8.9, for HSCH<sub>2</sub>CHCN, 7.1, and for HSCH<sub>2</sub>C(CH<sub>3</sub>)CO<sub>2</sub><sup>-</sup>, 9.5. A study of the temperature dependence of line broadening in <sup>-</sup>SCH<sub>2</sub>CHCO<sub>2</sub><sup>-</sup> and <sup>-</sup>SCH<sub>2</sub>C(CH<sub>3</sub>)CO<sub>2</sub><sup>-</sup> gave values for the activation energy for internal rotation by 180° about the CH<sub>2</sub>-C bond of 7.1 and 6.2 kcal mol<sup>-1</sup>, respectively.

## Introduction

Relatively little is known about reactions of the intermediates produced by oxidation of sulfide with OH radical. Hydroxyl radicals produced by radiolysis of aqueous solutions react rapidly with H<sub>2</sub>S or HS<sup>-</sup> depending on pH



with rate constants of  $1.1 \times 10^{10}$  and  $5.4 \times 10^6 \text{ M}^{-1} \text{ sec}^{-1}$ , respectively.<sup>2</sup> The resulting intermediates may include HS<sup>•</sup> and S<sup>-</sup> as well as complexes such as HSOH<sup>-</sup> and HS<sub>2</sub><sup>2-</sup> but the situation is not fully understood.<sup>2</sup> For the present purposes the intermediate (or intermediates) will be described by the simple name "sulfide radical". The reaction of this intermediate with the *aci* anion of nitromethane has been found<sup>3,4</sup> to produce the radical <sup>-</sup>SCH<sub>2</sub>NO<sub>2</sub><sup>-</sup> at high pH which is in equilibrium with HSCH<sub>2</sub>NO<sub>2</sub><sup>-</sup> at lower pH. The p*K* for this equilibrium can be estimated to be ~9.<sup>5</sup> Norman and Storey have also reported<sup>4</sup> adducts of the sulfide radical to acrylic acid and acrylonitrile in a flow-mixing system. The sulfide radical has also been detected by trapping with nitromethane in the photolysis of HS<sup>-</sup><sup>6</sup> and S<sub>2</sub>O<sub>3</sub><sup>2-</sup>.<sup>5</sup>

Because these earlier studies involve only a few reactants for the sulfide radical it is important to explore more fully the reactions of this species. The present paper describes *in situ* radiolysis-ESR experiments<sup>7</sup> in which radical products were sought with a wider range of unsaturated compounds.

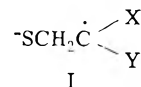
## Experimental Section

In all cases radicals were produced by irradiating a solution of sodium sulfide containing the desired compound. The irradiation (2.8-MeV electrons) was carried out directly in the ESR cavity as previously described.<sup>7</sup> The solution flowed through the flat silica cell at about 1 cc sec<sup>-1</sup> and its temperature was measured at the exit from the cell with a copper-constantan thermocouple. For measurement of ESR line positions, a second-derivative presentation was used (100-kHz and 200-Hz modulation). Where line widths were to be measured only the 100-KHz modulation was used and first-derivative spectra were recorded.

Sodium sulfide enneahydrate (Na<sub>2</sub>S·9H<sub>2</sub>O) was Baker Analyzed reagent. All of the organic chemicals employed were of the purest grade commercially available and used without further purification except for olefinic compounds containing stabilizers, which were distilled under atmospheric or reduced pressure. Water was distilled and freed from organic impurities by passing the vapor with oxygen through a silica tube at ~600°. Solutions were saturated with nitrous oxide which served both to remove oxygen and to convert e<sub>aq</sub><sup>-</sup> to ·OH. In the case of gaseous olefins, a mixture of the olefin and nitrous oxide (ratio ~4:1) was bubbled through the sulfide solution. The pH was adjusted with potassium hydroxide or perchloric acid; no buffer was used except where noted. Borate was added as Na<sub>2</sub>B<sub>4</sub>O<sub>7</sub> but concentrations are given in terms of H<sub>3</sub>BO<sub>3</sub>.

## Results and Discussion

*ESR Spectra of β-Mercaptoalkyl Radicals.* Basic (pH 12), N<sub>2</sub>O saturated solutions containing sodium sulfide (10–20 mM) and the desired olefinic compound (5–10 mM) were irradiated and the ESR spectra recorded. With acrylate, acrylonitrile, methacrylate, methacrylonitrile, and itaconate spectra were obtained which can be attributed to β-mercaptoalkyl radicals (I). The parameters for these radi-



cals are summarized in Table I. Because the nature of the intermediate sulfur containing radical is not clear (as mentioned above) it is possible that some reaction other than the net addition of S<sup>-</sup> has occurred. In particular the radicals designated by structure I could possibly be the adducts of some more complex group containing oxygen (or OH) as well as sulfur. However, the protonation equilibrium discussed in a later section is completely consistent with the structure as written so the simple structure is probably correct.

The spectrum obtained with acrylate (X = H, Y = CO<sub>2</sub><sup>-</sup>) is shown in Figure 1 with the expected six lines indicated

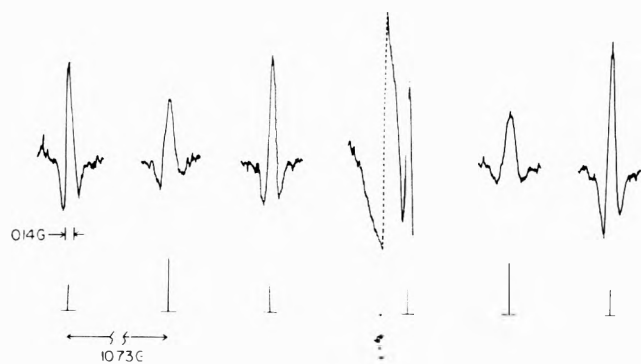
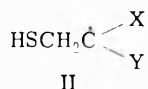


**Figure 1.** Second-derivative ESR spectrum of the radical produced by the addition of the sulfide radical to acrylate at pH 12 and  $19 \pm 2^\circ$ . No lines other than those shown were detected. The fourth line from the left is on the tail of the signal from the silica cell which necessitated the base line shift indicated by the dashed line. Note that the central lines of the triplets are broader and less intense.

by a "stick spectrum". The central lines (2 and 5) of the triplets caused by the  $\beta$ -methylene protons are weaker and broader than the other four lines. The peak height ratio of lines 1 and 2 under the conditions used is about 1:0.5 rather than the expected 1:2. Although some of the observed broadening is caused by the second-order splitting of 0.04 G this effect cannot reduce the intensity of lines 2 and 5 to such an extent and another source of broadening must exist. As discussed in a later section this broadening can be associated with hindered internal rotation. The same effect was present with methacrylate (i.e., with  $-\text{SCH}_2\dot{\text{C}}(\text{CH}_3)\text{CO}_2^-$ ) to an even greater degree such that the central lines of the triplets were hardly observable. In the case of the radical from itaconate ( $-\text{SCH}_2\dot{\text{C}}(\text{CO}_2^-)\text{CH}_2\text{CO}_2^-$ ) a broadening was observed for the central lines of the triplets associated with both sets of methylene protons. No selective line broadening was observed for the S<sup>-</sup> adducts of acrylonitrile and methacrylonitrile. The hyperfine constants for triplets which do show this effect are marked with an asterisk in Table I.

When acidic solutions were irradiated, spectra ascribable to the protonated radicals II were observed. Figure 2 shows



the spectrum obtained with acrylate at pH 5.5 and the doublet splitting produced by the HS proton (1.32 G) is clearly seen. The parameters of this radical and those obtained with acrylonitrile and methacrylate under similar conditions are given in Table I. Only a weak spectrum which could not be fully analyzed was observed with methacrylonitrile. None of the radicals of type II show the selective line broadening noted above for radicals of type I.

Parameters for the OH adducts of the five compounds under consideration are included in Table I for comparison purposes. All of these radicals (or the forms with the carboxyl groups protonated) have been observed previously. It is noteworthy that the OH adduct to itaconate shows a line broadening associated with the methylene protons of the  $\text{CH}_2\text{CO}_2^-$  group. The outstanding difference between the sulfur-containing radicals and the OH adducts is in the splittings by the methylene protons. All of the values for the sulfur-containing radicals are anomalously small. If the usual angular dependence for the splitting by a  $\beta$  proton is used ( $a_\beta = A + B \cos^2 \theta$ ) then the smallest splitting for

**TABLE I: ESR Parameters of Sulfide Radical Adducts<sup>a</sup>**

Parent molecule	$-\text{SCH}_2\dot{\text{C}}\text{XY}^b$				$\text{HSCH}_2\dot{\text{C}}\text{XY}^c$				$\text{HOCH}_2\dot{\text{C}}\text{XY}^d$										
	Hyperfine constants				Hyperfine constants, G				Hyperfine constants, G				Hyperfine constants, G						
	X	Y	$\text{CH}_2\text{S}^*$	$\alpha\text{-H}$	$\text{CH}_3$	N	$g$ factor	$\text{CH}_2\text{SH}$	SH	$\alpha\text{-H}$	$\text{CH}_3$	N	$g$ factor	$\text{CH}_2\text{OH}$	$\alpha\text{-H}$	$\text{CH}_3$	N	$g$ factor	
Acrylate	H	$\text{CO}_2^-$	10.73* (10.6 18.3) <sup>e</sup>	18.39 18.3) <sup>e</sup>			2.00307	11.29 (10.7 13.72)	1.32 1.4	19.81 19.5) <sup>f</sup>			2.00255	27.55 (27.58 20.45) <sup>g</sup>	20.43				2.00308
Acrylonitrile	H	CN	8.81 (8.8)	18.43 18.3		3.20 3.2) <sup>e</sup>	2.00288	13.72 (13.6)	1.12 1.1	19.94 19.6		3.34 3.3) <sup>f</sup>	2.00241	28.32 (28.15)	20.05			3.54 3.53) <sup>g</sup>	2.00280
Methacrylate	$\text{CH}_3$	$\text{CO}_2^-$	9.45*		19.87		2.00358	9.39	1.18		21.53		2.00305	20.20 (19.98)	20.10		22.90 23.03) <sup>g</sup>		2.00312
Methacrylonitrile	$\text{CH}_3$	CN	8.99		19.57	3.22	2.00332		1.00 <sup>h</sup>			3.32 <sup>h</sup>		23.62 (23.92)				3.48 3.44) <sup>g</sup>	2.00281
Itaconate	$\text{CH}_2\text{CO}_2^-$	$\text{CO}_2^-$	8.68*		11.88 <sup>i</sup>		2.00363					Not measured		21.55 (25.04)				14.17* <sup>j</sup> 13.75) <sup>k</sup>	2.00316

<sup>a</sup> All the measurements were made at about 20°. The hyperfine coupling constants are in gauss and accurate to  $\pm 0.03$  G. The  $g$  factors are accurate to  $\pm 0.00005$ ; second-order corrections have been made [R. W. Fessenden, *J. Chem. Phys.*, 37, 747 (1962)]. An asterisk indicates the hyperfine constants which show selective line broadening. <sup>b</sup> Measured at pH 12. <sup>c</sup> Measured at pH 5.5. <sup>d</sup> Measured at pH 11. <sup>e</sup> Values at pH 9 reported by Norman and Storey. <sup>f</sup> Values at pH 2 reported by Norman and Storey. <sup>g</sup> Values for strongly acidic solution. H. Fischer, *Z. Naturforsch.*, A, 19, 866 (1964). <sup>h</sup> The spectral intensities were weak due to the large number of lines. Only these two coupling constants could be determined. <sup>i</sup> Protons in  $\text{CH}_2\text{CO}_2^-$  group.

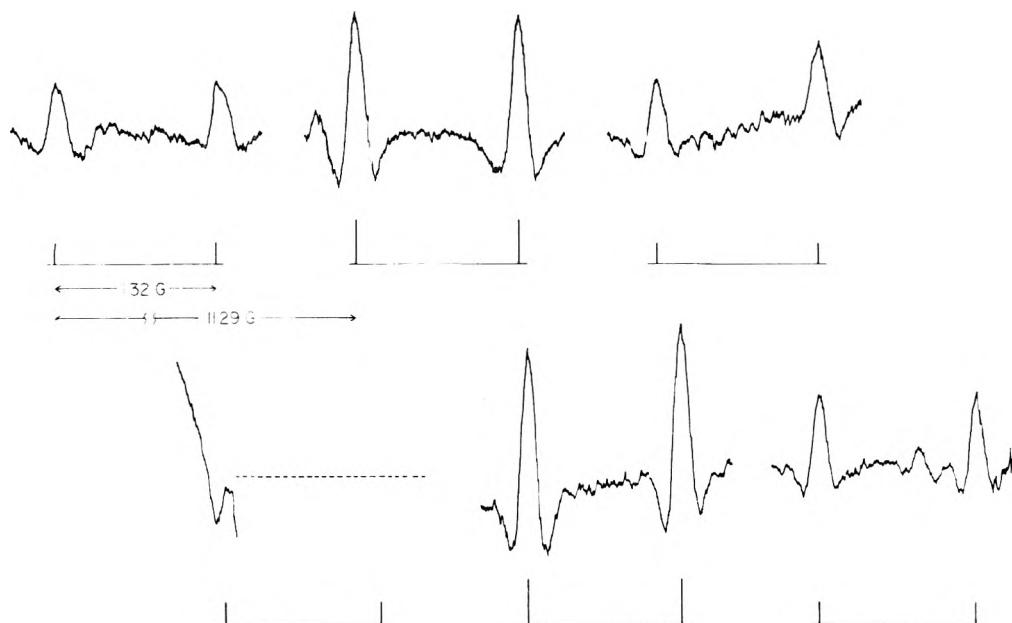
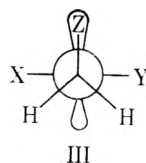


**Figure 2.** Second-derivative ESR spectrum (shown in two segments) of the radical produced by addition of the sulfide radical to acrylate at pH 5.5. Except for a few other weak lines of the size of those appearing between the main lines 2 and 3 and 11 and 12, no other lines were detected. The dashed line indicates the position of the signal from the cell.

equivalent methylene protons occurs for  $\theta = 2\pi/3$ . With the values  $A = 0$  and  $B = 2 \times 26.87^8$  the minimum splitting expected is 13.44 G. All but one of the values in Table I are significantly below this limit. Krusic and Kochi<sup>9</sup> have observed similar anomalies in other  $\beta$ -mercaptoalkyl radicals and have explained the low values by invoking a distortion at the  $\beta$  carbon which moves the  $\beta$  hydrogens away from the radical site and toward the nodal plane. Apparently similar effects exist here.

*Analysis of the Line Broadening.* The selective line broadening described in the preceding section can be attributed to hindered internal rotation around the  $C_{\alpha}$ - $C_{\beta}$  bond with the equilibrium conformation III. In this confor-



mation, if  $X \neq Y$ , the two methylene protons may have different coupling constants. An internal rotation by  $180^\circ$  interchanges the roles of the two  $\beta$  protons and makes possible line broadening. A radical held rigidly in conformation III will show a four-line subpattern of splitting by the methylene protons with the spacing of the central two lines equal to the difference of the two hyperfine constants. If rotation by  $180^\circ$  occurs, these two lines will broaden and eventually, at high rates of rotation, narrow again into a line of relative intensity two. The spectra observed here correspond to the latter stages where nearly complete averaging of the central line has occurred. Other possibilities exist, for which broadening can be associated with rotations of less than  $180^\circ$ , but these would require certain chance relationships between the hyperfine constants to explain the narrow outer lines in the methylene proton subpattern. The simpler situation with rotation by  $180^\circ$  automatically accounts for this latter fact because of the symmetry involved and so is more probable. Of the radicals

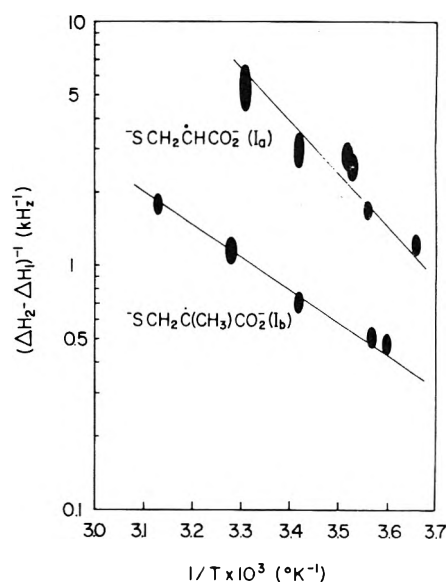


**Figure 3.** Temperature dependence of the line broadening for  $^{-}\text{SCH}_2\dot{\text{C}}\text{CO}_2^-$  (Ia) and  $^{-}\text{SCH}_2\dot{\text{C}}(\text{CH}_3)\text{CO}_2^-$  (Ib). The symbols  $\Delta H_1$  and  $\Delta H_2$  represent the line width in units of NMR frequency (kHz) for protons of the lowest and second-lowest field lines, respectively.

observed here only those in which both groups Z ( $\text{S}^-$  or  $\text{CO}_2^-$ ) and Y ( $\text{CO}_2^-$ ) had a negative charge showed line broadening. On this basis the main contribution to the potential barrier hindering rotation appears to be the repulsion between these substituents.

Near the fast exchange limit the line width caused by a hindered internal rotation is proportional to the correlation time of the internal rotation.<sup>10</sup> The temperature dependence of the correlation time  $\tau$  may be expressed in the form

$$\tau^{-1} \propto \exp(-E_a/RT)$$

where  $E_a$  is the potential barrier to the internal rotation. Plotting the logarithm of the inverse of the extra line width

**TABLE II: pK Values of  $\beta$ -Mercaptoalkyl Radicals and Their Corresponding Thiols**

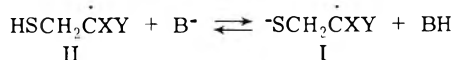
Radical	pK of radical	Thiol	pK of thiol
$\text{HSCH}_2\dot{\text{C}}\text{HCO}_2^-$	$8.9 \pm 0.2$	$\text{HSCH}_2\text{CH}_2\text{CO}_2^-$	10.84 <sup>a</sup>
$\text{HSCH}_2\dot{\text{C}}\text{HCN}$	$7.1 \pm 0.2$	$\text{HSCH}_2\text{CH}_2\text{CN}$	<i>b</i>
$\text{HSCH}_2\dot{\text{C}}(\text{CH}_3)\text{CO}_2^-$	$9.5 \pm 0.2$	$\text{HSCH}_2\text{CH}(\text{CH}_3)\text{CO}_2^-$	<i>c</i>

<sup>a</sup> Reference 12. <sup>b</sup> Not known. The value 8.63 may be estimated by means of the relationship between pK values and Taft  $\sigma^*$  for thiols  $\text{HSCH}_2\text{R}$ .  $\text{pK} = 10.54 - 1.47\sigma^*$ , reported by M. M. Kreevoy, E. T. Harper, R. E. Duvall, H. S. Wilgus, and L. T. Ditsch, *J. Am. Chem. Soc.*, 82, 4899 (1960). <sup>c</sup> Not known.

against  $1/T$  should give a straight line and with slope proportional to  $E_a$ . In Figure 3 are shown the results on the temperature dependence of the line broadening effect found for the radicals Ia ( $X = \text{H}$ ,  $Y = \text{CO}_2^-$ ) from acrylate and Ib ( $X = \text{CH}_3$ ,  $Y = \text{CO}_2^-$ ) from methacrylate. The two lines at the low-field end of the spectrum (the first and second lines from the left in Figure 1) were recorded in the first derivative presentation. Correction for modulation broadening was made according to Wahlquist.<sup>11</sup> The width of line 1 is independent of temperature within experimental error and was assumed to be the residual line width caused by effects other than the hindered rotation. The temperature range was from 0 to 29° for radical Ia and from 4 to 45° for radical Ib. The potential barriers determined from the slopes of the lines in Figure 3 are 7.1 kcal/mol for Ia and 6.2 kcal/mol for Ib.

The  $\beta$ -methylene proton couplings are also found to be temperature dependent. For example, with radical Ia the coupling constant changed from 10.51 G at 0° to 10.96 G at 38°. This result indicates that at higher temperatures the radical spends more time in conformations away from the equilibrium conformation III.

**Dissociation Equilibrium of the Sulfhydryl Protons.** At intermediate pH values a superposition of the discrete spectra of the ionized form I and the acid form II was observed. As the pH was changed no appreciable line broadening was observed even in the presence of 0.13 M borate or 0.5 M ammonium ion buffers. A plot of the logarithm of the concentration ratio  $[\text{I}]/[\text{II}]$  against pH should give a straight line with unit slope if an acid dissociation equilibrium exists between the two species:



where  $\text{B}^-$  represents an appropriate base. This analysis requires the time scale for reaching this equilibrium to be shorter than the decay time for either radical form. The result for the radicals Ia and IIa from acrylate is shown in Figure 4, where the peak height ratio of the unit intensity lines divided by two was taken as the concentration ratio (there was no appreciable difference between the widths of the unit lines of the radicals Ia and IIa). Taking into account the sizeable experimental errors we conclude that the equilibrium is realized in the radical lifetime although the slope seems slightly larger than one.

The pK value for the radical  $\text{HSCH}_2\dot{\text{C}}\text{HCO}_2^-$  (IIa) was determined from the data of Figure 4 to be  $8.9 \pm 0.2$ . The pK values for the other radicals II, i.e.,  $\text{HSCH}_2\dot{\text{C}}\text{HCN}$  and  $\text{HSCH}_2\dot{\text{C}}(\text{CH}_3)\text{CO}_2^-$ , were also determined in a similar way and are shown in Table II. These data indicate that a radi-

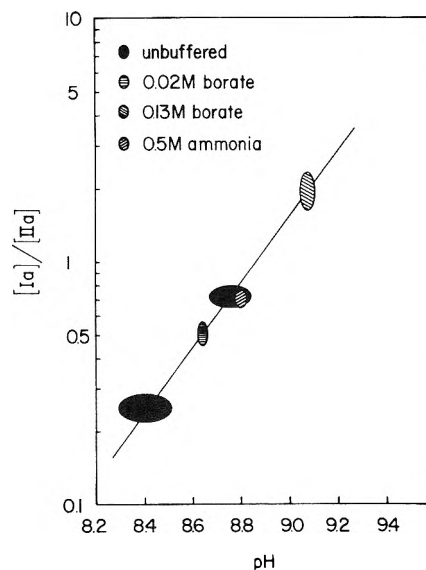
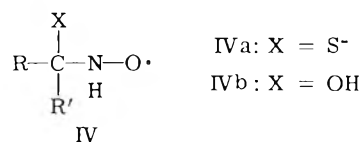


**Figure 4.** The pH dependence of the signal intensity ratio (as described in the text) for the dissociated (Ia) and undissociated (IIa) forms of the radical derived from acrylate. The slope of the line (1.4) is larger than the expected value of 1.

cal with a stronger electron-withdrawing substituent in the  $\beta$  position to the thiolic group is a stronger acid. The value of 8.9 for  $\text{HSCH}_2\dot{\text{C}}\text{HCO}_2^-$  is about two units lower than that for the corresponding thiol,  $\beta$ -mercaptopropionate, which is known to be 10.84.<sup>12</sup>

Because boric acid has a pK value of 9.14 which matches well that of the radicals examined, especially  $\text{HSCH}_2\dot{\text{C}}\text{HCO}_2^-$ , its addition was expected to increase the rate of exchange between the two forms of the radicals and, therefore, to result in broadening of the lines. However, this is not the case. These results indicate that the dynamics of the equilibrium between  $\text{HSCH}_2\text{CHCO}_2^-$  and  $-\text{SCH}_2\dot{\text{C}}\text{HCO}_2^-$  is slow enough ( $< \sim 10^6 \text{ sec}^{-1}$ ) even in the presence of 0.13 M borate buffer at pH 9.07 so that the discrete spectra of the two forms are observable. Thus the rate constant for the reaction between  $\text{HSCH}_2\dot{\text{C}}\text{HCO}_2^-$  and the basic species ( $\text{B}(\text{OH})_4^-$ ) must be less than  $10^7 \text{ M}^{-1} \text{ sec}^{-1}$ . This is much lower than that found for the reaction between some hydroxyalkyl radicals and phosphate ions<sup>13</sup> and may reflect the fact that SH protons can less readily form hydrogen bond bridges to the base. A similar conclusion must be reached for ammonium ion-ammonia buffer where the rate constant must be less than  $\sim 2 \times 10^6 \text{ M}^{-1} \text{ sec}^{-1}$ .

**Radicals Produced by Reaction with Oximes.** An  $\text{N}_2\text{O}$  saturated solution containing sodium sulfide at pH 12 and the desired oxime was irradiated. With acetaldoxime, acetoxime, and 2,3-butanedione monoxime spectra of rather broad lines (line width between points of maximum slope  $\sim 0.5 \text{ G}$ ) were observed which can be attributed to the nitroxide radical IVa ( $X = \text{S}^-$ ). The reaction of sulfide radi-



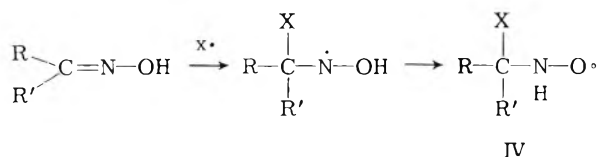
cals with these oximes is probably analogous to that of hydroxyl radicals,<sup>14</sup> i.e., addition of the radical to the carbon

TABLE III: ESR Parameters for Radicals Produced by Reaction with Oximes

R	R'	IVa				IVb			
		Hyperfine constants, G				Hyperfine constants, G			
		$a^N$	$a_{\text{NH}}^H$	$a_{\text{CH}}^H$	$g$ factor	$a^N = a_{\text{NE}}^H$	$a_{\text{CH}}^H$	$g$ factor	
CH <sub>3</sub>	H	14.60	13.76	10.24	2.00575	13.13	8.95	2.0059 <sup>a</sup>	
						13.2	9.0	<i>b</i>	
						13.2	8.8	<i>c</i>	
CH <sub>3</sub>	CH <sub>3</sub>	14.80	13.67		2.00581	13.3		2.0059 <sup>a</sup>	
						13.4		<i>b</i>	
						13.4		<i>c</i>	
CH <sub>3</sub> CO	CH <sub>3</sub>	14.32	13.68		2.00570	12.65	2.0059 <sup>a</sup>		

<sup>a</sup> Reference 14. <sup>b</sup> Reference 16. <sup>c</sup> Reference 15.

atom of C=N bond in the oxime followed by rearrangement.



The ESR parameters of the radicals IVa resulting from the reaction of sulfide radicals are shown in Table III together with those of the corresponding radicals IVb produced by the reaction of hydroxyl radicals.

It seems worth noting that the coupling constants for the nitrogen and N-H proton are different in the radicals IVa (X = S<sup>-</sup>) while they are known to be equal in the radicals of the type IV with X = OH,<sup>14,15</sup> CH<sub>2</sub>OH,<sup>14</sup> NH<sub>2</sub>,<sup>16</sup> or CO<sub>2</sub><sup>-17</sup> as well as in the radical H<sub>2</sub>NO.<sup>18,19</sup> Radicals of the type ROC(=O)N(H)O· are known to have different values for  $a^N$  and  $a_{\text{NH}}^H$ , as exemplified by <sup>-</sup>OC(=O)N(H)O· with  $a^N = 9.2$  G and  $a_{\text{NH}}^H = 12.7$  G.<sup>18</sup> However in these radicals  $a^N$  is smaller than  $a_{\text{NH}}^H$  while  $a^N$  is larger than  $a_{\text{NH}}^H$  in the radical IVa.

**Reactions with Other Compounds.** All experiments were carried out at an alkaline pH near 12. Concentrations of 10–30 mM in sodium sulfide and 1–10 mM in organic compound were used. In some experiments sodium sulfide was omitted and the reaction of hydroxyl radical with the unsaturated compound was examined for comparison.

Of the olefinic compounds studied (other than mentioned above) only two, furylacrylic acid and 3-(2-thienyl)-acrylic acid, gave ESR spectra attributable to sulfur-containing radicals. The predominant spectrum obtained with furylacrylic acid has the parameters  $a^H = 16.76, 9.26, 7.21, 1.71, 1.71$  G and  $g = 2.00292$ . This can be assigned to the radical (V),  $\text{OCH}=\text{CH}-\text{CH}=\text{C}\dot{\text{C}}\text{HCH}(\text{S}^-)\text{CO}_2^-$ . The spectrum from 3-(2-thienyl)-acrylic acid was too complex to be analyzed because of a superposition of lines from more than one radical, but the presence of the radical corresponding to V is likely since the total spread of the two spectra are very similar.

No sulfide adduct radicals were observed from methyl acrylate, acrylamide, crotonic acid, vinyl acetate, methyl vinyl ketone, ethyl vinyl ether, ethylene, propylene, isobutylene, and enols of acetylacetone and ethyl acetoacetate. The addition reaction to these compounds must be slow. Some of the compounds gave spectra which are due to the radicals produced directly from hydroxyl radicals and in one case hydrated electrons. It was shown qualitatively

from a series of experiments varying the concentration ratio of sodium sulfide and the organic compound that competition for the hydroxyl radicals occurred between sulfide and the organic compound so that sulfide radicals were indeed produced. With fumaric acid both the OH and  $e_{\text{aq}}^-$  adducts were observed. ESR parameters for the latter two radicals, except for the splitting due to the hydroxyl proton, are in full agreement with those reported by Neta.<sup>20</sup> (The OH splitting is lost at the high pH because of rapid exchange.) The  $e_{\text{aq}}^-$  adduct results from a portion of the hydrated electrons which escape scavenging by N<sub>2</sub>O. With allyl alcohol, abstraction of the allylic hydrogen by hydroxyl radicals takes place to give the two isomeric allylic radicals.<sup>21</sup> Weak lines were obtained from vinylacetic acid which appear also to be due to an allylic radical, but further analysis was not made. Of the six compounds having a C=N bond only the three mentioned above gave detectable signals. No ESR lines were observed from formaldoxime, formamidoxime, and benzyldimethylamine.

No radicals resulting from the addition of the sulfide radical to C=C and C=S bonds, benzene, furan, pyrrole, and thiophene rings were observed. The compounds examined were acetylenedicarboxylate, propargyl alcohol, 3-butyne-2-ol, 2-methyl-3-butyne-2-ol, 2-butyne-1,4-diol, thio-urea, thioacetamide, benzene-1,2,3-tricarboxylate, benzene-1,3,5-tricarboxylate, furan, 2,4-furandicarboxylate, 2-furoic acid, pyrrole, pyrrole-2-carboxylate, 2-thiophenecarboxylate, and 2-thiophenecarboxaldehyde as well as 2-furylacrylate and 3-(2-thienyl)-acrylate. In the case of the last two compounds, the sulfide addition took place to the C=C double bond in the side chain as described earlier and not to the ring.

The radicals produced by the reaction with hydroxyl radicals and observed even in the system containing sulfide are: HC=C-CHO· ( $g = 2.00372, a_{\text{N-H}} = 15.32$  G,  $a_{\text{H-H}} = 6.51$  G) from propargyl alcohol; HC=C-C(CH<sub>3</sub>)O· ( $g = 2.00335, a_{\text{CH}_3} = 13.99$  G,  $a_{\text{H-H}} = 4.42$  G) from 3-butyne-2-ol; HOCH<sub>2</sub>-C=C-CHO· ( $g = 2.00345, a_{\text{O-H}} = 15.15$  G,  $a_{\text{H-H}} = 5.59$  G) from 2-butyne-1,4-diol; three isomeric radicals<sup>22</sup> produced from 2-furoic acid and 3,4-furandicarboxylate by OH addition and ring rupture; two isomeric OH adduct radicals of benzene-1,2,3-tricarboxylate; and an OH adduct radical of benzene-1,3,5-tricarboxylate.

## Conclusions

Addition of the sulfur-containing intermediate produced by OH reaction with sulfide to a number of unsaturated compounds has been studied. Eight types of compounds were used: aliphatic compounds containing C=C (olefinic

compounds and enols), C≡C, C=N (oximes and an imine), or C=S bonds, benzenes, furans, pyrroles, and thiophenes. Adduct radicals containing sulfur were detected by their ESR spectra only in the case of certain olefinic compounds and oximes. The absence of detectable ESR lines for the other compounds can be the result of either slow reaction of the sulfide radical or broad lines for the sulfur containing radicals. From the fact that some sulfur containing radicals were observed it seems that slow reaction is the more likely reason. Values of the pK for the dissociation of sulfhydryl proton in three radicals of the type HSCH<sub>2</sub>CXY were determined and found to be about 1.5–2 units lower than in the corresponding thiol.

## References and Notes

- (1) Supported in part by the U.S. Atomic Energy Commission.
- (2) W. Karman, G. Meissner, and A. Henglein, *Z. Naturforsch. B*, **22**, 273 (1967).
- (3) D. Behar and R. W. Fessenden, *J. Phys. Chem.*, **76**, 1710 (1972).
- (4) R. O. C. Norman and P. M. Storey, *J. Chem. Soc. B*, 1009 (1971).
- (5) D. Behar and R. W. Fessenden, *J. Phys. Chem.*, **75**, 2752 (1971). Based on the spectrum shown for thiosulfate photolysis at pH 9.5 which shows more of the dissociated form, <sup>-</sup>SCH<sub>2</sub>NO<sub>2</sub><sup>-</sup>.
- (6) O. P. Chawla, Ph.D. Dissertation, Carnegie-Mellon University, Aug 1973.
- (7) K. Eiben and R. W. Fessenden, *J. Phys. Chem.*, **75**, 1186 (1971).
- (8) R. W. Fessenden, *J. Chim. Phys.*, **51**, 1570 (1964).
- (9) P. J. Krusic and J. K. Kochi, *J. Am. Chem. Soc.*, **93**, 846 (1971).
- (10) G. K. Fraenkel, *J. Phys. Chem.*, **71**, 139 (1967).
- (11) H. Wahlquist, *J. Chem. Phys.*, **35**, 1708 (1961).
- (12) R. J. Irving, L. Nelander, and I. Wadso, *Acta Chem. Scand.*, **18**, 769 (1964).
- (13) G. P. Laroff and R. W. Fessenden, *J. Phys. Chem.*, **77**, 1283 (1973).
- (14) P. Smith and W. M. Fox, *Can. J. Chem.*, **47**, 2227 (1969).
- (15) J. Q. Adams, *J. Am. Chem. Soc.*, **89**, 6022 (1967).
- (16) D. J. Edge and R. O. C. Norman, *J. Chem. Soc. B*, 182 (1969).
- (17) D. J. Edge and R. O. C. Norman, *J. Chem. Soc. B*, 1083 (1970).
- (18) C. J. W. Gutch and W. A. Waters, *J. Chem. Soc.*, 751 (1965).
- (19) J. Q. Adams, S. W. Nicksic, and J. R. Thomas, *J. Chem. Phys.*, **45**, 654 (1966).
- (20) P. Neta, *J. Phys. Chem.*, **75**, 2570 (1971).
- (21) M. Simic, P. Neta, and E. Hayon, *J. Phys. Chem.*, **77**, 2662 (1973).
- (22) R. H. Schuler, G. P. Laroff, and R. W. Fessenden, *J. Phys. Chem.*, **77**, 456 (1974).

## Protonation Reactions at Carbon Sites in the Anion Radicals of Certain Unsaturated Compounds and Aromatic Amino Acids<sup>1</sup>

C. Van Paemel, H. Frumin, V. L. Brooks, R. Failor, and M. D. Sevilla\*

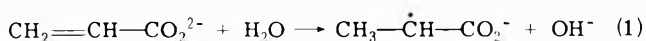
Department of Chemistry, Oakland University, Rochester, Michigan 48063 (Received October 9, 1974)

Publication costs assisted by the Petroleum Research Fund and the U.S. Atomic Energy Commission

The protonation reactions at carbon sites of the anion radicals of certain unsaturated compounds as well as aromatic amino acids and their analogs have been investigated in alkaline and neutral aqueous glasses by electron spin resonance spectroscopy. For the compounds acrylic acid, 3,3-dimethylacrylic acid, crotonic acid, acrylamide, and acrylonitrile protonation or deuteration is found to occur  $\beta$  to the electronegative group (R<sub>3</sub>) to form an  $\alpha$ -carbon radical: R<sub>1</sub>R<sub>2</sub>C=CHR<sub>3</sub><sup>-</sup> + H<sub>2</sub>O → R<sub>1</sub>R<sub>2</sub>CH— $\dot{C}$ HR<sub>3</sub> + OH<sup>-</sup>. The anions were found to be stabilized when R<sub>1</sub> (or R<sub>2</sub>) was a carboxyl (fumaric) or methyl (crotonic and 3,3-dimethylacrylic acid) group. The anions of acetylenedicarboxylic acid and hydrogen cyanide were also found to protonate in these aqueous glasses. The anions of four aromatic amino acids were found to protonate at carbon sites on the aromatic ring. Analogs of these amino acids which contain the aromatic ring were found to protonate at positions equivalent to those found in the amino acids. Molecular orbital calculations of the spin density and free valency show that the magnitude of these parameters can be correlated with the site of protonation and perhaps the tendency to protonate.

## Introduction

Evidence has been presented in several investigations that anion radicals of compounds with unsaturated hydrocarbon linkages undergo irreversible protonation reactions at carbon sites. These investigations have been of ions in aqueous solutions or in the solid state.<sup>2–7</sup> For example, the acrylic acid anion has been investigated in aqueous solution by ESR<sup>2</sup> and pulse radiolysis techniques,<sup>4</sup> as well as by ESR in glassy matrices.<sup>5–7</sup> These results show that the anion which is initially formed by electron attachment subsequently protonates (reaction 1).



This type of reaction is of interest to radiation chemistry of certain biochemical systems. For instance, in  $\gamma$ -irradiated DNA it is now considered likely that one of the radicals formed results from protonation at a carbon site on the anion of thymine.<sup>8</sup> Studies of other DNA bases<sup>9</sup> as well as aromatic amino acids<sup>10</sup> suggest protonation at carbon sites in these cases as well.

In this study we have investigated a series of model compounds to determine the type of unsaturated molecules which readily protonate in aqueous glasses. We have also studied a number of aromatic amino acids and their analogs to determine if protonation reactions occur and at which sites they occur. We briefly consider possible theoretical reasons for the particular site of protonation.

TABLE I: Radicals Formed by Electron Attachment to Molecules with Localized Multiple Bonds

Compounds	Radical	Matrix	Hyperfine splitting, G	Temp, °K
<b>A. Anions</b>				
3,3-Dimethylacrylic acid	$(\text{CH}_3)_2\text{C}=\text{CHCO}_2^-\text{H}$	LiCl-D <sub>2</sub> O	14.6 (6 H)	77
	$(\text{CH}_3)_2\text{C}=\text{CHCO}_2^{2-}$	NaOD	14.1 (6 H)	77
Crotonic acid	$\text{CH}_3\text{CH}=\text{CHCO}_2^{2-}$	NaOD	15 (4 H) <sup>a</sup>	77
Acetylenedicarboxylic acid	$\text{CO}_2^-\text{C}\equiv\text{CCO}_2^{2-}$	NaOD	4 G wide singlet	77
Fumaric acid	$\text{CO}_2^-\text{CH}=\text{CHCO}_2^{2-}$	NaOD	8 (2 H) <sup>a</sup>	77
<b>B. Protonated Radicals</b>				
Acrylic acid	$\text{CH}_2\dot{\text{C}}\text{HCO}_2^-$	LiCl or NaOH	24 (4 H) <sup>a, b</sup>	77
Acrylamide	$\text{CH}_2\dot{\text{C}}\text{HCONH}_2$	LiCl or NaOH	25 (4 H) <sup>a</sup>	77
Acrylonitrile	$\text{CH}_2\dot{\text{C}}\text{HC}\equiv\text{N}$	LiCl or NaOH	24.5 (4 H) <sup>a</sup>	77
Crotonic acid	$\text{CH}_3\text{CHD}\dot{\text{C}}\text{HCO}_2^-$	NaOD	40 (1 H)	165
	$(\text{CH}_3)_2\text{CH}\dot{\text{C}}\text{HCO}_2^-$	NaOH	27.5 (2 H)	160
3,3-Dimethylacrylic acid	$(\text{CH}_3)_2\text{CD}\dot{\text{C}}\text{HCO}_2^-$	LiCl	24.5 (2 H)	160
	$(\text{CH}_3)_2\text{CH}\dot{\text{C}}\text{HCO}_2^-$	NaOD	22 (1 H)	160
	$(\text{CH}_3)_2\text{CH}\dot{\text{C}}\text{HCO}_2^-$	LiCl-D <sub>2</sub> O	21 (1 H)	160
Acetylenedicarboxylic acid	$\text{CO}_2^-\text{CH}=\dot{\text{C}}\text{CO}_2^-$	LiCl or NaOH	57 (1 H)	77
	$\text{CO}_2^-\text{CD}=\dot{\text{C}}\text{CO}_2^-$	LiCl-D <sub>2</sub> O or NaOD	8.6 (1 D)	77
Hydrogen cyanide	$\text{H}_2\text{C}=\dot{\text{N}}^+$	LiCl	89 (2 H), $A_1^{\text{N}} = 32$ $A_1^{\text{N}} < 3.5$	110

<sup>a</sup> Further anisotropic structure was observed in these radicals, however, only the approximate isotropic result is reported. <sup>b</sup> The anisotropic structure in the ESR spectrum of this radical was interpreted (see text).

## Experimental Section

All reagents and solutes were obtained commercially and were used without further purification except for acrylic acid and histidine which were purified by distillation and recrystallization, respectively.

The experimental procedure has been explained in our previous work.<sup>11,12</sup> Both 8 M NaOH and 12 M LiCl glasses were employed in this study. Electrons were generated by photolysis of 10–20 mM K<sub>4</sub>Fe(CN)<sub>6</sub>. The concentration of solute was approximately 2 mM for most compounds. Higher concentrations of histidine (20 mM) were found to be necessary.

The anions formed were often found to protonate when exposed to white light. Thus filtered light ( $\geq 4300 \text{ \AA}$ ) was used for photobleaching trapped electrons.

The *g* values and hyperfine splittings in this work were measured relative to potassium peroxyaminedisulfonate ( $A_{\text{N}} = 13.0\text{G}$  and  $g = 2.0056$ ).

## Results and Discussion

**Molecules with Localized Double Bonds.** Electron attachment to a number of compounds with localized double bonds in neutral or alkaline matrices resulted in stable anion radicals in several cases (see Table I). We discuss these radical anions below.

**3,3-Dimethylacrylic Acid.** Electron attachment to 3,3-dimethylacrylic acid on NaOD at 77°K gave the ESR spectrum in Figure 1A. This spectrum which shows a 14.1-G hyperfine splitting due to the six methyl protons is clearly that of the dianion radical. This splitting is very close to that found for the acrylic acid anion in a nonaqueous matrix.<sup>6</sup> Similar results were found in LiCl-D<sub>2</sub>O (Table I). In H<sub>2</sub>O matrices some protonation occurred even at 77°K, so that the anion could not be isolated from the protonated species.

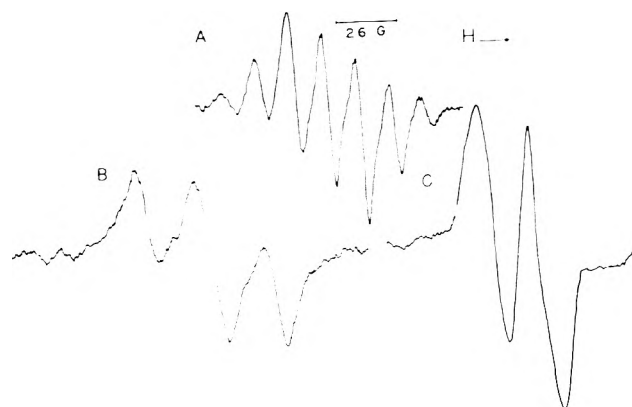
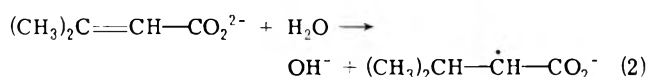


Figure 1. ESR spectra of radicals formed after electron attachment to 3,3-dimethylacrylic acid in alkaline glasses: (A) spectrum of the dianion at 77°K; (B) protonated radical,  $(\text{CH}_3)_2\text{CH}\dot{\text{C}}\text{HCO}_2^-$ , spectrum produced by photoprotonation of the dianion at 77°K in 8 M NaOH; (C) deuterated radical,  $(\text{CH}_3)_2\text{CD}\dot{\text{C}}\text{HCO}_2^-$ , spectrum produced by warming the dianion to 175°K in 8 M NaOD.

The anion (LiCl) or dianion (NaOH) was found to protonate or deuterate upon warming to 160°K or photobleaching with unfiltered visible light. In H<sub>2</sub>O matrices the protonated radical gave a spectrum consisting of a 24.5- to 27.5-G triplet due to two protons (Figure 1B). Of the two possible carbon sites available for protonation only protonation at the site  $\beta$  to the carboxyl as in reaction 2 could produce this spectrum.



In D<sub>2</sub>O matrices a 21- to 22-G doublet was observed as would be expected for the  $\alpha$  proton in the radical,  $(\text{CH}_3)_2\text{CH}-\dot{\text{C}}\text{H}-\text{CO}_2^-$  (Figure 1C). In contrast to our re-



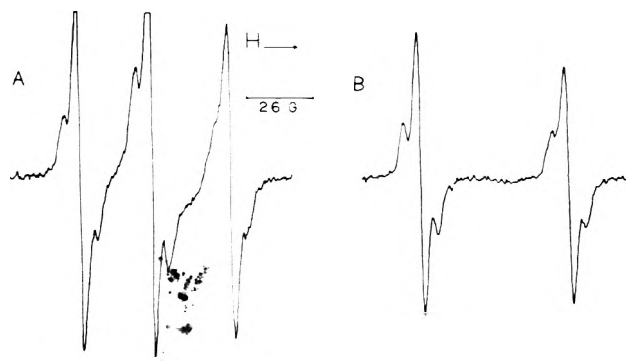


**Figure 2.** ESR spectra of radicals formed after electron attachment to acetylenedicarboxylic acid in 8 M NaOH: (A) spectrum at 77°K of the anion, protonated radical ( $\text{CO}_2^-\text{CH}=\text{CCO}_2^-$ ), and electron before photobleaching; (B) protonated radical spectrum at 110°K after removing the anion and electron by photobleaching. The structure on the major components in this spectrum is likely due to matrix interactions since it is not observed in  $\text{D}_2\text{O}$  matrices.

sults Neilson and Symons<sup>13</sup> report that both H atom bombarded and  $\gamma$ -irradiated solid dimethylacrylic acid added hydrogen to the  $\alpha$  carbon position. This may be a matrix effect or an inherent difference in the site of attack of the hydrogen atom.

An interesting concentration dependence was noted for the anion of 3,3-dimethylacrylic acid in  $\text{LiCl-H}_2\text{O}$ . Saturated solutions gave the anion without any protonation. Even warming did not result in complete protonation. This effect is considered to be due to agglomerates of the solute which hinder protonation by removing water from the reaction site.

**Acetylenedicarboxylic Acid.** The anion radical of acetylenedicarboxylic acid was observed at 77°K in alkaline matrices though it is overlapped with the protonated radical (Figure 2A). The anion was not observed in  $\text{LiCl}$  glasses under the same conditions. The singlet spectrum of the anion was distinguishable from the electron from its much narrower line width (4 G vs. 13 G). Complete protonation occurred upon photobleaching with unfiltered visible light or warming to 110°K (Figure 2B). The protonated radical ( $\text{CO}_2^-\text{CH}=\dot{\text{C}}-\text{CO}_2^-$ ) shows a 57-G splitting with some further structure in  $\text{H}_2\text{O}$ . Since this further structure was not observed for the protonated radical in  $\text{NaOD}$  (92% D) it is likely due to matrix interactions. The splittings for radicals in  $\text{D}_2\text{O}$  matrices (Table I) are very close to those predicted from those found in  $\text{H}_2\text{O}$  using the gyromagnetic ratio. The splittings found in this work are larger than those found in single crystal work (51–54 G)<sup>3</sup> or in aqueous solution at room temperature (50 G).<sup>2</sup> In both of these investigations the anion radicals were proposed as precursors to the protonated radicals; our results confirm this previous work.

**Crotonic and Fumaric Acids.** Both these compounds gave spectra expected for anion radicals in 8 M  $\text{NaOD}$  after electron attachment. The analysis of the spectra in terms of isotropic couplings is shown in Table I. Both spectra showed some anisotropic structure. Warming crotonic acid in  $\text{NaOD}$  resulted in an ESR spectrum which could only arise from deuteration at the  $\beta$  position (Table I). Fumaric acid did not protonate upon warming in  $\text{NaOH}$  to 180°K. The results for fumaric acid agree with those found in aqueous solution.<sup>2,14</sup>

Other compounds whose anion radicals did not protonate in these glasses were benzoic and muconic acids. Neta

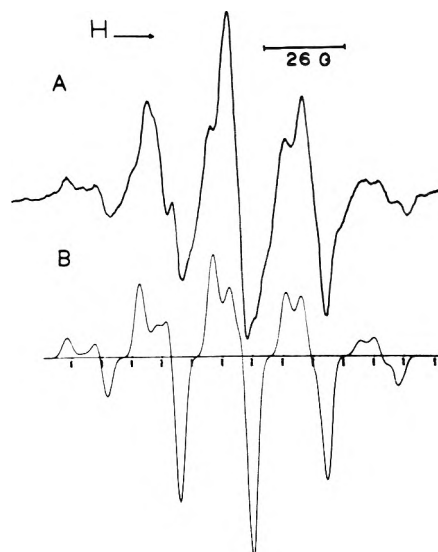


**Figure 3.** (A) ESR spectrum of the  $\text{CH}_3\text{CHCO}_2^-$  radical resulting from protonation at the  $\beta$  position in the acrylic acid anion at 77°K in 8 M NaOH. (B) Computer simulation of the anisotropic spectrum in A utilizing parameters described in the text.

and Fessenden report similar results in aqueous solution.<sup>2,29</sup>

The anions of the other compounds in Table I were not stable at 77°K in any of the aqueous glasses employed in this study. The spectral parameters of protonated (deuterated) radicals are reported in Table I and discussed below briefly.

**Acrylic Acid.** The acrylic acid protonated radical ( $\text{CH}_3\text{CHCO}_2^-$ ) gave spectra which showed the anisotropic structure of the  $\alpha$  proton in both  $\text{LiCl}$  and  $\text{NaOH}$  glasses (Figure 3A). In  $\text{D}_2\text{O}$  where deuteration occurred a well-resolved spectrum was found (Figure 4A). The protonated radical has been observed in several previous investigations of acrylic acid;<sup>5,6</sup> however, the anisotropic structure of the spectrum has not been interpreted. We have attempted such an interpretation and have employed a computer program which simulates anisotropic spectra to first order. The  $g$  and hyperfine tensors are assumed to be coaxial. From previous work on radicals of this type in single crystals as well as theory it is known that  $A_{xx} > A_{zz} > A_{yy}$  and  $g_{zz} > g_{xx} \approx g_{yy}$ . The  $z$  axis is perpendicular to the plane of the molecule. We have, therefore, employed these constraints on the variation of parameters for the  $\alpha$  hydrogen. The best fit to experiment, shown in Figure 3B, yields  $A_{\text{CH}_3} = 24$  G (assumed isotropic), the following parameters for the  $\alpha$  proton  $A_{xx}^{\text{H}} = 38$  G,  $A_{yy}^{\text{H}} = 11$  G,  $A_{zz}^{\text{H}} = 20$  G and  $g_{xx} \approx g_{yy}$  with  $g_{xx} - g_{zz} = 0.0016$ . As can be seen, the fit is best at the ends where the anisotropic structure of the  $\alpha$  proton is free from the methyl group structure. Our anisotropic parameters are similar to, but about 3 G larger than, those found for the same radical in alanine single crystals at room temperature.<sup>15</sup>

The reconstruction shown in Figure 4B for the radical  $\text{CH}_2\text{DCHCO}_2^-$  assumes the parameters for the  $\alpha$  proton, but a single isotropic (methyl) deuterium splitting of 3.7 G as well as two isotropic (methyl) protons at 24 G. Due to the fact the solution was not completely deuterated (92% D), the experimental spectrum was found to be overlapped with some of the protonated species. We estimated that about 20% of the radicals are protonated. The simulation, therefore, contains both deuterated (80%) and protonated

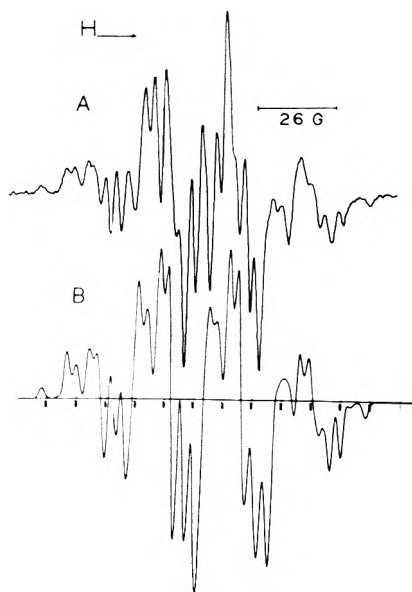


**Figure 4.** (A) ESR spectrum of the  $\text{CH}_2\text{DCHCO}_2^-$  and  $\text{CH}_3\text{CHCO}_2^-$  resulting from deuteration and protonation at the  $\beta$  position in acrylic acid anion at 77 K in 8 M NaOD (92% D). (B) Computer simulation of the anisotropic spectrum in A assuming 80%  $\text{CH}_2\text{DCHCO}_2^-$  and 20%  $\text{CH}_3\text{CHCO}_2^-$ . Parameters utilized in the reconstruction are described in the text.

(20%) radicals. The agreement for the end components is excellent and confirms that deuteration occurs at the same site as protonation.

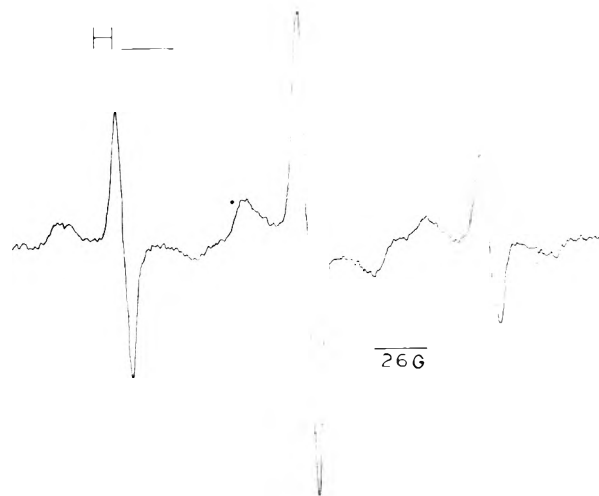
**Hydrogen Cyanide.** The results of electron attachment to HCN in LiCl-H<sub>2</sub>O at 77°K under acidic conditions is shown in Figure 5. This spectrum is assigned to the  $\text{CH}_2=\text{N}\cdot$  radical. The hyperfine parameters reported in Table I are in good agreement with those found in aqueous solution by Behar and Fessenden<sup>16</sup> and those found in the solid state.<sup>17,18</sup> The acidic conditions used, of course, mean that attack by hydrogen atoms as well as by electrons may have occurred. The previous work in aqueous solution, however, showed both these intermediates result in the same radical.<sup>16</sup>

**Acrylonitrile.** The anion of acrylonitrile was found to immediately protonate at 77°K to form the  $\text{CH}_3\text{CHCN}$  radical. The ESR spectrum in H<sub>2</sub>O glasses was an overall quintet with further resolution of the anisotropic structure of the  $\alpha$  proton similar to that found in acrylic acid. Resolution of nitrogen splittings was not found. The splitting reported in Table I is the average separation between the major peaks in the spectrum.

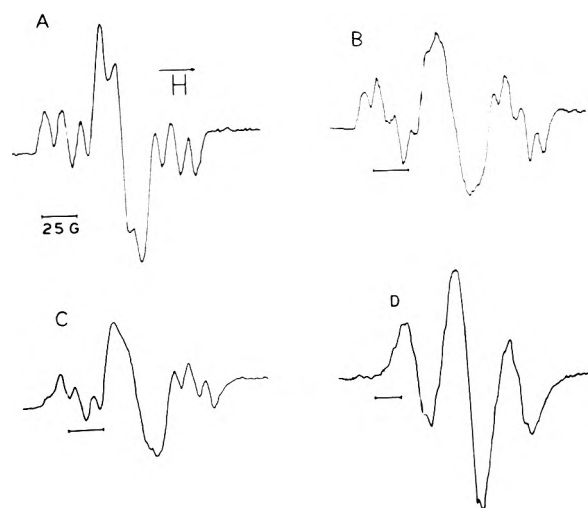
It was first thought that the results for acrylonitrile would test the relative tendency of a carbon-carbon double bond and the cyano group to protonate after electron attachment. However, the spin density distribution (discussed later) in the anion places most of the unpaired electron in the double bond. This compound is, therefore, not a reasonable test of the relative potentials for protonation.

**Acrylamide.** The results for acrylamide are reported in Table I. Spectra of the protonated anion of acrylamide were similar to those found for acrylic acid and acrylonitrile, i.e., a 25-G quintet with some further resolution of the  $\alpha$  proton anisotropy.

Seddon and Smith report results in  $\gamma$ -irradiated 8 M NaOH glasses containing acrylamide or acrylonitrile which are in agreement with those found here. A virtually identical spectrum with that found here for  $\text{CH}_2\text{DCHCO}_2^-$  was



**Figure 5.** ESR spectrum of the  $\text{H}_2\text{CN}$  radical in 12 M LiCl (H<sub>2</sub>O) at 110°K.

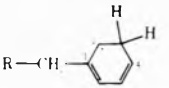
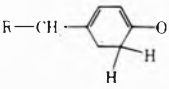
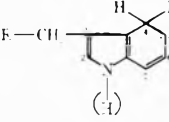
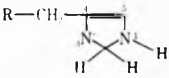


**Figure 6.** ESR spectra of carbon protonated radicals formed after electron attachment to aromatic amino acids: (A) tryptophan radical spectrum at 160°K; (B) phenylalanine radical spectrum at 160°K; (C) tyrosine radical spectrum at 160°; (D) histidine radical spectrum at 77°K.

found by Seddon and Smith for  $\text{CH}_2\text{DCHCOND}_2$ .<sup>19</sup> In view of the similarity in structure of the radicals this is reasonable; however, their interpretation included splittings arising from the amide group which are most likely a result of anisotropy in the  $\alpha$  proton coupling and overlap of the spectrum due to the protonated radical.

**Aromatic Amino Acids.** Electron attachment reactions with four aromatic amino acids were investigated. The ESR spectra immediately after electron attachment in alkaline and neutral glasses showed spectra indicative of protonation in all cases (except histidine in NaOH). The ESR spectra of the protonated anions of these amino acids (Figure 6) consist of a large triplet of 38–48 G between the components which are further split. The large splittings are due to the methylene protons produced by protonation on the aromatic ring. The further splittings are due to ring proton splittings. The assignment of specific sites of protonation from these results is not possible without recourse to theory. This is treated later. Table II gives the results of the analysis of the ESR spectra in both alkaline and neutral

TABLE II: Radicals Formed by Electron Attachment to Aromatic Amino Acids and Their Analogs

Compound	Suggested major radical <sup>a</sup>	Matrix	Hyperfine splittings, G		Temp, K
			Methylene	Ring protons	
Phenylalanine		NaOH	48(2 H)	11(3 H)	77
		LiCl	47(2 H)	11(3 H)	160
Tyrosine		NaOH	42(2 H)	12(2? H) <sup>b</sup>	77
		LiCl	40(2 H)	12(2? H)	77
Tryptophan		NaOH	38(2 H)	12(2 H)	165
		LiCl	39(2 H)	12(2 H)	165
Histidine		LiCl	47(2 H)	7 (even no H)	77
Imidazole	<i>c</i>	LiCl	47(2 H)		77
Phenylacetic acid	<i>d</i>	NaOH	46(2 H)	11(? H) <sup>b</sup>	170
Phenol	<i>e</i>	NaOH	42(2 H)	11(2 H)	77

<sup>a</sup> R = -CH(NH<sub>3</sub><sup>+</sup>)CO<sub>2</sub><sup>-</sup> in 12 M LiCl and -CH(NH<sub>2</sub>)CO<sub>2</sub><sup>-</sup> in 8 N NaOH. <sup>b</sup> The ESR spectrum for this radical suggests more than one protonated radical is present. <sup>c</sup> This structure is analogous to that found for histidine. <sup>d</sup> This structure is analogous to that found for phenylalanine. <sup>e</sup> This structure is analogous to that found for tyrosine.

glasses. Below we discuss the extent of protonation in the various glasses.

For phenylalanine and histidine protonation in 12 M LiCl was nearly complete immediately after electron attachment, i.e., photolysis and photobleaching. Partial protonation was noted for tyrosine and tryptophan at this point. Upon warming to 165°K the ESR spectra (Figure 6) were essentially that of the protonated radicals. This is considered to be due to the loss of the other less stable radicals formed, i.e., anions and possible deaminated species, upon warming. The conversion of anion to protonated radical upon warming could not be proven owing to (1) an overall loss in signal intensity and (2) attack of hydrogen atoms which are produced by electron reaction with the matrix and mobilized on warming.

The results for histidine in NaOH showed no protonation. Only a weak singlet ESR spectrum indicative of the anion was found. All other aromatic amino acids showed partial protonation at 77°K in NaOH. The phenylalanine anion again protonated to the greatest extent. The fact that tryptophan, tyrosine, and phenylalanine protonate under both neutral and alkaline conditions is good evidence that the anion is the immediate precursor of the protonated radicals. For histidine the pK of the methylene proton in the protonated species could be such so as to be protonated in the LiCl glass but not in the NaOH glass. Alternatively, the anion of histidine in the neutral glass could react to form hydrogen atoms which then would attack the original or neighboring molecules. Further experiments utilizing different techniques will be necessary to distinguish between these hypotheses.

In previous investigations of amino acids with aliphatic side chains in aqueous glasses we found that in a neutral glass deamination of the zwitterion readily occurs at 77°K.<sup>11,20</sup> The results of this investigation suggest that

electron attachment and protonation at carbon sites in aqueous media can effectively compete with this deamination step in aromatic amino acids. Recent pulse radiolysis results of Mittal and Hayon confirm this conclusion.<sup>21</sup> Their results suggest that electron reaction with phenylalanine yields 60% of the ring protonated radical and 40% deaminated radical.

*Analogs of the Aromatic Amino Acids.* Since the aromatic ring is a site of attack in aromatic amino acids, several compounds which contain only the aromatic ring were investigated. The results of electron attachment to imidazole, phenol, and phenylacetic acid are reported in Table II. The extent of protonation was only partial for phenol and phenylacetic acid. Since warming did not induce more protonation, the protonation of the anion may have been induced by light during photolysis or photobleaching. Imidazole anion completely protonated in LiCl but showed no protonation in NaOH. As would be expected from the similar structures, the results for the analogs are nearly identical with those found for the aromatic amino acids. Experiments with indole, the analog of tryptophan, were unsuccessful due to its very low solubility in 8 N NaOH or 12 M LiCl.

Lamotte and Gloux have investigated  $\gamma$ -irradiated imidazole.<sup>22</sup> They identify the stable radical at room temperature as the same as that found here. They report the two methylene proton splittings differ in magnitude by 5 G, but their average value is 47 G as is found here.

*Assignment of Sites of Protonation. MO Calculations and Further Experiments.* Although the sites of protonation are unequivocally determined by analysis of the ESR spectra for the radicals from the localized bond compounds, in the case of the aromatic amino acids more information is needed. McLachlan MO calculations have been performed to aid in the assignment of the site of protona-

TABLE III: McLachan Spin Density ( $\rho$ ) and HMO Free Valency ( $F$ ) Calculations for Anion Radicals

Position	Acrylic Acid		Acrylonitrile		Phenylalanine		Histidine		Tryptophan	
	$\rho$	$F$	$\rho$	$F$	$\rho$	$F$	$\rho$	$F$	$\rho$	$F$
1	0.55	1.12 <sup>a</sup>	0.54	1.15 <sup>a</sup>	-0.07	0.40	0.14		0.03	
2	0.25	0.58	0.37	0.68	0.29	0.65 <sup>c</sup>	0.60	1.04 <sup>b</sup>	0.29	0.74 <sup>e</sup>
3	0.10	0.23	0.02	0.46	0.29	0.65 <sup>b</sup>	0.21		0.04	0.47
4	0.09		0.08		0.07	0.40	0.10	0.42	0.28	0.63 <sup>b</sup>
5	0.01						0.15	0.66 <sup>c</sup>	0.04	0.43
6									0.17	0.53
7									0.21	0.55 <sup>e</sup>
8									0.04	0.18
9									0.08	0.33 <sup>d,f</sup>
	$\begin{array}{c} \text{CH}_2=\text{CH}-\overset{4}{\text{C}}-\text{OH} \\ \text{1} \quad \text{2} \quad \text{3} \quad \text{5} \end{array}$		$\begin{array}{c} \text{CH}_2=\text{CH}-\text{C}\equiv\text{N}^- \\ \text{1} \quad \text{2} \quad \text{3} \quad \text{4} \end{array}$		<i>d, e</i>		<i>d</i>			

<sup>a</sup> This site is unequivocally determined by experiment to be the site of protonation. For acrylic acid ref 2, 5, and 6 have shown this as well.

<sup>b</sup> Comparison of spin densities calculated for the protonated radicals with experiment suggest these sites are the likely sites of protonation.

<sup>c</sup> A possible site which is somewhat less likely as the protonation site. Sites b and c could not be distinguished in our spectra. <sup>d</sup> See Table II for the numbering scheme. <sup>e</sup> The MO calculations for tyrosine gave very similar results to those of phenylalanine. <sup>f</sup> The MO calculations for tryptophan are for the structure with the nitrogen at position 1 protonated. <sup>g</sup> Possible protonation site from MO calculations which experiments with 7-methyltryptophan show to be unlikely as the site of protonation in tryptophan.

tion as well as to gain an understanding of the protonation process. Parameters have been employed which have been successful in predicting spin densities in other heterocyclic ion radicals.<sup>11,23</sup> Parameters for the ring methylene groups were those of Levy.<sup>24</sup>

Calculations were performed for all the possible protonated radicals of each aromatic amino acid. Those sites labeled b in Table III are those considered most likely to be sites of protonation from a comparison of experiment with the theoretical calculation. Those labeled c are possible sites which cannot be eliminated by the calculation alone. For phenylalanine and tyrosine these additional sites arise because the methylene protons in the amino acid side chain could orient so as to produce a single proton splitting of about the proper splitting. The ESR spectra could consist of both the radicals at sites b and c since they could not be distinguished experimentally.

The MO calculations for tryptophan suggest three possible sites of protonation (2, 4, 7). To further aid in this assignment experiments were performed with 4-methyl- and 7-methyltryptophan in 8 N NaOH. Analysis of the ESR spectrum for 7-methyltryptophan gave two protons at 38 G split by four protons at 13 G. Since the splitting due to four protons indicates coupling to the methyl group at position 7, the site of protonation must be position 4. This is the only protonation site which produces the required spin density at position 7 after protonation. The spectrum for 4-methyltryptophan showed less protonation. However, the spectrum did show an overall triplet of ca. 40 G. This indicates protonation at one of the other sites (2 or 7) and suggests that methyl substitution can shift the site of protonation. Therefore these experiments cannot conclusively show the site of protonation in tryptophan itself. However, the results suggest that position 4 is the major site of protonation.

MO calculations for the precursors, the anions, were also performed. In Table III we report the spin density and free valency distributions for the anions of the aromatic amino acids as well as those of acrylic acid and acetonitrile.

For acrylic acid and acrylonitrile the site of protonation

is the carbon site of highest spin density and free valency. This appears to hold true for the aromatic amino acids as well. The sites which are the likely sites of protonation are also the sites of high spin density and free valency. Our calculations of the charge density showed that this parameter did not appear to be as good an indicator as the free valency or spin density.

It would be of interest to be able to compare our assignments of the site of protonation to those found from less ambiguous methods such as ESR of single crystals. However, studies of  $\gamma$ -irradiated single crystals of aromatic amino acids<sup>25,27</sup> have reported H-addition radicals only in the case of histidine<sup>25</sup> and its analog imidazole.<sup>22</sup> In these cases, however, the H addition occurs at the position predicted by the free valency calculation. Liming and Gordy report radicals analogous to those found here in  $\gamma$ -irradiated polymeric aromatic amino acids.<sup>28</sup> They interpret their results in a similar manner to this work; however, they consider attack of hydrogen atoms instead of protonation of anions. Our results as well as those of Mittal and Hayon<sup>21</sup> suggest that protonation is the mechanism at least in aqueous media.

## Conclusions

The results for the compounds in Table I show that the anions of compounds with structure  $R_1R_2C=CHCO_2^-$  are stabilized when  $R_1$  is a carboxyl or a methyl group. The stabilization of the carboxylic group was also found by Neta and Fessenden.<sup>2,29</sup> They attributed this to further delocalization of the electron over the carboxylic group. They considered the protonation to be related to localized double bond structure. However, we have shown that even aromatic ring structures can protonate, if the free valency is appropriately large. The stabilization caused by a methyl group is likely due to steric effects. The methyl group most likely tends to protect the carbon site from the approach of water. This same effect of methyl substitution has been observed by Hayon et al. in pulse radiolysis study of substituted acrylic acids as well.<sup>4</sup> The fact that the protonation reactions occur as readily in NaOH as in LiCl shows the

reaction is with  $\text{H}_2\text{O}$  not  $\text{H}_3\text{O}^+$ . This conclusion is also in agreement with previous work.<sup>2</sup>

Recent work by Fessenden and Chawla has shown that the acrylate dianion protonates at the  $\beta$  carbon more readily than the acrylic acid anion.<sup>2b</sup> Neither anion was stable at low temperature in our results, thus we were unable to observe this effect.

The experimental results for the aromatic amino acids show that some protonation on the ring structure occurs in each case. Examination of the free valency calculations for the anions of aromatic amino acids and other compounds indicate that protonation occurs at sites with high values of the free valency (about 0.63 or greater). The three anions which showed no carbon protonation in our studies, i.e., the anions of fumaric, benzoic, and muconic acids, have free valencies equal to or under 0.60.

As we mentioned initially, the anion of the DNA base thymine has been found to protonate in an alkaline glass at a carbon site (position 6). The free valency at this position is 0.77. The anions of the purine DNA bases, which have less of a tendency to protonate, have free valencies under 0.65.<sup>30</sup> However, cytosine and uracil which have similar free valencies to thymine have not been found to protonate.

Taken all together the facts suggest that the free valency is indicative but is not alone sufficient to predict whether or not rapid protonation at carbon sites will occur (for example, steric factors must be considered). Free valency calculations, however, seem able to predict the likely site or sites of protonation if the reaction does occur.

*Acknowledgment.* Acknowledgment is made to the Donors of the Petroleum Research Fund, administered by the American Chemical Society, for partial support of this research. This research was also supported in part by the U.S. Atomic Energy Commission.

## References and Notes

- (1) This research was supported by the U.S. Atomic Energy Commission and by the Petroleum Research Fund.
- (2) (a) P. Neta and R. W. Fessenden, *J. Phys. Chem.*, **76**, 1957 (1972); (b) R. W. Fessenden and O. P. Chawla, *J. Am. Chem. Soc.*, **96**, 2262 (1974).
- (3) H. Muto, K. Toriyama, and M. Iwasaki, *J. Chem. Phys.*, **57**, 3016 (1972).
- (4) E. Hayon, N. N. Lichtin, and V. Madhavan, *J. Am. Chem. Soc.*, **95**, 4762 (1973).
- (5) T. Gillbro, *J. Polym. Sci. Lett. Ed.*, **11**, 309 (1973).
- (6) M. Iwasaki, M. Fukaya, S. Fujii, and H. Muto, *J. Phys. Chem.*, **77**, 2739 (1973).
- (7) I. S. Ginns and M. C. R. Symons, *Chem. Commun.*, 893 (1971).
- (8) R. A. Holroyd and J. W. Glass, *Int. J. Radiat. Biol.*, **14**, 445 (1968).
- (9) M. D. Sevilla and P. A. Mohan, *Int. J. Radiat. Biol.*, **25**, 635 (1974).
- (10) V. T. Srinivasan and A. Van de Vorst, *Int. J. Radiat. Biol.*, **19**, 133 (1971).
- (11) M. D. Sevilla and V. L. Brooks, *J. Phys. Chem.*, **77**, 2954 (1973).
- (12) M. D. Sevilla, R. Failor, and G. Zorman, *J. Phys. Chem.*, **78**, 696 (1974).
- (13) G. W. Neilson and M. C. R. Symons, *J. Chem. Soc., Perkin Trans. 2*, 397 (1973).
- (14) N. H. Anderson, A. J. Dobbs, D. J. Edge, R. O. C. Norman, and P. R. West, *J. Chem. Soc. B*, 1003 (1971).
- (15) J. W. Sinclair and M. W. Hanna, *J. Phys. Chem.*, **71**, 84 (1967).
- (16) D. Behar and R. W. Fessenden, *J. Phys. Chem.*, **76**, 3945 (1972).
- (17) F. J. Adrian, E. L. Cochran, and V. A. Bowers, *J. Chem. Phys.*, **36**, 1938 (1962).
- (18) J. A. Brivati, K. D. J. Root, M. C. R. Symons, and J. A. Tining, *J. Chem. Soc. A*, 1942 (1969).
- (19) W. A. Seddon and D. R. Smith, *Can. J. Chem.*, **45**, 3083 (1967).
- (20) M. D. Sevilla, *J. Phys. Chem.*, **74**, 2096 (1970).
- (21) J. P. Mittal and E. Hayon, *J. Phys. Chem.*, **78**, 1790 (1974).
- (22) B. Lamotte and P. Gloux, *J. Chem. Phys.*, **59**, 3365 (1973).
- (23) M. D. Sevilla, C. Van Paemel, and C. Nichols, *J. Phys. Chem.*, **76**, 3571 (1972).
- (24) D. H. Levy, *Mol. Phys.*, **10**, 233 (1966).
- (25) H. C. Box, H. G. Freund, and K. T. Lilga, *J. Chem. Phys.*, **46**, 2130 (1967); F. Q. Ngo, E. E. Budzinski, and H. C. Box *ibid.*, **60**, 3373 (1974).
- (26) E. L. Fasanella and W. Gordy, *Proc. Natl. Acad. Sci. U.S.A.*, **62**, 299 (1969).
- (27) E. L. Fasanella and W. Gordy, *Proc. Natl. Acad. Sci. U.S.A.*, **64**, 1 (1969).
- (28) F. G. Liming and W. Gordy, *Proc. Natl. Acad. Sci. U.S.A.*, **60**, 798 (1968).
- (29) P. Neta and R. W. Fessenden, *J. Phys. Chem.*, **77**, 620 (1973).
- (30) There are results [see J. Schmidt and D. C. Borg, *Radiat. Res.*, **46**, 36 (1971)] which suggest protonation in crystalline irradiated purine DNA bases. Protonation in glasses has been shown under certain conditions. See ref 9.

## Complexes of Aromatic Electron Donors with *N*-Methylsuccinimide and *N*-Methylmaleimide

Norman Kulevsky\*

Chemistry Department, University of North Dakota, Grand Forks, North Dakota

and Roy Foster

Chemistry Department, University of Dundee, Dundee, Scotland (Received October 8, 1974)

Evidence for weak complexes being formed between the cyclic imides and the aromatic hydrocarbon electron donors benzene, durene, and hexamethylbenzene in carbon tetrachloride was obtained from shifts of the imide NMR spectra. Formation constants for 1:1 complexes were determined from the NMR data using the Scatchard equation. The relative strength of the two imides in forming the complexes is interpreted in terms of dipole-induced-dipole interactions. From measurements made over a wide range of concentrations there is also evidence that complexes whose stoichiometry is not 1:1 are present.

### Introduction

NMR studies have been used to show that both the acyclic amides<sup>1-4</sup> and lactams<sup>5,6</sup> are capable of interacting with aromatic hydrocarbons. In these studies it was found that the proton resonance frequencies of the amides are strongly dependent on the solvent, i.e., the frequencies in benzene or toluene solutions are shifted upfield relative to the positions of the same protons in carbon tetrachloride solutions. These observed shifts were attributed to the formation of 1:1 amide-hydrocarbon complexes, even though the amide molecules are, in dilute solutions, completely surrounded by an envelope of solvent molecules. According to Ronayne and Williams these complexes form because of local dipole-induced-dipole interactions between the polar amides and the polarizable hydrocarbons.<sup>7</sup> Studies by Sandoval and Hanna on the equilibria involving dimethylformamide and aromatic hydrocarbons in carbon tetrachloride are consistent with a 1:1 stoichiometry for these complexes.<sup>8</sup>

The analogous interactions of aromatic hydrocarbons with cyclic imides have not been as extensively studied. There are, however, two studies in which upfield shifts of the resonance frequencies of imide protons in benzene relative to carbon tetrachloride solutions were interpreted as indicating the formation of 1:1 complexes.<sup>9,10</sup> In order to obtain a quantitative measure of the strength of this type of interaction as well as the stoichiometry, we have followed the change in chemical shifts of the protons of *N*-methylsuccinimide (MS) and *N*-methylmaleimide (MM) in carbon tetrachloride as the electron donors (D) benzene, durene, and hexamethylbenzene were added to the solutions. To explore the possibility that complexes whose stoichiometry is not 1:1 are present, the experiments were carried out over a wide range of electron donor concentrations. MS and MM were chosen since it was likely that comparisons of their complexing ability with a common donor would be useful in determining the importance of the unsaturated center in these interactions.

### Experimental Section

Spectral grade carbon tetrachloride dried over molecular sieves was used without further purification. Commercial MS and MM were recrystallized twice and vacuum sublimed before use. The donor molecules were purified by procedures given in previous reports.<sup>11,12</sup> All solutions were

prepared by weight. In the usual experiment the concentration of MS was ca.  $4 \times 10^{-3}$  M and MM ca.  $7 \times 10^{-3}$  M. The ranges of concentration for the donors were benzene 0.025–1.2 mol/kg of solution, durene 0.023–1.2 mol/kg of solution, and hexamethylbenzene 0.021–0.6 mol/kg of solution. For each of the complexes, at least 16 different concentrations of donor (in some cases 24 different concentrations) were used. NMR measurements were made with a Bruker HX-90 operating at 90 MHz and a probe temperature of 34.5°. TMS was used as an internal reference.

### Results and Discussion

The NMR spectra of MS and MM in carbon tetrachloride have two absorption peaks, one due to the ring protons and one due to the *N*-methyl protons. For both imides the two sets of protons are shifted to higher fields when aromatic hydrocarbons are added to the solutions. The magnitude of these upfield shifts increase as the concentration of added hydrocarbon increases. For a given concentration of hydrocarbon, the shifts of the ring protons are two to three times the upfield shifts of the *N*-methyl protons. Dilution of imide-carbon tetrachloride solutions by more solvent has little or no effect on the frequencies of either sets of protons, indicating that the shifts observed when hydrocarbons are added are not due to any changes in self-association of the imides.

Methods have been described by which the equilibrium constants ( $K$ ) for the formation of weak molecular complexes (AD) from the components A and D may be determined from the change of the proton frequencies in A as a function of the concentration of added aromatic hydrocarbon ( $C_D^0$ ).<sup>11-13</sup> The difference between the frequency of a given imide proton in pure solvent and in a solution containing D ( $\Delta_{\text{obsd}}$ ) can be related to  $K$  and  $C_D^0$  by the Scatchard equation:

$$\Delta_{\text{obsd}}/C_D^0 = -K\Delta_{\text{obsd}} + K\Delta_0$$

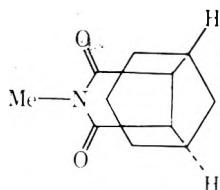
where  $\Delta_0$  is the difference between the frequency of the proton in pure A and in the complex AD. This equation is valid if only a 1:1 complex is formed,  $C_D^0 \gg C_A^0$ , and the concentrations are low enough for activities to be replaced by concentrations. Under these conditions a plot of  $\Delta_{\text{obsd}}/C_D^0$  vs.  $\Delta_{\text{obsd}}$  should be a straight line with a slope =  $-K$  and intercept =  $K\Delta_0$ .

TABLE I: Equilibrium Constants and Chemical Shifts of Complexes in CCl<sub>4</sub> at 34.5°

	Ring protons		N-Methyl protons	
	<i>K</i> , kg/mol	$\Delta_0$ , Hz	<i>K</i> , kg/mol	$\Delta_0$ , Hz
N-Methylsuccinimide-benzene	0.25 ± 0.01	121 ± 4	0.21 ± 0.02	47 ± 3
N-Methylsuccinimide-durene	0.42 ± 0.01	122 ± 4	0.30 ± 0.05	70 ± 5
N-Methylmaleimide-benzene	0.22 ± 0.01	112 ± 6	0.13 ± 0.05	70 ± 5
N-Methylmaleimide-durene	0.28 ± 0.01	146 ± 6	0.27 ± 0.05	72 ± 5
N-Methylmaleimide-hexamethylbenzene	0.38 ± 0.02	165 ± 9	0.39 ± 0.05	75 ± 5

Data obtained for both the ring and methyl protons of the MM and MS solutions were treated using this equation. Values of *K* and  $\Delta_0$  as well as the standard deviations on them were obtained from a standard least-squares fit. Since the frequency shifts for the methyl protons are smaller than those of the ring protons, the data for the methyl protons cover a narrow range of values and the scatter is large. For this reason the error limits on the values of *K* and  $\Delta_0$  obtained from the methyl protons are larger than the limits found when the ring protons are used. From the results in Table I it is clear that for any given complex, both sets of protons give equilibrium constants that are in reasonable agreement when the large error limits are considered.

From the data given in Table I it is also apparent that the order of complexing abilities for the aromatic hydrocarbons with imides is similar to that found in other studies of weak molecular complexes: hexamethylbenzene > durene > benzene. Further, comparison of the data for the MS and MM complexes indicates that toward benzene and durene, both imides have similar complexing ability. This leads to the supposition that the olefinic bond of MM is not necessary for complex formation. This would confirm the claim by Matsuo that charge transfer forces play only a small role in the formation of these complexes and that specific interactions occur between the polarizable hydrocarbons and the polar groups of the imides.<sup>10</sup> Since the *N*-methyl protons are less shifted than the ring protons it is likely that the structure of the complex is such that the two components lie in two parallel planes with the ring protons of the imide close to the center of the aromatic ring. The oxygen atoms and the methyl group would then be pointed away from the aromatic ring. As the charge transfer forces are negligible there is no need to have any significant overlap between  $\pi$  orbitals of the two interacting species and the structure given by Bryce-Smith and Hems is plausible.<sup>9</sup>



Taking this structure for the *N*-alkyl maleimide-benzene complexes, these authors have calculated the shift of the olefinic protons as a function of the distance between these protons and the plane of the benzene ring. They obtained values ranging from 1.63 ppm at a distance of 2.09 Å to 0.49 ppm at 4.17 Å. For the MM-benzene complex the data in Table I indicate a shift of 1.24 ppm.

The absolute accuracy of the above results is dependent on the validity of the assumption that only 1:1 complexes exist in the solutions, even though the experiments were

carried out on solutions in which  $C_D^0 > C_A^0$ . Recent studies of other weak molecular complexes have shown that 1:2 complexes such as AD<sub>2</sub> are formed in some cases.<sup>11,13</sup> Inclusion of two equilibrium processes in the treatment of the NMR data leads to an equation similar to the Scatchard equation except that plots of  $\Delta_{\text{obsd}}/C_D^0$  vs.  $\Delta_{\text{obsd}}$  are no longer linear:

$$\Delta_{\text{obsd}}/C_D^0 = -\Delta_{\text{obsd}}K_1[1 + C_D^0K_2] + K_1\Delta_0(1) + \Delta_0(2)C_D^0$$

In this equation *K*<sub>1</sub> and  $\Delta_0(1)$  are the equilibrium constant and chemical shift for the complex AD while *K*<sub>2</sub> and  $\Delta_0(2)$  are the equilibrium constant and shift for the complex AD<sub>2</sub>. Over a small range of concentrations (or saturation fraction) the deviation of the experimental data from linearity may be very small. Examination of the experimental data for all of the complexes studied here reveals that plots of  $\Delta_{\text{obsd}}/C_D^0$  vs.  $\Delta_{\text{obsd}}$  for the ring protons are not linear when values of  $\Delta_{\text{obsd}}$  less than 10 Hz are included in the plots (for these solutions the values of  $C_D^0$  range from 0.023 to 0.04 mol/kg). That these deviations are not due to random errors that are magnified because of the low values of  $\Delta_{\text{obsd}}$  is indicated by the observation that in all cases the deviations from the linear portion of the curves are in the same direction. A non-linear least-squares computer program based upon procedures given by Wolberg was used to obtain the best fit of the data to the four parameters and their standard deviations.<sup>15</sup>

The values of the parameters obtained by this procedure have two apparent faults. First, it was found that the standard deviations on each of the parameters were very large (in some cases, 100% of the value of the parameter). Second even if these values are meaningful, they are unrealistic. As an example, for MM-benzene the values obtained are *K*<sub>1</sub> = 5.8 kg/mol, *K*<sub>2</sub> = 0.14 kg/mol,  $\Delta_0(1)$  = 5.6 Hz, and  $\Delta_0(2)$  = 153 Hz. The values of *K*<sub>1</sub> are much too large and  $\Delta_0(1)$  much too low, while the ratio between  $\Delta_0(2)$  and  $\Delta_0(1)$  is too low. These types of values are found for each of the other complexes. The failure to obtain reasonable parameters for a system of 1:1 and 1:2 complexes could be explained on the basis that even higher complexes or clusters are present. For these reasons the values of *K* and  $\Delta_0$  in Table I are apparent values that indicate only the relative stabilities of the complexes.

## References and Notes

- (1) J. V. Hatton and R. E. Richards, *Mol. Phys.*, **3**, 253 (1960).
- (2) J. V. Hatton and R. E. Richards, *Mol. Phys.*, **5**, 139 (1962).
- (3) J. V. Hatton and W. G. Scheider, *Can. J. Chem.*, **40**, 1285 (1962).
- (4) R. M. Moriarty, *J. Org. Chem.*, **28**, 1296 (1963).
- (5) R. M. Moriarty and J. M. Klegman, *J. Org. Chem.*, **31**, 3007 (1966).
- (6) R. M. Moriarty and J. M. Klegman, *Tetrahedron Lett.*, 891 (1966).
- (7) J. Ronayne and D. H. Williams, *J. Chem. Soc. B*, 540 (1967).
- (8) A. A. Sandoval and M. W. Hanna, *J. Phys. Chem.*, **70**, 1203 (1966).
- (9) D. Bryce-Smith and M. A. Hems, *J. Chem. Soc. B*, 812 (1967).
- (10) T. Matsuo, *Can. J. Chem.*, **45**, 1829 (1967).

- (11) B. Dodson, R. Foster, and A. A. S. Bright, *J. Chem. Soc. B*, 1283 (1971).  
 (12) R. Foster and C. A. Fyfe, *Trans. Faraday Soc.*, **61**, 1626 (1965).  
 (13) R. Foster in "Molecular Complexes", Vol. 2, R. Foster, Ed., Elek Science, London, 1974.  
 (14) R. Foster, "Organic Charge Transfer Complexes", Academic Press, New York, N.Y., 1969, Chapter 7.  
 (15) J. R. Wolberg "Prediction Analysis", Van Nostrand, Princeton, N.J., 1967, Chapter 3.

## Magnetic Criteria for Aromaticity

Rois Benassi, Paolo Lazzeretti,\* and Ferdinando Taddei

*Istituto di Chimica Organica, Università, 41100 Modena, Italy (Received July 12, 1974)*

The coupled Hartree-Fock perturbation theory is used within the framework of the Pariser-Parr-Pople approximation to compute the magnetic susceptibility, NMR shielding constants, and electric dipole polarizability of aromatic molecules. It is shown that the contribution to the magnetic susceptibility component perpendicular to the molecular plane serves as a more reliable aromaticity index than that based on magnetic anisotropy or NMR data.

### Introduction

The concept of "aromaticity" dates back to the early days of chemistry, the first definition being that of Kekulé. Its current popularity among chemists is largely due to its successful applications: the familiar model of the electronic structure in benzene as a "sandwich" molecule provides both a useful visualization of the effects arising from delocalized electrons (reactivity data, molecular geometries, heats of formation and hydrogenation, enhanced diamagnetism, spectroscopic properties, and so on) and a reasonable hypothesis by which to rationalize them. Several suggestions have been put forward as to the most appropriate criterion with which to describe "aromaticity," and a rigorous, quantitative basis for such a criterion has often been felt necessary: semiempirical and ab initio methods of quantum chemistry have been employed to quantify the degree of aromaticity and to set up aromaticity scales.<sup>1-14</sup> Magnetic properties provide considerable insight into the concept of aromaticity: since the early days of quantum chemistry the anomalous diamagnetism of benzene has been related to delocalization of  $\pi$  electrons.<sup>15,17</sup> More recently, NMR data have been interpreted within the framework of the "ring current" model to explain the low-field chemical shifts of conjugated cyclic molecules.<sup>13,18-22</sup>

Accurate measurements of diamagnetic anisotropy have become available from the Zeeman splitting of microwave spectra, and these data have also been proposed for a proper definition of aromatic character.<sup>9-11</sup> On the other hand, magnetic criteria would appear rather contradictory: for instance, pyrones, which are fully aromatic according to the classical definition based on their chemical properties,<sup>24</sup> are classified as nonaromatic in light of magnetic anisotropy<sup>23</sup> and partially aromatic for what concerns their NMR chemical shifts.<sup>24</sup> As a matter of fact, the magnetic anisotropy criterion does not seem to be altogether reliable: even if this quantity is split into local and nonlocal contributions, the latter being more properly related to aromaticity,<sup>11</sup> it unavoidably accounts for terms contributed by  $\sigma$  electrons which are not directly responsible for aromatic

behavior. In a recent paper, the contribution provided by  $\pi$  electrons to the magnetic susceptibility component perpendicular to the molecular plane was chosen as an index of aromaticity;<sup>12</sup> it is purpose of this paper to show that, of magnetic criteria, this is the most reliable, whereas magnetic anisotropy measurements alone can be misleading. Electric polarizability of the  $\pi$  electron cloud is also considered in an attempt to clarify the concept of aromaticity and to restate a standard related to chemical reactivity.

### Outline of Calculations

The present paper relates to a set of molecules for which contradictory results are found in the literature. Contributions to second-order properties arising from  $\pi$  electrons, which essentially determine aromaticity, were computed by the coupled Hartree-Fock perturbation theory<sup>25,26</sup> starting from a semiempirical PPP zero-order wave function.<sup>19,22</sup> The approach employed is basically that first described by McWeeny,<sup>23,26</sup> with slight modifications. Allowing for the perturbation  $f^{(1)}$  and  $f^{(2)}$ , the first-order molecular orbitals are expanded as linear combinations of unperturbed orbitals:

$$\Phi_i^{(1)} = \sum_{k \neq i} C_{ki}^{(1)} \Phi_k \quad (1)$$

the coefficients  $C_{ki}^{(1)}$  in (1) are given by

$$C_{ki}^{(1)} = (\mathbf{C}_k^* \Delta^{(1)} \mathbf{C}_i) / (\epsilon_i - \epsilon_k) \quad (2)$$

where

$$\Delta^{(1)} = \mathbf{f}^{(1)} + \mathbf{G}(\mathbf{R}^{(1)}) \quad (3)$$

contains one and two electron perturbation terms:

$$f_{pq}^{(1)} = \langle p | f^{(1)} | q \rangle$$

$$G(\mathbf{R}^{(1)})_{pr} = \sum_{sq} R_{sq}^{(1)} \{ 2[pq | rs] - [pq | sr] \}$$

and the first-order density matrix  $\mathbf{R}^{(1)}$  is resolved into two components:



$$\mathbf{R}^{(1)} = \mathbf{X}^{(1)} + \mathbf{X}^{(1)*}$$

$$\mathbf{X}^{(1)} = \sum_i^{\text{occ}} \sum_k^{\text{unocc}} C_{ki}^{(1)*} \mathbf{C}_i \mathbf{C}_k^* \quad (4)$$

to be determined iteratively starting with  $\mathbf{R}^{(1)} = 0$  in (3).

Second-order properties are then expressed via second-order energy:

$$E^{(2)} = \text{tr} \mathbf{f}^{(1)} \mathbf{R}^{(1)} + 2 \text{tr} \mathbf{f}^{(2)} \mathbf{R} \quad (5)$$

The approximations to one-electron perturbation matrices  $\mathbf{f}^{(1)}$  are the same as in previous studies,<sup>19,20,27</sup> and the computer program used in this study is an implemented version of an earlier one.<sup>28</sup> For electric polarizabilities the dipole moment matrix  $\mathbf{f}^{(1)}$  is approximated by atomic coordinates assuming that  $\pi$  electrons are perfectly localized.<sup>33</sup> Then the  $\mu\nu$  component of polarizability tensor is

$$\alpha_{\mu\nu} = -2 \sum_p R_{p\mu}^{(\mu)} X_p^{(\nu)} \quad \mu, \nu = 1, 2, 3$$

The magnetic susceptibility component perpendicular to molecular plane<sup>19</sup> can then be expressed as

$$\chi = 2 \text{tr} \mathbf{R}^{(1)} \mathbf{f}^{(10)} + 2 \text{tr} \mathbf{R}^{(0)} \mathbf{f}^{(20)}$$

$$f_{p\alpha}^{(10)} = \alpha H_{p\alpha} S_{p\alpha} \quad f_{p\alpha}^{(20)} = \frac{1}{2} \alpha^2 H_{p\alpha} S_{p\alpha}^2$$

and the average shielding constant as

$$\sigma = \frac{2}{3} \text{tr} \mathbf{R}^{(1)} \mathbf{f}^{(01)} + \frac{2}{3} \text{tr} \mathbf{R}^{(0)} \mathbf{f}^{(11)}$$

$$f_{p\alpha}^{(01)} = \alpha H_{p\alpha} K_{p\alpha} S_{p\alpha} \quad f_{p\alpha}^{(11)} = \alpha^2 H_{p\alpha} K_{p\alpha} S_{p\alpha}^2$$

In these equations  $\alpha$  is the fine structure constant,  $\mathbf{H}$  is the zero-order hamiltonian and

$$S_{p\alpha} = \frac{1}{2} \mathbf{R}_p \times \mathbf{R}_\alpha \cdot \mathbf{n} \quad K_{p\alpha} = R_p^{-3} + R_\alpha^{-3}$$

where  $\mathbf{n}$  is the unit vector perpendicular to the molecular plane and  $\mathbf{R}_p$  is the position vector of atom  $p$  with respect to a reference frame which can be chosen arbitrarily: since a GIAO basis<sup>19</sup> is assumed, calculated magnetic properties are origin independent. The parameters used in the PPP calculation were taken from the literature,<sup>29</sup> as were available molecular geometries;<sup>30</sup> otherwise, standard bond lengths and bond angles were employed.

Different approximations were tested for the resonance integrals in benzene isomers: if  $\beta_{i,j}$  is assumed to be roughly  $-2.39$  eV for all bonds, the description is poorer. Slightly better results are obtained from the formula  $\beta_{ij} = 17r_{ij}^{-6}$ , and some improvement is generally achieved allowing for the empirical relationship<sup>31</sup>

$$\beta_{ij} = -2.39 \exp(2.5(1.397 - r_{ij})) \quad (6)$$

$$r_{ij} = 1.520 - 0.186 P_{ij}$$

which gives the  $\beta_{ij}$ 's as exponential functions of bond distances  $r_{ij}$ , in turn related to the bond orders  $P_{ij}$  at each iteration. A few results were compared with those obtained by means of the uncoupled Hartree-Fock perturbation theory<sup>21,27,32</sup> and found virtually identical.

The contributions from  $\pi$  electrons to electric dipole polarizability, magnetic susceptibility, and NMR shielding are reported in Table I.

The magnetic susceptibility data are partitioned for benzene and its isomers according to eq 7 outlined else-

$$\chi_i = n_C \chi_{C_i} + n_H \chi_{H_i} + \chi_\pi$$

$$\chi_m = \frac{1}{3} (\chi_i + 2(n_C \bar{\chi}_C + n_H \bar{\chi}_H)) \quad (7)$$

$$\Delta \chi = \chi_i - (n_C \bar{\chi}_C + n_H \bar{\chi}_H)$$

where;<sup>20,30</sup> similar formulae are used to assess contributions to molecular polarizabilities provided by  $\sigma$  bonds<sup>33</sup>:

$$\alpha = (\alpha_\pi/\epsilon) + \alpha_\sigma$$

$\alpha_\sigma$  is obtained assuming an additive scheme for C-C and C-H bonds:

$$\alpha_{C-C} = \frac{1}{3} (2\alpha_{C-C}^\perp + \alpha_{C-C}^\parallel)$$

$$\alpha_{C-H} = \frac{1}{3} (2\alpha_{C-H}^\perp + \alpha_{C-H}^\parallel)$$

the parameters  $\alpha_{C-C}^\perp$ ,  $\alpha_{C-H}^\perp$ ,  $\alpha_{C-C}^\parallel$ ,  $\alpha_{C-H}^\parallel$ , and  $\epsilon$  are those of ref 33.

A slightly different approach and additive bond parameters were used for molecules containing oxygen.<sup>34</sup> In Table I,  $\Delta = \chi_m(\text{expt}) - \chi_m(\text{calcd})$  is the magnetic exaltation according to Hoarau<sup>35</sup> ( $\chi_m(\text{calcd})$  is calculated from Pascal constants given by the same author) and can be considered a quasiexperimental measurement of delocalization effects.

## Results and Discussion

From the results in Table I it is seen that magnetic properties of benzene are fully rationalized by this calculation. The results for cyclopentadiene (a hyperconjugative model is assumed in the calculation<sup>7</sup>) are also in nice agreement with experimental findings: its relatively high magnetic anisotropy<sup>10,11</sup> is accounted for, but the aromaticity is roughly one-third that of benzene. The value of  $\chi_\pi$  puts cyclopentadiene at the lower end of the aromaticity scale in five-membered heterocycles;<sup>12</sup> comparison must, however, be established with some care because of different approximations retained in ref 12. A less exact agreement is found for 3,4-dimethylenecyclobutene and fulvene, which are nonaromatic according to our calculation (small paramagnetic contributions from  $\pi$  electrons). It is interesting to note that the exaltation  $\Delta$  given by Hoarau<sup>35</sup> is also paramagnetic for 3,4-dimethylenecyclobutene but diamagnetic for fulvene. As a matter of fact, even if the CHF estimate is paramagnetic for fulvene, the values obtained are quite close to those of Hoarau; in any event they are rather low, so that the interpretation of fulvene and 3,4-dimethylenecyclobutene as nonaromatic conjugated dienes is quite reasonable. Calculated results for trimethylenecyclopropane show that ring conjugation is completely absent, in agreement with Dewar;<sup>8b</sup> unfortunately, experimental magnetic properties of this molecule are not available for comparison.

The trend of the contributions to shielding constants arising from  $\pi$  electrons ( $\sigma$  in Table I) can also be roughly related to aromatic behavior; moreover, a preliminary inspection of the results shows that a relationship similar to (1) of ref 12 can be derived to discuss experimental chemical shifts. On the other hand, the connection between PMR chemical shifts and aromatic character is only qualitative: in our calculations it was found that the results are rather sensitive to C-H bond lengths, which must be known with great accuracy since ring current effects fall rapidly as the distance from the molecular periphery increases. On account of this additional dependence on distance, shielding would appear to be an inadequate yardstick of aromaticity. For pyrones, the calculations predict a weak aromatic char-

TABLE I: Calculated and Experimental (in Parentheses) Electric and Magnetic Second-Order Properties

	$\sigma$	$\alpha_{xx}$	$\alpha_{yy}$	$\bar{\alpha}$	$\chi_z$	$\chi_x$	$\chi_m$	$\Delta\chi$	$\Delta$	Exptl geom- etry
	2.648	6.014	6.014	10.38 (10.32 <sup>a</sup> )	-32.17	-95.76 (-96.4 <sup>b</sup> )	-55.60 (-55.2 <sup>b</sup> )	-60.24 (-59.10 <sup>b</sup> ; -59.7 <sup>c</sup> )	-15.3	<i>d</i>
	1 -0.140 2 -0.138 3 -0.024	10.034	2.517	10.51	1.27	-62.33 (-67.6 <sup>e</sup> )	-44.45 (-42.9 <sup>e</sup> )	-26.81 (-37.0 <sup>e</sup> )	-3	<i>f</i>
	1 -0.273 2 -0.045 3 -0.047	7.745	4.908	10.53	1.81	-61.78 (-51.3 <sup>e</sup> )	-44.27 (-36.9 <sup>e</sup> )	-26.27 (-21.7 <sup>e</sup> )	+3	<i>g</i>
	0.0	7.556	7.556	11.11	0.0	-63.60	-44.88	-28.08		<i>h</i>
	1 1.270 2 1.295 3 0.403	3.348	4.284	8.95 (8.90 <sup>i</sup> )	-12.12	-67.22 (-67.5 <sup>j</sup> )	-43.93 (-44.7 <sup>j</sup> )	-34.93 (-34.3 <sup>j</sup> )	-6.7	<i>d</i>
	0.192	3.738	2.000	4.68	-0.69			(-17.8 <sup>k</sup> )		<i>d</i>
	0.303	3.588	3.191	6.02	-2.92	(-52.5 <sup>l</sup> )	(-42.8 <sup>l</sup> )	(-14.5 <sup>l</sup> )	-2.5	<i>l</i>
	-0.094	9.873	1.932	7.68 (7.57 <sup>m</sup> )	0.85	(-53.5 <sup>l</sup> )	(-35.8 <sup>l</sup> )	(-26.6 <sup>l</sup> )	-4.4	<i>n</i>
	1 0.574 2 0.567	10.843	2.085	9.20	-6.87			(-22.9 <sup>o</sup> )		<i>d</i>
	1 0.535 2 0.531 3 0.539 4 0.548	10.028	5.183	9.74	-6.52			(-24.8 <sup>o</sup> )		<i>d</i>
	-0.097	15.664	1.556	10.69 (10.24 <sup>p</sup> )	1.216		(-34.4 <sup>o</sup> )	(-40.2 <sup>o</sup> )	+5	<i>d</i>

<sup>a</sup> Reference 41. <sup>b</sup> Reference 35. <sup>c</sup> Reference 42. <sup>d</sup> Reference 30a. <sup>e</sup> Reference 11. <sup>f</sup> Reference 30b. <sup>g</sup> Reference 30c. <sup>h</sup> Reference 30f. <sup>i</sup> Reference 39. <sup>j</sup> References 10, 36, 37. <sup>k</sup> Reference 38. <sup>l</sup> Reference 30d. <sup>m</sup> Reference 34. <sup>n</sup> Reference 30e. <sup>o</sup> Reference 23. <sup>p</sup> Reference 40. <sup>q</sup> Reference 35. <sup>r</sup> Reference 43.

acter (one-fifth of that of benzene), which is consistent with chemical data. Mean experimental susceptibility is available for 2,6-dimethyl-4-pyrone,<sup>24</sup>  $\chi_m = -53.52$ , whereas according to Hoarau  $\Delta\chi = +3.28$  and, more recently,<sup>24</sup>  $-2.19$ . Benson et al.<sup>23</sup> conclude that these molecules are not aromatic from their rationalization of experimental  $\Delta\chi$ 's. Experimental PMR chemical shifts support the presence of ring currents;<sup>24</sup> from these data one can reasonably argue that pyrones are essentially diene systems which ex-

hibit a low homocyclic conjugation. For other molecules considered here (paraquinone, vinylen carbonate, maleic anhydride) our classification coincides with that of Benson and Flygare.<sup>11</sup>

With regards to dipole polarizabilities, comparison between calculated and available experimental results shows good agreement and confirms the reliability of the semiempirical CHF approach; from the data displayed in Table I it is seen that both methods<sup>33,34</sup> employed here to account for

the  $\sigma$ -bond contribution work fairly well. It is also evident that the average  $\pi$  polarizability  $\alpha_\pi = \frac{1}{3}(\alpha_{xx} + \alpha_{yy})$  cannot even qualitatively be related to aromaticity. In principle, electric polarizability of a molecule would be naively connected with reactivity toward electrophilic reactions and henceforth furnish an aromaticity index. This is evident for a series of molecules with quite similar geometry; in the series benzene, pyridine, pyrimidine, triazine<sup>27</sup> the trend of  $\alpha_\pi$ 's closely parallels that of  $\chi_\pi$ 's. In the case of the molecules considered here it is seen that  $\alpha_\pi$ 's also depend on branchings and side groups in the molecule, which suggests that  $\alpha_\pi$  should be discarded as a general aromaticity index. Moreover, connections between reactivity and aromaticity must be considered with some care since the former is determined by several parameters of ground and excited states and any classification set up merely in terms of reactivity must be regarded at least as incomplete.

### Conclusions

The calculations reported here provide a satisfactory rationalization of the magnetic properties of the molecules studied. Hence one can reasonably conclude that the aromaticity index given by  $\chi_\pi$  seems more reliable than that based on  $\Delta\chi_{\text{nonlocal}}$  which contains spurious contributions from the  $\sigma$  core; the former can be used to set up "aromaticity scales" which, for benzene and its isomers, almost coincide with ab initio results,<sup>5</sup> which are much more difficult to obtain. The experimental data for benzene isomers recently discussed by Benson and Flygare<sup>11</sup> and considered as "surprising" and "puzzling" by the authors can be easily interpreted, and the resulting fundamental point is that high magnetic anisotropy does not necessarily imply aromaticity, as our calculations clearly show. On the other hand, the arguments expounded here suggest that an absolute definition of aromaticity explaining both reactivity and magnetic properties would be hard to set up (e.g., cyclopentadiene, pyrones), whereas, if we limit ourselves to magnetic criteria,  $\chi_\pi$  reasonably provides the chief means whereby to build up nomenclatures and relative degrees of aromatic character.

*Acknowledgment.* The authors wish to thank Professor G. Barbieri for stimulating and helpful discussion.

### References and Notes

- (1) D. P. Craig, "Theoretical Organic Chemistry", Kekulé Symposium, Butterworths, London, 1955, p 20
- (2) M. J. S. Dewar and C. De Llano, *J. Am. Chem. Soc.*, **91**, 789 (1969)
- (3) R. W. Hakaia, *Int. J. Quantum Chem.*, **1**, 187 (1967)
- (4) A. Julg and P. Francois, *Theor. Chim. Acta*, **8**, 249 (1967)
- (5) R. E. Cristoffersen, *J. Am. Chem. Soc.*, **93**, 4104 (1971)
- (6) N. C. Baird and M. J. S. Dewar, *J. Am. Chem. Soc.*, **91**, 352 (1969)
- (7) H. J. Dauben, J. D. Wilson, and J. L. Laity, *J. Am. Chem. Soc.*, **91**, 1991 (1969)
- (8) M. J. S. Dewar and G. J. Gleicher, *J. Am. Chem. Soc.*, **87**, 685, 692 (1965)
- (9) D. H. Sutter and W. H. Flygare, *J. Am. Chem. Soc.*, **91**, 4063, 6895 (1969)
- (10) R. C. Benson and W. H. Flygare, *J. Am. Chem. Soc.*, **92**, 7523 (1970)
- (11) R. C. Benson and W. H. Flygare, *J. Chem. Phys.*, **58**, 2366 (1973)
- (12) E. Corradi, P. Lazzeretti, and F. Taddei, *Mol. Phys.*, **26**, 11 (1973), and references quoted therein.
- (13) J. A. Elvidge, *Chem. Commun.*, 160 (1965)
- (14) M. H. Palmer and R. H. Findlay, *Tetrahedron Lett.*, **3**, 253 (1974)
- (15) P. E. Ehrenfest, *Phys. Grav.*, **5**, 388 (1925)
- (16) L. V. Raman and K. S. Krishnam, *Proc. Roy. Soc., Ser. A*, **113**, 511 (1927)
- (17) L. Pauling, *J. Chem. Phys.*, **4**, 673 (1936)
- (18) J. W. Emsley, J. Feeney, and L. H. Sutcliffe, "High Resolution Nuclear Magnetic Resonance Spectroscopy", Pergamon Press, New York, N.Y., 1965
- (19) G. G. Hall and A. Hardisson, *Proc. Roy. Soc., Ser. A*, **268**, 328 (1962)
- (20) P. Lazzeretti and F. Taddei, *J. Chem. Soc. Faraday Trans. 2*, **68**, 839, 1825 (1972)
- (21) H. G. Ff Roberts, *Theor. Chim. Acta*, **15**, 63 (1969)
- (22) T. G. Edwards and R. Mc Weeny, *Chem. Phys. Lett.*, **10**, 283 (1971)
- (23) R. C. Benson, C. L. Norris, W. H. Flygare, and P. Beak, *J. Am. Chem. Soc.*, **93**, 5591 (1971)
- (24) H. C. Smitherman and L. N. Ferguson, *Tetrahedron*, **24**, 923 (1968)
- (25) W. N. Lipscomb, "Theoretical Chemistry", W. Byers Brown, Ed., Butterworths London, 1972, p 167
- (26) R. Mc Weeny, *Phys. Rev.*, **128**, 1028 (1962); *Chem. Phys. Lett.*, **1**, 567 (1968)
- (27) P. Lazzeretti, *Mol. Phys.*, **28**, 1389 (1974)
- (28) P. Lazzeretti, "L'Elaborazione Automatica", Vol. 1. Casalecchio, Bologna, 1973, p 61
- (29) H. G. Ff Roberts, *Theor. Chim. Acta*, **16**, 151 (1970)
- (30) (a) L. E. Sutton, *Chem. Soc., Spec. Publ.*, No. **11** (1958); No. **18** (1965); (b) P. A. Baron, R. D. Brown, F. R. Burden, and J. E. Kent, *J. Mol. Spectrosc.*, **43**, 401 (1972); (c) A. Skancke, *Acta Chem. Scand.*, **22**, 3239 (1968); (d) W. F. White and J. E. Boggs, *J. Chem. Phys.*, **54**, 4714 (1971); (e) R. E. Marsh, E. Ubell, and H. E. Wilcox, *Acta Crystallogr.*, **15**, 35 (1962); (f) E. A. Dorko, J. L. Hencher, and S. H. Bauer, *Tetrahedron*, **24**, 2425 (1968)
- (31) Y. Mikami, S. Miyai, and T. Nakajima, *Bull. Chem. Soc. Jpn.*, **46**, 787 (1973)
- (32) A. T. Amos and H. G. Ff Roberts, *J. Chem. Phys.*, **50**, 2375 (1969)
- (33) P. Lazzeretti and F. Taddei, *J. Chem. Soc. Faraday Trans. 2*, **70**, 1153 (1974)
- (34) J. W. Le Fevre and A. Sundaram, *J. Chem. Soc.*, 4009 (1962)
- (35) J. Hoarau, *Ann. Chim. (Paris)*, **1**, 544 (1956)
- (36) J. Hoarau, *Bull. Soc. Chim. Fr.*, **17**, 1153 (1950)
- (37) J. Farquarson, *Trans. Faraday Soc.*, **32**, 219 (1935)
- (38) R. C. Benson and W. H. Flygare, *J. Chem. Phys.*, **58**, 2651 (1973)
- (39) J. W. Le Fevre and K. M. S. Sundaram, *J. Chem. Soc.*, 3518 (1964)
- (40) J. W. Le Fevre and A. Sundaram, *J. Chem. Soc.*, 974 (1963)
- (41) M. F. Vuks, *Opt. Spectrosc.*, **20**, 361, 644 (1966)
- (42) L. Caralp and J. Hoarau, *J. Chim. Phys.*, **66**, 642 (1969)
- (43) M. A. Lasheen, *Phil. Trans. Roy. Soc., Ser. A*, **256**, 357 (1964)

# Search for Isotope Effects in the Self-Diffusion of Benzene and Cyclohexane at 25°

R. Mills

Diffusion Research Unit, Research School of Physical Sciences, Australian National University, Canberra, A. C. T., Australia  
(Received December 2, 1974)

Publication costs assisted by Australian National University

A search has been made for possible isotope effects in the self-diffusion of benzene, cyclohexane, and their deuterated analogs at 25°. The diaphragm cell method was used throughout. No isotopic effect could be detected within average error limits of  $\pm 0.3\%$ . This finding is in agreement with the theoretical predictions of Friedman.

There has been some controversy in recent years as to whether or not measurable isotope effects occur in certain types of diffusion in organic liquids. The type of diffusion being considered is that in which molecules differing only in isotopic composition are diffusing in trace amounts in the same solvent. The solvent in most of the cases studied has been itself another isotopic form of the diffusing molecules. The controversy first arose for benzene self-diffusion with the molecules being labeled with varying numbers of  $^{14}\text{C}$  atoms. Eppstein<sup>1</sup> and Eppstein and Albright<sup>2</sup> observed that singly and doubly labeled benzene molecules diffused in normal benzene at different rates whose dependence appeared to follow approximately the inverse square root of the mass. Dunlop and coworkers<sup>3-5</sup> on the other hand have measured the self-diffusion of benzene samples containing on average from one to five  $^{14}\text{C}$  atoms and found only a very slight linear dependence on mass. These latter results are in accord with a recent analysis by Friedman<sup>6</sup> who used correlation function theory to predict that, for the type of system outlined above, there should be little or no dependence on the mass of the diffusing particle.

One of the problems associated with the  $^{14}\text{C}$  studies is knowing precisely the number of radioactive atoms in each tracer molecule so that the molecular mass can be specified. The average number of carbon atoms labeled in a particular batch can be estimated from its specific activity and knowledge of any dilution steps during synthesis. Such an estimate assumes perfect yields and disregards isotope effects. There is also a fairly broad spread in the number of  $^{14}\text{C}$  atoms in each molecule around the most probable number and only an average can be used. The molecular weight of 88 assigned to our previous  $^{14}\text{C}$ -labeled benzene results quoted later in this paper was obtained in this way.

We have used a different approach to the problem by tritiating two sets of normal and fully-deuterated species and used conditions under which the isotopic masses are exactly specified. This procedure not only overcame the uncertainties applying to  $^{14}\text{C}$ -labeled molecules but also in the cyclohexane case gave a large mass difference (11 units) with which to test the theoretical predictions.

## Experimental and Discussion

Small samples of normal and fully deuterated benzene were labeled by treatment with tritiated water using methylaluminum chloride as catalyst as described by Long, Garnett, and Vining.<sup>7</sup> Normal and fully deuterated cyclohexane were tritiated by mixing the tritium gas with Raney nickel as catalyst as reported by Long, Odell, and

TABLE I:

Tracer	Isotopic mass	Solvent	$10^{-9}D^*$ , $\text{m}^2 \text{sec}^{-1}$
$\text{C}_6\text{H}_5\text{T}$	80	$\text{C}_6\text{H}_6$	$2.203 \pm 0.004$
$\text{C}_6\text{D}_5\text{T}$	85	$\text{C}_6\text{H}_6$	$2.207 \pm 0.007$
$\text{C}_5^{14}\text{C}^{12}\text{H}_6$	88	$\text{C}_6\text{H}_6$	$2.205 \pm 0.005$
$\text{C}_6\text{H}_{11}\text{T}$	86	$\text{C}_6\text{H}_{12}$	$1.457 \pm 0.002$
$\text{C}_6\text{D}_{11}\text{T}$	97	$\text{C}_6\text{H}_{12}$	$1.463 \pm 0.001$

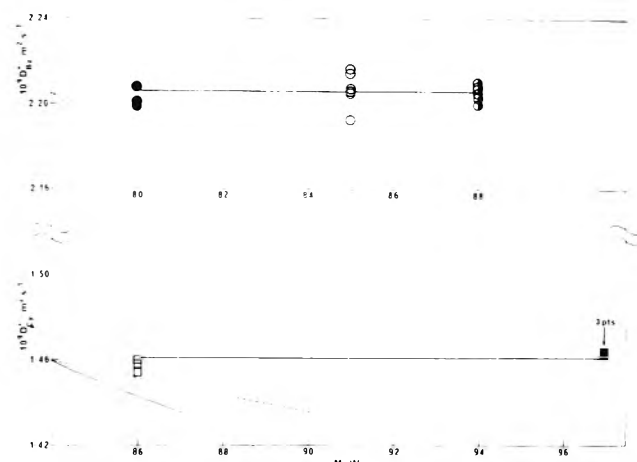


Figure 1. Self-diffusion coefficients for benzene and cyclohexane at 25°: ●,  $\text{C}_6\text{H}_5\text{T}$  in  $\text{C}_6\text{H}_6$ ; ○,  $\text{C}_6\text{D}_5\text{T}$  in  $\text{C}_6\text{H}_6$ ; ○,  $^{14}\text{C}_5^{12}\text{CH}_6$  in  $\text{C}_6\text{H}_6$ ; □,  $\text{C}_6\text{H}_{11}\text{T}$  in  $\text{C}_6\text{H}_{12}$ ; ■,  $\text{C}_6\text{D}_{11}\text{T}$  in  $\text{C}_6\text{H}_{12}$ ; —, inverse square-root mass; - - - -, inverse square-root reduced mass.

Richardson.<sup>8</sup> The amount of tritium activity admitted during the exchange process was regulated so that only one molecule in about  $10^6$  was labeled. This procedure ensured that only one place in the respective rings was labeled so allowing exact knowledge of the molecular mass. Thus the four tracers formed were  $\text{C}_6\text{H}_5\text{T}$ ,  $\text{C}_6\text{D}_5\text{T}$ ,  $\text{C}_6\text{H}_{11}\text{T}$ , and  $\text{C}_6\text{D}_{11}\text{T}$ . The normal benzene and cyclohexane used as the solvent for these tracers were purified in the usual way by fractional distillation. The diffusion measurements were made by the diaphragm cell technique which has been described previously.<sup>9</sup> The precision of the measurements was on average somewhat better than  $\pm 0.3\%$ .

The self-diffusion data are presented graphically in Figure 1 and are summarized in Table I. In the benzene case, data for  $^{14}\text{C}$ -labeled benzene previously reported by Mills<sup>10</sup>

are also presented. Examination of Figure 1 indicates that the data in both cases show no relation to the inverse square root of either the mass or reduced mass. To this extent we agree in the benzene case with the conclusions of Allen and Dunlop<sup>4</sup> for their  $^{14}\text{C}$ -labeled studies. There is, however, a slight divergence of interpretation concerning the results for benzene insofar as Allen and Dunlop<sup>4</sup> deduce a very small linear dependence on mass whereas our results both for this and the cyclohexane case are virtually constant. It may be remarked here that in a previous paper on the benzene system reported by Harris, Pua, and Dunlop<sup>3</sup> this linear dependence is not evident. Friedman's<sup>6</sup> theoretical analysis allows a small linear dependence so that his equation can accommodate either conclusion. In any event it can be said that his theoretical development for nonelectrolyte tracer diffusion has been experimentally confirmed.

*Acknowledgment.* The author is very grateful to Dr. M.A. Long of the University of New South Wales who prepared the various tracers by tritiation techniques.

## References and Notes

- (1) L. B. Eppstein, *J. Phys. Chem.*, **73**, 269 (1969).
- (2) L. B. Eppstein and J. G. Albright, *J. Phys. Chem.*, **75**, 1315 (1971).
- (3) K. R. Harris, C. K. N. Pua, and P. J. Dunlop, *J. Phys. Chem.*, **74**, 3518 (1970).
- (4) G. G. Allen and P. J. Dunlop, *Phys. Rev. Lett.*, **30**, 316 (1973).
- (5) S. J. Thornton and P. J. Dunlop, *J. Phys. Chem.*, **78**, 346 (1974).
- (6) H. L. Friedman, "Molecular Motions in Liquids", J. Lascombe, Ed., D. Reidel, Dordrecht, 1974, p. 87.
- (7) M. A. Long, J. L. Garnett, and R. S. W. Vining, *J. Am. Chem. Soc.*, **94**, 8632 (1972).
- (8) M. A. Long, A. L. Odell, and J. B. Richardson, *J. Catal.*, **9**, 8410 (1967).
- (9) R. Mills and L. A. Woolf, "The Diaphragm Cell", A.N.U. Press, Canberra, 1968.
- (10) R. Mills, *Trans. Faraday Soc.*, **67**, 1654 (1971).

## Kinetics of the Conversion of Monetite to Calcium Pyrophosphate

Nancy Wolejko Wikholm, Ralph A. Beebe,\*

Department of Chemistry, Amherst College, Amherst, Massachusetts 01002

and J. S. Kittelberger

Xerox Corporation-W114, Webster, New York 14580 (Received October 31, 1974)

The kinetics of the solid-state phase change, monetite  $\rightarrow$  pyrophosphate, is investigated by a mass spectrometric thermal analysis (MTA) technique closely related to flash desorption. Supporting evidence of ir, X-ray diffraction, DTA, and TGA is collected. Under the conditions used, monetite dehydrates near  $500^\circ$  to  $\gamma\text{-Ca}_2\text{P}_2\text{O}_7$ , which converts to  $\beta\text{-Ca}_2\text{P}_2\text{O}_7$  over the range  $500\text{--}750^\circ$ . The enthalpies and activation energies for the two steps are discussed. The activation energy for the dehydration step is  $49 \pm 1$  kcal/mol from the MTA experiments, and is estimated to be 53 kcal/mol from the two DTA experiments.

### Introduction

The thermal conversion of  $\text{CaHPO}_4$  (monetite) to pyrophosphate under various conditions has been the subject of several studies.  $\text{Ca}_2\text{P}_2\text{O}_7$  can be obtained from  $\text{CaHPO}_4$  by heating in air in the range  $325\text{--}700^\circ$  for extended periods.<sup>1</sup> A more precise examination yielded  $390^\circ$  for the decomposition temperature in air.<sup>2</sup> Yet another study found that in air  $\text{CaHPO}_4$  decomposed at  $250^\circ$  in a discrete step which was complete about  $350^\circ$ .<sup>3</sup> Skinner has reported the equilibrium temperature for the phase change, monetite  $\rightarrow \beta$ -pyrophosphate, to be  $323^\circ$  at 2 kbars and  $343^\circ$  at 4 kbars water pressure.<sup>4</sup> The conversion of acid phosphates to pyrophosphates forms the basis for the important analytical method for acid phosphates.<sup>5</sup> The rather wide range of conversion temperatures cited above suggests sluggish kinetics for this solid-state reaction. It seemed important, therefore, to determine kinetic parameters for this phase change.

Additionally, this laboratory has been engaged in thermal analyses of several of the calcium phosphates as well as other systems. The temperature programmed dehydration (TPD) method<sup>6</sup> has been applied to a model system,

$\text{CuSO}_4 \cdot 5\text{H}_2\text{O}$ ,<sup>7</sup> and to an in vitro amorphous calcium phosphate.<sup>8</sup> A mass spectrometric thermal analysis (MTA) technique directly related to the original flash desorption method has been applied to the dehydration of octacalcium phosphate (OCP).<sup>9</sup> Since the conversion of  $\text{HPO}_4^{2-}$  to  $\text{P}_2\text{O}_7^{4-}$  is involved in both the decomposition mechanism of OCP<sup>1,3,9</sup> and of calcium apatite systems,<sup>5,10,11</sup> an understanding of the monetite dehydration kinetics should assist in understanding these other systems.

The present work, therefore, is a study of the dehydration of monetite to calcium pyrophosphate, with some emphasis on the product phase(s) formed.

### Experimental Section

The MTA apparatus has been described recently,<sup>9</sup> but a few details are repeated here. The powdered sample is spread on the floor of an oven programmed for various linear heating rates. The oven is mounted in a 36-l. metal vacuum chamber; pressures ranged from  $1 \times 10^{-7}$  to  $5 \times 10^{-7}$  Torr during these experiments. Estimated pumping speed near the sample is about 400 l./sec from a diffusion pump,

**TABLE I: MTA Peak Temperatures ( $T_M$ ) at Various Heating Rates ( $\beta$ )**

Peak	$T_M$ , °C	$\beta$ , deg/min
A	472	4.4
B	487	8.8
C	496	13.1
D	503	17.3
E	507	22.3

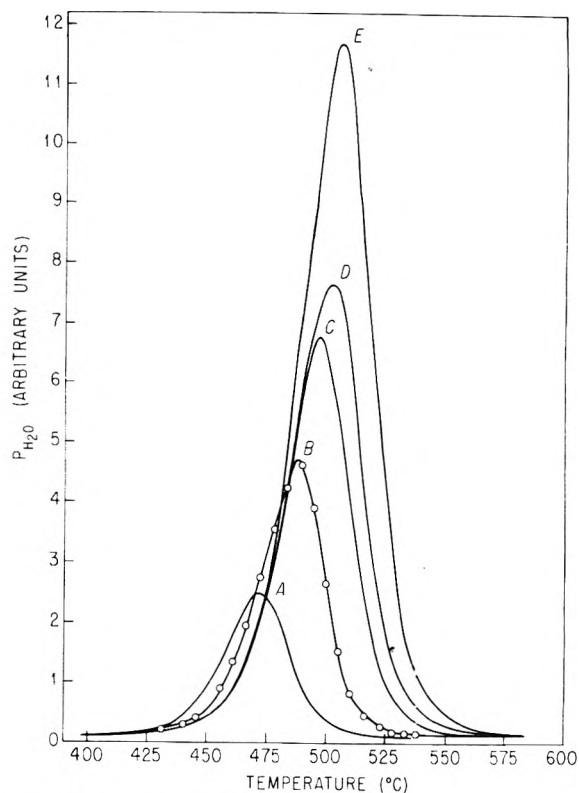
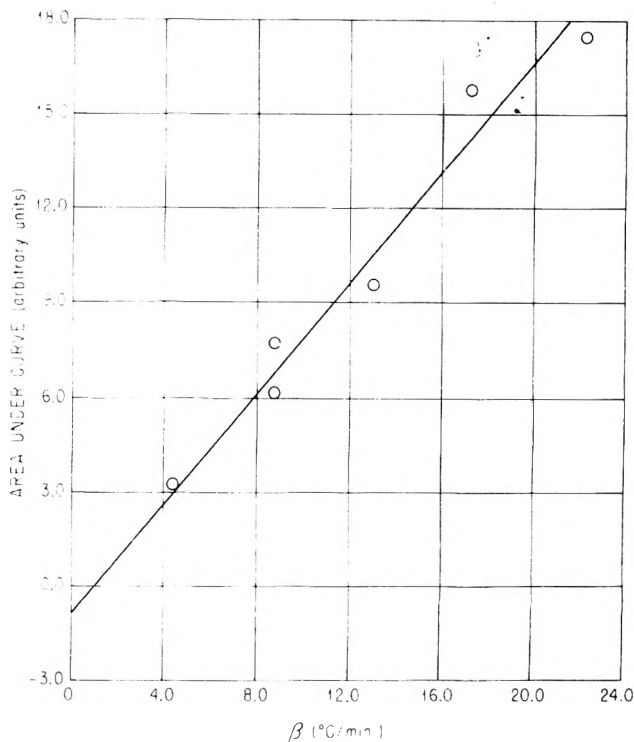
with an additional contribution of about 1500 l./sec (for  $H_2O$ ) from a liquid-nitrogen cryopump. Detection of gaseous decomposition products is via a quadrupole mass spectrometer mounted in a differentially pumped detector chamber. The portion of the mass spectrum  $17 \leq m/e \leq 46$  is scanned and recorded every 30 sec. At a heating rate of  $10^\circ/\text{min}$ , therefore, the partial pressure of  $H_2O$  (taken here as the height of the  $m/e$  18 peak) is recorded every  $5^\circ$ . Sample temperature determination is made with chromel-alumel thermocouples. Thermocouple calibration for this apparatus has been discussed previously.<sup>9</sup> The reported values of the peak temperature ( $T_M$ ) in the MTA spectrum of evolved water should be accurate to  $\pm 1^\circ$ . Each MTA run spanned the range from ambient room temperature to about  $580^\circ$ . Samples for each run consisted of 5-mg aliquots of Fisher Certified reagent anhydrous  $CaHPO_4$ . Infrared spectra of this reagent dispersed to about 2 wt % in dried KBr agreed with previously reported spectra of monetite.<sup>1</sup> X-Ray diffraction on the powdered samples confirmed the reagent as well-crystallized monetite.<sup>12</sup>

To further characterize the processes occurring in the temperature range covered by the MTA studies, differential thermal analysis (DTA) and thermogravimetric analysis (TGA) were conducted on monetite samples. Two DTA runs, 10 and  $20^\circ/\text{min}$ , were conducted under dry  $N_2$  flowing at 100 ml/min. A single TGA scan, at  $10^\circ/\text{min}$ , was carried out with the same  $N_2$  flow conditions.

## Results

The dehydration spectra of monetite obtained in the MTA apparatus at the several heating rates are shown in Figure 1. The temperatures ( $T_M$ ) at which the partial pressure of water reaches a maximum for each heating rate ( $\beta$ ) are recorded in Table I. A single sharp peak attributed to this dehydration was obtained for each  $\beta$  between 425 and  $575^\circ$ . Above and below these temperatures the spectrum adhered to the level of background water of the empty oven. The area under the single peak found in the MTA spectrum rises monotonically with heating rate, as a casual inspection of Figure 1 will reveal. The peak areas, measured with a polar planimeter and expressed in arbitrary units, are plotted against  $\beta$  in Figure 2. The intercept of the least-squares line which appears in Figure 2 is within one standard deviation of the origin.

Ir spectra of the pyrolysis product produced during the MTA runs agree closely with those obtained previously<sup>1</sup> for  $\gamma\text{-Ca}_2\text{P}_2\text{O}_7$ . X-Ray diffraction patterns of the pyrolysis product reveal a poorly crystallized  $\gamma\text{-Ca}_2\text{P}_2\text{O}_7$  with a small amount of  $\beta\text{-Ca}_2\text{P}_2\text{O}_7$  present. The TGA scan at  $10^\circ/\text{min}$  reveals a single discrete weight loss of 7.2%; the inflection point ( $d^2w/dT^2 = 0$ ) occurs at  $474^\circ$ , within the range of peak temperatures in the MTA spectra. Theoretical weight loss for the complete dehydration of monetite to diphosphate is 6.6%.


**Figure 1.** MTA spectra of  $CaHPO_4$ .

**Figure 2.** Area under peak near  $500^\circ$  in MTA spectra of  $CaHPO_4$  vs. heating rate,  $\beta$ .

The DTA scan of monetite displays a strong endothermic process at  $473^\circ$  for  $\beta = 10^\circ/\text{min}$  and at  $487^\circ$  for  $\beta = 20^\circ/\text{min}$ , and an exothermic process over the range  $500\text{--}750^\circ$ .

## Discussion

The ir, TGA, DTA, and X-ray results unequivocally identify the process occurring in the MTA spectra near 480° as the conversion to  $\gamma$ -Ca<sub>2</sub>P<sub>2</sub>O<sub>7</sub>. The exothermic process observed in the DTA scan from 500 to 750° is probably the phase change  $\gamma$ -Ca<sub>2</sub>P<sub>2</sub>O<sub>7</sub> →  $\beta$ -Ca<sub>2</sub>P<sub>2</sub>O<sub>7</sub>. Skinner<sup>4</sup> has found the equilibrium product formed from monetite at about 330°, using a hydrothermal bomb, to be the  $\beta$  phase. However, up to 60 days were required to produce the stable  $\beta$  form at these temperatures. Heating monetite at 550° can produce the  $\gamma$  phase in 11 days.<sup>4</sup> Preparation of the  $\beta$  phase from monetite is achieved by heating at 800° in air for 3 hr.<sup>4</sup> Since the DTA-observed process is rather diffuse (extending from about 500 to 750°), and since a small fraction of the product produced by heating to 580° in the MTA runs was  $\beta$ -Ca<sub>2</sub>P<sub>2</sub>O<sub>7</sub>, we assign the process from 500 to 750° observed in the DTA curve to the conversion of  $\gamma$ - to  $\beta$ -Ca<sub>2</sub>P<sub>2</sub>O<sub>7</sub>.

The activation energy ( $E_A$ ) can be calculated from a series of MTA scans at varying values of  $\beta$ , if certain conditions are met. For a single-step kinetic process with an Arrhenius rate constant,  $E_A$  independent of reagent concentrations, kinetic order  $n \geq 1$ , and pumping speed  $\rightarrow \infty$ , it has been shown<sup>13</sup> that

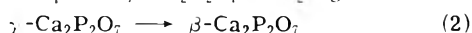
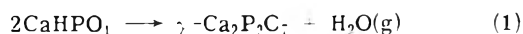
$$\ln \left( \frac{T_M^2 \theta_M^{n-1}}{\beta} \right) = \frac{E_A}{RT_M} - \ln \left( \frac{E_A}{nAR} \right)$$

where  $T_M$  is the peak temperature,  $\theta_M$  the reagent concentration at  $T_M$ ,  $A$  is the Arrhenius frequency factor,  $\beta$  is the linear heating rate,  $R$  is the gas constant, and  $n$  is the reaction order. For the case where  $E_f = f(\theta)$ , it has been shown<sup>14</sup> that broad, rather flat-topped peaks result. Since this peak shape is not found in our MTA spectra, a plot of  $\ln (T_M^2/\beta)$  vs.  $1/T_M$  should presumably yield a line with slope  $E_A/R$ , the corrections for  $n > 1$  being negligible.<sup>13b</sup> The effects of finite pumping speed do, however, need to be considered. The dependence of MTA peak area on  $\beta$  shown in Figure 2 is predicted for experiments conducted at finite pumping speed, as shown in Appendix I. The shift in  $T_M$  produced by finite pumping speed can be approximated from Redhead's work<sup>13a</sup> for a first-order process only. This is shown in Appendix I to produce a negligible error in  $E_A$ , and assumed to be valid for the dehydration observed here.

The plot of  $\ln (T_M^2/\beta)$  vs.  $1/T_M$  for the MTA data is shown in Figure 3. From the slope,  $E_A = 49$  kcal/mol with a standard deviation of 1 kcal/mol.

Activation energies can be derived from DTA peak temperatures in the same manner.<sup>15</sup> Using  $T_M$  values derived from the DTA data at two heating rates and plotting  $\ln (T_M^2/\beta)$  vs.  $1/T_M$ , the slope of the line connecting the two points gives  $E_a = 53$  kcal/mol. With only two data points, no standard deviation can be calculated.

Under the conditions of the MTA and DTA experiments reported here, the stable product  $\beta$ -Ca<sub>2</sub>P<sub>2</sub>O<sub>7</sub> is produced in two semidiscrete steps:



From Skinner's observation<sup>4</sup> of two equilibrium temperatures and H<sub>2</sub>O pressures for the overall process (reaction 1 + reaction 2) we have calculated the enthalpy change by using the Clausius-Clapeyron equation. We find  $\Delta H_1 + \Delta H_2 = 25$  kcal/mol; no error limits can be set, since only two data points exist. Reaction 2 is observed to be exothermic by our DTA measurements, as required if the  $\beta$  phase

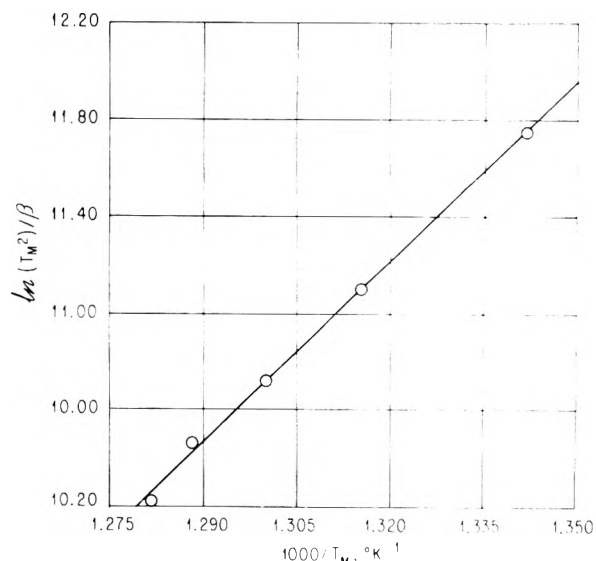


Figure 3. Plot of  $\ln (T_M^2/\beta)$  vs.  $1000/T_M$  for the peak in the MTA spectrum of CaHPO<sub>4</sub>. From the slope of the line  $E_A = 49$  kcal/mol.

is more stable than the  $\gamma$  phase, and if entropic effects are small. Thus for reaction 1,  $25 < \Delta H_1 \leq E_{A1} = 50$  kcal/mol, and for reaction 2,  $-25 \leq \Delta H_2 < 0$  kcal/mol. Here we ignore the differences in the conditions under which  $E_{A1}$  and  $(\Delta H_1 + \Delta H_2)$  were measured, and the small difference between energy and enthalpy. The observation of  $\gamma$ -Ca<sub>2</sub>P<sub>2</sub>O<sub>7</sub> as a metastable intermediate in the conversion of CaHPO<sub>4</sub> to  $\beta$ -Ca<sub>2</sub>P<sub>2</sub>O<sub>7</sub>, under these conditions, parallels previous work of Skinner<sup>4</sup> which indicates that crystal structural rearrangements involving PO<sub>4</sub> → P<sub>2</sub>O<sub>7</sub> and  $\gamma$  →  $\beta$  are probably the rate-determining steps in the reaction. It might be added that the crystallographic identity and thermodynamic stability of  $\gamma$ -Ca<sub>2</sub>P<sub>2</sub>O<sub>7</sub> are not well established. This material may not be a well crystallized phase, but the present work sheds little light on that point.

Furthermore, it should be kept in mind that both particle size and impurities, which may act as fluxes, can affect solid state rates. Such effects have not been identified in this work. The point could be checked by determining the activation energy for samples of different purity and particle size with due attention to size distribution.

*Acknowledgments.* We acknowledge with thanks our helpful discussions with C. Murphy and the assistance of R.J. Wikholm and J. Bykowski, and in particular the assistance of Dr. H.C.W. Skinner, who employed the facilities of her laboratory to characterize the monetite samples used here. Financial support from NIH Grant No. AM-2896 is gratefully acknowledged.

## Appendix I

At equilibrium in a system into which gas leaks at a constant rate of  $L$  molecules/sec and is pumped away at a constant speed of  $S$  l./sec

$$L = KSp_{\text{eq}} \quad (\text{A1})$$

where  $p_{\text{eq}}$  is the equilibrium pressure, and  $K = 3.27 \times 10^{19}$  molecules/Torr l. at 295°K.

When gas evolves from the sample (and adsorption is negligible)

$$A \frac{dn}{dt} + L = KSp + K1 \frac{dp}{dt} \quad (\text{A2})$$

where  $dn/dt$  is the desorption or decomposition rate in molecules/cm<sup>2</sup> sec,  $A$  is the sample area, and  $V$  is the system volume. (A1) and (A2) can be combined to yield

$$\frac{dp^*}{dt} + \frac{p^*}{\tau} = a \frac{dn}{dt} \quad (\text{A3})$$

where  $a = A/KV$ ,  $\tau = V/S$ , the characteristic pumping time for the system, and  $p^* = p - p_{\text{eq}}$ . The development above is given by Redhead.<sup>13a</sup>

To evaluate the area under a pressure-temperature gas evolution curve, eq A3 can be integrated from the starting temperature  $T_0$  to any temperature of interest, if the time-temperature relationship is known. For linear heating rates ( $dT/dt = \beta$ ) this produces

$$a\beta \int_{T_0}^T dn = \frac{1}{\tau} \int_{T_0}^T p^* dT + \beta p^*$$

since  $p^* = 0$  at  $T = T_0$ . If the integration is carried to infinite temperature

$$\int_{T_0}^{\infty} p^* dT = \tau\beta \left[ a \int_{T_0}^{\infty} dn - p^*_{T=\infty} \right] \quad (\text{A4})$$

The left-hand side of the equation is just the area under the pressure-temperature gas evolution curve (measured from a baseline of  $p = p_{\text{eq}}$ ), and is proportional to the heating rate  $\beta$ .

Redhead has shown<sup>13a</sup> that finite pumping speed causes the maximum in the  $P$ - $T$  curve to shift toward higher tem-

perature. The shift ( $\Delta T$ ) is a fixed fraction of  $T_M$  for fixed  $E_A$  and  $\tau$ . Redhead<sup>13a</sup> has treated the first-order case by numerical methods, and this allows us to estimate the temperature shift  $\Delta T$ . The worst case is the smallest pumping speed or the greatest  $\tau$ . Assuming only diffusion pumping in our system  $\tau \approx 10^{-1}$  sec. For  $E_A = 50$  kcal and  $\tau = 10^{-1}$  sec,  $\Delta T = 0.7\%$  for first-order kinetics.

We have corrected the  $T_M$  values in Table I for this effect and determined  $E_A$  for the monetite conversion using the corrected temperatures. The corrected value is 49.0 instead of 49.4 kcal. The difference is not significant given the 1 kcal standard deviation of the plot.

## References and Notes

- (1) B. O. Fowler, E. C. Moreno, and W. E. Brown, *Arch. Chem. Phys.*, **11**, 477 (1966).
- (2) A. Boullé and M. Dupont, *C. R. Acad. Sci.*, **241**, 42 (1955).
- (3) N. Newesely, *Monatsh. Chem.*, **98**, 379 (1967).
- (4) H. C. W. Skinner, *Mater. Res. Bull.*, **5**, 437 (1970).
- (5) A. Gee and V. R. Dietz, *J. Am. Chem. Soc.*, **77**, 2961 (1955).
- (6) R. J. Cvetanović and Y. Amenomiya, *J. Phys. Chem.*, **67**, 144 (1963).
- (7) J. M. Sedlak and R. A. Beebe, *Thermochim. Acta*, **9**, 251 (1974).
- (8) J. M. Sedlak and R. A. Beebe, *J. Colloid Interface Sci.*, **47**, 48 (1974).
- (9) C. W. Anderson, R. A. Beebe, and J. S. Kittelberger, *J. Phys. Chem.*, **76**, 1631 (1974).
- (10) S. J. Joris and C. H. Amberg, *J. Phys. Chem.*, **75**, 3172 (1971).
- (11) This laboratory, unpublished results.
- (12) X-Ray analysis was performed by Dr. H. C. W. Skinner of Yale University. The structure of monetite is discussed by Skinner<sup>4</sup> or by V. L. Jones and D. W. H. Cruickshank, *Z. Kristallogr.*, **116**, 101 (1961).
- (13) (a) P. A. Redhead, *Vacuum*, **12**, 203 (1962); (b) F. M. Lord and J. S. Kittelberger, *Surface Sci.*, **43**, 173 (1974).
- (14) R. Cvetanović and Y. Amenomiya, *Catal. Rev.*, **6**, 21 (1972).
- (15) See T. Ozawa, *J. Thermal Anal.*, **2**, 301 (1970), for example.

# COMMUNICATIONS TO THE EDITOR

## Rotational Freedom of Adsorbed Molecules

Publication costs assisted by the National Research Council of Canada

*Sir:* In a recent communication de Lara and Delaval<sup>1</sup> suggested, on the basis of spectroscopic evidence, that the CH<sub>4</sub> molecule retains appreciable rotational freedom when adsorbed on type A zeolites. This conclusion is supported by independent thermodynamic evidence.

The Henry's law adsorption equilibrium constant (defined by  $c = Kp$ ) may be expressed as the ratio of the partition functions for adsorbed and gaseous molecules, or, in terms of the configuration integral ( $Z$ ):

$$K = Zf_{\text{int}}/f'_{\text{g}} kT \quad (1)$$

In this expression  $f$  is the rotational partition function and  $f_{\text{int}}$  the internal vibrational partition function for an adsorbed molecule;  $f'_{\text{g}}$  is the partition function per unit volume for a gaseous molecule,  $k$  is Boltzmann's constant, and  $z$  is defined by

$$Z = \int_V \exp(-u(\mathbf{r})/kT) d\mathbf{r} \quad (2)$$

where  $u(\mathbf{r})$  is the potential energy at a point specified by position vector  $\mathbf{r}$ . For a monatomic species  $f = 1$  and  $f'_{\text{g}}$  is simply the translational partition function per unit volume ( $f'_{\text{trans}}$ ) so that

$$K = Z/f'_{\text{trans}} kT \quad (3)$$

while for a polyatomic species  $f'_{\text{g}} = f'_{\text{trans}} f'_{\text{rot}} f'_{\text{int}}$  and, assuming  $f_{\text{int}}$  to be the same for gaseous and adsorbed species, we have

$$K = Zf/f'_{\text{trans}} f'_{\text{rot}} kT \quad (4)$$

where  $f_{\text{rot}}$  is the rotational partition function for the gaseous (polyatomic) species.

For nonpolar molecules the potential energy profile within a zeolite cavity arises from the sum of the dispersion, repulsion, and polarization energies and, in any given crystal framework, these energies are determined principally by the size and polarizability of the adsorbed molecule. For a monatomic molecule and a symmetrical polyatomic molecule of the same size and polarizability the potential energy profiles, and the configuration integrals for any particular zeolite, should therefore be essentially the same



**TABLE I: Parameters for Sorption in 5A (Linde) Zeolite<sup>a</sup>**

	Kr	CH <sub>4</sub>	Ar	O <sub>2</sub>
$\sigma$ , Å	3.6	3.8	3.44	3.5
$10^{25}\alpha$ , cm <sup>3</sup> molecule <sup>-1</sup>	25	26	16.3	16.0
$f_{\text{rot}}$ (at 298°K)	1	72	1	71
$K_0$ , molecule cavity <sup>-1</sup>	$1.26 \times 10^{-6}$	$1.9 \times 10^{-6}$	$1.04 \times 10^{-6}$	$1.48 \times 10^{-6}$
$q_0$ , kcal mol <sup>-1</sup>	4.24	4.54	3.36	3.30
$K_{\text{poly}}/K_{\text{mono}}$ (at 298°K)	2.56		1.24	
$f$ (at 298°K)		15		22

<sup>a</sup> The Henry constant is given by  $K = K_0 \exp(q_0/RT)$ . Values of  $K_0$  and  $q_0$  for CH<sub>4</sub>, Ar, and Kr are taken from the thesis of Derrah.<sup>2</sup> The values for O<sub>2</sub> are from unpublished data obtained in this laboratory. Values of  $\sigma$  and  $\alpha$  are from Hirschfelder et al.<sup>3</sup>

and, from eq 3 and 4, the ratio of the Henry constants will be given by

$$\frac{K_{\text{poly}}}{K_{\text{mono}}} = \left( \frac{f}{f_{\text{rot}}} \right)_{\text{poly}} \frac{f'_{\text{trans mono}}}{f'_{\text{trans poly}}} \quad (5)$$

Since the ratio of translational partition functions is simply the ratio of molecular weights raised to the three-halves power:

$$f = \frac{K_{\text{poly}}}{K_{\text{mono}}} \left( \frac{M_{\text{poly}}}{M_{\text{mono}}} \right)^{3/2} f_{\text{rot}} \quad (6)$$

Comparative data for the sorption of CH<sub>4</sub>/Kr and O<sub>2</sub>/Ar in 5A (CaA) zeolite are given in Table I. For these pairs of molecules the conditions of equal size (as measured by the Lennard-Jones  $\sigma$ ) and polarizability are very nearly fulfilled and the limiting heats of sorption ( $q_0$ ) for the species of each pair are almost the same, as is to be expected if the configuration integrals are similar. The rotational partition functions for the adsorbed molecules estimated according to eq 6, are 15 for CH<sub>4</sub> and 22 for O<sub>2</sub>. These values, which may be compared with values of 71–72 for the freely rotating gaseous molecules, suggest that although rotation is somewhat restricted in the adsorbed state an appreciable degree of rotational freedom is retained, in accordance with the spectroscopic evidence.

**References and Notes**

- (1) E. Cohen de Lara and Y. Delaval, *J. Phys. Chem.*, **78**, 2180 (1974).
- (2) R. I. Derrah, Ph.D. Thesis, University of New Brunswick, Fredericton, New Brunswick, Canada, 1973.
- (3) J. O. Hirschfelder, C. F. Curtiss, and R. B. Bird, "Molecular Theory of Gases and Liquids", Wiley, New York, N.Y., 1954.

Department of Chemical Engineering  
University of New Brunswick  
Fredericton, New Brunswick, Canada

**D. M. Ruthven**

Received January 8, 1975

**A Correction and Improvement of "On the Kinetics of Step-Wise Micelle Association" by E. A. G. Aniansson and S. N. Wall<sup>1</sup>**

Sir: The part of ref 1 from eq 31b up to and including eq 37

should be exchanged for the following treatment. Expand

$$\xi(z, t) = \sum_{n=0}^{\infty} c_n(t) H_n(z) \quad (32)$$

where  $H_n$  is the Hermite polynomial<sup>2</sup> of order  $n$  obeying

$$H_n'' - 2zH_n' + 2nH_n = 0 \quad (33a)$$

$$\int_{-\infty}^{\infty} H_n(z) H_m(z) \exp(-z^2) dz = 2^n n! \sqrt{\pi} \delta_{nm} \quad (33b)$$

$$H_n'(z) = 2nH_{n-1}(z) \quad (33c)$$

and

$$2zH_n(z) = H_{n+1}(z) + 2nH_{n-1}(z) \quad (33d)$$

The conservation of total material gives

$$\xi_1(t) = -ac_0(t) - a \frac{\sqrt{2}\sigma}{\bar{n}_3} c_1(t) \quad (34)$$

where

$$\sqrt{2}\pi A_0 = \bar{A}_{\text{exc}} / \sigma \bar{n}_3 \quad (35)$$

has been used and we have introduced

$$a = \bar{A}_{\text{exc}} / \bar{A}_1 \quad (36)$$

Inserting (32) and (34) into (28) and utilizing (33a-d) one finds

$$c_0(t) = c_0(0) \quad (37a)$$

and

$$c_1(t) = \left( c_1(0) - \frac{a \frac{\sigma}{\sqrt{2}} c_0(1 + c_0)}{1 + \frac{\sigma^2}{\bar{n}_3} a(1 + c_0)} \right) e^{-t/\tau} - \frac{a \frac{\sigma}{\sqrt{2}} c_0(1 + c_0)}{1 + \frac{\sigma^2}{\bar{n}_3} a(1 + c_0)} \quad (37b)$$

where

$$\frac{1}{\tau} = \frac{k^+}{a^2} + \frac{k^-}{\bar{n}_3} a(1 + c_0) \quad (37c)$$

The time dependence of the higher  $c_n$ 's can be found similarly and will contain successively smaller time constants given by

$$1/\tau_n = nk^-/\sigma^2 \quad (37d)$$

In relaxation experiments the quantity measured is  $\xi_1(t)$  or its equivalent so that until new experimental methods sensitive to the finer details of the micellar size distributions are developed only  $c_0$  and  $c_1$  are needed.

Under the present assumptions, then, only one relaxation time constant governs the fast rearrangement process even at very large deviations from equilibrium. At small deviations from equilibrium  $c_0 \ll 1$  so that  $k^-/\bar{n}_3$  is then directly obtainable from the slope and  $k^-/\sigma^2$  from the intercept at  $a = 0$  in a plot of  $1/\tau$  vs.  $a$ . Since  $\bar{n}_3$  can be obtained from scattering or other measurements both  $k^-$  and  $\sigma$  should, for the first time, be directly obtainable. The fallacy of the previous treatment resided in an inability of  $p_1(z)$  to give properly convergent integrals for the higher  $n$ 's in the previous eq 37, even after addition to it of suitable amounts of homogenous solutions of the previous eq 30 for  $\mu = 2$ .

**Reference and Notes**

- (1) E. A. G. Aniansson and S. N. Wall, *J. Phys. Chem.*, **78**, 1024 (1974).

(2) G. Arfken, "Mathematical Methods for Physicists", Academic Press, New York, N.Y., 1966; ref 32 in ref 1.

Department of Chemistry  
The University of Göteborg and  
Chalmers University of Technology  
Gothenberg, Sweden

E. A. G. Aniansson\*  
S. N. Wall

Received November 11, 1974

## Rate of Phase Separation in Liquid Mixtures Studied by T-Jump Experiments under Pressure

Publication costs assisted by Verband der Chemischen Industrie e. V., Fonds der Chemischen Industrie

Sir: In this paper some preliminary results for the time dependence of the phase separation into two liquid phases of homogeneous mixtures of pyridine, water, and potassium chloride under pressure are reported.

In recent years the pressure dependence of immiscibility phenomena in liquid mixtures has been extensively investigated, and demixing phenomena in aqueous solutions of nonelectrolytes were also studied as a function of pressure, temperature, concentration, and content of added salts. Figure 1 shows a plot of demixing temperatures as a function of pressure for pyridine-water mixtures with various amounts of potassium chloride added, according to measurements by Russo and Schneider;<sup>1</sup> regions where two liquid phases coexist are indicated by hatching. Starting from conditions of temperature and pressure in the homogeneous region just below the curves plotted, heterogeneous states can be reached rapidly by a relatively small temperature jump. By measuring the degree of turbidity as a function of time some knowledge can be obtained for the time dependence of demixing phenomena in these mixtures.

Measurements were made in a temperature jump apparatus that has been developed for the investigation of fast reactions in solutions under high pressure. Here the temperature jump is generated by discharging a high voltage capacitor. The measuring cell with optical windows for spectroscopic measurements is mounted in a high-pressure autoclave. Details of the experimental device have been reported elsewhere.<sup>2</sup>

With only slight modifications this apparatus was used for the measurements of this paper. The system was pressurized and temperature jumps between 2.4 and 5.4° were created within 3.5  $\mu$ sec. Turbidity was observed by measuring the change of optical transmission; the wavelength used was 560 nm. The current of the photomultiplier was recorded on a storage oscilloscope. Figure 2 shows a typical trace of the oscilloscope for a pyridine-water mixture (wt % pyridine/wt % water = 35/65) with KCl added (14.6 g of KCl in 100 g of H<sub>2</sub>O) starting from 85 bar and 58.2°. The vertical scale is in arbitrary units of decreasing optical transmission (according to increasing turbidity); the horizontal scale is 200  $\mu$ sec per large scale division. After the temperature jump is initiated at  $t = 0$ , the transmission first remains nearly constant for approximately 80  $\mu$ sec.

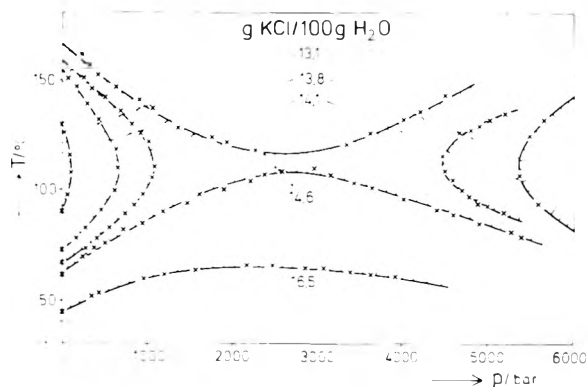


Figure 1. Liquid-liquid phase separation temperatures for the system pyridine-water-KCl as a function of pressure (wt % pyridine/wt % H<sub>2</sub>O = 35/65; salt concentration in g of KCl/100 g of H<sub>2</sub>O; two-phase regions are indicated by hatching).

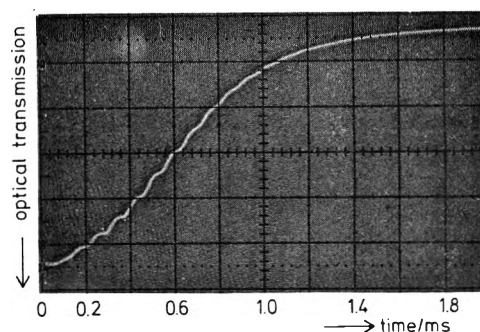


Figure 2. Typical temperature jump trace for the phase separation in a pyridine-water-KCl mixture (wt % pyridine/wt % H<sub>2</sub>O = 35/65; 14.6 g of KCl/100 g of H<sub>2</sub>O; starting conditions  $p = 85$  bar,  $T = 58.2^\circ$ ,  $\Delta T = 5.4^\circ$ ,  $\lambda = 560$  nm).

Then the transmission decreases rapidly until finally an approximately constant value is reached after about 1 msec. Experiments with a shorter wavelength show that in this case the decrease of the transmission starts earlier after the temperature jump.

Assuming a diffusion-controlled growth of the turbidity creating droplets a time of approximately 100  $\mu$ sec can be calculated considering a mean diffusion coefficient of  $D \approx 10^{-5}$  cm<sup>2</sup> sec<sup>-1</sup> until the droplets reach a diameter on the order of the wavelength used. It follows from the above experiments that the growth of the droplets will probably start immediately after the temperature jump without considerable supersaturation.

## References and Notes

- (1) G. M. Schneider and C. Russo, *Ber. Bunsenges. Phys. Chem.*, **70**, 1008 (1966).
- (2) A. Jost, *Ber. Bunsenges. Phys. Chem.*, **78**, 300 (1974).

Department of Chemistry  
University of Bochum  
4630 Bochum  
German Federal Republic

A. Jost  
G. M. Schneider\*

Received December 2, 1974

**If you must have  
reliable data  
on physical  
and chemical  
properties . . .  
you need . . .**

The Journal of Physical and  
Chemical Reference Data.

Now in its third year, this valuable  
publication has proved that it fills  
the important gaps for you in the  
literature of the physical sciences.

Published by the American Institute  
of Physics and the American  
Chemical Society for the National  
Bureau of Standards, this quarterly  
gives you quantitative numerical data,  
with recommended values and  
uncertainty limits chosen by experts  
in the field.

Critical commentary on methods of  
measurement and sources of error,  
as well as full references to the  
original literature, is an integral part  
of each of your four issues a year.

Can you afford to be without this  
prime source of reliable data on  
physical and chemical properties? To  
start receiving your copies, just fill  
in the order form and drop into the  
mail. If you do use a purchase order,  
please attach the printed form as this  
will help us to expedite your order.

Send for complete list of reprints!



. . . another ACS service

# The Journal of Physical and Chemical Reference Data

**JOURNAL OF PHYSICAL AND CHEMICAL REFERENCE DATA**

**1975**

**American Chemical Society**

1155 Sixteenth Street, N.W.  
Washington, D.C. 20036

Yes, I would like to receive the JOURNAL OF PHYSICAL AND CHEMICAL REFERENCE DATA at the one-year rate checked below.

	<b>U.S. &amp; Canada</b>	<b>PUAS</b>	<b>Mexico</b>	<b>Other Nations</b>
<b>ACS*, AIP and affiliated societies members:</b>	<input type="checkbox"/> \$25.00	<input type="checkbox"/> \$28.00	<input type="checkbox"/> \$25.00	<input type="checkbox"/> \$28.00
<b>Nonmembers:</b>	<input type="checkbox"/> \$75.00	<input type="checkbox"/> \$78.00	<input type="checkbox"/> \$75.00	<input type="checkbox"/> \$78.00

Name \_\_\_\_\_

Address  Home  Office \_\_\_\_\_

City \_\_\_\_\_ State \_\_\_\_\_ Zip \_\_\_\_\_

Check enclosed  Bill Company  Bill Me

\*ACS member rates are for personal use only.

Journal subscriptions start on January '75

# RADIONUCLIDES IN THE ENVIRONMENT

## ADVANCES IN CHEMISTRY SERIES NO. 93

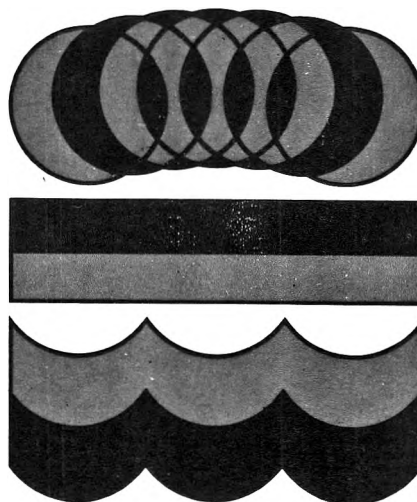
Twenty-eight papers from a symposium sponsored by the Division of Nuclear Chemistry and Technology, chaired by E. C. Freiling.

Pollution . . . a growing concern . . . a concept not generally associated with radionuclides. The successful control of this hazardous waste product of nuclear energy is essential to the continued use and development of nuclear power. Critical to this problem is an understanding of the processes by which radionuclides are produced, dispersed, and retained in the environment.

The papers in this volume discuss and evaluate the properties and problems relating to radionuclides, including

- mechanisms of release, absorption, uptake, transport
- behavior, measurement and characterization, specific weapons tests
- specific activity, public health aspects, fallout
- new methods and equipment

522 pages with index Clothbound (1968) \$15.00  
Set of L.C. cards with library orders upon request.



Other books in the ADVANCES IN CHEMISTRY SERIES OF related interest include:

No. 89 Isotope Effects in Chemical Processes. Methods of separating isotopes and labeled molecules—chemical exchange, electromigration, photochemical processes, and distillation—are examined, along with factors that suit a process to isotope separation—single stage fractionation, exchange rate, and reflux.  
278 pages cloth (1969) \$13.00

No. 82 Radiation Chemistry—II. Thirty-six papers and 17 abstracts on radiation chemistry in gases, solids, and organic liquids. Includes three plenary lectures. 558 pages cloth (1968) \$16.00

No. 81 Radiation Chemistry—I. Forty-one papers and 17 abstracts on radiation chemistry in aqueous media, biology, and dosimetry. From the international conference at Argonne National Laboratory. 616 pages cloth (1968) \$16.00. No. 81 and 82 ordered together \$30.00

No. 72 Mass Spectrometry in Inorganic Chemistry. A basic tool for chemical manipulations, the mass spectrometer is a conventional monitor for any stage in a research problem to help establish what is going on. 21 Research reports. 329 pages cloth (1968) \$12.00

No. 68 The Mössbauer Effect and Its Application in Chemistry. Ten papers that will familiarize chemists with Mössbauer spectroscopy as an analytical tool for studying chemical bonding, crystal structure, electron density, magnetism, and other properties.

178 pages cloth (1967) \$8.00

No. 66 Irradiation of Polymers. Eighteen papers survey radiation mechanics in polymers, the chemical nature of reactive species produced, crosslinking and scission, homopolymerization, graft copolymerization, and the effects of ultraviolet light radiation.

275 pages cloth (1967) \$10.00

No. 58 Ion-Molecule Reactions in the Gas Phase. Eighteen papers survey spectrometric and other methods for producing and studying ion-molecule reactions such as pulsed sources for studying thermal ions, reactions in flames and electrical discharges.

336 pages cloth (1966) \$10.50

No. 50 Solvated Electron. Reviews of theory, structure, reactions of solvated and hydrated electrons; detailed papers on electrical transport properties, photochemistry, theory of electron transfer reactions, structure of solvated electrons, hydrated electron research. 304 pages cloth (1965) \$10.50

Postpaid in U. S. and Canada; plus 30 cents elsewhere.

Order from:

**SPECIAL ISSUES SALES  
AMERICAN CHEMICAL SOCIETY  
1155 SIXTEENTH ST., N.W.  
WASHINGTON, D. C. 20036**